ELSEVIER

Physics Reports 269 (1996) 1–131

PHYSICS REPORTS

# Statistical physics of polymer gels

Sergei Panyukov[1], Yitzhak Rabin

*Department of Physics, Bar-Ilan University, Ramat-Gan 52900, Israel*

Received July 1995; editor: I. Procaccia

**Contents**

1. Introduction 4
2. The model 12
  2.1. Pre-cross-linked polymer 13
  2.2. Instantaneous cross-linking and cross-link saturation threshold 13
  2.3. Edwards formulation 15
  2.4. Field theory 21
3. Mean-field solution 25
  3.1. The mean-field equation 25
  3.2. Homogeneous solution 27
  3.3. Inhomogeneous solution 27
  3.4. Mean-field free energy 32
  3.5. Stability of the mean-field solution 34
  3.6. Uniqueness of the ground state 37
  3.7. Local deviations from affinity 41
4. Static inhomogeneities and thermal fluctuations 45
  4.1. RPA free energy density functional 45
  4.2. Inhomogeneous equilibrium density profile 49
  4.3. Thermal and structure averages 50
  4.4. Density correlation functions 52
  4.5. Analytical expressions for the correlators 53
  4.6. Gels in polymeric solvents 59
5. Gels in good solvents 71
  5.1. Renormalization and scaling 72
  5.2. Thermodynamics 75
  5.3. Interpenetration and desinterpenetration of network chains 78
  5.4. Density correlation functions 78
6. Connection with continuum theory of elasticity 85
  6.1. Anisotropic moduli of homogeneous deformed networks 86
  6.2. Equilibrium state of deformed inhomogeneous gels and the butterfly effect 89
7. Discussion 91
Appendix A. Field theoretical preliminaries 95
  A.1. Functional integrals 95
  A.2. Field representation for Gaussian chains 96
Appendix B. Mean-field Hamiltonian 97
  B.1. Replica space integration 97
  B.2. The longitudinal subspace 99
Appendix C. Spectrum of fluctuations 100
  C.1. Homogeneous solution 100
  C.2. Inhomogeneous solution 101
Appendix D. Ultra-short wavelength corrections to free energy 110
  D.1. Rotational partition function 111
  D.2. Partition function of shear and density modes 112
  D.3. Elimination of divergences 113
  D.4. Wasted loops corrections to free energy 116
Appendix E. Correlation functions of the replica system 117
  E.1. Calculation of $g_{\Lambda}^{00}$ 118
  E.2. Calculation of $g_{\Lambda}^{kl}$ 119
Appendix F. Derivation of the entropy density functional 125
  F.1. Elimination of shear fluctuations and of density fluctuations in the initial state 125
  F.2. Diagonalization in the replicas 127
Appendix G. Asymptotic expressions for correlators $g_q$ and $v_q$ 128
References 130

[1] Permanent address: Lebedev Physics Institute, Russian Academy of Sciences, Moscow 117924, Russia.


*SSDI* 0370-1573(95)00068-2

# STATISTICAL PHYSICS OF POLYMER GELS

**Sergei PANYUKOV, Yitzhak RABIN**

*Department of Physics, Bar-Ilan University, Ramat-Gan 52900, Israel*


ELSEVIER

AMSTERDAM – LAUSANNE – NEW YORK – OXFORD – SHANNON – TOKYO

**Abstract**

This work presents a comprehensive analysis of the statistical mechanics of randomly cross-linked polymer gels, starting from a microscopic model of a network made of instantaneously cross-linked Gaussian chains with excluded volume, and ending with the derivation of explicit expressions for the thermodynamic functions and for the density correlation functions which can be tested by experiments.

Using replica field theory we calculate the mean field density in replica space and show that this solution contains statistical information about the behavior of individual chains in the network. The average monomer positions change affinely with macroscopic deformation and fluctuations about these positions are limited to length scales of the order of the mesh size.

We prove that a given gel has a unique state of microscopic equilibrium which depends on the temperature, the solvent, the average monomer density and the imposed deformation. This state is characterized by the set of the average positions of all the monomers or, equivalently, by a unique inhomogeneous monomer density profile. Gels are thus the only known example of equilibrium solids with no long-range order.

We calculate the RPA density correlation functions that describe the statistical properties of small deviations from the average density, due to both static spatial heterogeneities (which characterize the inhomogeneous equilibrium state) and thermal fluctuations (about this equilibrium). We explain how the deformation-induced anisotropy of the inhomogeneous equilibrium density profile is revealed by small angle neutron scattering and light scattering experiments, through the observation of the butterfly effect. We show that all the statistical information about the structure of polymer networks is contained in two parameters whose values are determined by the conditions of synthesis: the density of cross-links and the heterogeneity parameter. We find that the structure of instantaneously cross-linked gels becomes increasingly inhomogeneous with the approach to the cross-link saturation threshold at which the heterogeneity parameter diverges.

Analytical expressions for the correlators of deformed gels are derived in both the long wavelength and the short wavelength limits and an exact expression for the total static structure factor, valid for arbitrary wavelengths, is obtained for gels in the state of preparation. We adapt the RPA results to gels permeated by free labelled chains and to gels in good solvents (in the latter case, excluded volume effects are taken into account exactly) and make predictions which can be directly tested by scattering and thermodynamic experiments. Finally, we discuss the limitations and the possible extensions of our work.

## 1. Introduction

Polymer gels are fascinating materials which differ in many respects from ordinary solids. Although they possess all the normal characteristics of solids such as stability of shape, resistance to shear, etc., they can absorb solvent and swell to dimensions much larger than their dry size and exhibit linear elastic response to deformation at strains exceeding (and sometimes, far exceeding) unity. The fact that the gel is a solid permeated by solvent means that it can be thought of as a combination of a solid and a liquid, and that its state of equilibrium is determined by the interplay between the two components. The above statement applies even to dry polymer networks in which the "liquid" component can be identified with the un-cross-linked monomers which interact repulsively through short range excluded volume forces. When the network is deformed, the osmotic pressure of the liquid component adjusts itself to balance the local elastic stresses. If the liquid component changes its characteristics (by change of temperature, solvent, etc.), the network stresses adjust to the new osmotic pressure, resulting in a new equilibrium. This interplay determines the response of the gel to all external perturbations under which the network maintains its integrity (i.e., does not break).

Polymer gels can be synthesized by cross-linking a polymer solution or a melt (they can also be formed by polymerizing a mixture of monomers and multi-functional cross-linkers). Although, in principle, it is conceivable to cross-link a crystalline polymer solid and, upon melting, obtain a gel which "remembers" its original lattice structure, to the best of our knowledge, this has not been done to date. Accordingly, gels are disordered solids, the structure of which reflects the state of the polymeric solution from which they were formed. The memory of the initial state is frozen into the network during its formation and reveals itself in all experiments performed on the network, long after the process of cross-linking is terminated. Thus, if one attempts to model the response of the gel to some external deformation, one has to know not only the state of the gel immediately prior to the deformation but also the conditions under which it was prepared.

At first sight, the existence of memory effects suggests that in order to understand the behavior of polymer networks, one needs to have complete information about their complicated frozen structure, i.e., one has to specify a vast number (of the order of the Avogadro number) of parameters. If this was the case, it would undermine any attempt to obtain a *probabilistic* description of the physics of polymer gels by the usual methods of statistical physics. This seemingly intractable problem can be overcome by noticing, as was done by Edwards and his coworkers [1, 2], that if the gel is formed by *instantaneous* cross-linking of a polymer solution, the probability of observing a particular network structure is identical to the probability of observing a state of a polymer liquid in which some monomers (a fraction of which will be cross-linked immediately afterwards) are in contact with each other. The latter probability distribution can be characterized by only a small number of parameters which define the conditions of preparation, such as temperature, solvent quality, degree of cross-linking and density in the initial state. Similar tricks can be applied to other methods of gel preparation such as equilibrium polycondensation, etc., for which we can characterize the post-cross-linking state in terms of a known probability distribution of the pre-cross-linking state.

Using the above approach the problem can be reformulated in statistical terms, in which the answers to all experimentally relevant questions about the behavior of polymer gels are given in terms of averages of the physical quantities we are interested in. In this way the problem reduces to

finding the probability distribution associated with the physical quantity of interest and averaging with respect to this distribution. The possibility of obtaining such a reduced description is related to the fact (which will be proved latter) that, in spite of their complexity and frozen randomness, gels have a unique state of microscopic equilibrium. Although there is an obvious loss of ergodicity associated with the process of cross-linking (of the same kind which accompanies the crystallization of a liquid), gels differ from glasses due to the fact that once they are formed (by irreversible cross-linking), their equilibrium state is uniquely determined by (and only by) the parameters that characterize this state (temperature, quality of solvent, etc.) and does not depend on their "history" *after* preparation (as long as the integrity of the network is maintained). For example, if a gel is synthesized at temperature $T^{(0)}$ and subsequently studied at a temperature $T$, its state will depend only on $T$ and not on the history of heating process (heating to $T' > T$ and subsequently cooling to $T$ results in the same final state of equilibrium as heating directly from $T^{(0)}$ to $T$). In spin glasses the final state will depend, in general, on the history of its preparation (after the synthesis of the system).

This work is based on the Edwards model of *instantaneously cross-linked networks of Gaussian chains with excluded volume* [1]. No additional constraints are introduced to describe the fact that real chains cannot cross each other and, therefore, this model does not account for the contribution of permanent topological entanglements to the elasticity of polymer networks (recall that although all theories of polymer solutions consider only temporary entanglements [3], permanent entanglements may also be present in irreversibly cross-linked networks). In choosing the above model of polymer networks we are guided by considerations of simplicity. Although more complicated models (including entanglements and non-Gaussian elasticity) are more realistic, our aim is to start with the simplest well-defined microscopic theory and to present a *strict* mathematical analysis of the problem which will serve as a point of reference for future generalizations. We will show that the statistical mechanics of this model can be solved exactly (i.e., on the same level of rigor as other solved problems of polymer physics) and, in the process, obtain important insights about the physics of polymer gels, solve some long-standing puzzles and make new predictions which can be tested by scattering experiments on these systems.

The unusual length of this manuscript is dictated by the need to make a self-contained and (hopefully) coherent presentation of our ideas about the statistical mechanics of polymer gels and to reach different scientific communities which may be interested in this subject. We would like to stress that although this work uses much of the state-of-the-art machinery of theoretical physics, the mathematical concepts involved are fairly standard and simple and the more complicated derivations are described in considerable detail in the corresponding Appendices. Since this is mostly an account of original work, much of which has never been published before, we will refrain from reviewing the history of the subject and will refer to the contributions of other investigators (and to our own previous work), in the appropriate places in this manuscript.

In Section 2 we introduce the Edwards formulation of the statistical mechanics of polymer networks [1]. We discuss the hitherto unnoticed fundamental property of the instantaneous cross-linking process, namely, the existence of the *cross-link saturation threshold*, which defines the maximal achievable density of cross-links in the present model (at this point the number of cross-links becomes equal to the average number of inter-monomer "contacts" in the pre-cross-linked polymer solution). It will be shown later that when this saturation threshold is approached, the length scale associated with the quenched heterogeneity of network structure diverges and static heterogeneities appear on all length scales in the gel.

We use the self-averaging property of the total free energy in order express it as an average (with respect to the probability of synthesis of a given network structure) of the logarithm of the partition function of the deformed gel. In order to avoid the inconvenient averaging of the logarithm we introduce the standard *replica trick* (define one replica of the initial state and $m$ replicas of the final state) and express the true thermodynamic free energy as the derivative of the replica free energy with respect to $m$, in the limit $m \to 0$. The constraints introduced by the cross-links are replaced by an effective attractive potential through the introduction of the grand canonical representation which is then extended to all the monomers (i.e., both the number of monomers and the number of cross-links are allowed to fluctuate, so that only their average numbers are determined by the monomer chemical potential and by the fugacity of cross-links). This illustrates the immense computational simplification produced by the transformation to the abstract replica space (defined as the space of the coordinates in all the $1 + m$ replicas): *frozen inhomogeneities of network structure (in real space) can be treated as thermal fluctuations in replica space* and the seemingly intractable calculation of frozen disorder can be performed using the usual methods of equilibrium statistical mechanics! While excluded volume interactions act independently in each of the replicas, the interactions which represent the cross-links act identically in all the replicas (this is an expression of the solid character of the gel) and, therefore, introduce a coupling between the replicas. Finally, the thermodynamic free energy is expressed through the grand canonical partition function of the replica system.

Although the interactions (both excluded volume ones and those associated with cross-links) are non-local along the chain contour, they are local both in the 3-dimensional physical space and in the $3(1 + m)$-dimensional replica space. This fact is used in Section 3 where we transform to collective coordinates (field theory) and rewrite the interactions in terms of replica space densities (for the cross-links) and densities in each of the replicas (for the excluded volume). We then use a generalization of de Gennes' $n = 0$ method [3] to eliminate the elastic entropy term in the replica partition function by introducing a field theoretical representation of the entropy in terms of a $n$-component vector field $\varphi$ (the limit $n = 0$ is taken at the end of the calculation), and relate this field to the density in replica space. The details of the transformation to the field representation for Gaussian chains are given in Appendix A. We represent the replica partition function as a functional integral of Boltzmann weights defined by a replica generalization of a $\varphi^4$-type field Hamiltonian, and discuss the various continuous and discrete symmetries of this Hamiltonian (rotations in $n$ vector space, permutations of the replicas of the final state, rotations in each of the replicas and translations in replica space).

In Section 3 we proceed to look for a mean-field solution which minimizes the field Hamiltonian and, therefore, gives the steepest descent estimate of the replica partition function. We derive the field equations the solutions of which correspond to the extrema of the Hamiltonian. Guided by the expectation that the ground state solution must have the maximal possible symmetry, we first consider the constant (in replica state) solution which has the full symmetry of the underlying Hamiltonian. However, as is shown in Appendix C, this solution corresponds to the saddle point rather than to a minimum of the Hamiltonian and must be rejected.

The analogy with crystalline solids which can be thought of as solutions with spontaneously broken translational symmetry (in real space) which minimize a translationally invariant (i.e., which has the symmetry of a liquid) Hamiltonian [4], suggests that we look for a solution with *spontaneously broken translational symmetry in replica space* which obeys the physical condition

that it gives rise to a constant mean density in the three-dimensional space associated with each of the replicas [5]. The above condition imposes a constraint on the dependence of the mean-field solution on the replica space coordinates, i.e., the solution must be invariant under simultaneous translation (by a constant) along the principal axes of deformation in each of the replicas of the final state. Introducing a partition of the replica space into a 3-dimensional longitudinal (along the principal axes of deformation in each of the final state replicas) and a $3m$-dimensional transverse subspace, we show that the mean-field solution depends only on the coordinates of the transverse subspace and is invariant under rotations in this subspace. This allows the replacement of the $3(1 + m)$-dimensional non-linear partial differential equation by a simple non-linear differential equation from which the mean-field solution is calculated numerically. We find that the solution is localized around a 3-dimensional surface (the longitudinal subspace; see Appendix B) in replica space, defined by the *affine* relation between the coordinates in the initial and in each of the final replicas, with a characteristic width of the order of the mesh size of the network. The fact that the solution is *replica symmetric* (i.e., invariant under permutations of the replicas of the final state) means that *the position of any given monomer is nearly identical (up to thermal fluctuations on the scale of a mesh) in all of the replicas of the final state and that the average position of each monomer changes affinely with the deformation of the network.*

Using this inhomogeneous solution, we perform the steepest descent calculation of the replica partition function and obtain the mean-field thermodynamic free energy of the gel (details of the calculation are given in Appendix B). Our free energy coincides with the Deam and Edwards variational estimate [1] which is qualitatively similar (apart from a numerical coefficient and logarithmic corrections) to that of classical theories of network elasticity due to Flory and Rehner [6, 7] and James and Guth [8]. We then calculate the fluctuation corrections to the mean-field free energy (Appendix D). We find that the most important corrections due to frozen fluctuations of network structure come from ultra-short wavelengths of the order of the monomer size, due to the contributions of small "wasted" loops which decrease the number of elastically effective cross-links and therefore decrease the elastic modulus. The resulting corrections agree with those obtained by Deam and Edwards [1].

We proceed to examine the stability of the mean-field solution and check whether or not it corresponds to a true minimum of the replica Hamiltonian. To this end we calculate all the eigenvalues and eigenfunctions of the operator which gives the energy of fluctuations about this solution (the calculation is presented in Appendix C and uses the expressions for the replica space correlation functions derived in Appendix E). We find that the fluctuation energy evaluated on the homogeneous solution has some negative eigenvalues and therefore does not correspond to a true minimum. On the other hand, all the eigenvalues (corresponding to rotations in the space of the $n$-vector model and to shear and density modes in replica space) associated with our inhomogeneous solution are positive. This proves that *the inhomogeneous solution minimizes the Hamiltonian and is stable with respect to arbitrary small fluctuations in replica space*, including those which break the symmetry with respect to permutations of the replicas of the final state.

The next step is to check whether the minimum we found is a global one. The existence of other solutions with lower or equal energy would undermine the validity of our steepest descent calculation of the partition function (since, in the thermodynamic limit, the functional integral will be dominated by the true ground state). On a more fundamental level, the issue here is whether polymer gels belong to the class of spin glasses (which have multiple minima) or to the class of

ordinary solids (which have a single equilibrium state under given thermodynamic conditions). Since our inhomogeneous mean-field solution describes a network in which excluded volume effects are accounted for by introducing a uniform external field which fixes the average monomer density in the system, we proceed to calculate the partition function of a network without excluded volume, the surface of which is fixed to walls which enforce the constant density constraint (the *elastic reference state*). As all the functional integrals over the monomer positions are Gaussian, they can be calculated exactly and we are left with (also Gaussian) integrals over the coordinates of the cross-links and of the monomers which are bound to the walls. Representing each cross-link coordinate as the sum of a mean position and the deviation from it, we write the cross-link Hamiltonian as sum of quadratic contributions (in the mean cross-link positions and in the deviations from these positions) and a term which is linear in the deviations from the mean positions. The requirement that the linear term in the expansion must vanish is equivalent to the condition of mechanical equilibrium, i.e., to vanishing average force on each cross-link due to the "spring"-mediated forces of its immediate neighbors. We find that a single solution exists, i.e., that the number degrees of freedom (cross-links) is equal to the number of constraints (force balance conditions), provided that the matrix of second derivatives of the cross-link Hamiltonian with respect to the cross-link coordinates has no vanishing eigenvalues. We show that each such vanishing eigenvalue corresponds to a collective mode which does not affect the energy of the network (zero-energy mode). Using the properties of the second derivative matrix of a Gaussian network, we find that there is only one zero-energy mode and show that it corresponds to uniform translation of all the cross-links. This mode is eliminated if one fixes the position of even a single cross-link (or of the center of mass of the network) and we conclude that a randomly cross-linked network does not have any zero-energy modes. Thus, *our inhomogeneous solution defines the only mechanically stable state of the gel* and no other minima exist (this eliminates not only other stable states but also metastable ones). *A randomly cross-linked polymer network has a single microscopic state of equilibrium in which the average positions of cross-links (and of all monomers) are uniquely defined under given thermodynamic conditions*!

We proceed to analyze the physical content of the mean-field expression for the density of monomers in replica space, which is analogous to the Edwards–Anderson order parameter [9] familiar from the theory of spin glasses, and find that it contains *statistical* information about the frozen structure of the network. This order parameter defines the probability distribution of deviations of network monomers from their mean (i.e., affinely displaced) positions, from which the average localization length which determines the length scale of thermal fluctuations of monomers, is calculated. Contrary to the Flory assumption [6], we find that *both the monomers and the cross-links fluctuate over length scales of the order of the mesh size.*

The above order parameter can also be used to find how the distribution function of the end-to-end distances of chains of given contour length is affected by the deformation of the network. We present the results of calculations reported elsewhere [10, 11] (their derivation requires the use of methods which differ from the ones used in this work) which show that the average deformation of such chains depends both on their length and on the local environment in which they are embedded, and that *only chains which are larger than the local mesh size are stretched affinely with the macroscopic deformation.* Strong deviations from affinity are obtained for shorter network chains (those much shorter than the local mesh size react to deformation only through desinterpenetration). These intriguing results also follow from the observation that the rms

distance between the ends of a network chain is the sum of a contribution of the average distance between the ends (which deforms affinely with the network) and a fluctuation contribution (which is not affected by the deformation) and that the latter is important only on length scales of the order of the mesh size (the characteristic length scale of thermal fluctuations). Under uniaxial extension, the average mesh size deforms affinely along the direction of stretching and its transverse dimensions are not affected by the deformation.

Section 4 begins with the observation that, to make contact with scattering experiments which probe the static inhomogeneities and the thermal density fluctuations of the monomer density in swollen and stretched networks, we have to eliminate (i.e., integrate over) the contributions of the shear modes and of the density modes in the state of preparation. In order to make the calculation feasible we assume that the deviations from the average density are small and can be treated within the *random phase approximation* (RPA) [3] which corresponds to keeping only quadratic terms in these deviations. We show later that while this assumption always holds for frozen density inhomogeneities (for gels prepared away from the cross-link saturation threshold), it breaks down for thermal density fluctuations in gels in good solvents where such fluctuations are strong (we show in Section 5 that, on length scales larger than the "blob" size, these strong fluctuations can be accounted for by an appropriate renormalization of the RPA parameters). The elimination of the "irrelevant" shear and density modes is done by introducing auxiliary fields which couple between the replicas of the final state (the calculation is presented in Appendix F). Diagonalization of these couplings allows us to calculate the non-averaged free energy functional of the Fourier components of the monomer density ($\rho_q$) and a random field ($n_q$) which represents the structure of the network, and to obtain the (Gaussian) distribution function $P(n_q)$ (the probability to observe a given amplitude of the random field $n_q$ in the gel). We find the *equilibrium density distribution* $\rho_q^{eq}$ which minimizes the free energy functional and show that it corresponds to the *static inhomogeneous density profile of the gel, which is uniquely defined by the structure of the network and by the thermodynamic conditions in the final deformed state*, and which can be detected through the observation of static speckle patterns in the intensity of light scattered from gels. We show that the field $n_q$ can be interpreted as the inhomogeneous equilibrium density profile of the elastic reference state (i.e., of a stretched gel, without excluded volume interactions). Using the free energy functional (quadratic in $\rho_q$ and $n_q$) and the distribution function $P[n]$, we can compute all the statistical information about the static density inhomogeneities and thermal density fluctuations in a deformed gel. We relate our theoretical predictions to scattering experiments which measure static density correlations (averaged over both space and time), by showing that averaging over the ensemble of all possible network structures (consistent with thermodynamic conditions in the state of preparation) is equivalent to averaging over the volume of a single polymer gel, and that averaging over the ensemble of gels with a given network structure (thermal averaging) is equivalent to time averaging over the configurations of a single gel.

All the information which enables us to calculate the experimentally observable density correlation functions is contained in two functions, $g_q$ and $v_q$, where the former is the correlator of thermal density fluctuations in the elastic reference state and the latter is the structure averaged correlator which measures the spatial correlations of the inhomogeneous equilibrium density profile in this state (explicit analytical RPA expressions for these functions, in both the short wavelength and the long wavelength limits, are given in Appendix G). An exact (within the RPA) expression for the total structure factor, valid in the entire range of scattering wave vectors, is obtained for gels in

the state of preparation. Asymptotic expressions (in both the long wavelength and the short wavelength limits) for the experimentally observable density correlators in the final deformed state are also given and it is shown that all the structural information about the gel is contained in two parameters: the density of cross-links in the state of preparation and the *heterogeneity parameter* which measures the distance from the cross-link saturation threshold. *The total static structure factor is dominated by scattering from static monomer density inhomogeneities and when gels are subjected to uniaxial extension, the amplitudes of the (long wavelength) Fourier components of this static density profile are enhanced along the stretching direction and suppressed normal to it, resulting in "butterfly"-like contours in plots of the isointensity lines.* These butterfly patterns have been observed in small angle neutron scattering [12] and light scattering [13] experiments. The thermal structure factor exhibits the reverse anisotropy, an effect which also has been observed in (dynamic light scattering) experiments [14].

We show that under most conditions, *the thermal structure factor has a peak at a finite wave vector* which lies outside the range of our asymptotic expressions. We conjecture that the characteristic wavelength associated with the peak is of the order of the mesh size and, therefore, that thermal fluctuations are anomalously enhanced at this wavelength. *Microphase separation in poor solvent*, as the result of the expulsion of the solvent from the denser regions of the inhomogeneous profile, is predicted.

We apply our RPA formalism to the problem of a *network permeated by free labelled polymers*, in which thermal fluctuations are suppressed by strong screening [15]. We find that the structure factor depends on an *effective heterogeneity parameter* which vanishes both in the absence of frozen heterogeneities (i.e., for networks prepared away from the cross-link saturation threshold) and in the limit of vanishing concentration of the free labelled chains. The scattering increases with the heterogeneity parameter (e.g., with the density of cross-links) and with the degree of swelling. We analyze the case of uniaxial extension and show that the scattering is enhanced in direction of stretching and suppressed normal to it, and that butterfly patterns appear, as the result, in plots of the isointensity lines. All the above results are in qualitative agreement with experimental observations on gels permeated by polymeric solvents and on blends of short and long chains (in which entanglements act as effective cross-links) [16–18]. We also study segregation (i.e., expulsion of the free chains from the gel) and find that *the spinodal is shifted by externally applied anisotropic deformations* (which promote segregation) and that, for uniaxial extension, it is first reached for fluctuations which are normal to the stretching direction. Related experiments on sheared blends indicate that segregation is indeed promoted by deformation [19].

In Section 5 we consider *semi-dilute gels in good solvents* and present a simple method which allows one to account for the effect of strong fluctuations by combining renormalization group and scaling ideas. We argue that the coarse graining of the microscopic Hamiltonian leads to the renormalization of the bare parameters of this Hamiltonian (e.g., monomer size and second virial coefficient) and use the known scaling blob parameters [3] to find the fixed points of the corresponding renormalization group transformations. This procedure leads to a non-trivial renormalization of the mean-field free energy which can no longer be decomposed into independent osmotic and elastic parts, indicating the *breakdown of the classical additivity assumption* [20]. We show that *the celebrated $c^*$ theorem* [3] *applies only at the cross-link saturation threshold and that, under normal preparation conditions, there are many chains within the volume of the average mesh of the network.* The number of interpenetrating chains is not affected by swelling (no

desinterpenetration), but increases with compression (through expulsion of solvent). We calculate the equilibrium swelling ratios and elastic and osmotic moduli and show how these moduli are affected by externally applied osmotic pressure.

We proceed to calculate the density correlation functions for gels swollen in good solvents. *Density fluctuations are enhanced by isotropic swelling and under uniaxial extension, butterfly patterns appear in the isointensity plots of the structure factor.* In the high $q$ limit (i.e., for wave vectors much larger than the inverse mesh size) the scattering reduces to that of a semi-dilute solution of uncross-linked and unstretched chains. In the long wavelength limit (for wavelengths much larger than the mesh size), we find that for gels prepared near the cross-link saturation threshold, scattering from static inhomogeneities always dominates over that from thermal fluctuations. Away from the cross-link saturation threshold, *thermal fluctuations dominate in the state of preparation (in the reaction bath), but static heterogeneities give an increasingly larger contribution with progressive swelling and dominate the fluctuation intensity at swelling equilibrium in excess solvent.* The effect of uniaxial stretching is to enhance the static inhomogeneities compared to the thermal fluctuations, in the direction of stretching. The effect is reversed normal to the direction of stretching. In all cases, butterfly patterns oriented along the direction of stretching (in plots of the isointensity contours) are predicted, in agreement with experiment [12]. This holds even when thermal fluctuations dominate, since in this regime the thermal fluctuation intensity is nearly angle-independent and the entire angular dependence comes from static inhomogeneities. Another interesting (and totally unexpected) prediction is the existence of *a maximum at a finite wave vector, in the thermal structure factor of neutral gels in good solvents.* The presence of this maximum may explain the observed complicated shapes of the total scattered intensity curves, under conditions when thermal fluctuations make an important contribution to the static scattering profiles (e.g., in lightly cross-linked gels, close to the density of preparation).

In Section 6 we return to the butterfly effect, the observation of which was the first clear demonstration of the failure of the classical theories of gels and prompted our own interest in this problem. In order to obtain a simple physical picture of the inhomogeneous equilibrium state of stretched polymer networks in terms of balance of forces, we proceed to establish the connection between our theory and the continuum theory of elasticity of solids [21]. Following Alexander [22], we show that the classical theory of network elasticity (as well as ours) which predicts linear elastic response at strains exceeding unity, corresponds to a version of the usual continuum theory of elasticity of homogeneous solids, in which one takes into account the usually neglected non-linear contributions to the strain tensor. *The elastic modulus of a stretched homogeneous network is a tensor which depends on both the magnitude and the direction of stretching.* When the theory is generalized to the case of inhomogeneous continua and osmotic (excluded volume) contributions are included, minimization of the free energy yields the force balance condition between forces associated with the stretched "springs" (present even in homogeneous networks), forces which drive the network towards the inhomogeneous equilibrium state and osmotic forces which tend to swell the gel. The resulting inhomogeneous equilibrium density distribution displays the characteristic anisotropy observed in static scattering experiments and we conclude that *the butterfly effect arises as the result of the interplay among the three phenomena which underlie the physics of polymer gels: the elastic response of stretched springs (deformation-dependent modulus), the presence of "liquid-like" degrees of freedom (osmotic forces) and the existence of frozen inhomogeneities of network structure (inhomogeneous equilibrium state).*

In Section 7 we summarize the main results obtained in this work. We argue that gels do not belong to any of the known classes of solids. Unlike amorphous materials (e.g., glasses), once they are formed, they have a single well-defined state of microscopic equilibrium. Unlike crystalline solids, they possess no long-range order and their "atoms" (i.e., monomers and cross-links) fluctuate over distances which exceed the average distance between neighboring "atoms". This new class of materials can be called *soft disordered equilibrium solids*. We end this work by discussing the limitations of our theory and suggesting possible extensions and generalizations.

## 2. The model

Consider the following situation: a chemically cross-linked polymer network is immersed in a good solvent and subjected to mechanical deformation. As long as the deformation does not affect the chemical structure of the gel (i.e., as long as the network does not break), the response will be determined by both the external conditions (deformation, solvent quality, temperature, etc.) which can be varied at will, and by the fixed *network structure*. The structure of the network is uniquely defined by specifying which monomers are joined at each cross-link point and is fixed once and for all at the time of preparation of the gel. It can depend on the method of cross-linking (irradiation, chemical reaction, etc.) and on the physical conditions (solvent quality, temperature . . .) to which the system was subjected during synthesis. In the following, we will refer to the state of preparation (following cross-linking) as the *initial* state. The *final* state of the swollen and deformed network depends indirectly on the conditions of network preparation, since they determine the frozen structure of the network.

We start with the Edwards model of a *randomly cross-linked network of Gaussian chains with excluded volume* [1]. While this microscopic model does not contain explicit topological constraints which would account for the presence of permanent entanglements in real networks, it is conceivable that such effects are implicitly contained in the model, due to excluded volume interactions that prevent chains from crossing each other. Although we do not have a definitive proof that this is not the case (because of our incomplete understanding of the microscopic nature of entanglements of polymers), we can easily give a counter example. Consider, for instance, a discrete model of a polymer made of beads of finite volume ("monomers"), connected by "phantom" springs which can pass freely through each other (the minimal length of a spring is larger than the bead diameter). This model gives rise to the same universal static exponents (e.g., the scaling of end-to-end distance with molecular weight) as a non-phantom model in which the springs are not allowed to cross each other but, unlike the latter, cannot describe entanglements (notice that both models reduce to the Edwards Hamiltonian in the continuum limit where both the length of the springs and the size of the beads are taken to zero). While such entanglement effects can be treated by the ad hoc introduction of an "entanglement tube" into the present model, they cannot be described with the same degree of mathematical rigor as the simpler "phantom" chains (the concept of an "entanglement tube" does not arise naturally in the microscopic model and has to be introduced by hand into our formulation).

Following Deam and Edwards [1], we neglect dangling ends and assume that the network is formed by cross-linking very long chains, well above the gelation point (which corresponds to the minimal concentration of cross-links at which an infinite connected network is formed). In order to

avoid difficulties associated with the description of a dense polymer liquid, it is assumed that the network is prepared by cross-linking chains in a semi-dilute solution in a good solvent, in which the interaction between monomers can be described by an effective second virial coefficient, $w^{(0)}$. Since chain-end effects can be neglected for sufficiently long percursor chains, the polymer solution can be replaced by a single chain of $N_{\rm tot}$ monomers where $N_{\rm tot}$ is the total number of monomers in the original solution (this replacement is allowed as long as we do not consider the conformations of individual chains). The constraint of average monomer density $\rho^{(0)}$ in the pre-cross-linked polymer solution is satisfied by confining the chain to a volume $V^{(0)}$ such that $\rho^{(0)} = N_{\rm tot}/V^{(0)}$.

### 2.1. Pre-cross-linked polymer

The conformation of a polymer in a good solvent is defined by the spatial position $\boldsymbol{x}(s)$ of the $s$th monomer ($s$ takes values from 1 to the number of monomers in a chain). In a continuum description of the chain, $s$ becomes a continuous contour parameter which varies between 0 and $N_{\rm tot}$, and the polymer is modeled by the Edwards Hamiltonian [23],

$$\frac{\mathscr{H}^{(0)}[\boldsymbol{x}(s)]}{T^{(0)}} = \frac{1}{2a^2}\int_0^{N_{\rm tot}} \mathrm{d}s\left(\frac{\mathrm{d}\boldsymbol{x}}{\mathrm{d}s}\right)^2 + \frac{w^{(0)}}{2}\int_0^{N_{\rm tot}}\mathrm{d}s\int_0^{N_{\rm tot}}\mathrm{d}s'\delta[\boldsymbol{x}(s)-\boldsymbol{x}(s')]\,, \tag{2.1}$$

where $a$ is the monomer size and $T^{(0)}$ is the temperature in the state of preparation (here and in the following we take the Boltzmann constant to be unity).

The statistical weight of a particular configuration of the chain $\{\boldsymbol{x}(s)\}$ is given by the canonical distribution function

$$\begin{aligned}\mathscr{P}_{\rm liq}[\boldsymbol{x}(s)] &= Z_{\rm liq}^{-1}\exp(-\mathscr{H}^{(0)}[\boldsymbol{x}(s)]/T^{(0)})\,,\\ Z_{\rm liq} &= \int \mathrm{D}\boldsymbol{x}(s)\exp(-\mathscr{H}^{(0)}[\boldsymbol{x}(s)]/T^{(0)})\,.\end{aligned} \tag{2.2}$$

Here $\int \mathrm{D}\boldsymbol{x}(s)$ implies functional integration over all the configurations of the chain and $Z_{\rm liq}$ is the partition function of the polymer (the subscript liq refers to the liquid-like state of the polymer, prior to the introduction of cross-links).

### 2.2. Instantaneous cross-linking and cross-link saturation threshold

In order to elucidate the physics of the process of cross-linking in the above model (to the best of our knowledge, this point was never discussed before), let us consider an instantaneous configuration of a *constrained* polymer in a good solvent (with average monomer density $\rho^{(0)}$) in which there are exactly $K$ binary contacts between monomers (these contacts form and disappear due to thermal fluctuations). During a contact event, two monomers share a contact volume $v$ (in the mean field approximation, the definition of the contact volume coincides with the definition of the excluded volume parameter, $v = w^{(0)}$, which appears in the Edwards Hamiltonian, Eq. (2.1)). The partition function of the constrained polymer is given by

$$Z_{\rm liq}(K) = \int \mathrm{D}\boldsymbol{x}(s)\exp(-\mathscr{H}^{(0)}[\boldsymbol{x}(s)]/T^{(0)})\int \mathrm{d}\boldsymbol{S}_K \prod_{\{i,j\}} v\delta[\boldsymbol{x}(s_i)-\boldsymbol{x}(s_j)]\,, \tag{2.3}$$

where the product is taken over all the $K$ pairs of monomers $\{i,j\}$ which are in contact with each other. The integration over $\boldsymbol{S}_K$ goes over the contour positions of the $2K$ monomers which participate in the contacts

$$\int \mathrm{d}\boldsymbol{S}_K \equiv \frac{1}{2^K K!} \prod_{\{i,j\}} \int_0^{N_{\mathrm{tot}}} \mathrm{d}s_i \int_0^{N_{\mathrm{tot}}} \mathrm{d}s_j \tag{2.4}$$

and accounts for the fact that such contacts can occur with equal probability at any location along the chain contour. The normalization factor $K!$ arises because all contact pairs are indistinguishable and the factor $2^K$ accounts for the indistinguishability of the two monomers which form each contact.

We can now define the probability that the polymer has exactly $K$ contacts as

$$P(K) = Z_{\mathrm{liq}}(K) \Big/ \sum_{K=0}^{N_{\mathrm{tot}}/2} Z_{\mathrm{liq}}(K) \,. \tag{2.5}$$

The average number of contacts is given by

$$\bar{K} = \sum_{K=0}^{N_{\mathrm{tot}}/2} K P(K) \tag{2.6}$$

and can be easily estimated from mean-field arguments. Notice that since the excluded volume of a monomer is given by the second virial coefficient $w^{(0)}$, each monomer can be represented by an impenetrable sphere of volume $w^{(0)}$. The volume fraction occupied by such spheres is $w^{(0)}\rho^{(0)}$ and, therefore, the average number of binary contacts between the spheres is

$$\bar{K} \simeq \tfrac{1}{2} N_{\mathrm{tot}} w^{(0)} \rho^{(0)} = \tfrac{1}{2} V^{(0)} w^{(0)} (\rho^{(0)})^2 \,. \tag{2.7}$$

When a polymer is *instantaneously* cross-linked by irradiation or by other means, a fraction of all monomers which are at a distance of the order of $(w^{(0)})^{1/3}$ from each other (i.e., form a contact) become cross-linked (see Fig. 2.1). The number of such cross-linked monomers ($2N_c$) depends on the intensity of irradiation and determines the average number of monomers between neighboring cross-links, $\bar{N} = N_{\mathrm{tot}}/(2N_c)$. As long as the required density of cross-links $\rho^{(0)}/(2\bar{N})$ is smaller than the average density of monomer contacts $w^{(0)}(\rho^{(0)})^2/2$ in the polymer liquid (prior to irradiation), the former can be increased by increasing the intensity of irradiation. The saturation density of cross-links (or, equivalently, the minimal chain length between cross-links) is obtained by equating the two densities $(\rho^{(0)}/2\bar{N})^{\max} \simeq w^{(0)}(\rho^{(0)})^2/2$ and yields the *cross-link saturation threshold*

$$w^{(0)} \rho^{(0)} \bar{N}^{\min} = 1 \,. \tag{2.8}$$

We conclude that the physically meaningful range of parameters describing the initial state corresponds to $w^{(0)}\rho^{(0)}\bar{N} > 1$. This simple mean-field estimate should be revised for semi-dilute gels in good solvents where strong thermal fluctuations on length scales smaller than the "blob" size should be taken into account (by scaling methods [3]). We will show in the section dealing with such gels that the maximal attainable density of cross-links corresponds to a situation in which there is one cross-link per blob and that the cross-link saturation threshold condition becomes

$$(a^2 w^{(0)})^{3/5} \rho^{(0)} (\bar{N}^{\min})^{4/5} \simeq 1 \,. \tag{2.9}$$

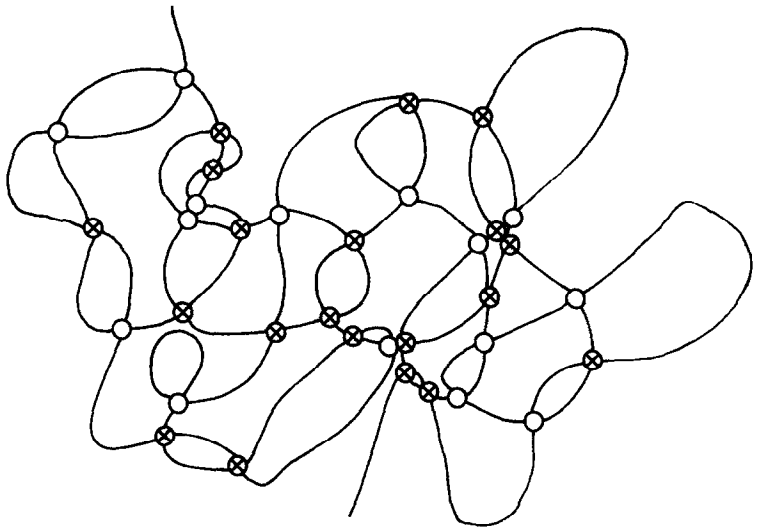

Fig. 2.1. Schematic drawing of a network, in the moment of cross-linking. Inter-monomer contacts (○) and cross-link points (×) are shown.

Note that the crossover between the mean field and the scaling regimes takes place at $\rho^{(0)} \simeq w^{(0)}/a^6$, which coincides with the usual limit of applicability of mean-field treatments of excluded volume effects [23].

What happens when the cross-link saturation threshold is approached (e.g., by increasing the intensity of irradiation)? We will show later in this work that the structure of the gel becomes increasingly inhomogeneous in the sense that the characteristic length scale of density fluctuations increases dramatically as the saturation threshold is approached. We would like to emphasize that although the existence of the saturation threshold has only been demonstrated here for instantaneous cross-linking of long chain polymers and therefore may be considered as an artifact of the present model, similar phenomena were observed in computer simulations where other methods of cross-linking were used [24].

### 2.3. *Edwards formulation*

Consider a network containing $N_c$ cross-links which has been prepared by instantaneous cross-linking, below the saturation threshold. Since at each cross-link point a chemical bond is formed between two monomers of the chain (the functionality of cross-links is 4), the resulting $N_c$ cross-links are characterized by the set of monomers $\{i, j\}$ with corresponding positions $\{s_i, s_j\}$ on the chain contour. The set $\boldsymbol{S} \equiv \{s_i, s_j\}$ uniquely defines the structure (topology) of the network. The probability distribution which describes the gel under conditions of preparation is given by that of a polymer in a solvent, Eq. (2.2), supplemented by the constraint of a given configuration $\boldsymbol{S}$ of $N_c$ monomer contacts,

$$\mathscr{P}^{(0)}[\boldsymbol{x}(s), \boldsymbol{S}] = [Z^{(0)}(\boldsymbol{S})]^{-1} \exp(-\mathscr{H}^{(0)}[\boldsymbol{x}(s)]/T^{(0)}) \times \prod_{\{i,j\}} \delta[\boldsymbol{x}(s_i) - \boldsymbol{x}(s_j)] , \tag{2.10}$$

where the partition function of the gel in the state of preparation is defined by the normalization condition $\int \mathrm{D}\boldsymbol{x}(s)\mathscr{P}^{(0)}[\boldsymbol{x}(s), \boldsymbol{S}] = 1$ (the integration goes over all the configurations in the volume $V^{(0)}$ occupied by the gel in the state of preparation):

$$Z^{(0)}(\boldsymbol{S}) = \int \mathrm{D}\boldsymbol{x}(s) \exp(-\mathscr{H}^{(0)}[\boldsymbol{x}(s)]/T^{(0)}) \prod_{\{i,j\}} \delta[\boldsymbol{x}(s_i) - \boldsymbol{x}(s_j)] \tag{2.11}$$

The above distribution function gives the complete statistical mechanical description of the gel in the state of preparation, including its response to small perturbations (linear response). However, unlike usual solids, polymer networks display linear elastic response to stretching and swelling well into the large deformation regime, which cannot be described by $Z^{(0)}$. The partition function $Z(\boldsymbol{S})$ of an arbitrarily deformed gel differs from that of the undeformed one in the following respects: first, the swelling modifies the effective second virial coefficient, i.e., $w^{(0)}$ is replaced by $w$ in the Edwards Hamiltonian and in the subsequent equations. Second, the deformation changes the volume ($V^{(0)}$) occupied by the network and the integration over the polymer coordinates extends over the new volume $V$. Third, one has to introduce the forces which act on the surface of the gel and produce the stretching. The effect of these forces will be represented by introducing the appropriate *deformation ratios* $\{\lambda_\alpha\}$ along the principal axes of deformation. Furthermore, in general, we have to allow for the possibility that the temperature in the final state, $T$, differs from that in the state of preparation $T^{(0)}$ (see Fig. 2.2).

Since the calculation of the partition function for a given realization of the network structure $\boldsymbol{S}$ is prohibitively difficult, we proceed to simplify the problem by the use of the *self-averaging* property of the free energy of a macroscopic system. This property follows from the additivity of the free energy. Imagine that we divide the entire sample into a large number of small but still macroscopic domains, each of which has its own unique structure (Fig. 2.3). In the limit of an infinitely large number of such domains, the probability $\mathscr{P}(\boldsymbol{S})$ of appearance of a domain with a given structure $\boldsymbol{S}$ is determined by the process of cross-linking. Since, in the case of instantaneous cross-linking of a polymer in a solvent, the initial state of the gel prior to deformation is a particular realization of the equilibrium state of this polymer and since the solution is ergodic, the probability is given by the Gibbs distribution function

$$\mathscr{P}(\boldsymbol{S}) = Z^{(0)}(\boldsymbol{S}) \Big/ \int \mathrm{d}\boldsymbol{S}' Z^{(0)}(\boldsymbol{S}') \,. \tag{2.12}$$

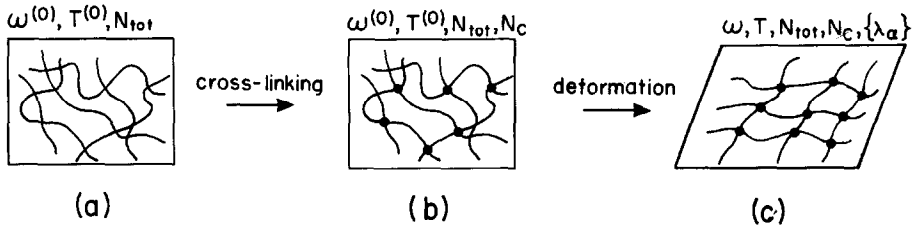


Fig. 2.2. (a) Polymer solution prior to cross-linking (characterized by parameters $w^{(0)}$, $T^{(0)}$, $N_{\mathrm{tot}}$), (b) initial undeformed gel (parameters $w^{(0)}$, $T^{(0)}$, $N_{\mathrm{tot}}$, $N_{\mathrm{c}}$, $\{\lambda_\alpha\}$).

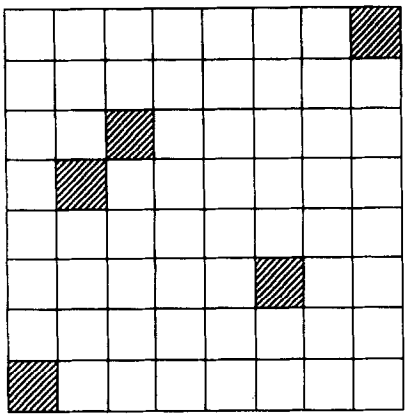

Fig. 2.3. Partitioning of the gel into macroscopic regions characterized by different network structures. Domains with a particular structure $S$ are shaded.

The total free energy $\mathscr{F}(\boldsymbol{S})$ of a macroscopic network with a given structure $\boldsymbol{S}$, can be written as the sum of free energies of such domains. This sum can be replaced by the sum over all possible realizations of network structures. The contribution of each of these structures is weighted by the distribution function (2.12), yielding:

$$\mathscr{F}(N_{\mathrm{tot}}, N_{\mathrm{c}}) = -T\int \mathrm{d}\boldsymbol{S}\,\mathscr{P}(\boldsymbol{S})\ln Z(\boldsymbol{S})\,. \tag{2.13}$$

In writing down this formula we took the thermodynamic limit in which the free energy is independent of the particular choice of network structure and depends only on thermodynamic properties such as the total numbers $N_{\mathrm{tot}}$ and $N_{\mathrm{c}}$ of monomers and of cross-links, on volume, temperature and quality of solvent.

*2.3.1. Replica formalism*

The averaging in (2.13) can be performed using the *replica* method which is based on the identity [1]

$$\ln Z = \lim_{m\to 0}(Z^m - 1)/m\,. \tag{2.14}$$

The trick consists of introducing the "replica" free energy $\mathscr{F}_m(N_{\mathrm{tot}}, N_{\mathrm{c}})$ of a network with $N_{\mathrm{tot}}$ monomers and $N_{\mathrm{c}}$ cross-links

$$\exp[-\mathscr{F}_m(N_{\mathrm{tot}}, N_{\mathrm{c}})/T] \equiv \int \mathrm{d}\boldsymbol{S}\,Z^{(0)}(\boldsymbol{S})Z^m(\boldsymbol{S})\,. \tag{2.15}$$

At this stage, $\mathscr{F}_m$ has no obvious physical meaning and is introduced only to avoid the cumbersome averaging of the logarithm in (2.13). It is easy to show that the physical free energy $\mathscr{F}(N_{\mathrm{tot}}, N_{\mathrm{c}})$ (2.13) is related to the replica free energy by the expression

$$\mathscr{F}(N_{\mathrm{tot}}, N_{\mathrm{c}}) = \left.\frac{\mathrm{d}\mathscr{F}_m(N_{\mathrm{tot}}, N_{\mathrm{c}})}{\mathrm{d}m}\right|_{m=0}. \tag{2.16}$$

Since we are only interested in the $m \to 0$ limit, the function $\mathscr{F}_m$ can be expanded in a power series in $m$. Eq. (2.16) implies that in the calculation of $\mathscr{F}_m$ one should retain terms only up to first order in $m$.

Some intuition about the physical meaning of the replica free energy can be gained by considering the limit $m \to 0$ in Eq. (2.15). This yields

$$\exp[-\mathscr{F}_0(N_{\text{tot}}, N_c)/T] = \int d\boldsymbol{S} Z^{(0)}(\boldsymbol{S}) \equiv \boldsymbol{Z}_{\text{liq}}(N_c) \tag{2.17}$$

and we conclude that in this limit the replica free energy reduces to the free energy $-T \ln \boldsymbol{Z}_{\text{liq}}(N_c)$ of the constrained partition function of a polymer in a good solvent, with a given number ($N_c$) of binary contacts between monomers.

Going back to Eq. (2.15) we note that, for integer $m$, the product $Z^{(0)}(\boldsymbol{S})Z^m(\boldsymbol{S})$ can be interpreted as the partition function of a replica system which consists of $1 + m$ non-interacting systems (replicas). The 0th replica represents the initial non-deformed gel (with partition function $Z^{(0)}(\boldsymbol{S})$ corresponding to a particular realization $\boldsymbol{S}$ of network structure) and the other $m$ identical replicas represent the final deformed gel (each with partition function $Z(\boldsymbol{S})$). The Hamiltonian and the partition function of the 0th replica are given by (2.1) and (2.11), respectively, where for clarity of notation we label the monomer coordinates by the superscript (0). Similarly, the Hamiltonian of the $k$th replica ($1 \le k \le m$) is

$$\frac{\mathscr{H}^{(k)}[\boldsymbol{x}^{(k)}(s)]}{T} = \frac{1}{2a^2}\int_0^{N_{\text{tot}}} ds \left(\frac{d\boldsymbol{x}^{(k)}}{ds}\right)^2 + \frac{w}{2}\int_0^{N_{\text{tot}}} ds \int_0^{N_{\text{tot}}} ds' \delta[\boldsymbol{x}^{(k)}(s) - \boldsymbol{x}^{(k)}(s')] , \tag{2.18}$$

where we have used the fact that the quality of solvent and the temperature are identical in all the replicas ($k \ge 1$) corresponding to the final state of the gel, i.e., $w^{(k)} = w$ and $T^{(k)} = T$, respectively. The partition function of the $k$th replica is

$$Z^{(k)}(\boldsymbol{S}) = \int D\boldsymbol{x}^{(k)}(s) \exp(-\mathscr{H}^{(k)}[\boldsymbol{x}^{(k)}(s)]/T) \prod_{\{i,j\}} \delta[\boldsymbol{x}^{(k)}(s_i) - \boldsymbol{x}^{(k)}(s_j)] , \tag{2.19}$$

where the integration goes over all chain configurations in the volume $V$ occupied by the deformed gel.

Substituting expressions (2.11) and (2.19) into Eq. (2.15) yields

$$\exp[-\mathscr{F}_m(N_{\text{tot}}, N_c)/T] = \int d\boldsymbol{S} \prod_{k=0}^{m} \int D\boldsymbol{x}^{(k)}(s) \times \exp(-\mathscr{H}^{(k)}[\boldsymbol{x}^{(k)}(s)]/T) \prod_{\{i,j\}} \delta[\boldsymbol{x}^{(k)}(s_i) - \boldsymbol{x}^{(k)}(s_j)] . \tag{2.20}$$

Since the replica Hamiltonians in the above equation do not contain the cross-link contour coordinates $\boldsymbol{S}$, we can pull the integrals over these coordinates in front of the product of the

$\delta$-functions and perform $N_c$ integrations over the cross-linked pairs of monomers $\{i,j\}$. Each of these integrations produces a factor

$$B[\{\boldsymbol{x}^{(k)}\}] = \int_0^{N_{tot}} ds_i \int_0^{N_{tot}} ds_j \prod_{k=0}^{m} \delta[\boldsymbol{x}^{(k)}(s_i) - \boldsymbol{x}^{(k)}(s_j)] \tag{2.21}$$

and, therefore, the integration over $\boldsymbol{S}$ introduces the factor $(B[\{\boldsymbol{x}^{(k)}\}])^{N_c}$ into the integrand in (2.20).

*2.3.2. Grand canonical representation*

Instead of working directly with the constraints introduced by substituting the $\delta$-functions (Eq. (2.21)) into Eq. (2.20), we can replace them by effective interactions, using the following identity:

$$B^{N_c} = \frac{N_c!}{2\pi i} \oint \frac{dz_c}{z_c^{N_c+1}} e^{z_c B} . \tag{2.22}$$

This relation is analogous to the usual thermodynamic transformation from the canonical to the grand canonical ensemble which suggests that $z_c$ can be interpreted as the *fugacity* which defines the average number of cross-links in the latter ensemble. Apart from mathematical convenience, the use of the grand canonical ensemble reflects the physical observation that only the average number of cross-links can be fixed by any physical or chemical method of gel preparation.

In order to complete the transformation to the grand canonical ensemble we introduce the chemical potential $\mu$ of monomer units (it differs from the usual thermodynamic definition of the chemical potential by a factor of $T$) through the identity

$$\delta(N_{tot} - M) = \frac{1}{2\pi i} \oint d\mu e^{\mu(N_{tot} - M)} . \tag{2.23}$$

As a result the replica partition function (2.15) takes the form

$$\exp[-\mathscr{F}_m(N_{tot}, N_c)/T] = \left[\frac{1}{2\pi i} \oint d\mu e^{\mu N_{tot}}\right]\left[\frac{1}{2\pi i} \oint \frac{dz_c}{z_c^{N_c+1}}\right] \Xi_m(\mu, z_c) , \tag{2.24}$$

where $\Xi_m$ is the grand canonical partition function:

$$\Xi_m(\mu, z_c) = \int_0^{\infty} dM e^{-\mu M} \int D\hat{\boldsymbol{x}}(s)$$
$$\exp\left\{ -\frac{1}{2a^2} \int_0^M ds \left(\frac{d\hat{\boldsymbol{x}}}{ds}\right)^2 + \frac{z_c}{2} \int_0^M ds \int_0^M ds' \delta[\hat{\boldsymbol{x}}(s) - \hat{\boldsymbol{x}}(s')] \right.$$
$$\left. - \sum_{k=0}^{m} \frac{w^{(k)}}{2} \int_0^M ds \int_0^M ds' \delta[\boldsymbol{x}^{(k)}(s) - \boldsymbol{x}^{(k)}(s')] \right\} . \tag{2.25}$$

In writing (2.25) we introduced the $3(1 + m)$-dimensional vector $\hat{\boldsymbol{x}}$ in the space of the replicas (replica space), with components $x_\alpha^{(k)}$ ($\alpha = x, y, z$; $k = 0, \ldots, m$) and used the identities

$$\left(\frac{d\hat{\boldsymbol{x}}}{ds}\right)^2 = \sum_{k=0}^{m} \left(\frac{d\boldsymbol{x}^{(k)}}{ds}\right)^2 \tag{2.26}$$

and

$$\delta[\hat{\boldsymbol{x}}(s) - \hat{\boldsymbol{x}}(s')] = \prod_{k=0}^{m} \delta[\boldsymbol{x}^{(k)}(s) - \boldsymbol{x}^{(k)}(s')] \,. \tag{2.27}$$

Notice that the expression inside the curly brackets in the exponent in Eq. (2.25) can be interpreted as (minus) the effective Hamiltonian of a polymer chain in an abstract replica space. Network constraints due to the cross-links (which were present in the original physical space) are replaced, in this replica space, by an effective attractive interaction with strength proportional to $z_c$. Unlike the usual excluded volume interaction which is expressed as the sum of $\delta$-functions with coefficients $w^{(k)}$ and, therefore, is *diagonal* in the replicas, the effective attractive interaction due to the cross-links appears as a product of $\delta$-functions (Eq. (2.27)) which *couples* the different replicas. This statement can be further clarified by the observation that a total Hamiltonian describes a set of non-interacting systems, only if it can be represented as the sum of the Hamiltonians of the constituents.

On a more physical level, the difference between the effects of excluded-volume and cross-links stems from the different ways in which they enter the replica formulation of the statistical mechanics of polymer networks. Thermal fluctuations take place *independently* in the different replicas and, therefore, different monomer pairs interact via excluded volume in different replicas. On the other hand, all the replicas have, by definition, the *same* network structure (they all correspond to the same realization of this structure) and thus, the same monomer pairs interact through attractive interactions (which account for the presence of cross-links), in all the replicas.

The cross-link-induced coupling between the replicas has a dramatic effect on the typical conformation of the polymer in the abstract replica space. While the attractions due to the cross-links can be stabilized by excluded volume repulsions *in each* of the replicas, there is nothing to balance the attractions *between different* replicas, with the consequence that (as will be shown in detail in the following) the true ground state of the replica system corresponds not to a state of uniform density in replica space but, rather, to a *collapsed* state of the polymer in this space!

In the thermodynamic limit, $N_{tot}, N_c \to \infty$, the integrals over $\mu$ and $z_c$ in (2.24) can be evaluated by the method of steepest descent, with the result

$$\mathscr{F}_m(N_{tot}, N_c)/T = -\ln \Xi_m(\mu, z_c) - N_{tot}\mu + N_c \ln z_c \,, \tag{2.28}$$

where the fugacity $z_c$ of cross-links and the chemical potential $\mu$ of monomers can be obtained by minimizing the right-hand side of (2.28)

$$N_{tot} = -\partial \ln \Xi_m(\mu, z_c)/\partial \mu \,, \qquad N_c = \partial \ln \Xi_m(\mu, z_c)/\partial \ln z_c \,. \tag{2.29}$$

Substituting Eq. (2.28) into Eq. (2.16), we relate the physical free energy to the replica partition function of the grand canonical ensemble:

$$\begin{aligned}\mathscr{F}(N_{tot}, N_c) = &- T \left.\frac{\partial \ln \Xi_m(\mu, z_c)}{\partial m}\right|_{m=0} - T \left.\frac{\partial \ln \Xi_m(\mu, z_c)}{\partial \mu}\right|_{m=0} \left.\frac{\partial \mu}{\partial m}\right|_{m=0} \\ &- T \left.\frac{\partial \ln \Xi_m(\mu, z_c)}{\partial \ln z_c}\right|_{m=0} \left.\frac{\partial \ln z_c}{\partial m}\right|_{m=0} - N_{tot} \left.\frac{\partial \mu}{\partial m}\right|_{m=0} + N_c \left.\frac{\partial \ln z_c}{\partial m}\right|_{m=0} \\ = &- T \left.\frac{\partial \ln \Xi_m(\mu, z_c)}{\partial m}\right|_{m=0} ,\end{aligned} \tag{2.30}$$

where the last equality is obtained using (2.29). The monomer chemical potential and the fugacity of cross-links which parametrize the grand canonical partition function in Eq. (2.30), should be expressed in terms of the parameters $N_{tot}$ and $N_c$ using Eq. (2.29), in the limit $m = 0$.

In order to calculate the free energy, Eq. (2.30), one has to evaluate functional integrals over the set of trajectories $\{\hat{x}(s)\}$ in replica space, in Eq. (2.25). Direct calculation of such integrals is prohibitively difficult and, following the usual approach in polymer physics [23], we will transform the problem into a more tractable one by going over to collective coordinates (field theory).

### 2.4. Field theory

Inspection of the grand canonical partition function reveals the source of the mathematical difficulties which arise in theories of interacting string-like objects. While the elastic term (Eqs. (2.25) and (2.26)) is local in this representation (i.e., depends only on a single coordinate along the chain, $s$), the interaction terms in Eq. (2.25) are non-local (depend on two coordinates, $s$ and $s'$). An attempt to confront these difficulties head-on was made by Deam and Edwards [1], who used a variational method to calculate the thermodynamic free energy of an instantaneously cross-linked polymer gel. Such an approach is known to give good results for the ground state energy (we will see that the variational bound on the thermodynamic free energy obtained by the above authors coincides with our result) but is difficult to apply to the calculation of density fluctuations for which one has to have complete information about the ground state. In this work we take a different path which was proposed by Edwards and Vilgis [25] (for modelling end-linked networks, without excluded volume), and which is based on the realization that while the interactions are non-local along the chain contour, due to the presence of the $\delta$-functions they are local in real (and in replica) space. Therefore, it is advantageous to transform to a description in terms of fields over spatial coordinates (i.e., to collective coordinates), in which the local character of the interaction terms is made explicit [23]. We now proceed to construct the field theoretical representation of the grand canonical partition function.

#### 2.4.1. Density functional

We start with the definition of the microscopic (i.e., non-averaged) monomer density in replica space

$$\rho(\hat{x}) \equiv \int ds \delta[\hat{x} - \hat{x}(s)] = \int ds \prod_{k=0}^{m} \delta[x^{(k)} - x^{(k)}(s)] . \tag{2.31}$$

The thermal average of this expression, $\langle \rho(\hat{x}) \rangle$, is identical to the Edwards–Anderson-order parameter in the theory of spin glasses [9] and is a measure of the correlations between the replicas. It vanishes (in the thermodynamic limit) in the "liquid" phase where there is no correlation between the monomer positions in different replicas and has a finite value in the "solid" phase in which the conformations of the network in the different replicas are strongly correlated due to its fixed structure [26].

Knowledge of this abstract density can be used to calculate the monomer density in the $k$th replica by integrating over the coordinates of all the other replicas

$$\rho^{(k)}(\boldsymbol{x}^{(k)}) \equiv \prod_{l \neq k} \int \mathrm{d}\boldsymbol{x}^{(l)} \rho(\hat{\boldsymbol{x}}) = \int \mathrm{d}s \delta[\boldsymbol{x}^{(k)} - \boldsymbol{x}^{(k)}(s)] \,, \tag{2.32}$$

which can also be represented in the form

$$\rho^{(k)}(\boldsymbol{x}) = \int \mathrm{d}\hat{\boldsymbol{x}} \rho(\hat{\boldsymbol{x}}) \delta[\boldsymbol{x} - \boldsymbol{x}^{(k)}] \,. \tag{2.33}$$

We now return to the expression for the grand canonical partition function, Eq. (2.25). Contour integration over a non-local (in the contour coordinates $s$) $\delta$-function can be replaced by a spatial integral over a local (in space) function of the density, as follows. We introduce the identity

$$\int \mathrm{d}s \int \mathrm{d}s' \delta[\hat{\boldsymbol{x}}(s) - \hat{\boldsymbol{x}}(s')] \equiv \int \mathrm{d}s \int \mathrm{d}s' \int \mathrm{d}\hat{\boldsymbol{x}} \delta[\hat{\boldsymbol{x}} - \hat{\boldsymbol{x}}(s)] \delta[\hat{\boldsymbol{x}} - \hat{\boldsymbol{x}}(s')] = \int \mathrm{d}\hat{\boldsymbol{x}} \rho^2(\hat{\boldsymbol{x}}) \,, \tag{2.34}$$

where the second equality is obtained by changing the order of the integrals and using the definition of $\rho(\hat{\boldsymbol{x}})$, Eq. (2.31). Similarly, we derive an analogous relation for the $k$th replica:

$$\int \mathrm{d}s \int \mathrm{d}s' \delta[\boldsymbol{x}^{(k)}(s) - \boldsymbol{x}^{(k)}(s')] \equiv \int \mathrm{d}\boldsymbol{x}^{(k)} [\rho^{(k)}(\boldsymbol{x}^{(k)})]^2 \,. \tag{2.35}$$

The next step is to replace the integration over the monomer coordinates $\{\hat{\boldsymbol{x}}(s)\}$ by the integration over the collective coordinates $\{\rho(\hat{\boldsymbol{x}})\}$. This is done by inserting the representation of unity

$$1 \equiv \int \mathrm{D}\rho(\boldsymbol{x}) \delta\left( \rho(\hat{\boldsymbol{x}}) - \int_0^M \mathrm{d}s \delta[\hat{\boldsymbol{x}} - \hat{\boldsymbol{x}}(s)] \right) \tag{2.36}$$

in front of the exponential in (2.25) and moving the integration over $\rho(\hat{\boldsymbol{x}})$ to the leftmost end of the expression on the right-hand side of this equation. Using identities (2.34) and (2.35), the grand canonical partition function can be represented as a functional integral over the replica density field:

$$\Xi_m(\mu, z_c) = \int \mathrm{D}\rho(\hat{\boldsymbol{x}}) \exp\left\{ S(\mu, [\rho(\hat{\boldsymbol{x}})]) + \frac{z_c}{2} \int \mathrm{d}\hat{\boldsymbol{x}} \rho^2(\hat{\boldsymbol{x}}) - \sum_{k=0}^{m} \frac{w^{(k)}}{2} \int \mathrm{d}\boldsymbol{x}^{(k)} [\rho^{(k)}(\boldsymbol{x}^{(k)})]^2 \right\} . \tag{2.37}$$

Here, the term proportional to $z_c$ accounts for the contribution of cross-links, the terms proportional to $w^{(k)}$ represent the excluded volume interactions, and $S(\mu, [\rho(\hat{\boldsymbol{x}})])$ is the replica analog of the elastic entropy of the polymer chain, with the given monomer density $\rho(\hat{\boldsymbol{x}})$ in replica space:

$$\begin{aligned} \exp\{S(\mu, [\rho(\hat{\boldsymbol{x}})])\} = & \int_0^\infty \mathrm{d}M \mathrm{e}^{-\mu M} \int \mathrm{D}\hat{\boldsymbol{x}}(s) \\ & \times \delta\left( \rho(\hat{\boldsymbol{x}}) - \int_0^M \mathrm{d}s \delta[\hat{\boldsymbol{x}} - \hat{\boldsymbol{x}}(s)] \right) \exp\left\{ -\frac{1}{2a^2} \int_0^M \mathrm{d}s \left( \frac{\mathrm{d}\hat{\boldsymbol{x}}}{\mathrm{d}s} \right)^2 \right\} \end{aligned} \tag{2.38}$$

*2.4.2. Elastic entropy*

We now derive a field theoretical representation of $\exp\{S\}$. Introducing the exponential representation of the $\delta$-function

$$\delta\left(\rho(\hat{x}) - \int_0^M \mathrm{d}s\,\delta[\hat{x} - \hat{x}(s)]\right) \equiv \int \mathrm{D}h(\hat{x}) \exp\left[\mathrm{i}\int \mathrm{d}\hat{x}\,h(\hat{x})\rho(\hat{x}) - \mathrm{i}\int_0^M \mathrm{d}s\,h(\hat{x}(s))\right] \tag{2.39}$$

and moving the integration over $h(\hat{x})$ to the leftmost end of the term on the right-hand side of Eq. (2.38), gives

$$\exp\{S(\mu, [\rho(\hat{x})])\} = \int \mathrm{D}h(\hat{x}) \exp\left[\mathrm{i}\int \mathrm{d}\hat{x}\,h(\hat{x})\rho(\hat{x})\right] \int \mathrm{d}\hat{x}_1 \int \mathrm{d}\hat{x}_2\, \hat{G}\{\hat{x}_1, \hat{x}_2, [\mathrm{i}h(\hat{x})]\}\,, \tag{2.40}$$

where

$$\hat{G}\{\hat{x}_1, \hat{x}_2, [\mathrm{i}h(\hat{x})]\} = \int_0^\infty \mathrm{d}M \mathrm{e}^{-\mu M} \int_{\hat{x}_1}^{\hat{x}_2} \mathrm{D}\hat{x}(s) \exp\left\{-\int_0^M \mathrm{d}s \left[\frac{1}{2a^2}\left(\frac{\mathrm{d}\hat{x}}{\mathrm{d}s}\right)^2 + \mathrm{i}h(\hat{x}(s))\right]\right\} \tag{2.41}$$

can be interpreted as the grand canonical partition function of an ideal Gaussian chain with ends fixed at points $\hat{x}_1$ and $\hat{x}_2$, in an external field $\mathrm{i}h(\hat{x})$ (in a $3(1 + m)$-dimensional replica space). In order to avoid explicitly handling the constraints associated with the connectivity of the chain, we transform the Gaussian chain problem into a field theory [27] (Appendix A). Using the replica space generalization ($x \to \hat{x}$) of the usual trick of relating the polymer problem to the $n = 0$ limit of the $n$-vector model (Appendix A), $\hat{G}$ is represented as a functional integral over an $n$-component vector field $\boldsymbol{\varphi}(\hat{x})$, with components $\varphi_i(\hat{x})$ ($i = 1, \ldots, n$). Analytic continuation to the limit $n \to 0$ yields

$$\hat{G}\{\hat{x}_1, \hat{x}_2, [\mathrm{i}h(\hat{x})]\} = \int \mathrm{D}\boldsymbol{\varphi}\, \varphi_1(\hat{x}_1)\varphi_1(\hat{x}_2) \exp\{-H_0[\mathrm{i}h(\hat{x}), \boldsymbol{\varphi}(\hat{x})]\}\,, \tag{2.42}$$

where the effective (dimensionless) Hamiltonian $H_0$ has the form

$$H_0[\mathrm{i}h(\hat{x}), \boldsymbol{\varphi}(\hat{x})] = \int \mathrm{d}\hat{x}\left[\tfrac{1}{2}(\mu + \mathrm{i}h(\hat{x}))\boldsymbol{\varphi}^2(\hat{x}) + \frac{a^2}{2}(\hat{\nabla}\boldsymbol{\varphi}(\hat{x}))^2\right]. \tag{2.43}$$

Here $\hat{\nabla}$ is the $3(1 + m)$-dimensional gradient operator with respect to replica space coordinates. Notice that we now have three different spaces and, in order to avoid confusion, we use different designations for vectors embedded in them: $\boldsymbol{x}$ is the usual 3-dimensional vector with components $x_\alpha$ ($\alpha = x, y, z$), the vector $\hat{x}$ is defined in $3(1 + m)$-dimensional replica space and has components $x_\alpha^{(k)}$ ($\alpha = x, y, z$; $k = 0, \ldots, m$); and the $n$-dimensional vector $\boldsymbol{\varphi}$ has components $\varphi_i$ ($i = 1, \ldots, n$).

We now substitute Eqs. (2.42) and (2.43) into (2.40) and integrate over the field $h$, using the identity

$$\int \mathrm{D}h(\hat{x}) \exp\left[\mathrm{i}\int \mathrm{d}\hat{x}\,h(\hat{x})(\rho(\hat{x}) - \boldsymbol{\varphi}^2(\hat{x})/2)\right] \equiv \delta(\rho(\hat{x}) - \boldsymbol{\varphi}^2(\hat{x})/2)\,. \tag{2.44}$$

The resulting field theoretical representation of the elastic entropy $S$, is

$$\exp\{S(\mu,[\rho(\hat{x})])\} = \int D\varphi(\hat{x})\left[\int d\hat{x}\varphi_1(\hat{x})\right]^2 \delta(\rho(\hat{x}) - \varphi^2(\hat{x})/2) \times \exp\left\{-\int d\hat{x}\left[\tfrac{1}{2}\mu\varphi^2(\hat{x}) + \frac{a^2}{2}(\hat{\nabla}\varphi(\hat{x}))^2\right]\right\}. \tag{2.45}$$

Note that, as a byproduct, we obtain the important relation between the vector field $\varphi$ and the monomer density in the replica space:

$$\rho(\hat{x}) = \varphi^2(\hat{x})/2 \tag{2.46}$$

This formula is an exact relation between the two fluctuating fields $\varphi$ and $\rho$. It is the generalization of a well-known relation in the $n = 0$, $\varphi^4$ formulation of the excluded volume problem [3] (which relates the *average* of the square of the abstract field $\varphi$ to the physically observable mean density $\langle\rho\rangle$).

*2.4.3. Field Hamiltonian*

Substituting Eq. (2.45) into Eq. (2.37) and carrying out the trivial (due to the $\delta$-function) integration over the field $\rho(\hat{x})$, we obtain an explicit representation for the grand canonical partition function of a Gaussian network, in terms of the field $\varphi(\hat{x})$:

$$\Xi_m(\mu, z_c) = \int D\varphi(\hat{x})\left[\int d\hat{x}\varphi_1(\hat{x})\right]^2 \exp\{-H[\varphi(\hat{x})]\}. \tag{2.47}$$

In evaluating this expression one has to perform the functional integration over the field $\varphi$ and then make the analytic continuation from integer $n$ to $n = 0$ (where $n$ is the number of components of this vector field). The Hamiltonian $H$ is given by

$$H[\varphi] = \int d\hat{x}\left[\tfrac{1}{2}\mu\varphi^2(\hat{x}) + \frac{a^2}{2}(\hat{\nabla}\varphi(\hat{x}))^2 - \frac{z_c}{8}(\varphi^2(\hat{x}))^2\right] + \sum_{k=0}^{m}\frac{w^{(k)}}{2}\int dx^{(k)}\left[\prod_{l\neq k}\int dx^{(l)}\varphi^2(\hat{x})\right]^2. \tag{2.48}$$

This effective Hamiltonian is a straightforward extension of the $\varphi^4$ zero-component field theory of a polymer chain with excluded volume to the $3(1 + m)$-dimensional replica space. It has a number of discrete and continuous symmetries:

1. Arbitrary rotations in the abstract space of the $n$-vector model.
2. Permutation of the replicas of the final state.
3. Arbitrary rotations in the space of *each* of the replicas. Due to the presence of the excluded volume terms, the Hamiltonian is not invariant under arbitrary rotations in replica space which would, in general, mix the different replicas (the densities in each of the replicas, $\rho^{(k)}(x^{(k)})$, that enter the excluded volume interaction term in the Hamiltonian, are not invariant under rotations in replica space $\{\hat{x}\}$ which mix the different replicas).
4. Translation by an arbitrary constant vector in replica space.

The existence of the symmetry under translation in replica space suggests (wrongly!) that our field theory describes a polymer "liquid" in replica space, with cross-links replaced by effective attractions between monomers. Consider, for example, the single replica, $m = 0$, version of our model. In this case, $\prod_{l\neq 0}\int d\boldsymbol{x}^{(l)}$ is replaced by unity and the corresponding Hamiltonian (2.48) becomes

$$H[\varphi]|_{m=0} = \int d\boldsymbol{x}^{(0)}\left[\tfrac{1}{2}\mu\varphi^2(\boldsymbol{x}^{(0)}) + \frac{a^2}{2}(\nabla\varphi(\boldsymbol{x}^{(0)}))^2 + \frac{(w^{(0)} - z_c)}{8}(\varphi^2(\boldsymbol{x}^{(0)}))^2\right], \tag{2.49}$$

which is identical to the Hamiltonian of the $n \to 0$ model of a polymer chain in a solvent, without cross-links but with an excluded volume parameter $w^{(0)} - z_c$. Substitution of this Hamiltonian to Eq. (2.47) gives the grand canonical partition function of a constrained polymer with a second virial coefficient $w^{(0)} - z_c$, confined to a volume $V^{(0)}$. The reduction of the excluded volume parameter compared to its bare value $w^{(0)}$ reflects the fact that some of the inter-monomer contacts in any configuration of this polymer ($N_c$ of them, on the average), represent the cross-links and do not contribute to the excluded volume interaction energy.

Although the above conclusion is perfectly valid for the single-replica case, it misses the fact that our model contains not only the replica of the initial state but also $m$ replicas of the final state, and that the calculation has to be performed in the $3(1 + m)$-dimensional replica space *before* taking the limit $m \to 0$. Inspection of Eq. (2.37) shows that while excluded volume repulsions act only within the individual replicas (only the sum $\sum_{k=0}^{m} w^{(k)}[\rho^{(k)}(\boldsymbol{x})]^2$ appears in the exponent in Eq. (2.37)), cross-link-induced attractions ($z_c[\rho(\hat{\boldsymbol{x}})]^2$) introduce a coupling between all the replicas. The presence of this coupling reflects the fact that our model describes a *solid*.

## 3. Mean-field solution

### 3.1. The mean-field equation

We now proceed to calculate the functional integral (2.47). Due to the presence of the $\varphi^4$ terms, this integral is not Gaussian and cannot be calculated exactly. Instead, we resort to a mean-field estimate by the method of *steepest descent*, which is equivalent to finding the solution $\varphi_{mf}$ that minimizes the effective Hamiltonian (2.48). The condition that $\varphi_{mf}$ corresponds to an extremum of $H$ is

$$\left(\mu + \sum_{k=0}^{m} w^{(k)}\rho_{mf}^{(k)}(\boldsymbol{x}^{(k)}) - a^2\hat{\nabla}^2 - \frac{z_c}{2}\varphi_{mf}^2(\hat{\boldsymbol{x}})\right)\varphi_{mf}(\hat{\boldsymbol{x}}) = 0\,, \tag{3.1}$$

where, from Eqs. (2.31)–(2.33), the mean-field density of monomer units in the $k$th replica is

$$\rho_{mf}^{(k)}(\boldsymbol{x}^{(k)}) \equiv \prod_{l\neq k}\int d\boldsymbol{x}^{(l)}\rho_{mf}(\hat{\boldsymbol{x}})\,, \quad \text{where } \rho_{mf}(\hat{\boldsymbol{x}}) = \varphi_{mf}^2(\hat{\boldsymbol{x}})/2\,. \tag{3.2}$$

The thermodynamic parameters $\mu$ and $z_c$ which appear in (3.1) can be related to the physical parameters which characterize the gel in the state of preparation, i.e., the average monomer density

$\rho^{(0)} = N_{\rm tot}/V^{(0)}$ and the average number of monomers between cross-links which are nearest neighbors along the chain contour, $\bar{N} = N_{\rm tot}/(2N_{\rm c})$. The parameters $\mu$ and $z_{\rm c}$ should be calculated from Eq. (2.29), with the corresponding derivatives evaluated at $m = 0$. In the mean-field approximation, this equation can be replaced by

$$N_{\rm tot} = \left.\frac{\partial H[\varphi_{\rm mf}]}{\partial \mu}\right|_{m=0}, \quad N_{\rm c} = -\left.\frac{\partial H[\varphi_{\rm mf}]}{\partial \ln z_{\rm c}}\right|_{m=0}, \tag{3.3}$$

where the Hamiltonian $H$ (for $m = 0$) is defined in Eq. (2.49).

Since we are looking for a solution of Eq. (3.1) which describes the spatially homogeneous initial state of the gel (with density $\rho^{(0)}$), the mean-field solution is obtained by setting the expression in the brackets in this equation to zero. We obtain

$$\rho^{(0)} = \varphi_{\rm mf}^2/2 = \mu/(z_{\rm c} - w^{(0)}) . \tag{3.4}$$

Substituting this solution into Eq. (2.49) and using Eqs. (3.3) yields $N_{\rm tot} = \rho^{(0)}V^{(0)}$ and $N_{\rm c} = z_{\rm c}V^{(0)}(\rho^{(0)})^2/2$. Using these relations and the definition of $\bar{N}$, we obtain the mean-field expressions for $\mu$ and $z_{\rm c}$ in terms of $\rho^{(0)}$ and $\bar{N}$

$$\mu = 1/\bar{N} - w^{(0)}\rho^{(0)}, \qquad z_{\rm c} = 1/(\rho^{(0)}\bar{N}) . \tag{3.5}$$

We would like to emphasize that in order to calculate the free energy, Eq. (2.30), it is not enough to obtain the solution of the mean-field equation (3.1) and that there are two further conditions which must be satisfied by this mean-field solution.

1. We have to verify that the solution *minimizes* the effective Hamiltonian. Notice that since Eq. (3.1) was obtained from the condition $\delta H/\delta\varphi = 0$, its solutions correspond to the *extrema*, but not necessarily to the minima of $H$. A solution of this equation minimizes $H$ if the second derivative operator

$$K_{ij}(\hat{x}, \hat{x}') \equiv \left.\frac{\delta^2 H}{\delta\varphi_i(\hat{x})\delta\varphi_j(\hat{x}')}\right|_{\varphi=\varphi_{\rm mf}}, \tag{3.6}$$

whose eigenvalues $\{\Lambda\}$ give the "energies" of small (but otherwise arbitrary) fluctuations ($\{\delta\varphi\cdot\}$) about the mean-field ground state, has only non-negative eigenvalues. The spectrum of eigenvalues can be found from the secular equation

$$\sum_{j=1}^{n}\int d\hat{x}' K_{ij}(\hat{x}, \hat{x}')\psi_j(\hat{x}') = \Lambda\psi_i(\hat{x}) , \tag{3.7}$$

where $\psi$ are the eigenfunctions corresponding to these eigenvalues (the indices $i$ and $j$ enumerate the components of the $n$-vector field). A complete analysis of this eigenvalue problem will be presented later in this work (Section 3.5 and Appendix C).

2. We have to show that our solution corresponds to the true ground state of the Hamiltonian since, in the thermodynamic limit, the steepest descent estimate of the replica partition function is dominated by the lowest minimum of $H$ (ground state dominance). This problem will be considered in Section 3.6.

### 3.2. Homogeneous solution

We now proceed to look for a solution of Eq. (3.1) for arbitrary integer $m$. In principle, this complicated non-linear equation may admit many solutions which would correspond to different extrema of $H$. One should find all the solutions, compare their "energy" (by substituting the corresponding solution in the definition of $H$, Eq. (2.48)) and find the one which describes the true ground state of the Hamiltonian. A less tedious strategy is based on symmetry arguments, i.e., on the expectation that such a solution must have the full symmetry of $H$, provided, of course, that it minimizes the Hamiltonian. Inspection of $H$, Eq. (2.48) shows that it is invariant under the displacement of the replica space coordinates by an arbitrary constant vector, $\hat{x} \to \hat{x} + \hat{u}$, a condition which is trivially satisfied by the spatially homogeneous (in replica space) solution,

$$\varphi_{\mathrm{mf}}(\hat{x}) = \boldsymbol{n}\varphi_{\mathrm{mf}} , \tag{3.8}$$

where $\boldsymbol{n}$ is a constant unit vector in the space of the $n$-vector model. It is easy to check that Eq. (3.1) has indeed a constant (in replica space!) solution which can be determined from this equation by setting the expression in the brackets to zero. In the limit $m \to 0$, we get

$$\varphi_{\mathrm{mf}} = \sqrt{2/z_c \bar{N}} . \tag{3.9}$$

However, as will be shown later in this work, the analysis of the spectrum of eigenvalues of the second derivative operator $K$ defined in Eq. (3.6) (evaluated on this homogeneous solution) shows that some of the eigenvalues are negative, and therefore the constant solution corresponds to a *saddle point* rather than to a minimum of $H$. We conclude that the homogeneous solution must be rejected and proceed to look for another solution of the mean-field equation.

### 3.3. Inhomogeneous solution

The fact that the homogeneous (in replica space) solution does not minimize $H$, forces us to look for a solution that has a lower symmetry than the Hamiltonian, a situation which is commonly referred to as *spontaneous symmetry breaking*. Such a phenomenon arises in crystalline solids in which the energy is invariant under arbitrary translations but the ground state is invariant only under translations by multiples of lattice vectors, along the symmetry axes of the crystal lattice [4]. This suggests an interesting analogy between crystalline and amorphous solids: from the knowledge that spontaneous symmetry breaking of translational symmetry in *real space* gives rise to *crystalline solids*, we expect that the breaking of this symmetry in *replica space* leads to the general class of *disordered solids*. Note, that according to this view, the difference between a disordered solid and a liquid stems only from the breaking of translational symmetry in the former, and no additional symmetry breaking is necessary in general. Therefore, since the Hamiltonian is invariant under the permutation of the ($k \neq 0$) replicas, we will first look for replica symmetric solutions and examine whether they minimize $H$. After we find the solution which minimizes the Hamiltonian, we will show that there are no other solutions which satisfy the condition of local equilibrium and, therefore, this solution corresponds to the unique ground state of the Hamiltonian.

*3.3.1. Spontaneous breaking of translational symmetry in replica space*

We proceed to look for a mean-field solution with spontaneously broken translational symmetry which is inhomogeneous in replica space (the analysis below was first given by one of us, (SP), in Ref. [5]). Since the average density should be constant in real space, in both the initial and the final states of the network, we look for solutions of the form $\rho_{\rm mf}^{(k)}(\boldsymbol{x}) = \text{const}$. We now show that this form is consistent with Eq. (3.2) if the field $\varphi(\hat{\boldsymbol{x}})$ (and, consequently, $\rho_{\rm mf}(\hat{\boldsymbol{x}})$) depends on the coordinates of the replicas only through the linear combinations

$$\boldsymbol{y}^{(k)} \equiv \boldsymbol{x}^{(k)} - \lambda^{(k)} \star \boldsymbol{x}^{(0)}; \quad k = 1, \ldots, m\,, \tag{3.10}$$

where $\lambda^{(k)}$ are arbitrary constants (the symmetry of Eq. (3.1) with respect to permutation of replicas with $k \geq 1$, implies that one should take $\lambda_\alpha^{(k)} = \lambda_\alpha$ for all these replicas) and where we define the $\star$ operation by

$$(\lambda \star \boldsymbol{x})_\alpha \equiv \lambda_\alpha x_\alpha \tag{3.11}$$

(no summation over $\alpha$!). A similar functional dependence of the mean-field solution on the replica coordinates (in the momentum representation) was introduced by Goldbart and coworkers [28] for the case of an undeformed gel, $\{\lambda_\alpha = 1\}$.

Clearly, we can always replace $\rho_{\rm mf}(\hat{\boldsymbol{x}}) = \rho_{\rm mf}(\boldsymbol{x}^{(0)}, \{\boldsymbol{x}^{(k)}\})$ by a different function of the arguments $x_\alpha^{(0)}$ and $y_\alpha^{(k)}$ $(k \geq 1)$, i.e., write $\rho_{\rm mf}(\hat{\boldsymbol{x}}) = f(\boldsymbol{x}^{(0)}, \{\boldsymbol{y}^{(k)}\})$. From Eqs. (3.2), the density in the $k$th replica can be expressed as

$$\rho_{\rm mf}^{(0)}(\boldsymbol{x}^{(0)}) = \prod_{l \neq 0} \int \mathrm{d}\boldsymbol{y}^{(l)} f(\boldsymbol{x}^{(0)}, \{\boldsymbol{y}^{(l)}\}) \quad \text{for } k = 0\,, \tag{3.12}$$

$$\rho_{\rm mf}^{(k)}(\boldsymbol{x}^{(k)}) = \int \mathrm{d}\boldsymbol{x}^{(0)} f^{(k)}(\boldsymbol{x}^{(0)}, \boldsymbol{x}^{(k)} - \lambda \star \boldsymbol{x}^{(0)}) \quad \text{for } k \neq 0\,, \tag{3.13}$$

where

$$f^{(k)}(\boldsymbol{x}^{(0)}, \boldsymbol{y}^{(k)}) = \prod_{l \neq k} \int \mathrm{d}\boldsymbol{y}^{(l)} f(\boldsymbol{x}^{(0)}, \{\boldsymbol{y}^{(l)}\})\,. \tag{3.14}$$

In eqs. (3.12) and (3.14), we shifted the integrations by $\mathrm{d}\boldsymbol{x}^{(l)} \to \mathrm{d}\boldsymbol{y}^{(l)}$. Our proof follows immediately from inspection of the above integrals, which shows that, for $\rho_{\rm mf}^{(k)}$ to be independent of $\boldsymbol{x}^{(k)}$ (for all $k$) as required, $f$ must depend on $\boldsymbol{x}^{(k)}$ *only* through the linear combination $\boldsymbol{x}^{(k)} - \lambda^{(k)} \star \boldsymbol{x}^{(0)}$ (for example, if $f$ was a function of both $\boldsymbol{x}^{(0)}$ and $\{\boldsymbol{y}^{(l)}\}$, upon performing the integration in Eq. (3.12), we would obtain a function of $\boldsymbol{x}^{(0)}$ and not a constant!). Furthermore, in order for Eqs. (3.12) and (3.14) to be meaningful, the integrals which appear in these equations must be convergent, i.e., the function $f(\{\boldsymbol{y}^{(k)}\})$ must be a sufficiently rapidly decreasing function of its arguments.

In order to relate the parameters $\lambda_\alpha$ to the characteristics of the deformed network, we use the fact that the function $f^{(k)}$ depends only on $\boldsymbol{y}^{(k)}$ and, therefore, we can replace $\int \mathrm{d}\boldsymbol{x}^{(0)}$ by $\int \mathrm{d}\boldsymbol{y}^{(k)}/(\lambda_x \lambda_y \lambda_z)$. Inserting the expression for $f^{(k)}$ (Eq. (3.14)) and comparing with (3.12), we obtain a relation between the mean density of the undeformed gel and that of the deformed one (i.e., any one of the identical replicas of the deformed state):

$$\rho_{\rm mf}^{(k)} = \rho_{\rm mf}^{(0)}/(\lambda_x \lambda_y \lambda_z)\,, \quad k \neq 0\,. \tag{3.15}$$

Notice that under an arbitrary stretching or compression, the linear dimensions of the system, $L_{0x}, L_{0y}, L_{0z}$, change to $L_x, L_y, L_z$. The volume changes from $V_0 = L_{0x}L_{0y}L_{0z}$ to $V = L_xL_yL_z$ and, thus, the relation between the final density $\rho$ and the density prior to the deformation, $\rho_0$, is given by $\rho = \rho_0(L_{0x}L_{0y}L_{0z}/L_xL_yL_z)$. Comparison with Eq. (3.15) shows that $\lambda_x$, $\lambda_y$ and $\lambda_z$ must be identified with the extension ratios along the principal axes of the deformation of the network,

$$\lambda_\alpha = L_\alpha/L_{0\alpha} \quad \text{for } \alpha = x, y, z\ . \tag{3.16}$$

It is easy to check that any function (e.g., our solution) which depends only on the argument $\boldsymbol{x}^{(k)} - \lambda \star \boldsymbol{x}^{(0)}$, is invariant under the following displacement of replica space coordinates:

$$\hat{\boldsymbol{x}} \to \hat{\boldsymbol{x}} + \sum_\alpha u_\alpha \hat{\boldsymbol{e}}_\alpha\ , \tag{3.17}$$

where $u_\alpha$ are the components of an arbitrary constant three-dimensional vector and $\hat{\boldsymbol{e}}_\alpha$ is a unit vector in the $3(1+m)$-dimensional replica space:

$$\hat{\boldsymbol{e}}_\alpha = \left(\frac{\boldsymbol{e}_\alpha}{(1+m\lambda_\alpha^2)^{1/2}}, \frac{\lambda_\alpha \boldsymbol{e}_\alpha}{(1+m\lambda_\alpha^2)^{1/2}}, \cdots, \frac{\lambda_\alpha \boldsymbol{e}_\alpha}{(1+m\lambda_\alpha^2)^{1/2}}\right). \tag{3.18}$$

Here $\boldsymbol{e}_\alpha$ is a unit vector along the direction $\alpha$ ($\alpha = x, y, z$) in the usual three-dimensional space.

The condition of invariance under an arbitrary displacement along the axes $\hat{\boldsymbol{e}}_x$, $\hat{\boldsymbol{e}}_y$ and $\hat{\boldsymbol{e}}_z$ (Eq. (3.17)), singles out these three directions in replica space. An arbitrary vector $\hat{\boldsymbol{x}}$ can be decomposed as

$$\hat{\boldsymbol{x}} = \hat{\boldsymbol{x}}_{\mathrm{L}} + \hat{\boldsymbol{x}}_{\mathrm{T}}\ , \tag{3.19}$$

where $\hat{\boldsymbol{x}}_{\mathrm{L}} \equiv \sum_\alpha (\hat{\boldsymbol{e}}_\alpha \cdot \hat{\boldsymbol{x}})\hat{\boldsymbol{e}}_\alpha$ and $\hat{\boldsymbol{x}}_{\mathrm{T}}$ is orthogonal to $\hat{\boldsymbol{x}}_{\mathrm{L}}$. Condition (3.17) means that our solution can depend only on the transverse components $\hat{\boldsymbol{x}}_{\mathrm{T}}$ of the vector $\hat{\boldsymbol{x}}$. Furthermore, in the basis defined by the vectors $\hat{\boldsymbol{e}}_x$, $\hat{\boldsymbol{e}}_y$ and $\hat{\boldsymbol{e}}_z$ and their orthogonal complements (which can be constructed by the Graham–Shmidt procedure), only the first three components ($\hat{\boldsymbol{e}}_\alpha \cdot \hat{\boldsymbol{x}} \equiv x_{\mathrm{L}\alpha}$) of $\hat{\boldsymbol{x}}_{\mathrm{L}}$ are non-vanishing and thus, $\boldsymbol{x}_{\mathrm{L}}$ can be thought of as a three-dimensional vector. In the same way, we can define a $3m$-dimensional vector $\boldsymbol{x}_{\mathrm{T}}$.

Returning to Eq. (3.1), we note that since we are looking for a solution which depends only on $\boldsymbol{x}_{\mathrm{T}}$, the Laplacian $\hat{\nabla}^2$ can be replaced by $\nabla_{\mathrm{T}}^2$, where the gradient is taken only with respect to the components of the transverse vector. Since we are looking for the ground state of the Hamiltonian and the spherically symmetric solution has lower energy than the ones that break rotational symmetry (in the $3m$-dimensional subspace defined by the transverse coordinates), we conclude that the solution can depend only on the magnitude of $\boldsymbol{x}_{\mathrm{T}}$, i.e., on the scalar combination (see Fig. 3.1)

$$\varsigma \equiv \tfrac{1}{2}(\boldsymbol{x}_{\mathrm{T}})^2 = \tfrac{1}{2}\left[\hat{\boldsymbol{x}}^2 - \sum_\alpha (\hat{\boldsymbol{e}}_\alpha \cdot \hat{\boldsymbol{x}})^2\right]. \tag{3.20}$$

Therefore, the most general form of a solution with spontaneously broken symmetry under translation in replica space can be written as [5]

$$\boldsymbol{\varphi}_{\mathrm{mf}}(\hat{\boldsymbol{x}}) = \boldsymbol{n}\varphi_{\mathrm{mf}}(\varsigma)\ , \tag{3.21}$$

where the constant unit vector $\boldsymbol{n}$ was defined in Eq. (3.8).

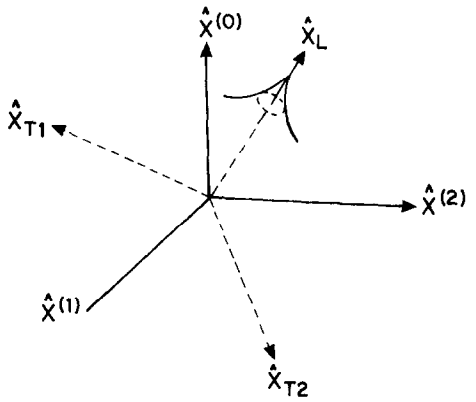


Fig. 3.1. The 3(1 + 2)-dimensional replica space (each axis in the figure represents a 3-dimensional subspace) in the original and the rotated (longitudinal and transverse) coordinates. The cylindrical symmetry of the inhomogeneous mean-field solution about the longitudinal subspace $\hat{x}_L$ (depends only on $\varsigma$) is illustrated by the cusp-shaped feature.

### 3.3.2. *Calculation of the inhomogeneous mean-field solution*

Inserting the mean-field solution, Eq. (3.21), into the field Hamiltonian, Eq. (2.48), we notice that the solution enters the Hamiltonian only through the combinations $\varphi_{mf}(\hat{x})$ and $[\hat{\nabla}\varphi_{mf}(\hat{x})]^2$. Upon the substitution $(\boldsymbol{n})^2 = 1$, the resulting Hamiltonian becomes independent of the number of components $n$ of the field and taking the limit $n \to 0$ does not affect the final results (the non-trivial character of the $n$-vector field will play a role only when we consider fluctuation corrections due to excluded volume effects).

The calculation of $\varphi_{mf}(\varsigma)$ can be further simplified by the observation that the effective Hamiltonian has to be known only up to the *first order* in $m$. This follows since the free energy is obtained by calculating

$$\left.\frac{dH}{dm}\right|_{m=0} = \left.\frac{\partial H[\varphi]}{\partial m}\right|_{m=0} + \int d\hat{x}\left.\frac{\delta H[\varphi]}{\delta\varphi(\hat{x})}\right|_{m=0}\left.\frac{\partial\varphi(\hat{x})}{\partial m}\right|_{m=0} = \left.\frac{\partial H[\varphi]}{\partial m}\right|_{m=0}, \tag{3.22}$$

where the second term in the first equation vanishes since we consider only solutions which minimize the Hamiltonian. According to Eq. (3.22), one should first compute the analytic continuation to the $m \to 0$ limit of the mean-field solution $\varphi_{mf}$ and then substitute it into $H$ and take the derivative with respect to $m$. Alternatively, the $m \to 0$ limit of $\varphi_{mf}$ can be directly calculated from Eq. (3.1), by keeping only the $k = 0$ term in the sum and dropping the term proportional to $m$ in the spherical part of the Laplacian, $(\nabla_r^2)_{sph} = 2\varsigma\partial^2/\partial\varsigma^2 + 3m\partial/\partial\varsigma$. This results in the following equation for the function $\varphi_{mf}(\varsigma)$:

$$(1/N - 2a^2\varsigma(\partial^2/\partial\varsigma^2) - (z_c/2)\varphi_{mf}^2(\varsigma))\varphi_{mf}(\varsigma) = 0\,, \tag{3.23}$$

where we used the equality $\mu + w^{(0)}\rho_{mf}^{(0)} = 1/\bar{N}$ (see Eq. (3.5)). Eq. (3.23) can be reduced to a dimensionless form by introducing the dimensionless variable $t \equiv \varsigma/(2a^2\bar{N})$ and writing

$$\varphi_{mf}(\varsigma) = \sqrt{(2/z_c\bar{N})}\chi(t)\,. \tag{3.24}$$

Substituting the expression (3.24) into Eq. (3.23) we find that the dimensionless function $\chi$ obeys the equation [5]

$$t\chi''(t) = \chi(t) - \chi^3(t)\,, \tag{3.25}$$

with the boundary conditions $\chi(0) = 1$ and $\chi(t \to \infty) \to 0$ (these choices are dictated by the form of the equation, assuming that $\chi''$ is finite at the origin and that $\chi$ is finite at infinity, respectively). The asymptotic ($t \to \infty$) behavior of this function can be easily found, since in this limit the function goes to zero and one can neglect the non-linear term in Eq. (3.25). Direct integration of the resulting linear equation yields

$$\chi(t) \sim t^{1/4} \exp(-2t^{1/2})\,, \quad t \gg 1\,. \tag{3.26}$$

For arbitrary $t$ the function $\chi(t)$ is computed numerically (see Fig. 3.2).

The observation that $\varphi_{\mathrm{mf}}$ (and, therefore, $\rho_{\mathrm{mf}}(\hat{\boldsymbol{x}})$) decreases rapidly with $\boldsymbol{x}^{(k)} - \lambda * \boldsymbol{x}^{(0)}$ means that if $\boldsymbol{x}^{(k)}$ is the position of a monomer in the $k$th replica, then

$$\boldsymbol{x}^{(1)} \simeq \cdots \simeq \boldsymbol{x}^{(m)} \simeq \lambda \star \boldsymbol{x}^{(0)}\,. \tag{3.27}$$

Thus,

1. the positions of monomers in different replicas of the final state (with $k \neq 0$) are nearly identical (up to thermal fluctuations on length scale $a\sqrt{\bar{N}}$),
2. the average monomer positions in the final state change affinely with the macroscopic deformation of the network.

The localization of the monomers in the final state of the network (in the sense that their average position is uniquely defined by their initial state and by the macroscopic deformation of the gel)

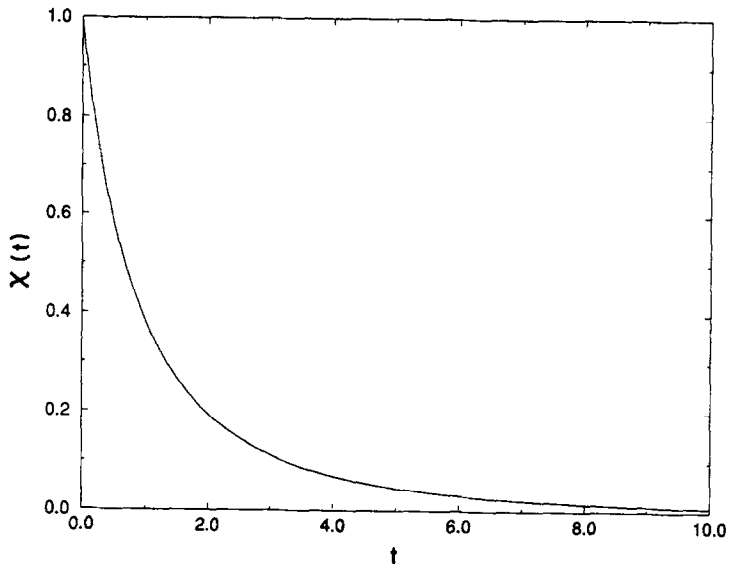


Fig. 3.2. The normalized mean-field solution $\chi(t)$ is plotted versus the dimensionless variable $t = \varsigma/(2a^2\bar{N})$.

arises as the consequence of spontaneous breaking of translational symmetry in replica space and reflects the *solid* character of the network.

As will be shown in the following, the monomer density in replica space

$$\rho_{\mathrm{mf}}(\hat{\boldsymbol{x}}) = \rho_{\mathrm{mf}}^{(0)} \chi^2 [x_{\mathrm{T}}^2/(4a^2\bar{N})] \tag{3.28}$$

contains statistical information about quantities such as the distribution of mesh sizes and their average deformation (or, equivalently, the average deformation of a network chain of a given length) and the average length scale associated with thermal fluctuations of monomers about their mean positions. It can, therefore, be used to study deviations from affine behavior due to small-scale thermal fluctuations.

A self-consistent scheme to calculate the mean-field density in replica space (which is the Edwards–Anderson-order parameter of this model) was proposed in Ref. [28] and numerical results were obtained for gels prepared near the gelation threshold (a more general result, valid for arbitrary conversion ratios, was obtained in Ref. [29]). The above group has also calculated the analog of the spin glass non-linear susceptibility (two-point replica space density correlation function), and it was shown that this function diverges at the gelation threshold [30].

### 3.4. *Mean-field free energy*

Anticipating that our inhomogeneous mean-field solution with spontaneously broken symmetry with respect to translation in replica space, corresponds to the true minimum of the Hamiltonian, we will use it to calculate the thermodynamic free energy of the network, via the steepest descent estimate of the functional integral, Eq. (2.47). To this end, we first calculate the mean-field Hamiltonian obtained by substituting the inhomogeneous mean-field solution, Eq. (3.24), into Eq. (2.48) (in this calculation we have to keep terms up to first order in $m$):

$$H_{\mathrm{mf}} = \int \mathrm{d}\hat{\boldsymbol{x}} \tilde{H}(\varsigma) + \frac{w^{(0)}}{2} V^{(0)} (\rho^{(0)})^2 + m \frac{w}{2} V \rho^2 \,. \tag{3.29}$$

Here $\tilde{H}(\varsigma)$ is the Hamiltonian density corresponding to the term in the first square bracket in Eq. (2.48). In writing down the last two contributions in the above equation, we use the fact that (a) the densities in all the replicas (evaluated on the mean-field solution) are constant and (b) that the densities in all the replicas of the final state are equal, $\rho \equiv \rho^{(1)} = \rho^{(2)} = \cdots = \rho^{(m)}$.

The calculation of $H_{\mathrm{mf}}$ is carried out in Appendix B. From this mean-field Hamiltonian one calculates (using Eq. (2.47)) the steepest descent estimate for the grand canonical partition function (in the thermodynamic limit, $V \to \infty$): $\ln \Xi_m = -H_{\mathrm{mf}}$. Substitution into Eq. (2.30) results in the following mean-field free energy of the stretched polymer network:

$$\frac{\mathscr{F}_{\mathrm{mf}}\{\lambda_\alpha\}}{VT} = \nu \left[ \frac{1}{2} \sum_\alpha \lambda_\alpha^2 + \ln(a\sqrt{\bar{N}})^3 \right] + \tfrac{1}{2} w \rho^2 \,, \tag{3.30}$$

where $\rho = N_{\mathrm{tot}}/V$ and $\nu \equiv \rho/(2\bar{N})$ is the density of cross-links in the final state of the gel (note that, both $\nu$ and $\rho$ depend only on the final volume of the gel and thus, depend on $\{\lambda_\alpha\}$ only through the product $\lambda_x\lambda_y\lambda_z$). This expression was previously derived by Edwards [1].

Eq. (3.30) differs in two important ways from the free energy of the classical theories of polymer networks. First, the coefficient in front of the elastic entropy term is $\nu/2$ instead of the classical $\nu$. Second, Flory's theory [6] contains a $\ln(\lambda_x\lambda_y\lambda_z)$ term which depends on the deformation of the network. The reasons for the discrepancy were discussed by Edwards [1]: the first discrepancy is attributed to the neglect of cross-link fluctuations about their mean positions in both the Flory–Rehner [6] and the James–Guth [8] theories and the second to the uniform density assumption in the former (but not in the latter) model.

In Appendix D we show that the dominant corrections to the mean-field free energy, Eq. (3.30) come from ultra-short wavelength (length scales $\sim a$) frozen inhomogeneities and thermal fluctuations. The former give rise to *wasted loop* corrections to the mean-field free energy (which were also considered in Ref. [1]) that arise due to the formation of small permanent loops (on the length scale of monomer size) which do not transmit elastic stresses in the network but contribute to monomer and cross-link density (see Fig. 3.3). The contribution of such loops is taken into account exactly, using the *effective action* method [31, 27]. The situation is more delicate with regard to thermal fluctuations. While ultra-short wavelength thermal fluctuations lead to a trivial shift of the chemical potential, the formation of large temporary loops due to long wavelength thermal fluctuations leads to the renormalization of the monomer size and of the second virial coefficient, in the initial and the final states of the gel. These renormalizations will be performed in a later section when we consider semidilute gels in good solvents, and will lead to a non-trivial modification of the thermodynamic free energy (i.e., to the violation of the classical additivity assumption of elastic and osmotic contributions to the free energy). Here we will assume that the excluded volume perturbation parameters $(w^{(0)}/a^6\rho^{(0)})^{1/2}$ and $(w/a^6\rho)^{1/2}$ in the initial and final states, respectively, are small and that all corrections due to long wavelength thermal fluctuations are negligible (this is equivalent to the strong screening assumption [23]).

Neglecting logarithmic corrections and constants, the renormalized free energy which includes ultra-short wavelength fluctuation corrections, is given by (the derivation is given in Appendix D)

$$\frac{\mathscr{F}_{sw}\{\lambda_\alpha\}}{VT} = \frac{\nu}{2}\left[1 + \sum_{N=1}^{\infty} P_N(0)/\rho^{(0)}\right]^{-1} \sum_\alpha \lambda_\alpha^2 + \tfrac{1}{2}w\rho^2 , \tag{3.31}$$

where $P_N(0)$ is the probability density of forming a loop of $N$ monomers. A similar expression was first derived by Deam and Edwards [1].

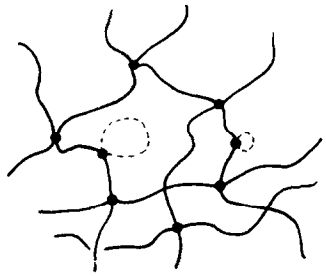

Fig. 3.3. Schematic drawing of the network. Wasted loops are shown by broken lines.

Note that in the idealized case of network chains which are Gaussian down to arbitrarily small scales, the sum $\sum_{N=1}^{\infty} P_N(0)$ diverges due to the contributions of small loops, and we conclude that strictly Gaussian networks have a vanishing elastic modulus due to the proliferation of wasted loops. For real chains with local stiffness, $\sum_{N=1}^{\infty} P_N(0)$ is a finite constant which decreases with increasing persistence length and can be calculated from models which account for the details of the local structure of the chain [32]. Finally, we would like to mention that the presence of wasted loop corrections is a characteristic feature of our model of networks formed by cross-linking mid-parts of extremely long chains. Modifications of this type do not appear in theories of networks formed by end-linking of polymers [25], although in this case one has to introduce corrections due to chains which contribute to the monomer density but not to the modulus of the network (i.e., dangling ends).

### 3.5. *Stability of the mean-field solution*

We found that the mean-field equation admits two solutions (i.e., the homogeneous one and the one with spontaneously broken symmetry with respect to translation in replica space) which are symmetric with respect to permutation of the $m$ replicas of the final deformed state of the gel. In order to check which of the mean-field solutions corresponds to a minimum of the Hamiltonian, we need to consider their stability with respect to small but otherwise arbitrary fluctuations.

Another important issue which comes up is the question of replica symmetry breaking (RSB) [33]. Although there is a trivial lack of symmetry between the 0th replica (of the initial undeformed gel) and all the other ones (those of the final deformed gel), the real issue is the presence or the absence of RSB between the $m$ replicas of the final system. A related question is: are gels regular solids, characterized by a single ground state or do they belong to the class of spin glasses which have multiple ground states separated by infinite barriers? This issue was first considered by Goldbart and Goldenfeld [34], who favored the second option. In more recent works of one of these authors [35] no RSB was found on a mean-field level for the present model in the absence of excluded volume interactions, but it was conjectured that RSB would appear if these interactions were included. In this subsection we will not deal with the issue of the existence of other, hitherto unknown ground states but, rather, will attempt to answer a more limited question: is the ground state solution we found stable against RSB (and other) fluctuations?

Consider small fluctuations $\delta\boldsymbol{\varphi}(\hat{\boldsymbol{x}}) = \boldsymbol{\varphi}(\hat{\boldsymbol{x}}) - \boldsymbol{\varphi}_{\mathrm{mf}}(\hat{\boldsymbol{x}})$ about the mean-field solutions we found. In order to test the stability of these solutions we have to calculate the spectrum of eigenvalues $\{\Lambda\}$ of the second derivative operator $K$ (evaluated on the appropriate mean-field solution), Eqs. (3.6) and (3.7), which gives the energy of these fluctuations and check whether all of them are positive (i.e., whether all small fluctuations increase the energy). In the harmonic approximation, the energy of these fluctuations is given by quadratic corrections (in $\delta\boldsymbol{\varphi}$) to the mean-field Hamiltonian:

$$\Delta H[\delta\boldsymbol{\varphi}] = H[\boldsymbol{\varphi}] - H_{\mathrm{mf}} = \tfrac{1}{2}\sum_{ij}\int \mathrm{d}\hat{\boldsymbol{x}} \int \mathrm{d}\hat{\boldsymbol{x}}'\, \delta\varphi_i(\hat{\boldsymbol{x}}) K_{ij}(\hat{\boldsymbol{x}}, \hat{\boldsymbol{x}}') \delta\varphi_j(\hat{\boldsymbol{x}}) \,. \tag{3.32}$$

The operator $\boldsymbol{K}$ which gives the energy spectrum of fluctuations about a particular mean-field solution $\boldsymbol{\varphi}_{\mathrm{mf}}$, can be obtained by substituting $\boldsymbol{\varphi}(\hat{\boldsymbol{x}}) = \boldsymbol{\varphi}_{\mathrm{mf}}(\hat{\boldsymbol{x}}) + \delta\boldsymbol{\varphi}(\hat{\boldsymbol{x}})$ into the Hamiltonian (Eq. (2.48)) and expanding up to second order in $\delta\boldsymbol{\varphi}$ (terms linear in $\delta\boldsymbol{\varphi}$ vanish since mean-field

solutions correspond to extrema of the Hamiltonian). From the general form of the solution, $\varphi_{mf}(\hat{x}) = \boldsymbol{n}\varphi_{mf}(\hat{x})$, we conclude that $\boldsymbol{K}$ can be decomposed using the projection operators $\boldsymbol{P}^{\parallel} \equiv \boldsymbol{nn}$ and $\boldsymbol{P}^{\perp} \equiv \boldsymbol{1} - \boldsymbol{nn}$, which project an arbitrary vector along directions parallel and perpendicular to $\boldsymbol{n}$, respectively. Thus,

$$\boldsymbol{K}(\hat{x}, \hat{x}') = K^{\parallel}(\hat{x}, \hat{x}')\boldsymbol{P}^{\parallel} + K^{\perp}(\hat{x}, \hat{x}')\boldsymbol{P}^{\perp} , \tag{3.33}$$

where

$$K^{\perp}(\hat{x}, \hat{x}') \equiv \delta(\hat{x} - \hat{x}')[1/\bar{N} - a^2\hat{\nabla}^2 - (z_c/2)\varphi_{mf}^2(\hat{x})] , \tag{3.34}$$

and

$$K^{\parallel}(\hat{x}, \hat{x}') \equiv \delta(\hat{x} - \hat{x}')[1/\bar{N} - a^2\hat{\nabla}^2 - 3(z_c/2)\varphi_{mf}^2(\hat{x})] + \varphi_{mf}(\hat{x})\varphi_{mf}(\hat{x}')\sum_{k=0}^{m} w^{(k)}\delta(\boldsymbol{x}^{(k)} - \boldsymbol{x}'^{(k)}) . \tag{3.35}$$

The operators $K^{\parallel}$ and $K^{\perp}$ have eigenfunctions $\psi^{\parallel}(\hat{x})$ and $\psi^{\perp}(\hat{x})$, with eigenvalues $\Lambda^{\parallel}$ and $\Lambda^{\perp}$, respectively, which are determined by the scalar (in the $n$-dimensional space) variants of Eq. (3.7),

$$\begin{aligned} &\int d\hat{x}' K^{\parallel}(\hat{x}, \hat{x}')\psi^{\parallel}(\hat{x}') = \Lambda^{\parallel}\psi^{\parallel}(\hat{x}) , \\ &\int d\hat{x}' K^{\perp}(\hat{x}, \hat{x}')\psi^{\perp}(\hat{x}') = \Lambda^{\perp}\psi^{\perp}(\hat{x}) . \end{aligned} \tag{3.36}$$

An important simplification results from the observation that since we are interested in the limit $m \to 0$, all eigenvalues can be expanded around $m = 0$, i.e., $\Lambda = \Lambda_0 + m\Lambda_1 +$ (higher-order terms in $m$). In order to test the stability of the mean-field solution, we only need to check whether the above eigenvalues are non-negative in this limit and, therefore, as long as $\Lambda_0 \neq 0$, the higher-order corrections to the spectrum need not be considered. However, if we want to calculate the eigenfunctions we cannot set $m = 0$, since symmetry under permutations of the $m$ replicas of the final state implies that these eigenfunctions are degenerate, and the degree of degeneracy must be kept a finite integer. The general rule to be followed in taking the limit $m \to 0$ is that one can safely take this limit in all analytical expressions, but one has to keep $m$ finite in all other cases (e.g., in summations over the index $k$, where $k = 1, \ldots, m$), until one arrives at analytic functions of $m$. This rule was already used to derive the mean-field solution where it led to dramatic simplification of replica calculations.

Another important simplification results from the fact that, in order to consider the stability of the mean-field solution, it is sufficient to obtain the eigenvalues corresponding to the lowest energy fluctuations. Since we expect that this energy is a monotonically decreasing function of the wavelength, in this section we will only study long wavelength fluctuations (i.e., fluctuations on length scales much larger than the mesh size of the network, $a\bar{N}^{1/2}$).

### *3.5.1. Homogeneous solution*

In order to examine the stability of the homogeneous solution we have to calculate the spectrum of eigenvalues of the operator $K^{\parallel}$ evaluated on this solution, Eq. (3.9). We will show that some of

the eigenvalues of this operator are negative and therefore will not study further the spectrum of the operator $K^{\perp}$ for the homogeneous mean-field solution. In Appendix B we show that the eigenfunctions of $K^{\parallel}$ are plane waves, $\psi^{\parallel}(\hat{x}) \sim \exp(i\hat{q}\cdot\hat{x})$, and that their eigenvalues can be positive (depending on the values of the excluded volume parameters in the initial and the final states) for wave vectors which are completely confined to the space of one of the replicas ($\hat{q}^{(i)} \equiv (0, \ldots q^{(i)}, \ldots 0)$). However, for all other wave vectors, which are not restricted to these sectors (i.e., $\hat{q} \equiv (q^{(0)}, \ldots q^{(k)}, \ldots q^{(m)})$), the eigenvalues become negative in the long wavelength limit. The presence of the negative eigenvalues shows that the constant solution corresponds to a saddle point, rather than to a minimum of the Hamiltonian. We conclude that the solution which has the full translational invariance of $H$ does not represent its true ground state, and proceed to examine the stability of solutions with spontaneously broken translational symmetry.

*3.5.2. Inhomogeneous solution*

We now consider the solutions of the secular equations, (3.36), which correspond to the inhomogeneous mean-field solution $\varphi_{mf}(\hat{x}) = \varphi_{mf}(\varsigma)$ (Eq. (3.24)). The details of the calculation are given in Appendix B and here we present a brief summary of the main results.

The general form of the eigenfunctions and of the corresponding eigenvalues can be determined from the observation that the mean-field solution is invariant under arbitrary translations in the 3-dimensional *longitudinal* subspace spanned by the three vectors $\hat{e}_{\alpha}$, $\alpha = x, y, z$ (Eqs. (3.18) and (3.19)). The fact that it is only a function of $x_T$ means that it does not depend on the 3-dimensional vector $x_L$, defined by the projection $x_{L\alpha}$ of the replica space vector $\hat{x}$ on the *longitudinal* subspace spanned by the three vectors $\hat{e}_{\alpha}$, $\alpha = x, y, z$ (Eqs. (3.18) and (3.19)). Thus, the eigenfunctions are plane waves in this subspace

$$\psi(\hat{x}) = \psi_{q_L}(x_T)\exp(iq_L\cdot x_L) \tag{3.37}$$

and both their amplitudes $\psi_{q_L}(x_T)$ and the corresponding eigenvalues $\Lambda(q_L)$ are characterized by the longitudinal wave vector $q_L$. We now proceed to classify these eigenvalues.

1. *Rotational modes*

The eigenvalues of the operator $K^{\perp}$ are

$$\Lambda^{\perp}(q_L) = a^2 q_L^2 . \tag{3.38}$$

The eigenfunctions corresponding to these eigenvalues are associated with the rotations of the vector $n$ in the abstract $n$-dimensional space and are gapless Goldstone modes, i.e., their eigenvalues are positive definite and vanish in the long-wavelength limit. The situation is equivalent to that of a ferromagnet (with $n \to 0$ spin components) where the Goldstone modes describe "soft" ($q \to 0$) rotations of the magnetization vector [36], though in our case these modes do not have a simple physical interpretation.

We proceed to calculate the spectrum of the operator $K^{\parallel}$ the eigenmodes of which are the shear and the density modes:

2. *Shear modes*

The lowest energy shear modes are Goldstone modes with eigenvalues

$$\Lambda_S(q_L) = a^2 q_L^2 , \tag{3.39}$$

which describe the infinitesimal displacement $\boldsymbol{x}_T \to \boldsymbol{x}_T + \boldsymbol{u}_T(\boldsymbol{x}_L)$ of the coordinate $\boldsymbol{x}_T$ (in the abstract transverse $3m$-dimensional subspace), subject to the condition that it does not affect the densities in any of the replicas.

3. *Density modes in initial state*

Eigenmodes for which the density fluctuations $\delta\rho^{(0)}(\boldsymbol{x}^{(0)})$ are not identically zero have eigenvalues

$$\Lambda_{\text{gap}}(\boldsymbol{q}_L) = (w^{(0)} - z_c)\varphi_{\text{mf}}^2 + a^2(\boldsymbol{q}_L)^2 \tag{3.40}$$

Since these eigenvalues do not vanish, in general, in the limit $q \to 0$, following the usual terminology we say that the corresponding solution is *massive* (i.e., has an energy gap). The gap vanishes at

$$z_c^{\max} = 1/\rho^{(0)}\bar{N}^{\min} = w^{(0)}, \tag{3.41}$$

which is identical to the cross-link saturation threshold condition, Eq. (2.8), that determines the maximal attainable density of cross-links in our model. Our inhomogeneous mean-field solution becomes unstable (and therefore unphysical) if this density exceeds the saturation threshold.

4. *Density modes in final state*

The eigenvalues of these modes (with $\delta\rho^{(k)}(\boldsymbol{x}^{(k)}) \neq 0$ in at least one of the replicas of the final state),

$$\Lambda_D(\boldsymbol{q}_L) = a^2\boldsymbol{q}_L^2 + 2w\rho^{(0)}a^2\bar{N}(\lambda^{-1} \star \boldsymbol{q}_L)^2 \tag{3.42}$$

vanish in the limit $\boldsymbol{q}_L \to 0$ and hence the corresponding fluctuations are Goldstone modes. The stability criterion $\Lambda_D(\boldsymbol{q}_L) > 0$ is always satisfied when the final state of the gel corresponds of good solvent conditions ($w \to 0$). Note that for large deformations the positivity condition can be satisfied even for moderately poor solvents ($w < 0$), since then the network is stabilized against collapse by the external forces applied to its surface.

We conclude that all the fluctuations about the inhomogeneous mean-field solution $\varphi_{\text{mf}}(\varsigma)$ (including those which break replica symmetry!) increase the energy of the system and, therefore, the above solution corresponds to a true minimum of the Hamiltonian. This shows a fundamental difference between the mean-field solution of our model and that of the Sherrington–Kirkpatrick model of spin glasses [37]. While our solution corresponds the true minimum of the Hamiltonian, the solution of Sherrington–Kirkpatrick model gives only the saddle point of the corresponding Hamiltonian. Note that although the above argument does not prove that our solution is the true *global* minimum of the Hamiltonian and that no other minima with lower energy exist, we will show that this is indeed the case and that polymer networks do not belong to the class of spin glasses. Further support for this statement comes from the work of Goldbart and coworkers [35], who use a variational approach to study the present model (neglecting excluded volume interactions) and find no solutions with RSB. Although the above authors argue that RSB should appear in a more complete treatment of the Edwards model of polymer networks which would account for excluded volume effects, we have shown by now that replica symmetry is maintained even when these interactions are exactly taken into account by the collective coordinates method.

### 3.6. *Uniqueness of the ground state*

We have found an inhomogeneous (in replica state) solution of the mean-field equations and showed that this solution is, at least, a local minimum of the Hamiltonian (i.e., is stable against

arbitrary small fluctuations). The question which is still unanswered is: are there other minima of the Hamiltonian or is the ground state we found unique? We will show now that under given thermodynamic conditions (temperature, solvent quality and forces at the boundaries) there exists a unique state of the gel, which is fully characterized by specifying the average positions of all the cross-links. In this state the network is in a mechanical equilibrium, i.e., the total force on each of the cross-links vanishes.

Our inhomogeneous mean-field solution (as well as any other mean-field solution which is characterized by constant monomer density $\rho$) describes a network in which excluded volume effects are taken into account by introducing a uniform external field $h = w\rho$ (recall that $\rho$ is the mean monomer density). The free energy is given by the sum of the energy of this external field $TN_{\mathrm{tot}}h$ and the elastic free energy $\mathscr{F}_{\mathrm{el}}$ which describes the elasticity of a network without excluded volume (which occupies the same volume as our original network, with excluded volume) i.e., $\mathscr{F} = TN_{\mathrm{tot}}h + \mathscr{F}_{\mathrm{el}}$. The physical meaning of the replacement of excluded volume by an external field is quite clear: on a mean-field level the only role of excluded volume is to fix the average monomer density in the gel and, therefore, we can replace it by external forces applied to the surface of the network which stretch it to this average density (against the restoring elastic forces of the stretched network). Thus, instead of considering our original problem, we can consider a network without excluded volume, the surface of which is fixed to the walls.

The partition function of this *elastic reference system* is given by

$$Z_{\mathrm{el}} = \mathrm{e}^{-\mathscr{F}_{\mathrm{el}}/T} = \int \mathrm{D}\boldsymbol{x}(s)\exp\left[-\frac{1}{2a^2}\int_0^{N_{\mathrm{tot}}} \mathrm{d}s\left(\frac{\mathrm{d}\boldsymbol{x}}{\mathrm{d}s}\right)^2\right]$$

$$\times \prod_{\{i,j\}} \delta[\boldsymbol{x}(s_i) - \boldsymbol{x}(s_j)] \prod_k \delta[\boldsymbol{x}(s_k) - \boldsymbol{x}_k^{\mathrm{b}}] \,, \tag{3.43}$$

where the first product of the $\delta$-functions expresses the constraints introduced by $N_{\mathrm{c}}$ cross-links (using the notation in Eq. (2.11)), and the second product introduces the constraints due to the attachment of $N_{\mathrm{b}}$ surface monomers to the walls (the $s_k$th surface monomer is fixed to the point $\boldsymbol{x}_k^{\mathrm{b}}$ on the wall). Integrating over the coordinates of all the monomers between cross-links, we are left with a functional of the positions of cross-links ($\boldsymbol{x}_i^{\mathrm{c}}$) and monomers attached to the boundary ($\boldsymbol{x}_i^{\mathrm{b}}$) only,

$$Z_{\mathrm{el}} = \mathrm{const} \cdot \prod_i \int \mathrm{d}\boldsymbol{x}_i^{\mathrm{c}} \exp[-H_{\mathrm{c}}\{\boldsymbol{x}_i^{\mathrm{c}}, \boldsymbol{x}_k^{\mathrm{b}}\}] \,, \tag{3.44}$$

where the integration is over the positions of the cross-links (the positions of the boundary monomers are fixed). The cross-link Hamiltonian $H_{\mathrm{c}}$ is a quadratic form in the distances $\boldsymbol{x}_{i+1} - \boldsymbol{x}_i$ between cross-links (or boundary monomers) which are neighbors along the chain contour

$$H_{\mathrm{c}}\{\boldsymbol{x}_i^{\mathrm{c}}, \boldsymbol{x}_k^{\mathrm{b}}\} = \sum_l{}' \sum_m \frac{(\boldsymbol{x}_l - \boldsymbol{x}_m)^2}{2a^2 N_{l,m}} \,. \tag{3.45}$$

In the above expression the summation over the index $m$ goes over all cross-links and boundary monomers and, for each $m$, the summation $\sum_l'$ goes over the four neighboring cross-links (or boundary monomers) along the chain contour ($N_{l,m}$ is the number of network monomers in the chains connecting the neighboring cross-links or boundary monomers $l$ and $m$).

Using the standard method of calculation of Gaussian integrals we represent each cross-link coordinate as

$$\boldsymbol{x}_i^{\mathrm{c}} = \langle \boldsymbol{x}_i^{\mathrm{c}} \rangle + \delta \boldsymbol{x}_i^{\mathrm{c}} , \tag{3.46}$$

where the average position of the cross-link is determined by the condition that there will be no linear terms in $\delta \boldsymbol{x}_i^{\mathrm{c}}$ in the Hamiltonian obtained by substituting Eq. (3.46) into Eq. (3.45):

$$H_{\mathrm{c}}\{\boldsymbol{x}_i^{\mathrm{c}}, \boldsymbol{x}_k^{\mathrm{b}}\} = H_{\mathrm{c}}\{\langle \boldsymbol{x}_i^{\mathrm{c}} \rangle, \boldsymbol{x}_k^{\mathrm{b}}\} + \sum_i \langle \boldsymbol{f}_i \rangle \cdot \delta \boldsymbol{x}_i^{\mathrm{c}} + H_{\mathrm{c}}\{\delta \boldsymbol{x}_i^{\mathrm{c}}, 0\} . \tag{3.47}$$

The coefficient of the linear term in the expansion, $\langle \boldsymbol{f}_i \rangle$, is given by

$$\langle \boldsymbol{f}_i \rangle = \sum_j{}' \frac{\langle \boldsymbol{x}_i^{\mathrm{c}} \rangle - \langle \boldsymbol{x}_j \rangle}{a^2 N_{i,j}} , \tag{3.48}$$

where the summation is taken over the four neighboring (along the chain contour) cross-links (or boundary monomers for which $\langle \boldsymbol{x}_j^{\mathrm{b}} \rangle = \boldsymbol{x}_j^{\mathrm{b}}$) of the given cross-link $i$. Note that $\langle \boldsymbol{f}_i \rangle$ is the total average force acting (through the connecting chains) on cross-link $i$. The condition that the linear terms in Eq. (3.47) vanish

$$\langle \boldsymbol{f}_i \rangle = 0 \tag{3.49}$$

is simply the condition of mechanical equilibrium in the system. Note that since the Hamiltonian can be written as the sum of independent contributions along the three axes $x$, $y$ and $z$, we can restrict our consideration to a one-dimensional problem.

Two scenarios can possibly arise, depending on the value of the determinant $\det \boldsymbol{M}$ of the matrix $\boldsymbol{M}$, the elements of which are

$$M_{kl} = \partial^2 H_{\mathrm{c}}\{x_i^{\mathrm{c}}, 0\} / \partial x_k^{\mathrm{c}} \partial x_l^{\mathrm{c}} . \tag{3.50}$$

If $\det \boldsymbol{M} \neq 0$, the resulting $N_{\mathrm{c}}$ linear equations (for each component of the force) impose $N_{\mathrm{c}}$ constraints on the $N_{\mathrm{c}}$ average positions ($\{\langle x_i^{\mathrm{c}} \rangle\}$) of the cross-links and guarantee the uniqueness of the state of mechanical equilibrium (it will be stable if all the eigenvalues of the matrix $\boldsymbol{M}$ are positive). In this case one can perform all the Gaussian integrations in Eq. (3.44) and obtain the free energy (up to an additive constant)

$$\mathscr{F}_{\mathrm{el}} = T H_{\mathrm{c}}\{\langle \boldsymbol{x}_i^{\mathrm{c}} \rangle, \boldsymbol{x}_k^{\mathrm{b}}\} . \tag{3.51}$$

If the network is deformed with deformation ratios $\{\lambda_\alpha\}$, the positions of the monomers attached to the boundary change affinely with the displacement of the boundaries, $x_k^{\mathrm{b}} \to \lambda_k x_k^{\mathrm{b}}$, etc. The linearity of the mechanical equilibrium conditions equation (3.49) ensures that the average positions of the cross-links also change affinely,

$$\langle x_i^{\mathrm{c}} \rangle \to \lambda_x \langle x_i^{\mathrm{c}} \rangle , \qquad \langle y_i^{\mathrm{c}} \rangle \to \lambda_y \langle y_i^{\mathrm{c}} \rangle , \qquad \langle z_i^{\mathrm{c}} \rangle \to \lambda_z \langle z_i^{\mathrm{c}} \rangle . \tag{3.52}$$

Substituting these values into the free energy gives the classical dependence of the free energy on the deformation ratios, $\mathscr{F}_{\mathrm{el}} \propto \lambda_x^2 + \lambda_y^2 + \lambda_z^2$.

The situation becomes more complicated when $\det \boldsymbol{M} = 0$. This happens when the rank of the matrix $\boldsymbol{M}$ is smaller than its dimensionality and some of the eigenvalues of the matrix $\boldsymbol{M}$ vanish.

The eigenvalues $\Lambda$ and corresponding eigenfunctions $X_i^l$ of the matrix $\boldsymbol{M}$ are determined by the secular equation ($l$ labels the eigenfunctions and the indices $i$ and $j$ label the cross-links and boundary monomers)

$$\sum_j M_{ij} X_j^l = \Lambda X_i^l \,. \tag{3.53}$$

To find the eigenfunctions corresponding to zero eigenvalues $\Lambda = 0$ (since these collective displacements do not change the Hamiltonian we will call them "zero-energy" modes), we can multiply both sides of Eq. (3.53) by $X_i^l$ and perform the summation over $i$. The resulting equation takes the form

$$\sum_{i,j} M_{ij} X_i^l X_j^l = \sum_i \frac{[X_{i+1}^l - X_i^l]^2}{a^2 N_{i,i+1}} = 0 \,. \tag{3.54}$$

Notice that this equation is equivalent to the set of conditions

$$X_{i+1}^l = X_i^l \tag{3.55}$$

and, therefore, all $X_i^l$ should be equal in a connected network, $\{X_i^l = X^l\}$. Furthermore, this condition must be satisfied for all the zero-energy modes and since the normalization of the eigenfunctions is arbitrary, we conclude that all these modes are identical and thus there is only a single zero-energy mode, $\{X_i^1 = X^1 = 1\}$ (we chose the normalization $X^1 = 1$).

In order to understand the physical meaning of this zero-energy mode we note that the coordinates of each cross-link can be expanded as a linear combination of the zero- and non-zero-energy modes (NZEM),

$$\boldsymbol{x}_i^c = \boldsymbol{a} X_i^1 + \text{contribition of NZEM} = \boldsymbol{a} + \text{contribition of NZEM} \,, \tag{3.56}$$

This is equivalent to shifting the coordinates of all cross-links by a constant vector $\boldsymbol{a}$ and we conclude that the zero-energy mode describes a global translation of the entire network! Applying the same expansion to the coordinates of the fixed boundary monomers, we find that the expansion coefficient $\boldsymbol{a}$ must vanish and thus such (trivial) translation cannot occur in a gel with a fixed boundary (or with any single fixed point, e.g., center of mass).

This completes our proof of the uniqueness of the state of mechanical equilibrium of the network and *since we have shown that our inhomogeneous mean-field solution corresponds to a minimum of the replica Hamiltonian (i.e., is stable against arbitrary small fluctuations), we conclude that the solution we found is indeed the true unique ground state of the gel.*

The existence of a unique ground state is of fundamental importance to the physics of polymer networks and means that *a gel with a given structure and subjected to given thermodynamic conditions, has a unique microscopic state of equilibrium defined by the complete set of the average positions of all the cross-links and, therefore, of all the monomers* (note that a similar conclusion has been reached already by James [38], in his study of localized phantom networks). In this sense, gels resemble crystalline solids and differ dramatically from spin glasses [33] and amorphous materials in which there are many distinct microscopic equilibrium states under given thermodynamic conditions. A corollary of this statement is the somewhat astonishing prediction that *if the thermodynamic parameters are changed in an arbitrary way (by changing the solvent, temperature, forces on the boundaries, etc., without rupturing the network) and then returned to their initial values,*

*all the network monomers will first undergo some displacement from their initial average positions and then will return to their original locations.* This prediction can be tested by experiments which probe the static inhomogeneous density distribution of the gel, e.g., by checking the reproducibility of the observed (seemingly random) specle patterns of the intensity of light scattered from the gel, following a cyclic variation ($A \to B \to A$) of thermodynamic parameters. In spin glasses such cyclic variations do, in general, change the microscopic state of the sample.

Although the above proof applies only to the uniqueness of the mean-field solution, we have also shown that while strong ultra-short wavelength fluctuations can change the mean-field solution, they do not affect its stability. Since the mean-field solution which accounts for these ultra small-scale fluctuations, minimizes the effective action Hamiltonian which differs from the original one only by the replacement of the bare parameters by their renormalized values (see Appendix D), it also describes a unique microscopic equilibrium state of the network. The uniqueness proof applies also to gels in good solvents where, as will be shown in Section 5, strong fluctuations on length scales smaller than the blob size renormalize the parameters of the mean-field Hamiltonian but do not affect its functional form. Finally, question the existence of a unique microscopic equilibrium state in models of polymer networks which account for the existence of entanglements. Note that the introduction of permanent (topological) entanglements (at the same the number of permanent cross-links) adds additional constraints on the mean positions of the cross-links (and of the monomers). Hence, we expect that the main effect of the entanglements is to suppress the fluctuations of the average positions of all the monomers (the minimum becomes "sharper") and that, in this case too, there exists a unique microscopic equilibrium state characterized by the set of these average positions.

### *3.7. Local deviations from affinity*

We have shown that our inhomogeneous mean-field solution $\varphi_{mf}(\varsigma)$ defines a unique microscopic state of the gel, in the sense that once we have specified the thermodynamic parameters, the *average* positions of all the cross-links are uniquely defined by these parameters and by their positions in the state of preparation. We will show now that $\varphi_{mf}(\varsigma)$ also tells us about how these positions fluctuate about their mean values.

#### *3.7.1. Fluctuations about affinely deformed monomer positions*

In order to gain some understanding about the information content of our solution, we notice that the mean-field density in replica space, $\rho_{mf}(\hat{\boldsymbol{x}}) = \varphi^2_{mf}(\varsigma)/2$ can be expressed in terms of the Laplace transform $\Pi(\sigma)$ of $\rho_{mf}(\hat{\boldsymbol{x}})/\rho_{mf}(0)$:

$$\frac{\rho_{mf}(\hat{\boldsymbol{x}})}{\rho_{mf}(0)} = \int_0^\infty d\sigma\, \Pi(\sigma)\exp(-\sigma\varsigma)\,. \tag{3.57}$$

Using the definition $\varsigma = \hat{\boldsymbol{x}}_1^2/2$ (Eq. (3.20)) we can express the exponential as

$$\begin{aligned}\exp(-\sigma\varsigma) &= \exp\left[-\frac{\sigma}{2}\sum_\alpha\sum_{k=0}^{m}(x_\alpha^{(k)})^2 + \frac{\sigma}{2}\sum_\alpha\left(\sum_{k=0}^{m}x_\alpha^{(k)}e_\alpha^{(k)}\right)^2\right]\\ &= \int\frac{d\boldsymbol{r}}{(2\pi)^{3/2}}\,\sigma^{3/2}\exp\left[-\frac{\sigma}{2}\sum_\alpha\sum_{k=0}^{m}(x_\alpha^{(k)} - r_\alpha e_\alpha^{(k)})^2\right],\end{aligned} \tag{3.58}$$

where the second equality can be easily checked by performing the Gaussian integration and using the normalization condition, $\sum_{k=0}^{m}(e_\alpha^{(k)})^2 = 1$. Since $\sigma$ has the dimensions of inverse length squared, it is convenient to introduce a length $R$ and define $\sigma \equiv 1/R^2$. With the above substitutions, Eq. (3.57) is recast into the form

$$\frac{\rho_{\mathrm{mf}}(\hat{x})}{\rho_{\mathrm{mf}}(0)} = \int \mathrm{d}r \int_0^\infty \mathrm{d}R P(R) \prod_\alpha \prod_{k=0}^{m} W(x_\alpha^{(k)} - r_\alpha e_\alpha^{(k)} \mid R) , \tag{3.59}$$

where

$$P(R) \equiv (2/R^3)\Pi(1/R^2) , \tag{3.60}$$

and

$$W(\Delta x \mid R) \equiv [1/(2\pi R^2)^{1/2}]\exp[-(\Delta x)^2/2R^2] . \tag{3.61}$$

Both functions are normalized to unity, $\int \mathrm{d}R P(R) = \int \mathrm{d}\sigma \Pi(\sigma) = 1$ and $\int \mathrm{d}(\Delta x) W(\Delta x \mid R) = 1$ and admit a simple physical interpretation. According to the definition of the function $\rho(\hat{x})$ (Eq. (2.31)), the left-hand side of Eq. (3.59) is simply the mean-field expression for the probability to find a given monomer at points $\{x^{(k)}\}$, in each of the replicas (i.e., $x^{(0)}$ in the zeroth replica, $x^{(1)}$ in the first replica, etc.). The function $W(x_\alpha^{(k)} - r_\alpha e_\alpha^{(k)} \mid R)$ can be interpreted as the conditional probability to observe a fluctuation of the monomer position $x_\alpha^{(k)}$ around its mean position $r_\alpha e_\alpha^{(k)}$ in the $k$th replica, given that the rms deviation from this mean position (*localization* length) is $R$. The function $P(R)$ is then the probability of finding a monomer with a localization length $R$. This function is expressed through the Laplace transform of the mean-field density and has the same characteristic scale of variation, $a\bar{N}^{1/2}$ (independent of the deformation $\lambda_\alpha$), as the mean-field solution $\varphi_{\mathrm{mf}}(\varsigma)$. It can be calculated numerically and is shown in Fig. 3.4. The function $\Pi(\sigma)$ (which determines the

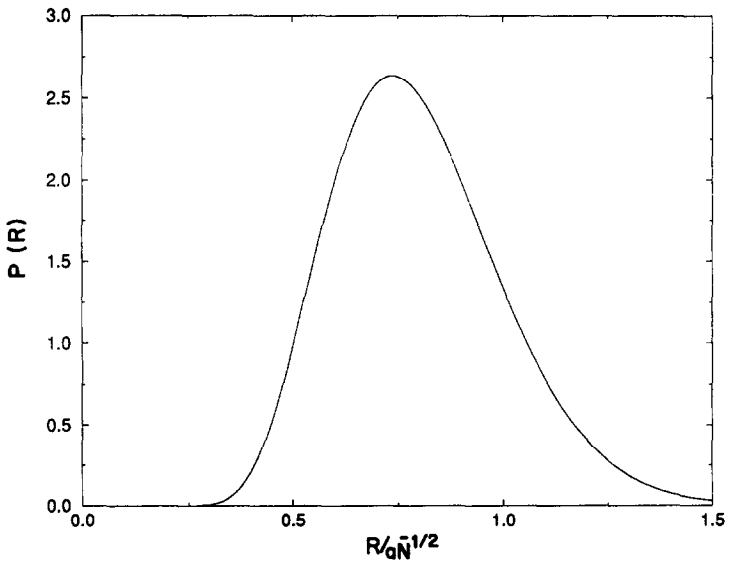


Fig. 3.4. The probability $P(R)$ of finding a monomer with localization length $R$, is plotted versus the dimensionless variable $R/(a\sqrt{2\bar{N}})$.

distribution of localization lengths, $P(R)$ – see Eq. (3.60)) was calculated numerically, for undeformed networks close to the gelation threshold, in Ref. [28].

The physical meaning of the above probabilities becomes clear in the limit $m \to 0$. In this case, Eq. (3.18) yields $e_\alpha^{(0)} = 1$ and $e_\alpha^{(k)} = \lambda_\alpha$ and the argument of the function W becomes $x_\alpha^{(0)} - r_\alpha$ and $x_\alpha^{(k)} - \lambda_\alpha r_\alpha$ (for $k > 0$). Thus, if the average position of a monomer in the initial state is $\langle x_\alpha^{(0)} \rangle = r_\alpha$, the corresponding average position in the replicas of the deformed state is $\langle x_\alpha^{(k)} \rangle = \lambda_\alpha \langle x_\alpha^{(0)} \rangle$ which means that *the average position of every monomer changes affinely with the deformation of the network*. The mean deviation from affine behavior of a typical monomer under deformation is given by $R$ and, therefore, the localization length $R$ can be interpreted as the length scale for thermal fluctuations of a typical monomer. It must be considered as a random variable which fluctuates in the space of the network (the probability of observing such a fluctuation is $P(R)$), both due to the frozen inhomogeneity of the structure of the network, and due to the fact that the thermal fluctuations of a given monomer will depend on its position along the contour.

We can show that the probability of having non-fluctuating monomers vanishes in our model ($P(0) = 0$), which means that all monomers, including cross-links, fluctuate about their average positions. If the cross-links were strictly pinned down (as in Flory's mode [6]), one would expect this probability to be of the order of the fraction of cross-links, $P(0) \sim \bar{N}^{-1}$.

Up to this point we considered the behavior of a single monomer and showed that, on the average, its position changes affinely with the deformation of the network and that deviations from affine behavior are only due to fluctuations. Different information can be obtained if we consider two-monomer quantities such as the rms distance between two end monomers of a network chain. The results of such a calculation [10] are discussed in the following.

### 3.7.2. *Non-affine deformation of network chains*

The analysis of this problem requires generating functional methods which differ from those used in this work and hence we will only present the results of calculations reported elsewhere [10]. In order to learn about the deformation of network chains of a given length $aN$ (averaged over all such chains in the network), we calculate the distribution function $W_N\{R_\alpha | \lambda_\alpha\}$ which gives the probability that a chain of contour length $aN$ has components of the end-to-end distance vector $R_\alpha$ ($\alpha = x, y, z$), given that the network is stretched by factors $\lambda_\alpha$ with respect to the initial state:

$$W_N\{R_\alpha | \lambda_\alpha\} = \int_0^\infty d\xi P(\xi) \prod_\alpha [2\pi \langle R_\alpha^2(N, \xi | \lambda_\alpha) \rangle]^{-1/2} \exp\left[ - \frac{R_\alpha^2}{2\langle R_\alpha^2(N, \xi | \lambda_\alpha) \rangle} \right]. \tag{3.62}$$

The normalized distribution function $P(\xi)$ defined in Eq. (3.60) is a function of the dimensionless variable $\xi/(a\bar{N}^{1/2})$ only and, in general, has to be calculated numerically from $\varphi_{mf}(\varsigma)$. The universal plot of $P(\xi)$ as a function of $\xi/(a\bar{N}^{1/2})$ is shown in Fig. 3.5. The average projection of the $\alpha$th component squared of the end-to-end distance vector for a given value of $\xi$, is given by

$$\langle R_\alpha^2(N, \xi | \lambda_\alpha) \rangle = a^2 N (1 + \lambda_\alpha^2 a^2 N/\xi^2)/(1 + a^2 N/\xi^2) \,. \tag{3.63}$$

Note that the above expression is the sum of two contributions: the first one, proportional to $\lambda_\alpha^2$, reflects the affine deformation of the average distance between the chain ends and the other one (independent of $\lambda_\alpha^2$) gives the purely fluctuational contribution which is not affected by the macroscopic deformation.

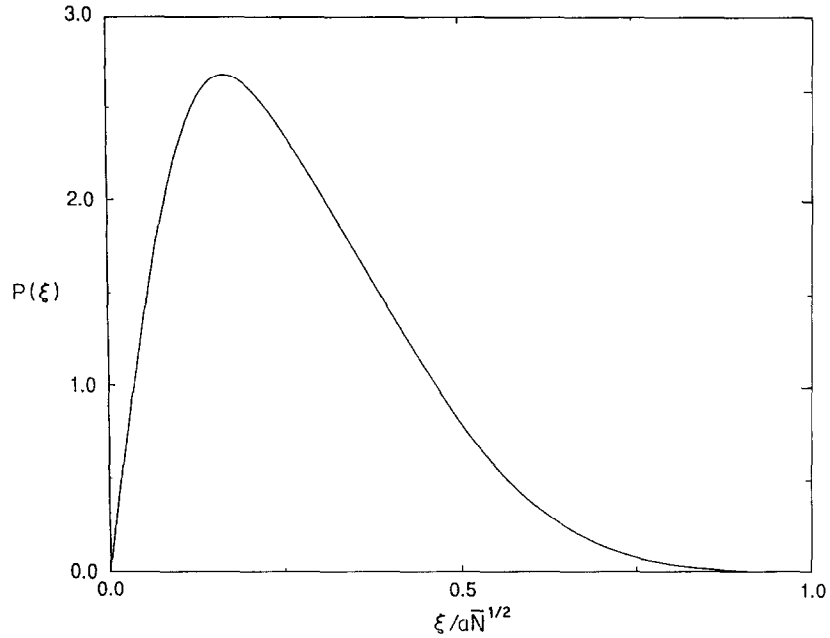


Fig. 3.5. Plot of the probability distribution $P(\xi)$ of the random length $\xi$, versus the dimensionless variable $\xi/(a\bar{N}^{1/2})$.

What is the physical interpretation of the length $\xi$? We know that $\xi$ is a random variable characterized by the distribution function $P(\xi)$ and that its average value is of the order of the unperturbed size of the average chain (mesh size), $\bar{\xi} \simeq 0.27a\bar{N}^{1/2}$ (see Fig. 3.5). Further insight can be obtained from Eq. (3.63) which describes the response of a chain of contour length $aN$ to a macroscopically-induced deformation. The fact that the chain under consideration is coupled to a network, the local properties of which (e.g., density of cross-links) may vary from point to point due to the random character of the cross-linking process, is reflected in the appearance of the random length $\xi$. We can distinguish between the following cases [11]:

*Case A*: In the direction of elongation, $\lambda_\alpha > 1$, and there are 3 regimes depending on $N$, $\xi$ and $\lambda_\alpha$ (these regimes become well-separated only in the limit $\lambda_\alpha \gg 1$)

1. For $N \ll [\xi/(a\lambda_\alpha)]^2$ the size of the chain is essentially unaffected by the macroscopic elongation. For such short chains, macroscopic deformation can only lead to desinterpenetration of undeformed chains.

2. Chains with number of monomers in the range $[\xi/(a\lambda_\alpha)]^2 \ll N \ll (\xi/a)^2$ are stretched non-affinely, with $R_\alpha^2 = (a^2N/\xi^2)a^2N\lambda_\alpha^2 \ll a^2N\lambda_\alpha^2$.

3. Finally, when $N \gg (\xi/a)^2$, the chain stretches affinely with the applied strain, i.e., the condition $R_\alpha^2 = a^2N\lambda_\alpha^2$ is satisfied. In this case, the rms distance between the ends of the chain is determined by the applied deformation and the fluctuational contribution is negligible.

*Case B*: In the direction of compression, $\lambda_\alpha < 1$ there are also three regimes of chain length:

1. Chains with $N$ smaller than $(\xi/a)^2$ interpenetrate without changing their undeformed size.

2. When $[\xi/(a\lambda_\alpha)]^2 \gg N \gg (\xi/a)^2$ the distance between chain ends is unaffected by compression and remains pinned down at $\xi$.

3. For $[\xi/(a\lambda_\alpha)]^2 \ll N$, the chains are compressed affinely with the network.

The most important geometric characteristic of the network is the average mesh size which can be defined as the rms end-to-end distance of an average chain (of $\bar{N}$ monomers). It follows from our analysis that the average mesh size deforms affinely under macroscopic *stretching or swelling*, i.e.,

$$\bar{R}^{\mathrm{str}}_{\mathrm{mesh}} \approx a\bar{N}^{1/2}\lambda\,, \tag{3.64}$$

but does not change under *compression* of the network (i.e., compression leads to enhanced interpenetration of the meshes [39, 40])

$$\bar{R}^{\mathrm{comp}}_{\mathrm{mesh}} \approx a\bar{N}^{1/2}\,. \tag{3.65}$$

We have seen that our mean-field solution tells us that *the average positions of all the monomers change affinely with the macroscopic deformation of the network.* It also gives us statistical information about the fluctuations of monomers about these mean positions and about the fluctuations of the end-to-end distance of chains of a given contour length. *Deviations from affine displacement of average monomer positions occur only due to thermal fluctuations and take place only on length scales smaller than the mesh size.*

Note that our mean-field solution, by its very nature, does not contain any information about the deviations of the monomer *density* from its average value. Such deviations occur due to static inhomogeneities introduced by the statistical nature of the cross-linking process and due to thermal fluctuations about this inhomogeneous density distribution. In the next section we proceed to study these density fluctuations and, in the process, gain important insights about the inhomogeneous structure of polymer networks.

## 4. Static inhomogeneities and thermal fluctuations

We now proceed to obtain all the statistical information concerning density fluctuations about the mean-field solution which, in spite of its rich physical contents, tells us nothing about the static inhomogeneities and the thermal fluctuations of the monomer density in polymer networks. Although we did study fluctuations about the mean-field solution (in order to test its stability), we have been working in an abstract replica space in which all fluctuations – those of the frozen structure of the network, as well as thermal ones – have been treated on the same footing (recall that the original reason for posing the problem in the language of replica field theory was to avoid dealing with the complicated averaging over the ensemble of different network structures and to treat static inhomogeneities in real space as thermal fluctuations in replica space). The price we had to pay is that we can no longer distinguish in a simple way between these two, physically very distinct, types of fluctuations. In order to recover the important information on the inhomogeneous structure of polymer networks and on the thermal fluctuations about this structure, we first eliminate all the collective coordinates which do not affect the monomer density and then to go back to real space in which the distinction between static inhomogeneities and thermal density fluctuations comes out naturally. This program will be carried out in the following.

### *4.1. RPA free energy density functional*

In principle, one can express the replica space fluctuation Hamiltonian (3.32) in terms of the shear and density modes and obtain the full information about all shear and density fluctuations in

the gel. In a similar way, the above Hamiltonian governs the response of the stretched and swollen network to small (in the linear response regime) deformations, on top of the stretching and swelling described by the deformation ratios $\{\lambda_\alpha\}$. The continuum limit of such a theory will give rise to a generalized theory of elasticity of two-component systems in which one of the components is a solid and the other a liquid [41, 29]. Such an approach (using a variational method) was used in Ref. [42] where elastic moduli describing small deformations of an unstretched network ($\lambda = 1$) were calculated. Although conceptually important, a mesoscopic (i.e., finite $q$) description of stress and strain fluctuations is of somewhat limited interest from the experimental point of view, since most scattering experiments do not measure the strain–strain (or stress–stress) correlation functions which can be calculated in this framework (information about such quantities can be obtained, in principle, from studies on the propagation of shear waves in the gel). In order to focus on issues which are of direct relevance to neutron and light scattering experiments which probe static density inhomogeneities and thermal *density* fluctuations in the gel, we will eliminate (i.e., integrate over) all the other degrees of freedom and obtain a reduced description in terms of the density fluctuations only.

Throughout this section we will assume that deviations from the mean density due to both thermal fluctuations and static inhomogeneities are small (this does not apply to the short wavelength fluctuations which were already taken into account in the preceding section) and can be described on a Gaussian (quadratic in the fluctuations) level. For thermal fluctuations this simplifying assumption is equivalent to the *random phase approximation* (RPA) which works well for concentrated polymer systems (for example, for polymer blends) but breaks down in the semi-dilute regime of polymer solutions in good solvents. Note, however, that RPA can be also applied to the study of long wavelength fluctuations in semi-dilute polymer solutions, provided that one uses renormalized (due to strong fluctuations on scales smaller than the correlation length) instead of the bare values of the parameters (monomer size, second virial coefficient) in the RPA Hamiltonian. This will be done in Section 5 where we discuss gels swollen in good low molecular weight solvents.

While the physical reasons for the breakdown of RPA due to the existence of strong thermal fluctuations on length scales smaller than the thermal correlation length (blob size) are well understood, nothing is known about the limits of applicability of RPA to static inhomogeneities. We will show in the next section that, when gels are prepared away from the cross-link saturation threshold, static inhomogeneities of monomer density are limited to length scales comparable to the average mesh size of the network and are therefore "weak". Thus, as long as one does not approach the "critical" regime of cross-link densities near the saturation threshold, one can safely assume the applicability of RPA to the study of such inhomogeneities.

Recall that the fluctuation Hamiltonian can be written as the sum of a rotational part ($\Delta H^{\perp}$) and a part which describes shear and density fluctuations ($\Delta H^{\parallel}$). Since rotational modes do not couple to the latter fluctuations, they do not contribute to the partition function of shear and density modes (defined by Eq. (D.4)),

$$\Xi_m^{SD} = \int D[\delta\varphi] \exp(-\Delta H^{\parallel}[\delta\varphi]) , \tag{4.1}$$

where the Hamiltonian of shear and density fluctuations in replica space can be written as

$$\Delta H^{\perp}[\delta\varphi] \equiv \frac{1}{2}\int d\hat{x}\, d\hat{x}'\, \delta\varphi(\hat{x}) K^{\perp}(\hat{x},\hat{x}')\, \delta\varphi(\hat{x}')$$

$$= \sum_{k=0}^{m} \frac{\Delta U^{(k)}[\delta\rho^{(k)}]}{T^{(k)}} - \Delta S[\delta\varphi]\,. \tag{4.2}$$

In the second equality we used the definition of the $K^{\perp}$ operator, Eq. (3.35), to represent the fluctuation Hamiltonian (for the shear and the density modes) as a sum of excluded volume

$$\Delta U^{(k)}[\delta\rho^{(k)}] \equiv \frac{w^{(k)}T^{(k)}}{2}\int dx^{(k)}[\delta\rho^{(k)}(x^{(k)})]^2 \tag{4.3}$$

and "entropic"

$$\Delta S[\delta\varphi] \equiv -\frac{1}{2}\int d\hat{x}\, \delta\varphi(\hat{x})\left[\frac{1}{\bar{N}} - a^2\hat{\nabla}^2 - \frac{3z_c}{2}\varphi_{mf}^2(\varsigma)\right]\delta\varphi(\hat{x}) \tag{4.4}$$

contributions. Here $T^{(k)}$ is the temperature (which can be different in replicas of the initial and the final state).

We proceed to eliminate the shear fluctuations and the density fluctuations in the initial state, i.e., integrate over those fluctuations which do not affect the densities in each of the replicas of the *final* state (we are only interested in density fluctuations in the final state; those in the state of preparation can be obtained from the latter by setting $T = T^{(0)}$, $w = w^{(0)}$ and $\{\lambda_\alpha = 1\}$). This is done by inserting the following representation of the unity:

$$1 = \prod_{k=1}^{m}\int D[\delta\rho^{(k)}]\delta[\delta\rho^{(k)}(x) - \int d\hat{x}\, \varphi_{mf}(\varsigma)\,\delta\varphi(\hat{x})\delta(x - x^{(k)})] \tag{4.5}$$

into the integrand in Eq. (4.1) and moving the integration over $\delta\rho^{(k)}$ to the leftmost side of the integral. We obtain

$$\Xi_m^{SD} = \prod_{k=1}^{m}\int D[\delta\rho^{(k)}]\exp\left(-\sum_{k=1}^{m}\frac{\Delta U^{(k)}[\delta\rho^{(k)}]}{T} + \Delta S_m[\{\delta\rho^{(k)}\}]\right), \tag{4.6}$$

where $T$ is the temperature in the final state, and

$$\exp(\Delta S_m[\{\delta\rho^{(k)}\}]) \equiv \int D[\delta\varphi]\exp\left(\Delta S[\delta\varphi] - \frac{\Delta U^{(0)}[\delta\rho^{(0)}]}{T^{(0)}}\right)$$

$$\times \prod_{k=1}^{m}\delta\left[\delta\rho^{(k)}(x) - \int d\hat{x}\varphi_{mf}(\varsigma)\delta\varphi(\hat{x})\delta(x - x^{(k)})\right]. \tag{4.7}$$

Note that although $\Delta S_m$ depends only on the replica densities $\delta\rho^{(k)}$ in the final state, it includes exactly all the contributions of both the density fluctuations in the initial state and the shear

fluctuations. The total entropy functional defined in Eq. (4.7) is calculated in Appendix E and can be written as

$$\exp\Delta S_m[\{\delta\rho^{(k)}\}] = \left\langle \prod_{k=1}^{m} \exp\Delta S[n, \delta\rho^{(k)}] \right\rangle_n , \tag{4.8}$$

where

$$\Delta S[n, \delta\rho^{(k)}] = -\int \frac{d\boldsymbol{q}}{(2\pi)^3} \frac{(\rho_q^{(k)} - n_q)(\rho_{-q}^{(k)} - n_{-q})}{2g_q} . \tag{4.9}$$

The entropy $\Delta S[n, \delta\rho^{(k)}]$ is a functional of the density in the $k$th replica and of a random field $n$ (the physical meaning of which will be discussed later). The averaging, $\langle\ \rangle_n$, in Eq. (4.8) is taken with respect to the distribution function (see Appendix E)

$$P[n] = \exp\left\{\frac{1}{2}\int \frac{d\boldsymbol{q}}{(2\pi)^3}\left[\ln(2\pi v_q) - \frac{n_q n_{-q}}{v_q}\right]\right\}, \tag{4.10}$$

with the correlator

$$\langle n_q n_{-q}\rangle_n = v_q . \tag{4.11}$$

General expressions for the function $g_q$ and for the correlator $v_q$ are given in Appendix G.

In order to derive the grand canonical partition function of the replica system, we substitute Eq. (4.8) into Eq. (4.6) and use the independence of the $n$ and the $\delta\rho^{(k)}$ fields to change the order of averaging (with respect to $n$) and integration (over $\rho^{(k)}$):

$$\Xi_m^{SD} = \left\langle \prod_{k=1}^{m} \int D[\delta\rho^{(k)}] \exp\left( -\frac{\Delta U^{(k)}[\delta\rho^{(k)}] - T\Delta S_n[\delta\rho^{(k)}]}{T} \right) \right\rangle_n . \tag{4.12}$$

Using the identity of the contributions from the different replicas of the final state and introducing the free energy functional

$$\mathcal{F}_n[\delta\rho] \equiv \Delta U[\delta\rho] - T\Delta S_n[\delta\rho] , \tag{4.13}$$

where

$$\Delta U[\delta\rho] \equiv \frac{wT}{2}\int \frac{d\boldsymbol{q}}{(2\pi)^3}\rho_q\rho_{-q} \tag{4.14}$$

and

$$\Delta S_n[\delta\rho] = -\int \frac{d\boldsymbol{q}}{(2\pi)^3} \frac{(\rho_q - n_q)(\rho_{-q} - n_{-q})}{2g_q} , \tag{4.15}$$

we can rewrite Eq. (4.12) as

$$\Xi_m^{SD} = \left\langle \left[ \int D[\delta\rho] \exp\left( -\frac{\mathcal{F}_n[\delta\rho]}{T} \right) \right]^m \right\rangle_n . \tag{4.16}$$

Substituting this expression into Eq. (D.2) and using Eq. (2.30), we obtain the final expression for the fluctuation contribution to the free energy of the deformed network, $\Delta\mathscr{F}\{\lambda_\alpha\} = \mathscr{F}\{\lambda_\alpha\} - \mathscr{F}_{sw}\{\lambda_\alpha\}$ ($\mathscr{F}_{sw}$ is defined in Eq. (3.31)),

$$\Delta\mathscr{F}\{\lambda_\alpha\} = -T\int \mathrm{D}nP[n]\ln\left[\int \mathrm{D}[\delta\rho]\exp\left(-\frac{\mathscr{F}_n[\delta\rho]}{T}\right)\right], \tag{4.17}$$

where $P[n]$ is given by Eq. (4.10), and

$$\frac{\mathscr{F}_n[\delta\rho]}{T} = \frac{1}{2}\int\frac{\mathrm{d}\boldsymbol{q}}{(2\pi)^3}\left[\frac{(\rho_q - n_q)(\rho_{-q} - n_{-q})}{g_q} + w\rho_q\rho_{-q}\right]. \tag{4.18}$$

Note that since all the functional integrals in Eq. (4.17) are Gaussian (see Eqs. (4.10) and (4.18)), they can be calculated exactly and one can obtain a complete expression for the thermodynamic free energy in which all fluctuation corrections are included on the RPA level. In order to carry out this program, one has to calculate Fourier integrals over combinations of the functions $v_q$ and $g_q$ for which only asymptotic (i.e., in the long and short wavelength limits) results are available at present. Since the resulting corrections are small (otherwise, our RPA calculation is inconsistent), we will not consider them here and come back to this issue in a latter section, where we study (by renormalization group and scaling methods) the effects of strong thermal fluctuations in semi-dilute gels in good solvents.

### *4.2. Inhomogeneous equilibrium density profile*

What is the physical meaning of the random field $n$? Comparison between the definition of the free energy functional $\mathscr{F}_n[\delta\rho]$ defined in Eq. (4.18) and the expression for the thermodynamic free energy, Eq. (2.13), shows that the probability functional $P[n]$, defined in Eq. (4.10), gives the probability of realization of a given network structure $\boldsymbol{S}$ which is characterized by the value of $n$ (in general $n$ is a complicated functional of $\boldsymbol{S}$ and depends on the deformation of the network)

$$P[n] = \int \mathrm{d}\boldsymbol{S}\mathscr{P}(\boldsymbol{S})\delta[n - n(\boldsymbol{S})], \tag{4.19}$$

where $\mathscr{P}(\boldsymbol{S})$ is defined in Eq. (2.12). As long as we are interested in observable quantities such as density correlation functions, which can be represented as statistical averages, we do not need the explicit functional form of $n(\boldsymbol{S})$ and it is sufficient to specify the probability functional $P[n]$ or, alternatively, the function $v_q$. It is shown in Appendix G that the function $v_q$ depends on the frozen structure of the network and on the deformation but does not depend on the quality of solvent in the final state.

In order to obtain further insight into the meaning of $n$, we note that the non-averaged free energy $\mathscr{F}_n[\delta\rho]$ defines (through the Boltzmann factor, $\exp\{-\mathscr{F}_n[\delta\rho]/T\}$) the probability of observing a thermal fluctuation of the monomer density (at a wave vector $\boldsymbol{q}$), $\rho_q^{th} = \rho_q - \rho_q^{eq}$, with respect to the inhomogeneous *equilibrium* density profile in the final deformed state of the network, $\rho_q^{eq}$ (in the following we will refer to the Fourier transform of the deviation from the average

monomer density as the "density" distribution, since the true density distribution can be reconstructed from it by inverse Fourier transform, $\rho^{eq}(\boldsymbol{x}) = \rho + \delta\rho^{eq}(\boldsymbol{x}) = \rho + \int [d\boldsymbol{q}/(2\pi)^3] \times \rho_{\boldsymbol{q}}^{eq} \exp(i\boldsymbol{q}\cdot\boldsymbol{x})$. The existence of a unique inhomogeneous equilibrium density profile which characterizes the state of the gel under given thermodynamic conditions is guaranteed by our demonstration (in Section 3.6) that a network which is stabilized against collapse by excluded volume forces or, equivalently, by external forces applied to its surface, has a unique microscopic equilibrium state characterized by the set of the average positions of all network monomers. In the collective coordinate representation this set of average monomer coordinates can be replaced by the (generally) inhomogeneous density field $\rho^{eq}(\boldsymbol{x})$.

The equilibrium monomer density profile is found by minimizing the free energy $\mathscr{F}_n[\delta\rho]$ with respect to $\rho_{\boldsymbol{q}}$. This gives

$$\rho_{\boldsymbol{q}}^{eq} = \frac{n_{\boldsymbol{q}}}{1 + w g_{\boldsymbol{q}}} . \tag{4.20}$$

Since, for $w = 0$, this density coincides with $n_{\boldsymbol{q}}$, we conclude that $n_{\boldsymbol{q}}$ can be interpreted as the *equilibrium density profile of the network in the absence of excluded volume interactions but under the constraint that the macroscopic deformation of the gel is the same as it was in our final deformed state in the presence of excluded volume forces* (the initial state is a particular case, with $\{\lambda_\alpha = 1\}$, $w = w^{(0)}$ and $T = T^{(0)}$). Under the above conditions (no excluded volume) only elastic forces act in the bulk of the network and, if no external forces were applied to its surface, the network would collapse to dimensions of the order of the mesh size. In view of the above, we will refer to the state characterized by the static density distribution $n_{\boldsymbol{q}}$, as the *elastic reference state.* Information about the static density profile in the elastic reference state can be obtained by the following procedure: first, a network is prepared in a good solvent ($w^{(0)} > 0$) and deformed. Then, the solvent is brought to its $\Theta$-point ($w = 0$) while keeping the macroscopic deformation fixed (if there was no external deformation applied initially, one should simply fix the surface of the gel in order to prevent it from shrinking). The inhomogeneous monomer density distribution in this elastic reference state can then be probed by scattering experiments.

In the general case ($w \neq 0$), *the presence of excluded volume interactions results in a new unique equilibrium state which is characterized by the inhomogeneous density distribution* $\rho_{\boldsymbol{q}}^{eq}$. As can be seen from Eq. (4.20), the new density profile will be more homogeneous than that of the corresponding elastic reference state (the presence of excluded volume tends to suppress local density fluctuations or, equivalently, to decrease the Fourier amplitudes of the density field). This static density distribution (which fluctuates in space but remains constant in time) leads to the stationary speckle patterns observed in light scattering from gels [43].

### *4.3. Thermal and structure averages*

Although, in principle, a given realization of network structure is described by the value of the field $n(\boldsymbol{x})$ at each point $\boldsymbol{x}$ in the gel, if we are interested in statistical information, we only have to know the probability $P[n(\boldsymbol{x})]$ (defined in Eq. (4.10)) of observing this particular value at this point in space. Thus, the only meaningful information about the density profile one can obtain from our statistical mechanical description involves *averages* of moments of the density field (e.g., density correlation functions).

We now introduce two important relations. The first is the consequence of our demonstration that a gel with a given network structure and thermodynamic parameters has a unique microscopic equilibrium state characterized by a density distribution $\rho_q^{eq}$. When the network is deformed, a new equilibrium state results which is characterized by a different equilibrium density distribution. Gels are, of course, non-ergodic in the sense that the configurational space available to the cross-linked network is smaller than that of the pre-cross-linked polymer solution. Nevertheless, the existence of a single state of equilibrium under given thermodynamic conditions implies that they possess *restricted ergodicity*, i.e., that if we prepare an ensemble of gels with *identical* structures, averaging over this ensemble with respect to the Gibbs distribution is the same as measuring time averages in a single gel. We therefore conclude that thermal (annealed) averaging is equivalent to time averaging.

The second relation is based on the fact that, as long as the cross-linking is done away from the cross-link saturation threshold, the resulting static density inhomogeneities will be uncorrelated over macroscopic distances. We can, therefore, mentally decompose the entire network into small but still macroscopic domains, each of which is characterized by a different structure. In the thermodynamic limit, the probability to find a region with a given structure $\boldsymbol{S}$ is the same as that to find a network with this structure, from the ensemble of networks with all possible structures (but prepared under the same conditions, i.e., temperature, density of cross-links, etc.). Thus, the *structure average* of a quantity over the latter ensemble is equivalent to the *spatial average* of this quantity over the volume of a single network. The averages we calculate are structure averages over the ensemble of different structures and the above equivalence implies that our results can be directly applied to scattering experiments which measure averages over the volume of a single gel with a unique structure.

We begin the calculation of the density correlation functions with the definition of thermal (time) and structure (spatial) averages. Thermal averages for a given network structure (which enters through the value of $n$) are taken with respect to the Gibbs probability distribution

$$\mathscr{P}_n[\delta\rho] \equiv \frac{\exp(-\mathscr{F}_n[\delta\rho]/T)}{\int \mathrm{D}[\delta\rho]\exp(-\mathscr{F}_n[\delta\rho]/T)}, \tag{4.21}$$

where $\mathscr{F}_n[\delta\rho]$ is defined in Eq. (4.18). The thermal average of a functional $A[\delta\rho]$ is denoted by

$$\langle A[\delta\rho]\rangle \equiv \int \mathrm{D}[\delta\rho]A[\delta\rho]\mathscr{P}_n[\delta\rho]\,. \tag{4.22}$$

The structure average of a functional $B[n]$ will be denoted by

$$\overline{B[n]} \equiv \int \mathrm{d}\boldsymbol{S}\mathscr{P}(\boldsymbol{S})B[n(\boldsymbol{S})] = \int \mathrm{D}nB[n]P[n] \equiv \langle B[n]\rangle_n\,, \tag{4.23}$$

where we used Eq. (4.19) to replace the averaging over the structure by averaging with respect to the density distribution in the elastic reference state, $n$. Finally, the complete structure and thermal (spatial and time) average of the functional $C_n[\delta\rho]$ is defined as

$$\overline{\langle C_n[\delta\rho]\rangle} \equiv \int \mathrm{D}nP[n]\int \mathrm{D}[\delta\rho]\mathscr{P}_n[\delta\rho]C_n[\delta\rho]\,. \tag{4.24}$$

### 4.4. Density correlation functions

One of the salient characteristics of gels is the presence of static spatial inhomogeneities of the density. While in liquids the time average of the density fluctuations vanishes ($\langle \delta\rho \rangle = 0$), in polymer gels static spatial density inhomogeneities are always present due to the statistical nature of the process of cross-linking which results in a unique equilibrium density distribution $\rho_q^{eq}$. Straightforward calculation (by Gaussian integration, using the probability distribution defined in Eq. (4.21)) of the thermally averaged Fourier component of the density fluctuations gives the amplitude of this density distribution:

$$\langle \rho_q \rangle = \frac{n_q}{1 + wg_q} = \rho_q^{eq} , \tag{4.25}$$

where the last equality follows from Eq. (4.20). Since every given realization of the network is characterized by a unique equilibrium density profile $\rho^{eq}(\boldsymbol{x}) = \rho + \delta\rho^{eq}(\boldsymbol{x}) = \rho + \int [d\boldsymbol{q}/(2\pi)^3] \times \rho_q^{eq} \exp(i\boldsymbol{q}\cdot\boldsymbol{x})$, the time-averaged density $\langle \rho(\boldsymbol{x}) \rangle$ will fluctuate in space across the network. This phenomenon has been recently detected through the observation of stationary speckle patterns and through the detection of a time-independent component in measurements of the temporal decay of intensity correlations in light scattering from gels [43, 44]. Finally, we note that $\overline{\rho_q^{eq}} \equiv \overline{\langle \rho_q \rangle} = 0$, as expected for an average deviation from the mean density $\rho \equiv N_{tot}/V$.

Using the above equation we can introduce the amplitude of thermal density fluctuations $\delta\rho^{th}(\boldsymbol{x}, t)$ as the deviation of the instantaneous density $\rho(\boldsymbol{x}, t)$ from its equilibrium value,

$$\delta\rho^{th}(\boldsymbol{x}, t) \equiv \rho(\boldsymbol{x}, t) - \rho^{eq}(\boldsymbol{x}) , \tag{4.26}$$

which, according to Eq. (4.25), satisfies $\langle \delta\rho^{th}(\boldsymbol{x}) \rangle = 0$ (we replace time averaging by ensemble averaging). We now proceed to calculate the different density correlators, evaluating Gaussian integrals by the method described in Appendix A.

The correlator of the thermal density fluctuations is given by

$$G_q \equiv \langle \rho_q^{th} \rho_{-q}^{th} \rangle = g_q/(1 + wg_q) . \tag{4.27}$$

The above expression can be rewritten in a form which emphasizes the similarity with the RPA relation of the theory of polymer liquids [23], that gives the effective Hamiltonian of thermal fluctuations ($G_q^{-1}$) as the sum of entropic and excluded volume contributions:

$$G_q^{-1} = g_q^{-1} + w . \tag{4.28}$$

Thus, $g_q$ *can be interpreted as the thermal structure factor of the gel, in the absence of excluded volume interactions* (i.e., in the elastic reference state).

The correlator of the static density inhomogeneities (the Fourier transform of the spatially averaged two-point correlation function $\overline{\delta\rho^{eq}(\boldsymbol{x})\delta\rho^{eq}(\boldsymbol{x}')}$) can be found using the definition (4.25) and Eq. (4.11)

$$C_q \equiv \overline{\rho_q^{eq} \rho_{-q}^{eq}} = v_q/(1 + wg_q)^2 . \tag{4.29}$$

Setting $w = 0$ in the above expression we conclude that $v_q$ *can be interpreted as the spatially averaged (structure averaged) equilibrium density correlator, in the absence of excluded volume interactions* (in the elastic reference state).

Using Eq. (4.26) we arrive at the following expression for the total structure factor, which includes the contributions of both static inhomogeneities and thermal fluctuations and which is a measure of the total deviation of the density from its mean value, $N_{tot}/V$:

$$S_q \equiv \overline{\langle \rho_q \rho_{-q} \rangle} = G_q + C_q \,. \tag{4.30}$$

This structure factor is proportional to the scattered intensity at a wave vector $\boldsymbol{q}$, measured in static scattering experiments.

### 4.5. *Analytical expressions for the correlators*

#### 4.5.1. *Initial state*

An exact (within the RPA) expression for the structure factor can be obtained in the important case of *density fluctuations in the initial undeformed state* of the gel. Note that this case can be obtained from our general results for the final deformed state by making the substitutions $\{\lambda_\alpha = 1\}$, $w = w^{(0)}$ and $T = T^{(0)}$. The symmetry of permutation of all the replicas (since in this case the final state coincides with the state of preparation) leads to drastic simplifications and, as shown in Appendix G, we arrive at the following RPA expression (valid for arbitrary $\boldsymbol{q}$),

$$S_q^{(0)} = 2\rho^{(0)}/(-2/\bar{N} + 2\rho^{(0)}w^{(0)} + a^2\boldsymbol{q}^2) \,. \tag{4.31}$$

The characteristic scale of fluctuations (correlation length), $a(2\rho^{(0)}w^{(0)} - 2/\bar{N})^{-1/2}$, diverges at the cross-link saturation threshold (Eq. (2.8)). We can define the dimensionless network *heterogeneity parameter*

$$X_{RPA} \equiv 1/(\rho^{(0)}w^{(0)}\bar{N} - 1) \,, \tag{4.32}$$

which diverges at the cross-link saturation threshold and goes to a small value away from it (for $\rho^{(0)}w^{(0)}\bar{N} \gg 1$). When the gel is prepared at the saturation threshold, $X_{RPA} \to \infty$, the long wavelength static fluctuations of network density become infinitely large and our RPA approximation for the static density inhomogeneities breaks down.

The physical reason for the increasingly inhomogeneous network density profile as the cross-link saturation threshold is approached, is as follows. At this threshold, nearly all the inter-monomer contacts which are present in a *typical* configuration of the pre-cross-linked polymer chain, are turned into cross-links. The introduction of any further cross-links cannot take place by cross-linking a typical configuration of the polymer (in which the average number of contacts is $\bar{K}$ – see Section 2.2) and the formation of a network with number of cross-links $N_c \geq \bar{K}$ can occur only starting from *atypical* (and therefore highly improbable) configurations of the polymer, in which $K > \bar{K}$. Since the probability of contacts is proportional to the square of the local monomer density, a higher number of contacts will arise in configurations with inhomogeneous density profiles than in those with more uniform density (the gain due to increased number of contacts in the high-density regions overcompensates for the loss due to their decreased number in the

low-density regions). This can be achieved either by increasing the contrast (i.e., the amplitude of density fluctuations), or by increasing the size of the inhomogeneous regions. Since large density gradients are penalized by "surface tension"-type forces, the latter mechanism will be energetically preferable and the dominant contribution will come from configurations characterized by large alternating domains which differ only slightly in monomer concentration (i.e., the amplitude of density fluctuations becomes progressively smaller with the approach to the cross-link saturation threshold). The above physical picture is similar to that of critical phenomena, where the correlation length diverges while the amplitude of the fluctuations goes to zero at the critical point. The predicted increase of the size of the inhomogeneities with degree of cross-linking (with decreasing $\bar{N}$) was observed in light scattering studies [45].

Away from the cross-link saturation threshold, the $2/\bar{N}$ term can be neglected and the predicted scattered intensity from a gel at the state of preparation is identical to that from a solution of disconnected chains at the same density and solvent conditions. Nearly identical scattering from gels and from solutions was reported in some cases [46,47], indicating that the networks were prepared away from the saturation threshold. In other cases, stronger scattering was observed from gels in the state of preparation than from solutions [48,49], apparently because the networks were prepared closer to the cross-link saturation threshold.

It is important to emphasize that the exact (for all $\boldsymbol{q}$) analytical expression for the total structure factor, Eq. (4.31), is obtained as the result of strong interference between the spatial density inhomogeneities and the thermal density fluctuations in the initial undeformed state of the network (the calculation of their separate contributions, for arbitrary $\boldsymbol{q}$, is prohibitively difficult). This interference arises due to the screening of the presence of static inhomogeneities by the thermal fluctuations which "adjust" themselves to the local distribution of the former [50].

We now proceed to discuss analytical results for the RPA density correlation functions in the final deformed state of the gel.

*4.5.2. Final state, long wavelength limit*

Simple analytical formulae for the functions $g_q$ and $v_q$ which enter the expressions (4.27)–(4.30) for the structure factor of the gel in the final state, can be obtained in the continuum limit $\boldsymbol{q} \to 0$ (these formulae are derived in Appendices E–G).

The continuum limit of the correlator of thermal fluctuations in the elastic reference state, $g_q$, is given by

$$g_{q\to 0} = 2\rho\bar{N}\boldsymbol{q}^2/(\lambda \star \boldsymbol{q})^2 \,. \tag{4.33}$$

Note that this function retains its angular dependence (associated with the direction of the wave vector $\boldsymbol{q}$) for anisotropic deformations, even in the limit $\boldsymbol{q} \to 0$. The presence of the $\boldsymbol{q}^2/(\lambda \star \boldsymbol{q})^2$ term is related the fact that $g_{q\to 0}$ is a response function which governs thermal fluctuations about an anisotropic deformed equilibrium state of the network (in the elastic reference state). It can be shown that the elastic moduli of such a deformed network depend on the deformation and are anisotropic and that this anisotropy results in the above dependence. This will be done in Section 6, where we analyze the connection between the long wavelength limit of the present theory and the continuum theory of elasticity of gels.

We now consider the correlator of the static inhomogeneities in the elastic reference state, $v_q$. In the long wavelength limit $v_q$ approaches a constant value:

$$v_{q\to 0} = \lim_{q\to 0} \overline{n_q n_{-q}} = \rho\bar{N}(6 + 9/(w^{(0)}\rho^{(0)}\bar{N} - 1)) , \tag{4.34}$$

where $\rho$ is the density of monomers in the *final* deformed state of the network. The quantity $v_{q\to 0}$ diverges at the cross-link saturation threshold, $\bar{N}^{\min} = 1/(w^{(0)}\rho^{(0)})$, at which the characteristic size of static spatial inhomogeneities of cross-link (and hence of monomer) density diverges. We would like to emphasize that the finite value of $v_{q\to 0}$ (away from the saturation threshold) does not mean that there are frozen clusters of macroscopic dimensions, but is a trivial consequence of the Fourier representation (*all* length scales contribute to the Fourier transform of the density in the limit $q \to 0$).

We can now estimate the amplitude of static density inhomogeneities and check the applicability of RPA. Away from the saturation threshold one can neglect the second term in the square brackets in Eq. (4.34) and write

$$\overline{(\delta n(x))^2} = \int \frac{dq}{(2\pi)^3} v_q \approx \frac{\rho\bar{N}}{(a\bar{N}^{1/2})^3} , \tag{4.35}$$

where we have used the fact that there are no static density inhomogeneities on length scales smaller than the mesh size $a\bar{N}^{1/2}$. The RPA assumption that the amplitude of inhomogeneities is much smaller than the mean density $\rho$, corresponds to the condition

$$\rho a^3 \bar{N}^{1/2} \gg 1 , \tag{4.36}$$

which is equivalent to the assumption that the volume of an average chain between cross-links is permeated by many other chains. In the following we will assume that this condition is always satisfied and that static inhomogeneities are correctly described in the RPA approximation.

It is interesting to consider the limiting case of cross-linking in the melt (strictly speaking, this case is outside the domain of applicability of our model since excluded volume in a melt cannot be described by a second virial coefficient). In this limit $w^{(0)} \sim 1/\rho^{(0)} \sim a^3$ and $v_{q\to 0} \simeq 6\rho\bar{N}$. The finite value of $v_{q\to 0}$ tells us that even though there are no density fluctuations in the melt, there are still finite inhomogeneities of the network structure which can be revealed upon swelling.

An explicit form for the correlators in the *final deformed state* of the network, can be given in the continuum limit ($q \to 0$), using expressions (4.33) and (4.34) for the functions $g_q$ and $v_q$ in Eqs. (4.27) and (4.29):

$$G_{q\to 0} = \frac{2\rho\bar{N}}{(\lambda \star q/|q|)^2 + 2w\rho\bar{N}} , \tag{4.37}$$

$$C_{q\to 0} = \frac{(\lambda \star q/|q|)^4 \rho\bar{N}(6 + 9/(w^{(0)}\rho^{(0)}\bar{N} - 1))}{[(\lambda \star q/|q|)^2 + 2w\rho\bar{N}]^2} . \tag{4.38}$$

Several general comments can be made regarding the properties of the RPA correlators in the continuum limit:

1. For anisotropic deformations both correlators have an angular singularity associated with the direction of the scattering wave vector $q$, even in the limit $q \to 0$. In the important case of

uniaxial deformations, *thermal fluctuations are suppressed along the extension axis and enhanced normal to it and static inhomogeneities exhibit the reverse behavior*. The enhancement of scattering along the stretching axis due to static inhomogeneities ($C_{q\to 0}$) has been predicted theoretically by Bastide et al. [51] and by Onuki [52]. It was observed in static small angle neutron scattering [12] and light scattering [13] from gels and is known as the *butterfly effect*. The fact that the anisotropy appears already is the limit $q \to 0$, is in agreement with experimental observations of this effect on the longest wavelengths probed by small angle neutron and light scattering. Suppression of thermal fluctuations along the stretching direction was predicted in Ref. [52] and observed (indirectly) in dynamic light scattering experiments [14] which monitored the decay rate of thermal density fluctuations (proportional to $G^{-1}_{q\to 0}$) in a stretched gel.

2. The only explicit dependence on the conditions of preparation of the gel (apart from the trivial dependence on the density of cross-links) appears in the correlator of the static inhomogeneities $C_{q\to 0}$ which diverges at the cross-link saturation threshold. The control parameter which measures the "strength" of these inhomogeneities is the *heterogeneity parameter*, $X_{\mathrm{RPA}} = (w^{(0)}\rho^{(0)}\bar{N} - 1)^{-1}$.

3. Static inhomogeneities are more sensitive than the thermal ones to deformation and swelling. Away from the $\Theta$-point ($w\rho\bar{N} \gg 1$), $G_{q\to 0} \sim 1/w$ is nearly independent of the deformation and of the density of cross-links. The intensity of scattering from static inhomogeneities, $C_{q\to 0} \sim (\lambda \star q/|q|)^4/(w^2\rho\bar{N})$, increases with the degree of cross-linking (this prediction is confirmed by experiments [48,49,53]). When the gel is uniformly swollen ($\lambda \sim 1/\rho^{1/3}$), scattering from static inhomogeneities increases with swelling (the RPA prediction of $1/\rho^{7/4}$ dependence will be modified for gels in good solvents – see Section 5.4.2). In uniaxial extension experiments it grows rapidly with the deformation ratio in the stretching direction (as $\lambda^4$) and decreases normal to it as ($1/\lambda^2$). In the vicinity of the $\Theta$-point, the intensity of thermal fluctuations $G_{q\to 0}$ decreases as $1/\lambda^2$ along the stretching direction (and increases as $\lambda$ normal to it) and $C_{q\to 0}$ approaches a constant (independent of $\lambda$).

*4.5.3. Final state, mesoscopic range (finite $q$)*

The explicit expressions for the density correlators, Eqs. (4.37) and (4.38), are valid only in the continuum limit ($q \to 0$). In order to relate to scattering experiments which probe the mesoscopic range of length scales (50–5000 Å), we have to include terms of higher order in $q$. This can be done by calculating the correlators in the elastic reference state $g_q$ and $v_q$ (Appendices E and F), to order $a^2\bar{N}q^2$. We first consider the thermal correlator $g_q$.

In the long wavelength limit $a^2\bar{N}q^2 \ll 1$, the thermal correlator $g_q$ of the elastic reference state is given by (to order $q^2$)

$$g_q = [2\rho\bar{N}/(\lambda \star \check{q})^2][1 + \alpha(\check{q})Q^2] , \tag{4.39}$$

where $\check{q} = q/|q|$ is the unit vector in the direction of the wave vector $q$, $Q$ is the dimensionless wave vector, defined as $Q^2 \equiv a^2\bar{N}q^2$ and

$$\alpha(\check{q}) = 2I_1[(\lambda \star \check{q})^2 - 1] + I_2(\lambda \star \check{q})^2 , \tag{4.40}$$

with the constants $I_1 \simeq 0.524$ and $I_2 \simeq 0.033$.

In the short wavelength limit $a^2\bar{N}q^2 \gg 1$, we get (to order $q^{-4}$)

$$g_q = (2\rho\bar{N}/Q^2)(1 + I_3/Q^2) , \tag{4.41}$$

where $I_3 \simeq 1.395$. The leading contribution ($\propto q^{-2}$) to this function is identical to that of a polymer solution.

We now present the long and short wavelength limits of the correlator of static density inhomogeneities $v_q$. We can write it, in general, in the form

$$v_q = 2\rho\bar{N}A_q + B_q S^{(0)}_{\lambda\star q}/\lambda_x\lambda_y\lambda_z \,, \tag{4.42}$$

where asymptotic expressions for the functions $A_q$ and $B_q$ were derived in Appendix G

$$A_q = \begin{cases} 3 - \{1 - 4I_1[(\lambda\star\check{q})^2 - 1] - 5I_2(\lambda\star\check{q})^2\}Q^2 & \text{for } Q \ll 1 \,, \\ (2 - I_3)^2 Q^{-4} & \text{for } Q \gg 1 \end{cases} \tag{4.43}$$

and

$$B_q = \begin{cases} 9 - 6\{1 - 4I_1[(\lambda\star\check{q})^2 - 1] - 4I_2(\lambda\star\check{q})^2\}Q^2 & \text{for } Q \ll 1 \,, \\ (2 - I_3)^4 Q^{-4} & \text{for } Q \gg 1 \end{cases} . \tag{4.44}$$

All the dependence on preparation conditions in Eq. (4.42) enters through the function $S^{(0)}_{\lambda\star q}$, defined by substituting $q \to \lambda\star q$ into Eq. (4.31).

Since the above RPA expressions for the structure factors cannot be directly applied to gels in good solvents (in which thermal fluctuations are strong), we will not analyze them any further here. In Section 5 we will show how these expressions can be adapted to the physically important case of gels in good solvents, by an appropriate renormalization of the RPA parameters.

*4.5.4. Spinodal decomposition in poor solvent*

Inspection of Eq. (4.40) shows that for $\alpha(\check{q}) > 0$, the thermal correlator $g_q$ increases linearly with $q^2$ for small wavelengths (Eq. (4.39)) and decreases as $q^{-2}$ in the short wavelength limit (Eq. (4.41)). This leads to the totally unexpected conclusion that the *thermal density correlation function of the elastic reference state has a maximum at some* wave vector $q = q_*$, the presence of which is a familiar feature of systems which exhibit microphase separation (such as diblock copolymers)! Since the maximum appears only for $\alpha(\check{q}) > 0$, it is present in the undeformed state ($\{\lambda_\alpha = 1\}$), under conditions of uniform swelling ($\{\lambda_z > 1\}$) and in uniaxially stretched swollen gels, for wave vectors along directions for which $(\lambda\star\check{q})^2 \geqslant 1$ (see Eq. (4.40)). The point $\alpha(\check{q}) = 0$ at which a maximum at a finite value of $q$ first appears, corresponds to $(\lambda\star\check{q})^2 \simeq 0.97$ (for smaller values it is located at $q_* = 0$).

What can we say about this maximum? Since the only length scale in our problem is the mesh size, we speculate that the maximum is achieved for wave vectors of the order of the inverse mesh size

$$1/q_* \sim a\bar{N}^{1/2} \tag{4.45}$$

and that it is shifted to $q_* = 0$ for $\alpha(\check{q}) \leqslant 0$. Unfortunately, wave vectors of such magnitude lie outside the region in which our asymptotic expressions for $g_q$ apply and therefore our results cannot be used to analyze the dependence of the maximum on the thermodynamic parameters.

What is the physical origin of this maximum? Using the equipartition theorem we conclude that $(1/2)Tg_q^{-1}\rho^{\text{th}}_q\rho^{\text{th}}_{-q}$ is the free energy cost of creating a thermal density fluctuation $\rho^{\text{th}}_q$ at a wave

vector $q$ around the spatially inhomogeneous equilibrium distribution $n_q$ (the elastic reference state). Although there is no ordering on any scale in the network, there is a characteristic wave vector associated with the static density inhomogeneities which is of the order of the inverse mesh size. The existence of a characteristic wave vector implies that the situation is quite similar to that arising in the ordered lamellar state of diblock copolymers, in which there is also a characteristic wave vector associated with the wavelength of the modulation (the analogy is quite close since in there is also no true long-range order in the lamellar state). In the case of diblock copolymers it was shown that the fluctuation energy about the modulated state has a minimum at a wave vector $q = q_*$ corresponding to the inverse wavelength of the pattern [54] and similar considerations can be applied to our system. Note that the observation that the maximum at finite $q$ disappears for $\alpha(\check{q}) \leqslant 0$ (in this regime $g_q$ has only a broad maximum at $q = 0$) is related to the fact that the density distribution in the reference state becomes homogeneous under compression (i.e., the contrast between dense and dilute regions disappears).

Can the maximum at $q = q_*$ be observed in scattering experiments which probe the thermal (time-dependent) contribution to the scattering intensity? Substitution into Eq. (4.27) shows that in the good solvent, small degree of swelling regime ($w\rho\bar{N} \gg 1$), the thermal structure factor $G_q$ becomes independent of $g_q$ and we conclude that a peak in thermal scattering (its position, $q_*$, is independent of the quality of solvent) can be observed either at large swelling degrees or in the vicinity of the $\Theta$-point.

Let us now consider a gel in a poor solvent ($w < 0$). Experimentally, macroscopic collapse can be prevented by fixing the volume of the gel (the way it is done in our calculation), or by performing the scattering experiment shortly upon the quench to poor solvent conditions, before the gel has the time to expel the solvent (since this happens by cooperative diffusion, collapse may take hours or days, depending on the volume of the gel). If the experiment is done by first deforming the gel in the good solvent and then (under conditions of constant deformation) bringing it into the poor solvent regime (e.g., by varying the temperature), the point at which thermal scattering intensity diverges defines the $q$-dependent spinodal of the gel:

$$1 + w_{sp} g_q = 0 . \tag{4.46}$$

Clearly, this condition is first satisfied at the maximum of $g_q$ (at $q = q_*$). Furthermore, since $g_q$ is largest in the direction of minimal extension ($\lambda_{min}$), the spinodal is first reached for wave vectors in this direction. For $\lambda_{min} < 0.97$, the spinodal occurs at $q_* = 0$ and corresponds to *macrophase* separation (the gel will expel the solvent and collapse if we remove the fixed volume constraint). For $\lambda_{min} > 0.97$, the spinodal occurs at a finite wave vector $q_*$, of the order of the inverse mesh size, at $w_{sp}$ given by Eq. (4.46). This corresponds to *microphase* separation, in the process of which solvent is expelled from the denser into the more "dilute" regions of the inhomogeneous static density profile (the characteristic size of such regions is of the order of the average mesh size). A peak at a finite $q$ value was observed in small angle neutron scattering from weakly charged gels but was attributed to electrostatic effects which are beyond the scope of this work [55].

The case $\lambda_{min} \simeq 0.97$ ($\alpha = 0$ in Eq. (4.40)) corresponds to the *Lifshitz point* [56] at which $q_* \to 0$.

In principle, we can now insert our RPA expressions for $g_q$ and $v_q$ into Eqs. (4.27)–(4.30), calculate the total structure factor as a function of the various parameters and compare with the results of experiments on light and SANS scattering from stretched, swollen gels. However, although our RPA results give a qualitatively correct picture of the effects of deformation and

swelling on static inhomogeneities and thermal fluctuations, quantitative comparison with experiments on gels swollen in good solvents is not possible since, in the derivation, we have assumed that thermal fluctuations are small. The above assumption is not valid for semi-dilute solutions and gels swollen in good solvents in which thermal fluctuations on length scales smaller than the "blob" size are large. This well-known problem received much attention in the context of semi-dilute solutions and several methods (e.g., renormalization group [27] and scaling [3]) were developed to deal with it. These methods have to be adapted to the problem of gels in a good solvent where simultaneous renormalization of the phenomenological parameters due to small scale fluctuations in both the initial and the final state of the gel is necessary. Such a scheme will be presented in Section 5. Instead of proceeding directly to gels in good low molecular weight solvents, we first apply our RPA results to the related problem of a gel in a polymeric solvent, where strong fluctuation effects are expected to be suppressed by screening. The replacement of a low-molecular weight solvent by a polymeric one, requires some modifications which will be discussed in the following.

### *4.6. Gels in polymeric solvents*

Consider a system which consists of free polymer chains in a network (Fig. 4.1) permeated by (small molecular weight) solvent, where the free chains have an arbitrary degree of polymerization, $L$, but the same chemical structure as the network (athermal case). The latter assumption is relaxed in the next subsection where we study the segregation of the free chains from the gel. We assume that the free chains have an initial monomer concentration $c^{(0)}$ and that $w^{(0)}c^{(0)}L \gg 1$ (this condition corresponds to neglecting the density fluctuations of the polymeric solvent in the initial state of the gel). In the final state, the network is, in general, stretched and swollen, with corresponding concentrations of network and free chain monomers $\rho$ and $c$, respectively, and with excluded volume parameter $w$ (for simplicity, this parameter is taken to be the same for both the network and the free chain monomers). We further assume that the free chains are confined to the volume of the gel and do not leave it following the deformation (this is usually the case in experiments [53]).

We proceed to construct the free energy of the network plus the free chains system in the spirit of the RPA method [3], by introducing the elastic entropy of the latter into the free energy, Eq. (4.18). The other, trivial, change is to replace the partial monomer density of the network by the total

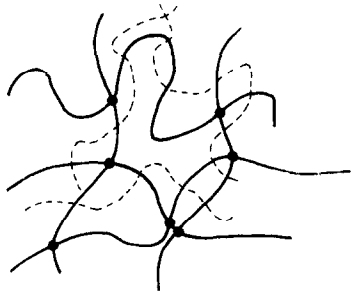

Fig. 4.1. Schematic drawing of the network. Free chains dissolved in the gel are shown by broken lines.

density due to both polymeric components. The resulting free energy is given by

$$\frac{\mathscr{F}_n[\rho,c]}{T}=\frac{1}{2}\int\frac{d\boldsymbol{q}}{(2\pi)^3}\left[\frac{(\rho_q-n_q)(\rho_{-q}-n_{-q})}{g_q}+\frac{c_q c_{-q}}{s_q}+w(\rho_q+c_q)(\rho_{-q}+c_{-q})\right], \tag{4.47}$$

where

$$s_q=cL/(1+a^2Lq^2/4) \tag{4.48}$$

is the (approximate) Debye structure factor of a free chain without excluded volume (note, that our $a^2$ differs by a factor of 3 from the usual definition [23]). The partition function of a network with a given structure (represented by $n$) is defined by

$$\int D[\delta c]\int D[\delta\rho]\exp\left(-\frac{\mathscr{F}_n[\rho,c]}{T}\right). \tag{4.49}$$

We now show that the free energy of a network permeated by a polymeric solvent is equivalent to the previously derived one (Eq. (4.18)), where we replace $w^{(0)}$ and $w$ by $q$-dependent virial coefficients which are determined by the properties of the free chains (e.g., $c$ and $L$). Since the free energy in Eq. (4.47) describes an arbitrary state of the gel, it can be applied to the initial state, by replacing all quantities by their values in this state (by adding a superscript $^{(0)}$).

In order to calculate the effective virial coefficient in the state of preparation of the gel, we first perform the $\delta c^{(0)}$ integration in the initial state analog of Eq. (4.49). This gives a free energy which depends on $n$ and $\rho^{(0)}$

$$\frac{\mathscr{F}_n^{(0)}[\rho^{(0)}]}{T^{(0)}}=\frac{1}{2}\int\frac{d\boldsymbol{q}}{(2\pi)^3}\left[\frac{(\rho_q^{(0)}-n_q)(\rho_{-q}^{(0)}-n_{-q})}{g_q}+\frac{w^{(0)}\rho_q^{(0)}\rho_{-q}^{(0)}}{1+w^{(0)}s_q^{(0)}}\right] \tag{4.50}$$

and we conclude that the effective virial coefficient in the initial state is given by

$$w_q^{(0)}\equiv w^{(0)}/(1+w^{(0)}s_q^{(0)})\,. \tag{4.51}$$

The factor $1+w^{(0)}s_q^{(0)}$ in the denominator of this expression reflects the screening of excluded volume interactions between network monomers due to the presence of free chains [3]. In the assumed limit, $w^{(0)}c^{(0)}L\gg 1$, the fluctuations of total density $\rho_q^{(0)}+c_q^{(0)}=\rho_q^{(0)}/(1+w^{(0)}s_q^{(0)})$, are strongly suppressed by screening and we obtain

$$w_q^{(0)}=1/s_q^{(0)}\,. \tag{4.52}$$

Since we will eventually consider only the density fluctuations of the polymeric solvent in the final state of the gel, we return to Eq. (4.49) and integrate over the density fluctuations of the network, $\delta\rho$. This yields the effective free energy functional which depends on the density of the free polymer chains and the structure of the network,

$$\frac{\mathscr{F}_n[c]}{T}=\frac{1}{2}\int\frac{d\boldsymbol{q}}{(2\pi)^3}\left[\frac{(c_q+n_q)(c_{-q}+n_{-q})}{g_q+1/w}+\frac{c_q c_{-q}}{s_q}\right]. \tag{4.53}$$

In the following we assume that $w\rho\bar{N} \gg 1$, in which case we can neglect the $1/w$ term in the denominator of Eq. (4.53). This is again equivalent to assuming that fluctuations of the total density $\rho_q + c_q = (c_q + n_q)/(1 + ws_q)$ are suppressed due to strong screening, a condition which guarantees the applicability of the RPA to our problem. Comparing Eq. (4.53) with Eq. (4.18), we conclude that the free energy of a network permeated by polymeric solvent is formally identical to that of a network of Gaussian chains, provided that we replace $w$ with the $q$-dependent effective virial coefficient $w_q = 1/s_q$ in Eq. (4.18). Since we limit ourselves to the case of small fluctuations of the density of the free chains, we need to impose the condition that there are many chains of that type in the volume occupied by one of them [3], i.e. $R_L^3 c/L \gg 1$, where $R_L = aL^{1/2}/2$ is the size of the free chain.

An exact (within the RPA) result for the structure factor valid for all $q$, can be obtained for the total structure factor under preparation conditions (i.e., an undeformed and unswollen network, $\lambda_x = 1$), by substituting $w^{(0)} \to 1/s_q^{(0)}$ into Eq. (4.31). This yields the Ornstein–Zernicke form

$$S_q^{(0)} = \rho^{(0)}\bar{N}X/[1 + (\xi^{(0)}q)^2] , \tag{4.54}$$

where the correlation length is defined by

$$(\xi^{(0)})^2 \equiv (a^2\bar{N}X/2)(1 + \rho^{(0)}/2c^{(0)}) \tag{4.55}$$

and where we defined the dimensionless *effective heterogeneity parameter* (the reason for this name will be clarified later on):

$$X \equiv ((\rho^{(0)}\bar{N}/c^{(0)}L) - 1)^{-1} . \tag{4.56}$$

Note that the parameter $X$ can be varied by changing the concentration, the length of the chains and the degree of cross-linking of the network, but is not affected by swelling (we assume that the labelled chains are trapped in the network throughout the process of swelling and, therefore, $\rho^{(0)}/c^{(0)} = \rho/c$). The cross-link saturation threshold for the network with the free chains, is given by $X \to \infty$ (inspection of Eqs. (4.52) and (4.48) shows that the RPA cross-link saturation threshold for a gel swollen by a low molecular weight solvent, Eq. (3.41), should be replaced by $\rho^{(0)}\bar{N}/s_0^{(0)} = \rho^{(0)}\bar{N}/c^{(0)}L = 1$ for a gel swollen by free polymer chains).

Near the cross-link saturation threshold $\xi^{(0)}$ diverges as $X^{1/2}$ and the intensity at $q \to 0$ diverges as $X$. Away from the cross-link saturation threshold, $(\xi^{(0)})^2 \to R_L^2(1 + 2c^{(0)}/\rho^{(0)})$ and the structure factor reduces to

$$S_q^{(0)}|_{X\to 0} \approx \frac{c^{(0)}L}{1 + R_L^2(1 + 2c^{(0)}/\rho^{(0)})q^2} , \tag{4.57}$$

i.e., the only dependence on network parameters comes through the initial density $\rho^{(0)}$.

The expression coincides (in the limit $X \to 0$) with the structure factor of a solution of chains of lengths $L$ (labelled monodisperse chains) and $\bar{N}$, of concentrations $c^{(0)}$ and $\rho^{(0)}$, respectively. Strictly speaking, the above statement is correct only if we assume that the distribution of the latter chain lengths is the same as in the network. It can be shown that, in the case of random cross-linking in the solution (or in the melt), the resulting distribution of chain lengths $f(N)$ is exponential [2], i.e.,

$$f(N) = (1/\bar{N})\exp(-N/\bar{N}) . \tag{4.58}$$

Although creating such a distribution may be non-trivial experimentally, it is obvious that a meaningful comparison of the scattering from free chains in a network with that from a solution,

must be performed under otherwise identical conditions. More generally, in the case of a solution with an arbitrary distribution of chains of average length $\bar{N}$, one has to replace $2c^{(0)}/\rho^{(0)} \to \eta c^{(0)}/\rho^{(0)}$ in the denominator of the structure factor (Eq. (4.57)) where the numerical factor $\eta$ is of order unity and can be calculated from the known molecular weight distribution [3]. Note that for $c^{(0)}/\rho^{(0)} \ll 1$ (this corresponds to the experimentally studied range of parameters [47, 57]), this factor drops out and the scattering from the gel in the state of preparation reduces exactly to that from an equivalent solution, independent of the molecular weight distribution. Since experiments report nearly identical scattering from both systems [47, 57] (in the absence of swelling or deformation) this suggests that the gels were prepared away from the cross-link saturation threshold (i.e., $X \leq 1$).

We now consider the case of a deformed network with free labelled chains inside. An explicit expression for the correlator $\overline{\langle c_q c_{-q}\rangle}$ can be derived by making the substitutions $1/s_q^{(0)}$ and $1/s_q$ instead of $w^{(0)}$ and $w$, in the RPA correlator of a gel in a small-molecule solvent obtained in the preceding subsection. The total structure factor can be represented in the form (using Eq. (4.42)):

$$S_q = [g_q/(1 + s_q^{-1} g_q)] + [1/(1 + s_q^{-1} g_q)^2][2\rho\bar{N}A_q + B_q S^{(0)}_{\lambda\star q}/\lambda_x\lambda_y\lambda_z] , \tag{4.59}$$

where the single free chain structure factor $s_q$ is defined in Eq. (4.48) and $S^{(0)}_{\lambda\star q}$ can be obtained by substituting $\boldsymbol{q} \to \lambda\star\boldsymbol{q}$ into the expression for the structure factor in the state of preparation, Eq. (4.54). Exact asymptotic expressions for the functions $g_q$, $A_q$ and $B_q$ have been calculated in the previous subsection.

We now introduce the reference state of a solution (blend) of free chains (polymers of length $\bar{N}$ and concentration $\rho$ and polymers of length $L$ and concentration $c$). Assuming the same concentrations as in the case of a network permeated by free chains and using the RPA, we obtain

$$S_q^{\mathrm{ref}} \equiv \langle c_q c_{-q}\rangle_{\mathrm{ref}} = \frac{2\rho\bar{N}}{1 + 2(\rho\bar{N}/cL)(1 + R_L^2\boldsymbol{q}^2)} . \tag{4.60}$$

Although the expressions for the scattering from free labelled chains in a network for arbitrary $\lambda_\alpha$ and $R_L^2\boldsymbol{q}^2$ are quite complicated, in the limit $\boldsymbol{q}^2 \gg \max\{(a^2\bar{N})^{-1}, R_L^{-2}\}$ the scattering becomes independent of $\lambda_\alpha$ and reduces to the corresponding limiting scattering from a solution of free chains, Eq. (4.48),

$$S_q \sim 4c/a^2\boldsymbol{q}^2 . \tag{4.61}$$

This behavior was observed by neutron scattering experiments [53].

*4.6.1. Isotropic swelling*

In order to understand the physical phenomena described by Eq. (4.59), we first consider the case of isotropic swelling, $\rho^{(0)} \to \rho$, starting from the state of preparation. The total structure factor is a function of the dimensionless parameters $X$ and the swelling degree $Q_{\mathrm{prep}} \equiv \rho^{(0)}/\rho$ (defined with respect to the state of preparation), since, in the case of isotropic swelling, $\lambda_\alpha = Q_{\mathrm{prep}}^{1/3}$. In Fig. 4.2 we present the dependence of the total scattered intensity at $\boldsymbol{q} = 0$, on the degree of swelling, for several values of $X$. The scattering increases monotonically with the degree of swelling (as was observed experimentally [53]), and grows dramatically with the approach to the cross-link saturation threshold, $X \to \infty$ (it approaches that from the reference solution of free chains for $X \to 0$). From

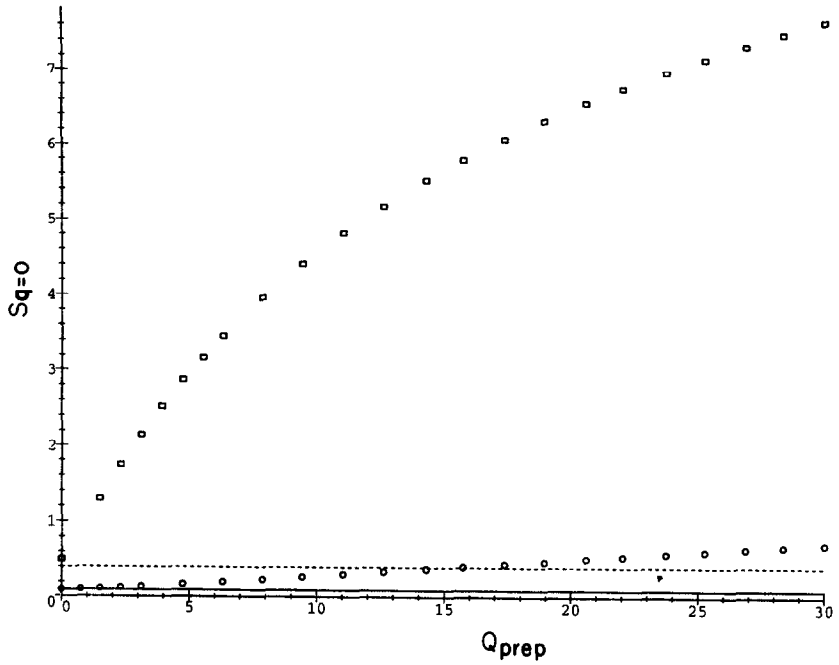


Fig. 4.2. The scattered intensity at $q = 0$ (normalized by $\rho\bar{N}$), as a function of the swelling degree $Q_{\text{prep}}$ with respect to preparation conditions (isotropic swelling), for $X = 0.1$ (circles) and 1 (squares). The $q = 0$ values for the corresponding reference solutions are given by the solid and the dashed lines, respectively.

inspection of Eq. (4.59) we conclude that the important quantity in the long wavelength limit is $Q_{\text{prep}}^{2/3}X/(1 + X)$. For small values of this parameter, the thermal scattering is practically independent of the degree of swelling while the scattering from static inhomogeneities increases as $Q_{\text{prep}}^{4/3}$. Although the range of $Q_{\text{prep}}^{2/3}X/(1 + X) \gg 1$ may be difficult to realize experimentally, we note that in this limit thermal scattering is suppressed (as $(1 + X)/XQ_{\text{prep}}^{2/3}$) and the scattered signal from static inhomogeneities approaches a swelling-independent constant.

We now turn to study the $q$-dependence of the structure factors. We consider only the long wavelength range ($R_L|q| \leq 1$; $N \ll L$), for which we have exact analytical expressions for the structure factors (the second condition ensures that the structure factors are monotonically decreasing functions of $q^2$). In Fig. 4.3 we compare the $q$ dependence of the full structure factor with that of the thermal part, for $X = 0.5$, $Q_{\text{prep}} = 10$ and $p \equiv 2\bar{N}/L = 0.1$. The scattered intensity from the reference solution (valid for all $q$) is also shown for comparison. We note that the thermal scattering from the chains in the gel is weaker than that in the reference solution and that the scattering from the static inhomogeneities dominates the signal (the effect increases with the degree of swelling).

We conclude that the observation of enhanced scattering from a swollen gel permeated by free labelled chains, compared to that from an equivalent solution of un-cross-linked chains, reflects the presence of static density heterogeneities in the network. These inhomogeneities affect the scattering through their screening effect on the interactions between the labelled monomers. This suggests that the effect of swelling on the scattering from the labelled chains is a *collective effect* which

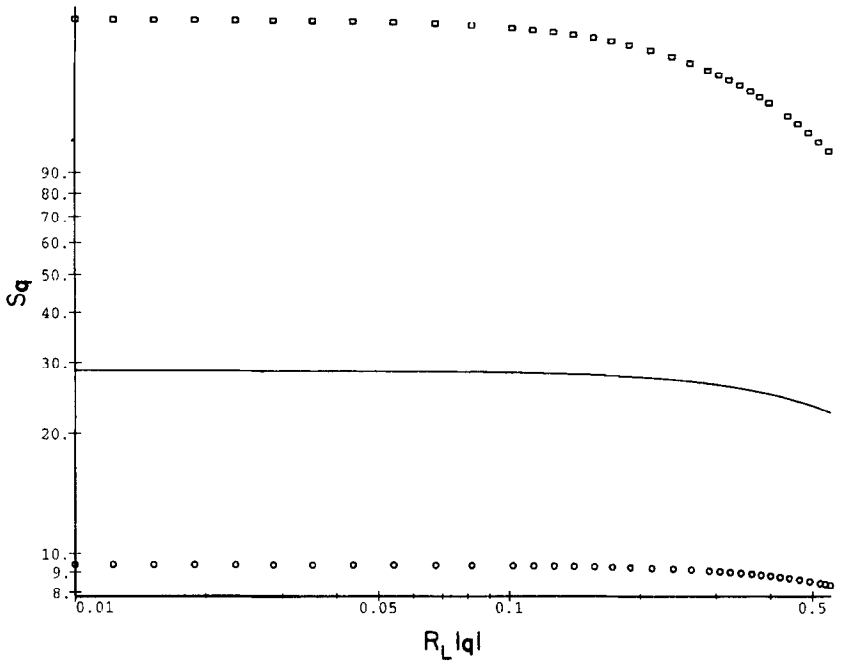


Fig. 4.3. Log–log plots of the full (squares) and the thermal (circles) structure factors (normalized by $\rho\bar{N}/100$) as a function of $R_L|\boldsymbol{q}|$, for the case of isotropic swelling. The parameters are $X = 0.5$, $Q_{\text{prep}} = 10$ and $p \equiv 2\bar{N}/L = 0.1$. The structure factor of the reference solution (solid line) is shown for comparison.

vanishes in the limit of vanishing concentration of these chains. Indeed, for fixed network density $\rho$, the limit $c^{(0)} \to 0$ corresponds to $X \to 0$, in which case $S_q \to s_q$ in Eq. (4.59), i.e., we recover the scattering from undeformed and non-interacting chains. This also shows that the deformation (i.e., swelling) of the network does not induce significant deformation of individual labelled chains and proves the collective origin of the enhanced scattering phenomenon. It is important to emphasize that the scattering off the free chains probes network heterogeneities only *indirectly*, through their effect on the local density of the free chains and that $X$ is an *effective* heterogeneity parameter which changes both with network structure and with the concentration and the length of the free chains.

*4.6.2. Uniaxial extension*

We consider the case of a network swollen in a good solvent (with degree of swelling $Q_{\text{prep}}$) and subsequently stretched along the $z$-axis, by a stretching ratio $\alpha$. We assume that the volume of the gel is not changed by the stretching and that the labelled chains remain trapped inside the network. In this case the deformation ratios $\lambda$ (which are affected by both the swelling and the stretching) are given by

$$\lambda_z = Q_{\text{prep}}^{1/3}\alpha\,, \qquad \lambda_x = \lambda_y = Q_{\text{prep}}^{1/3}\alpha^{-1/2}\,. \tag{4.62}$$

In Fig. 4.4 we present a log–log plot of the scattered intensities $S_q^{\parallel}$ and $S_q^{\perp}$ as a function of $R_L|\boldsymbol{q}|$ for $\alpha = 1.5$ (the structure factors for the unstretched gel and for the reference solution are included for comparison), with $X = 0.1$ and $Q_{\text{prep}} = 1$ (unswollen case). The scattered intensity is always

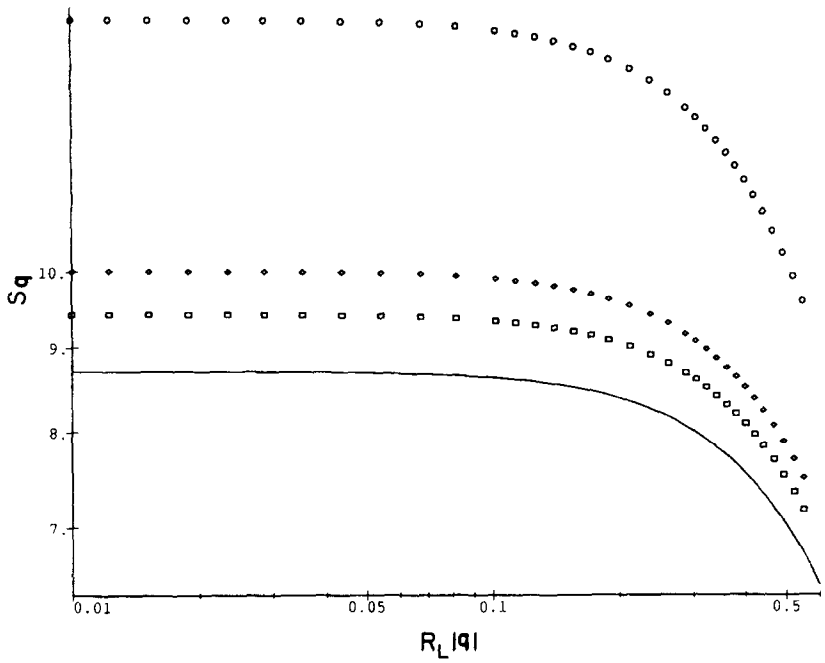


Fig. 4.4. Log–log plot of the scattered intensities in the direction of elongation (circles) and normal to it (squares) as a function of $R_L|\boldsymbol{q}|$, for $\alpha = 1.5$ (uniaxial extension), $X = 0.1$, $Q_{prep} = 1$ and $p = 0.1$ (in units of $\rho\bar{N}/100$). The structure factor of the undeformed gel (diamonds) and for the reference solution (solid line) are also shown.

enhanced along the stretching axis and suppressed normal to it, both effects increasing with $\alpha$ (the enhancement effect is much more pronounced than the suppression) [17, 18, 53]. The lines are drawn only in the region $R_L|\boldsymbol{q}| < 1$, where our exact (within the RPA) results for the structure factor apply.

In Figs. 4.5 and 4.6, the scattered intensities along and normal to the stretching direction, respectively, are plotted (on a log–log plot) versus $R_L|\boldsymbol{q}|$ with $Q_{\text{prep}} = 10$, $X = 0.25$ and $p = 0.1$, for several deformation ratios in the experimentally accessible range ($1 \leq \alpha \leq 2$).

In Fig. 4.7, the scattered intensities in the parallel and the perpendicular directions, at $\boldsymbol{q} = 0$, are plotted as a function of $X$, for the case $Q_{\text{prep}} = 10$, and $\alpha = 1.5$ (the $\boldsymbol{q} = 0$ structure factor of the undeformed network is included for comparison). The intensity increases with the approach to the cross-link saturation threshold ($X \gg 1$), and the effect is quite dramatic for $S^{\parallel}$. The latter observation suggests that the presence of static inhomogeneities has a strong effect on the scattering along the axis of stretching, even for rather small deformations ($\alpha \to 1$).

In Fig. 4.8 we plot the correlation lengths along and normal to the stretching axis as a function of $\alpha$, for $Q_{\text{prep}} = 10$ and $X = 0.25$, where the correlation lengths are defined as

$$\xi_{\parallel}^2 = -\left.\frac{\partial \ln S_{\boldsymbol{q}}^{\parallel}}{\partial \boldsymbol{q}^2}\right|_{\boldsymbol{q}=0} \quad \text{and} \quad \xi_{\perp}^2 = -\left.\frac{\partial \ln S_{\boldsymbol{q}}^{\perp}}{\partial \boldsymbol{q}^2}\right|_{\boldsymbol{q}=0}. \tag{4.63}$$

In Fig. 4.9 we present a contour plot (isointensity lines) of the scattered intensity in the $q_{\parallel}, q_{\perp}$ plane, for uniaxial stretching ($\alpha = 1.2$), with $Q_{\text{prep}} = 10$, $X = 0.25$ and $p = 0.1$. The butterfly pattern

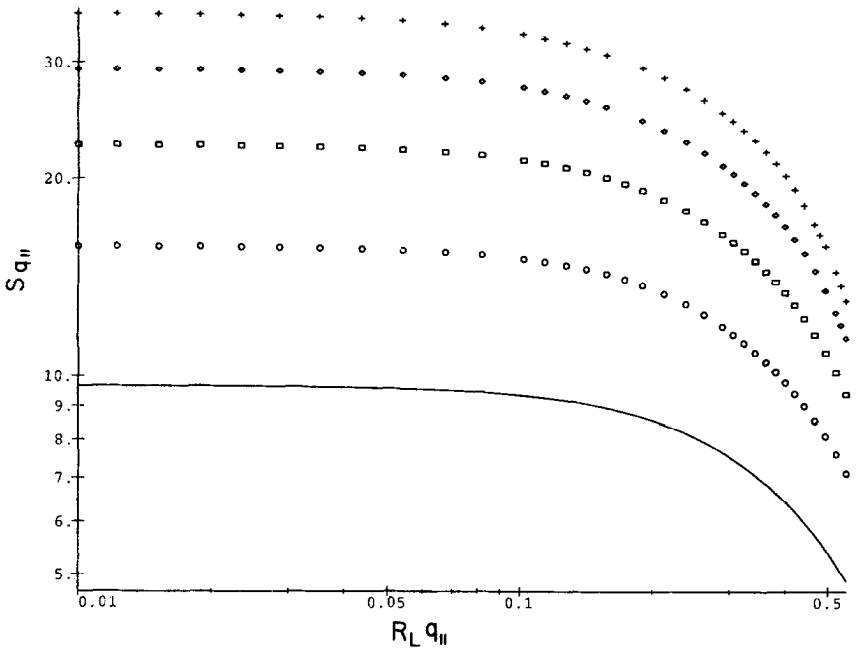


Fig. 4.5. Log–log plot of the scattered intensities in the direction of elongation (uniaxial extension) as a function of $R_L|\boldsymbol{q}|$, for $\alpha = 1.25$ (circles), 1.5 (squares), 1.75 (diamonds) and 2 (crosses), in units of $\rho\bar{N}/10$. The scattered intensity for the undeformed gel is given by the solid line. The parameters are $X = 0.25$, $Q_{\text{prep}} = 10$ and $p = 0.1$.

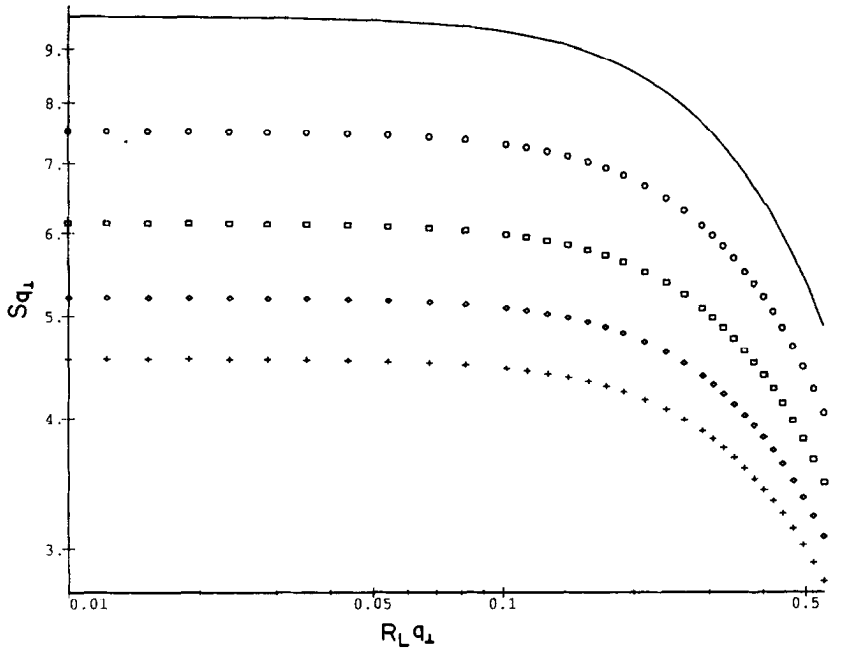


Fig. 4.6. Log–log plot of the scattered intensities normal to the direction of elongation (uniaxial extension) as a function of $R_L|\boldsymbol{q}|$. All the deformation ratios and parameters are as in Fig. 4.5.

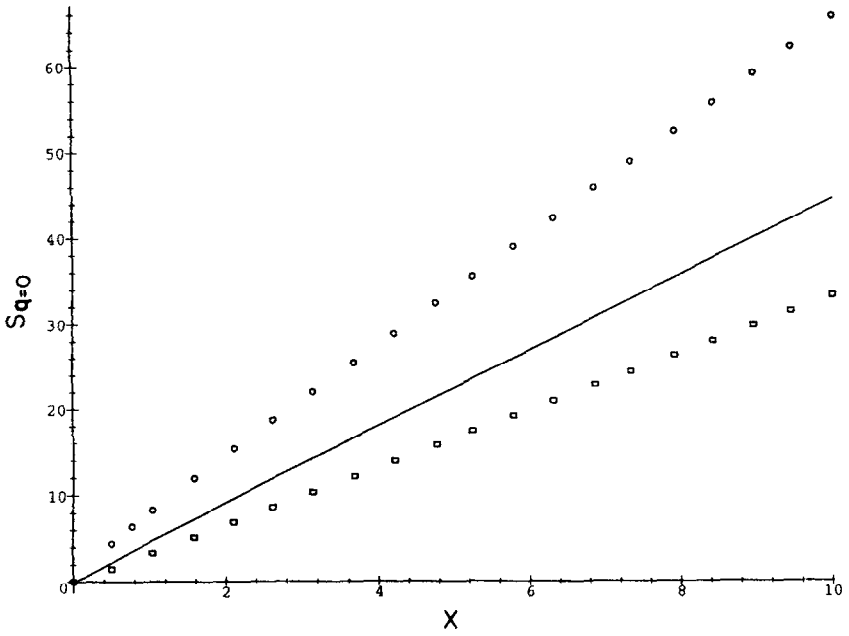


Fig. 4.7. The structure factors in the parallel (circles) and perpendicular (squares) directions are plotted in the $q = 0$ limit (for uniaxial extension) as a function of $X$, for $\alpha = 1.5$ and $Q_{prep} = 10$ (the undeformed case is given by the solid line).

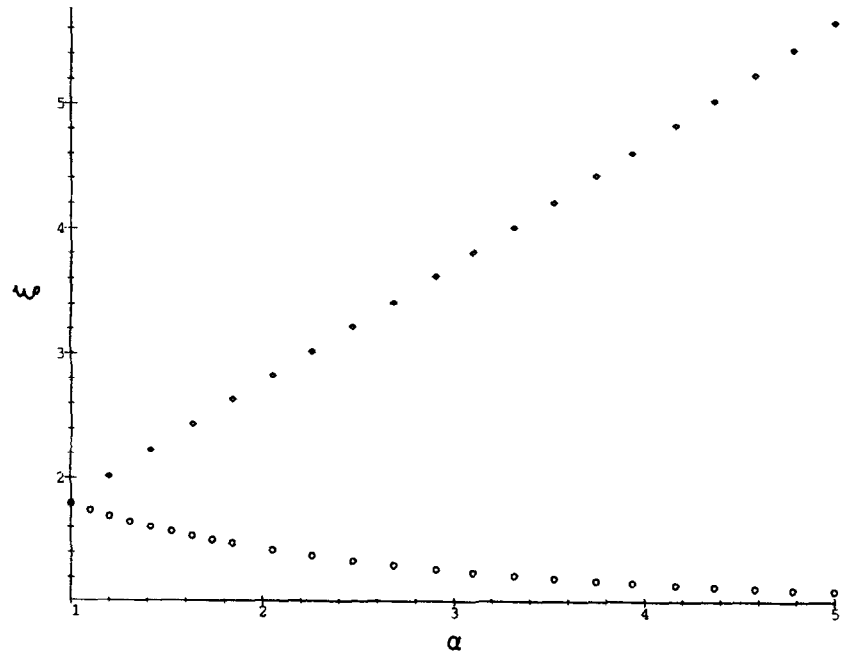


Fig. 4.8. Plot of the correlation lengths along (diamonds) and normal to (circles) the stretching direction (for uniaxial extension), as a function of $\alpha$, for $X = 0.25$ and $Q_{prep} = 10$.

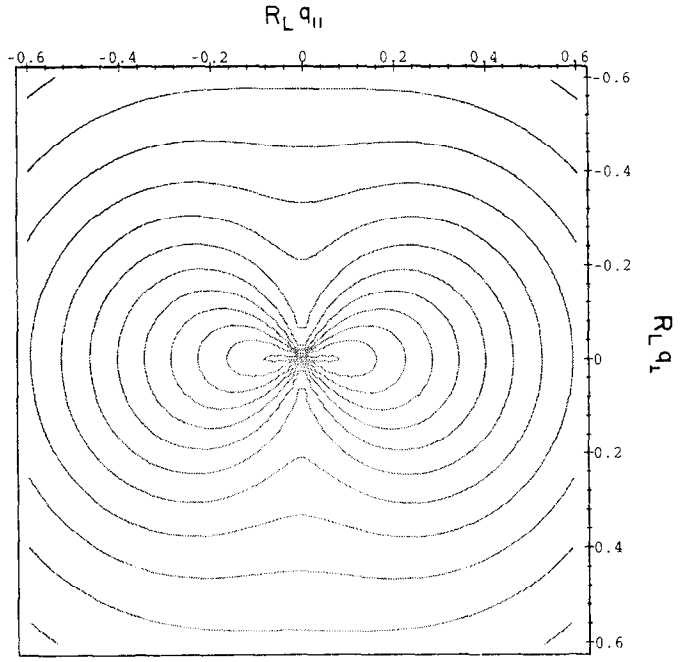


Fig. 4.9. Contour plot of the isointensity lines for wave vectors in the plane normal to the incident (neutron, laser) beam, for uniaxial extension with deformation ratio $\alpha = 1.2$. The parameters are $X = 0.25$, $Q_{prep} = 10$ and $p = 0.1$.

shows clearly the presence of an angular singularity at $\boldsymbol{q} = 0$ and the enhanced scattering along the direction of stretching observed in experiments [12]. The predicted contour plot for uniaxial compression, $\alpha = 0.8$ (where no experimental data are yet available) is shown in Fig. 4.10.

*4.6.3. Segregation of labelled chains*

Up to this point we assumed (for simplicity) that the network and the free chains are chemically identical (athermal case) and differ only in length. We now turn to the case of a network permeated by free chains (we assume that there is no small molecular weight solvent, i.e., $(\rho + c)a^3 = 1$), in which the interaction between the monomers of the free and the network monomers is described by the Flory–Huggins parameter $\chi$ (thermal case [3]). The interaction term in Eq. (4.47) is replaced by

$$\tfrac{1}{2} w(\rho_q + c_q)(\rho_{-q} + c_{-q}) \to a^3 \chi \rho_q c_{-q}\,, \quad c_q + \rho_q = 0 \tag{4.64}$$

and, as the result, Eq. (4.53) takes the form

$$\frac{\mathscr{F}_n[c]}{T} = \frac{1}{2} \int \frac{\mathrm{d}\boldsymbol{q}}{(2\pi)^3} \left[ \frac{(c_q + n_q)(c_{-q} + n_{-q})}{g_q} + c_q c_{-q} \left( \frac{1}{s_q} - 2a^3 \chi \right) \right]. \tag{4.65}$$

Comparison with Eq. (4.18) shows that the effective virial coefficient for the screened interaction between the monomers of the network is

$$w_q = s_q^{-1} - 2a^3 \chi\,. \tag{4.66}$$

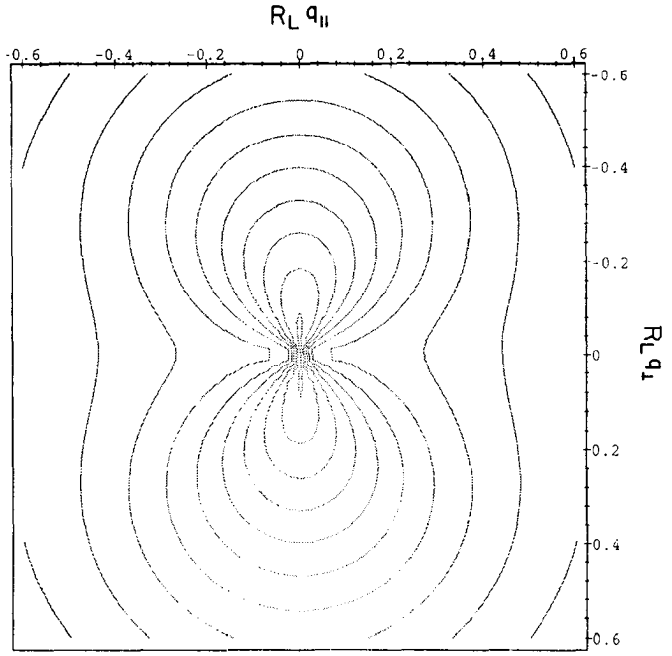


Fig. 4.10. The same as Fig. 4.9, for uniaxial compression, $\alpha = 0.8$.

The correlation functions can be obtained from Eqs. (4.37) and (4.38) by the replacement $w \to w_q$. Let us first consider the case of long free chains, $L \gg \bar{N}$ for which the presence of a maximum in $g_q$ does not show up in the structure factor. The spinodal (i.e., the onset of segregation) is found from the condition for the divergence of thermal fluctuations in the limit $q \to 0$ and is given by

$$2\chi_{sp} = [1/2(1-\phi_L)\bar{N}]\ (\lambda \star \boldsymbol{q}/|\boldsymbol{q}|)^2 + 1/\phi_L L\,, \tag{4.67}$$

where $\phi_L \equiv ca^3$ is the volume fraction of the free chains. This should be compared with well-known expression for the spinodal of a binary blend of free chains [3] with average lengths $\bar{N}$ (and the same exponential distribution of lengths as the network chains – see Eq. (4.58)) and $L$,

$$2\chi_{sp}^{blend} = 1/2(1-\phi_L)\bar{N} + 1/\phi_L L\,. \tag{4.68}$$

Note that in the absence of deformation ($\lambda_\alpha = 1$), $\chi_{sp} = \chi_{sp}^{blend}$.

Under uniaxial extension (by a factor of $\alpha$), thermal density fluctuations become anisotropic and the spinodal is first reached for fluctuations which are *normal* to the stretching direction:

$$2\chi_{sp} = 1/2\alpha(1-\phi_L)\bar{N} + 1/\phi_L L\,. \tag{4.69}$$

This effect is shown in Fig. 4.11. We conclude that phase separation resulting in the expulsion of the free chains from the gel may result when a gel is subjected to stretching (the effect should be most pronounced near the spinodal of the undeformed system). Such effects have been observed in sheared blends [19] (to which our theory cannot be directly applied, even though a generalization of the present approach to transient phenomena in polymer liquids in which temporary entanglements act as effective cross-links, appears plausible).

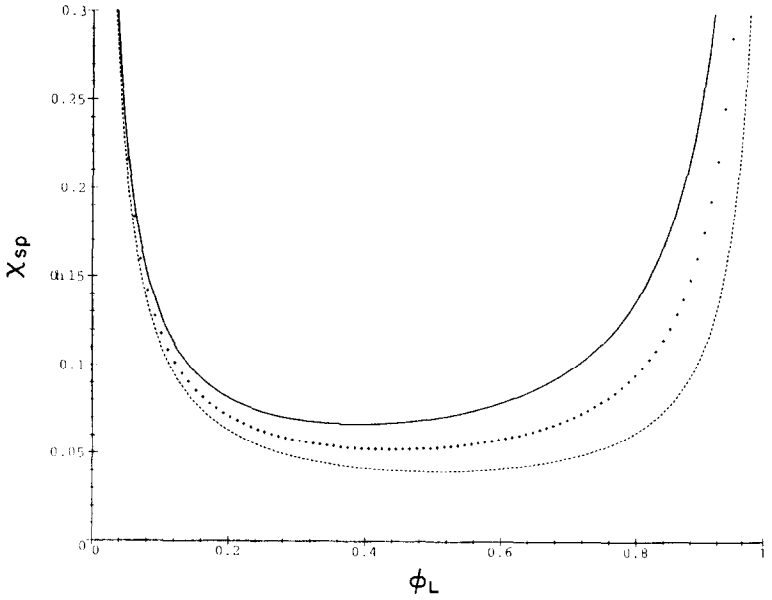


Fig. 4.11. Plot of spinodal values of the Flory–Huggins interaction parameter $\chi$ as a function of the volume fraction of the free chains inside the network, $\phi_L$, for $\bar{N}/L = 0.1$ and $\alpha = 1$ (solid line), 1.5 (crosses) and 2.5 (dashed line).

The prediction that the spinodal is first reached for fluctuations perpendicular to the stretching direction appears to contradict our previous conclusion that light or small angle neutron scattering is always enhanced in the direction of stretching (since the spinodal is usually assumed to be the point where the scattering signal diverges). Upon some reflection (see Eqs. (4.37) and (4.38)) we realize that the predicted enhancement (away from the spinodal) in the stretching direction comes from the $\lambda^4$ factor in the numerator of the correlator of static inhomogeneities. The spinodal condition corresponds to the point where the denominators of both the thermal correlator and the correlator of static inhomogeneities (in Eqs. (4.37) and (4.38)) vanish, and is first reached in the direction perpendicular to the stretching axis. This explains the observations of Ref. [58] where the enhancement of the scattering signal along the stretching direction (consistent with the butterfly effect) was interpreted as the signature of the spinodal. We therefore predict that scattering experiments on free chains dissolved in a network in the vicinity of the cross-link saturation threshold will observe an increase of the scattering in the parallel direction at moderate deformations, followed by the divergence of the scattered intensity in the perpendicular direction, at higher deformations (Fig. 4.12). From the asymmetry (with respect to composition) of the spinodal in the presence of uniaxial extension (see Fig. 4.11), significant stretching-induced shifts of the spinodal are expected to occur in networks which contain large concentration of free chains.

What happens when the free chains are shorter than the network chains, $64/(a^3c) \ll L \ll \bar{N}$ (the first inequality ensures the applicability of the RPA)? This situation is described by our RPA analysis of gels in small molecular weight solvents (since small free chains are equivalent to a low molecular weight solvent), with the spinodal condition replaced by (using Eqs. (4.46) and (4.66))

$$1 + (1/cL - 2a^3\chi_{sp})g_q = 0 \,. \tag{4.70}$$

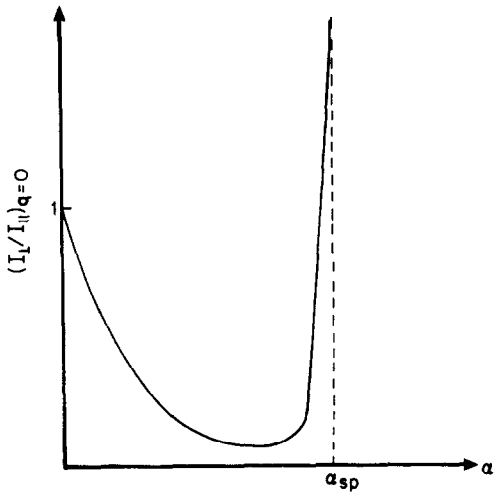


Fig. 4.12. Schematic drawing of the ratio of the intensities scattered perpendicular and parallel to the stretching axis ($I_\perp/I_\parallel$) as a function of the stretching ratio $\alpha$, for a network permeated by free labelled chains and prepared close to the spinodal.

The spinodal is first reached for fluctuations with wave vectors in the direction of minimal extension. According to the analysis in Section 4.5.4, there are different possible scenarios depending on the value of $\lambda_{min}$. For $\lambda_{min} \leqslant 0.97$ we have macrophase separation (at $q = 0$); otherwise, microphase separation at a characteristic wave vector of the order of the inverse mesh size will result. The spinodal curves ($\chi_{sp}$ vs. $\phi_L$) are qualitatively similar in both cases, but the one corresponding to microphase separation occurs at lower values of $\chi_{sp}$. The case $\lambda_{min} \simeq 0.97$ at which the transition from macro to microphase separation takes place corresponds to the Lifshitz point.

## 5. Gels in good solvents

Up to this point we assumed that both static inhomogeneities and thermal fluctuations in the gel are small and expanded the free energy to second order in the deviations from the mean density. This allowed us to carry out the resulting Gaussian integrals and to calculate the density correlation functions. While such an approach leads to physically meaningful results for gels permeated by polymeric solvent which can be adequately described on a mean-field level (by RPA), it fails to account for strong short wavelength thermal fluctuations of a network embedded in a good, low molecular weight solvent (we have shown that such a problem does not arise for static inhomogeneities which can be always described on the RPA level, for networks prepared away from the cross-link saturation threshold). However, since there exist well-known methods (e.g., renormalization group and scaling) for dealing with such problems in the case of semi-dilute solutions, we can adapt these methods to the present case and obtain a scaling description of gels in good solvents. The application of semi-dilute solution ideas to cross-linked gels is based on the fact that while static density inhomogeneities take place only on scales comparable to or larger than the

characteristic mesh size of the network, thermal fluctuations are dominated by small-scale phenomena which are quite similar to those in semi-dilute polymer solutions. The absence of static inhomogeneities on these small length scales means that, in deriving the long wavelength description (effective free energy) of the gel, the only contributions from the small scales will come from *thermal* fluctuations.

### 5.1. Renormalization and scaling

The fundamental distinction between the study of fluctuations in polymer networks and in polymer solutions is that, in the former case we have to consider fluctuations in both the initial and the final state. This observation stems from the fact that gels are prepared from polymer solutions and, consequently, thermal fluctuations in these solutions determine the structure of the resulting networks.

In order to describe long wavelength phenomena, we resort to the standard approach of renormalization group ($RG$) theory [59]. We recall the expression for the replica grand canonical replica partition function, Eq. (2.47) (from which we omitted the unimportant term which accounts for chain end effects),

$$\Xi_m = \int \mathrm{D}\varphi(\hat{x}) \exp\{ - H[\varphi(\hat{x})]\} . \tag{5.1}$$

Since strong fluctuations come from small scales it is convenient to separate the slowly ($\varphi_>(\hat{x})$) and the rapidly ($\varphi_<(\hat{x})$) spatially varying components of the field $\varphi$ (by rapidly varying we mean that the spatial variation is fast in at least one of the replicas). The separation is done by introducing the length scales $\{R^{(k)}\}$ in each of the replicas and writing

$$\varphi(\hat{x}) = \varphi_<(\hat{x}) + \varphi_>(\hat{x}) , \tag{5.2}$$

with the definitions

$$\varphi_>(\hat{x}) = \int_> \frac{\mathrm{d}\hat{q}}{(2\pi)^{3(1+m)}} \varphi_{\hat{q}} \exp(\mathrm{i}\hat{q}\cdot\hat{x}) , \tag{5.3}$$

and

$$\varphi_<(\hat{x}) = \int_< \frac{\mathrm{d}\hat{q}}{(2\pi)^{3(1+m)}} \varphi_{\hat{q}} \exp(\mathrm{i}\hat{q}\cdot\hat{x}) , \tag{5.4}$$

where $\int_<$ denotes integration over wave vectors $\hat{q} \equiv (q^{(0)}, q^{(1)}, \ldots, q^{(m)})$, with $|q^{(k)}| > 1/R^{(k)}$ in at least one of the replicas, and $\int_>$ describes integration over wave vectors which obey $\{|q^{(k)}| < 1/R^{(k)}\}$ in all of the replicas. The next step is to represent the partition function as a functional of a coarse grained Hamiltonian $H_>$, which depends only on the fluctuations of the $n$-component field $\varphi_>(\hat{x})$, on length scales larger than $\{R^{(k)}\}$:

$$\Xi_m = \int \mathrm{D}\varphi_>(\hat{x}) \exp\{ -H_>[\varphi_>(\hat{x})]\} , \tag{5.5}$$

where we define

$$\exp\{-H_{>}[\varphi_{>}(\hat{x})]\} \equiv \int D\varphi_{<}(\hat{x}) \exp\{-H[\varphi]\} . \tag{5.6}$$

It can be shown that our replica space theory is renormalizable in the sense that the above coarse graining procedure does not affect the functional form of the Hamiltonian [60] and thus,

$$H_{>}[\varphi_{>}] = \int d\hat{x} \left[ \frac{\mu}{2} \varphi_{>}^2(\hat{x}) + \frac{1}{2} \sum_{k=0}^{m} [a^{(k)}(R^{(k)})]^2 (\nabla^{(k)} \varphi_{>}(\hat{x}))^2 \right.$$
$$\left. - \frac{z_c}{4} (\varphi_{>}^2(\hat{x}))^2 \right] + \frac{1}{2} \sum_{k=0}^{m} w^{(k)}(R^{(k)}) \int dx^{(k)} \left[ \prod_{l \neq k} \int dx^{(l)} \varphi_{>}^2(\hat{x}) \right]^2 , \tag{5.7}$$

where $\nabla^{(k)}$ is a 3-dimensional gradient operator with respect to coordinates of $k$th replica. The integration in Eq. (5.6) leads only to the *renormalization* of the bare parameters of the field Hamiltonian (2.48), i.e., to their replacement by the cut-off dependent parameters in the initial

$$a^{(0)} \to a^{(0)}(R^{(0)}) , \qquad w^{(0)} \to w^{(0)}(R^{(0)}) \tag{5.8}$$

as well as the final state,

$$a \to a(R) , \qquad w \to w(R) , \tag{5.9}$$

where we used the identity of the replicas of the final state to write $a^{(k)}(R^{(k)}) \equiv a(R)$ and $w^{(k)}(R^{(k)}) \equiv w(R)$. The parameters $\mu$ and $z_c$, which determine the chemical structure of the gel, are not renormalized under the integration over fluctuations of the field $\varphi_{<}(\hat{x})$ with spatial scales smaller than the mesh size of the network (this is related to the previously made statement that fluctuations of network structure take place on scales of the order or larger than the mesh size).

The renormalized Hamiltonian $H_{>}[\varphi_{>}(\hat{x})]$ describes fluctuations in initial and final systems with spatial scales larger than $R^{(0)}$ and $R$, respectively. The scales $R^{(0)}$ and $R$ are connected by the condition that they determine the linear size of the *same* topological objects (i.e., network segments), but in *different* states. Note that, due to different physical conditions in the initial and final states, the renormalized monomer sizes $a^{(0)}(R^{(0)})$ and $a(R)$ differ one from another, even if they were identical in the bare Hamiltonian, $H = H_{>}(\{R^{(k)} = a\})$, Eq. (2.48). The coarse graining process is continued until one reaches the *fixed points* of the RG transformation [61]

$$a^{(0)}(R^{(0)}) \to a^{(0)}(\xi^{(0)}) \equiv a_{fp}^{(0)}, \quad a(R) \to a(\xi) \equiv a_{fp} \tag{5.10}$$

and

$$w^{(0)}(R^{(0)}) \to w^{(0)}(\xi^{(0)}) \equiv w_{fp}^{(0)}, \quad w(R) \to w(\xi) \equiv w_{fp} . \tag{5.11}$$

On the scales $R^{(0)} > \xi^{(0)}$ and $R^{(k)} > \xi$, density fluctuations in each of the replicas are suppressed by screening effects and there is no renormalization of the parameters of the Hamiltonian upon further coarse graining. One can, therefore, identify $\xi^{(0)}$ and $\xi$ with the correlation lengths in the initial and final states, respectively.

In order to describe the thermodynamic functions and the behavior of long wavelength fluctuations (with wave vectors $q^{(0)} \ll 1/\xi^{(0)}$ and $q^{(k)} \ll 1/\xi$), we can use our mean-field description, with the replacements

$$a \to a_{\rm fp}^{(0)}\,, \quad \lambda_\alpha \to \lambda_\alpha \frac{a_{\rm fp}^{(0)}}{a_{\rm fp}} \equiv \lambda_\alpha \bar{R}^{(0)}/\bar{R}\,, \tag{5.12}$$

where $\bar{R}^{(0)} \equiv a_{\rm fp}^{(0)} \bar{N}^{1/2}$ and $\bar{R} \equiv a_{\rm fp} \bar{N}^{1/2}$ are the sizes of chains of $\bar{N}$ monomers which depend only on the densities of the initial and the final states, respectively, (but not on the deformation of the network in these states). The second equality in Eq. (5.12) follows from the replacement of the coordinates in the replicas of the final state, $\boldsymbol{x}^{(k)} \to (a_{\rm fp}/a_{\rm fp}^{(0)})\boldsymbol{x}^{(k)}$ in the renormalized Hamiltonian, Eq. (5.7) (in order to recast it into the form given in Eq. (2.48)), and from the observation that as the result of this transformation $\lambda_\alpha$ is multiplied by a factor $a_{\rm fp}^{(0)}/a_{\rm fp}$.

Strictly speaking, the values of renormalized parameters in Eqs. (5.8) and (5.9) should be found from the solution of the RG equations. However, since the fixed points of these equations can be readily obtained by scaling methods, we will limit ourselves to simple scaling considerations. The fixed point parameters can be calculated by identifying them with their physically observable values, and estimating the latter using the de Gennes blob picture of semi-dilute solutions [3]. In the spirit of the scaling approach, we omit all numerical coefficients in the following.

Consider the case in which both the *initial and the final states of the network correspond to the semi-dilute regime* (in the important case of cross-linking in the melt, no renormalization of the initial state parameters is necessary) in an *athermal* solvent with $w^{(0)} = w = a^3$. The renormalized monomer sizes $a_{\rm fp}^{(0)}$ and $a_{\rm fp}$ in these states can be evaluated from the mean-field expressions for the corresponding correlation lengths,

$$\xi^{(0)} = a_{\rm fp}^{(0)} (g^{(0)})^{1/2}\,, \quad \xi = a_{\rm fp} g^{1/2}\,. \tag{5.13}$$

Using the well-known blob model estimates of the concentration dependence of the blob parameters, yields

$$g^{(0)} = (\rho^{(0)} a^3)^{-5/4}\,, \quad \xi^{(0)} = a^{-5/4} (\rho^{(0)})^{-3/4}\,, \tag{5.14}$$

where $g^{(0)}$ and $\xi^{(0)}$ are the number of monomers and the size of the blobs in the initial state. The analogous expressions for the final state are

$$g = (\rho a^3)^{-5/4}\,, \quad \xi = a^{-5/4} \rho^{-3/4}\,. \tag{5.15}$$

Note that although our approach differs from the standard one [3] in which the bare monomer size is used and the ideal chain exponents are replaced by their Flory values (i.e., $\xi = a g^{3/5}$), it leads to the same concentration dependence of the correlation length.

Substituting the above relations into Eq. (5.13) we find

$$a_{\rm fp}^{(0)} = a^{5/8} (\rho^{(0)})^{-1/8}\,, \quad a_{\rm fp} = a^{5/8} \rho^{-1/8} \tag{5.16}$$

and, therefore,

$$\bar{R}^{(0)} \equiv a_{\rm fp}^{(0)} \bar{N}^{1/2} = a^{5/6} (\rho^{(0)})^{-1/8} \bar{N}^{1/2} \tag{5.17}$$

and

$$\bar{R} \equiv a_{\mathrm{fp}} \bar{N}^{1/2} = a^{5/8} \rho^{-1/8} \bar{N}^{1/2} . \tag{5.18}$$

The values of renormalized virial coefficients $w_{\mathrm{fp}}^{(0)}$ and $w_{\mathrm{fp}}$ can be calculated by equating the renormalized excluded volume interaction terms in the free energy (the osmotic pressures in the initial and the final states) to their semi-dilute solution analogs:

$$T^{(0)} w_{\mathrm{fp}}^{(0)} (\rho^{(0)})^2 = T^{(0)}/(\xi^{(0)})^3 , \quad T w_{\mathrm{fp}} \rho^2 = T/\xi^3 . \tag{5.19}$$

This gives

$$w_{\mathrm{fp}}^{(0)} = a^{15/4} (\rho^{(0)})^{1/4} , \quad w_{\mathrm{fp}} = a^{15/4} \rho^{1/4} . \tag{5.20}$$

Note that the latter expression can be written as $w_{\mathrm{fp}} = a^3 (a^3 \rho)^{1/4}$. The reduction (in the semi-dilute regime $a^3 \rho \ll 1$) of the interaction parameters compared to their bare values is the consequence of the well-known correlation hole effect [3]. Eqs. (5.16) and (5.20) complete our discussion of the renormalization of our model. We conclude that in order to describe a gel in a good solvent, we only have to replace the bare parameters in the previously derived expressions for the free energy, correlation functions, etc., by their renormalized values.

The cross-link saturation threshold $w^{(0)} \rho^{(0)} \bar{N} = 1$ (Eq. (2.8)) takes the form

$$\rho_{\mathrm{min}}^{(0)} = a^{-3} \bar{N}^{-4/5} \equiv \rho^* , \tag{5.21}$$

which is identical to the condition for the threshold of overlap of chains of $\bar{N}$ monomers ($c^*$ theorem [3]). Thus, the conditions of preparation under which a gel can be formed, $\rho^{(0)} > \rho_{\mathrm{min}}^{(0)}$, correspond to a semi-dilute solution of such chains, $\rho^{(0)} > \rho^*$. Note that as $\rho^{(0)} \to \rho^*$ the fluctuations of network structure diverge and the gel becomes extremely heterogeneous.

### 5.2. *Thermodynamics*

In the following we use the scaling relations derived in the last subsection to formulate the thermodynamic description of deformation and swelling of networks in good solvents. Renormalizing the mean-field free energy, (3.30), with the aid of Eqs. (5.16) and (5.20) (neglecting the logarithmic term), we obtain the following expression for the free energy of the swollen gel [62–64]

$$\frac{\mathscr{F}\{\lambda_\alpha\}}{VT} = \nu \sum_\alpha \left( \frac{\lambda_\alpha \bar{R}^{(0)}}{\bar{R}} \right)^2 + \rho^{9/4} a^{15/4} . \tag{5.22}$$

The $\rho^{9/4}$ term contains the well-known fluctuation correction [3] to the mean-field value $\rho^2$ for the osmotic pressure. Although the elastic term resembles the usual expressions of classical theories of gel elasticity which also contain a correction factor $(\bar{R}^{(0)}/\bar{R})^2$, in the latter theories this ratio depends only on the difference of the qualities of solvent in the initial and the final states [65], and does not take into account the swelling-induced change in their respective sizes. In our case this ratio is given by

$$(\bar{R}^{(0)}/\bar{R})^2 = (\rho/\rho^{(0)})^{1/4} \tag{5.23}$$

from which the case of cross-linking in the melt is obtained by the substitution $\rho^{(0)} = a^{-3}$. The presence of the concentration-dependent $(\bar{R}^{(0)}/\bar{R})^2$ correction to the elastic term in the free energy leads to interesting new effects such as the prediction of a *negative effective Poisson ratio* at uniaxial deformations of order unity [64].

Minimizing the above free energy with the substitution $\lambda = (\rho^{(0)}/\rho)^{1/3}$ (i.e., balancing the osmotic and the elastic forces in the network) we obtain the volume swelling factor (defined with respect to the dry state of the gel),

$$Q \equiv (\rho a^3)^{-1} = (\rho^{(0)} a^3)^{-1/4} \bar{N}^{3/5} . \tag{5.24}$$

For networks prepared at the cross-link saturation threshold we can substitute Eq. (5.21) into the above equation and obtain $Q_{\max} \equiv (\rho^* a^3)^{-1}$ which corresponds to the $c^*$ theorem [3]. We conclude that the equilibrium swelling state of gels cross-linked away from the cross-link saturation threshold is much more concentrated than the $c^*$ state and thus there are many other network chains in the volume spanned by a chain which connects two adjacent cross-links. This means that the mental picture suggested by the $c^*$ theorem in which there is only one chain in the volume occupied by the average mesh, has to be replaced by one in which there are many chains per mesh volume and which corresponds to a semi-dilute solution of interpenetrating network chains. Note that while in the former picture, coarse graining over a mesh size leads to an ordered lattice, the latter picture corresponds to a topologically disordered gel (see Fig. 5.1).

The osmotic and the elastic (e.g., shear) moduli at equilibrium swelling in excess solvent, $G_{os}$ and $G_{el}$ can be read off the expression for the free energy, Eq. (5.22),

$$G_{os} = G_{el} = (T/a^3) Q^{-9/4} = (T\rho^*/\bar{N})(\rho^{(0)}/\rho^*)^{9/16} . \tag{5.25}$$

These moduli are larger than those predicted by the $c^*$ theorem (by a factor of $(\rho^{(0)}/\rho^*)^{9/16}$), due to the greater density of the equilibrium state.

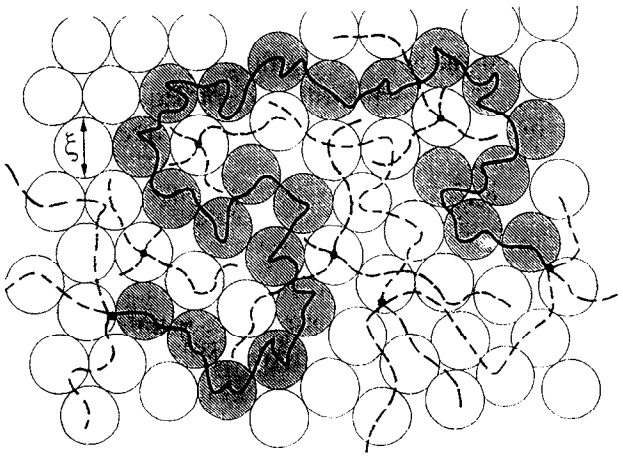


Fig. 5.1. Schematic drawing of a topologically disordered gel as a network made of chains of blobs. The blob size $\xi$ is shown.

The above expression for the moduli was derived under conditions of thermal equilibrium in excess solvent in which the density $\rho$ is completely determined by the conditions of preparation and the quality of solvent and can be varied only by changing the latter. We now proceed to examine the concentration dependence of the moduli in a network which is in thermal equilibrium in the presence of externally applied osmotic pressure. In this case, the density can be obtained from the thermodynamic relation

$$P = -\frac{\partial \mathscr{F}}{\partial V}\bigg|_{N_{\text{tot}}}, \quad \text{where } V = \frac{N_{\text{tot}}}{\rho_P}. \tag{5.26}$$

For large compressions, the elastic contribution to the free energy can be neglected with respect to the osmotic part and we obtain $P = Ta^{15/4}\rho_P^{9/4}$, which define the density $\rho_P$ corresponding to a given pressure $P$. This yields the moduli

$$G_{\text{os}}^P = (T/a^3)(a^3\rho_P)^{9/4} \tag{5.27}$$

and

$$G_{\text{el}}^P = T\rho_P^{7/12}(\rho^{(0)})^{5/12}/\bar{N}. \tag{5.28}$$

In the compression regime the elastic modulus is smaller than the osmotic one (the two become equal and are given by Eq. (5.25) in the limit $P \to 0$).

It is interesting to examine the limit in which $\rho_P = \rho^{(0)}$, i.e., the case when the externally applied osmotic pressure is large enough to increase the density to its value in the state of preparation. Substitution into Eq. (5.28) gives

$$G_{\text{el}}^P|_{\lambda=1} = T\rho^{(0)}/\bar{N}. \tag{5.29}$$

This simple result can be interpreted as follows: in the state in which the gel was originally cross-linked, the chains between cross-links are undeformed ($\lambda = 1$), and each of them carries $T$ of elastic free energy.

In the extreme case of compression to the dry state (i.e., all solvent is expelled) we obtain a universal relationship between the elastic modulus in the dry state and its equilibrium swelling factor in a good solvent $Q$, defined in Eq. (5.24):

$$G_{\text{el}}^{\text{dry}} = (T/a^3)Q^{-5/3}. \tag{5.30}$$

This relation does not depend on the structure of the network (characterized by $\bar{N}$) and can be tested by independent measurements of the factors on both sides of the equality.

The results obtained in this subsection apply to mechanical and osmotic experiments which probe the gel under conditions of thermal equilibrium. Since most mechanical experiments are done under conditions in which the gel is in thermal but not in osmotic equilibrium (long time, of the order of hours and days, may be needed to reach osmotic equilibrium in macroscopic polymer gels), it is important to stress that the above expressions can be applied even to situations in which osmotic equilibrium has not been reached.

### 5.3. Interpenetration and desinterpenetration of network chains

The number of interpenetrating chains in the volume $(\bar{R}^{(0)})^3$ of a mesh in the initial state can be estimated as

$$n^{(0)} = \rho^{(0)}(\bar{R}^{(0)})^3/\bar{N} = (\rho^{(0)}/\rho^*)^{5/8} = (\rho^{(0)}a^3)^{5/8}\bar{N}^{1/2}\,, \tag{5.31}$$

where we used Eqs. (5.13), (5.14) and (5.21) ($\bar{R}^{(0)}$ has been defined in Eq. (5.17)). This number characterizes the degree of topological disorder and varies between 1 (for gels prepared at the cross-link saturation threshold) and $\bar{N}^{1/2}$ (for networks cross-linked in the melt).

We now estimate the number of interpenetrating chains in a swollen network. We found in the mean-field approximation (Eq. (3.64)), that the effective mesh size changes affinely with the stretching as $R_{\text{mesh}} = a\bar{N}^{1/2}\lambda$. In order to transform this into the scaling picture we replace $a \to a_{\text{fp}}^{(0)}$, $\lambda \to \lambda\bar{R}^{(0)}/\bar{R}$ (Eq. (5.12)) and change the length scale as $x \to x\bar{R}^{(0)}/\bar{R}$. This gives

$$R_{\text{mesh}} = \bar{R}^{(0)}\lambda \tag{5.32}$$

from which the average number of interpenetrating chains per mesh in a swollen state is estimated as

$$n_{\text{str}} = \rho(\lambda\bar{R}^{(0)})^3/\bar{N} = n^{(0)} \tag{5.33}$$

and we conclude that this number remains constant during the swelling of the network.

The situation is more delicate if we consider the case in which the network is compressed in its final state, compared to its state of preparation (this can be done by applying osmotic pressure $P$, as discussed above). We showed (Eq. (3.65)) in the mean-field approximation, that in this case (i.e., $\lambda < 1$), the mesh size is $R_{\text{mesh}} = a\bar{N}^{1/2}$ which upon rescaling, becomes $\bar{R} = \xi(\bar{N}/g)^{1/2}$ (it depends on the final density as $\rho^{-1/8}$) and

$$n_{\text{comp}} = \rho\bar{R}^3/\bar{N} = (\rho/\rho^*)^{5/8} > n^{(0)}\,, \tag{5.34}$$

i.e., compression leads to increased overlap (interpenetration) of chains. Indirect support for this mechanism comes from measurements on labelled chains in a network which do not decrease significantly in size upon compression [46]. If the network is prepared in the semi-dilute regime, then dried (i.e., the solvent is removed) and, finally, stretched and reswollen in a good solvent, one will observe desinterpenetration of network chains compared to the dry state ($n_{\text{comp}}$ will decrease by a factor of $(\rho a^3)^{5/8}$ compared to the dry value, $\bar{N}^{1/2}$).

### 5.4. Density correlation functions

We proceed to calculate the density correlation functions of gels in good solvents. In the microscopic (short wavelength) range, $|q| \gg \xi^{-1}$, the analysis of the asymptotic behavior of the functions $v_q$ and $g_q$ shows that the scattering is identical to that from a semi-dilute solution in a good solvent (at the same monomer concentration $\rho$), i.e.,

$$C_q \to 0 \tag{5.35}$$

and

$$G_q \approx \rho(aq)^{-5/3} . \tag{5.36}$$

This behavior has been observed in neutron scattering from gels in good solvents [48].

*5.4.1. Mesoscopic range*

In the mesoscopic range $|q| \ll \xi^{-1}$ (where the correlation length $\xi$ is given by Eq. (5.15)), density fluctuations are suppressed by the screening of excluded volume interactions and we can use the RPA expressions for the structure factors (Section 4.5.3), in which we replace the mean-field parameters by their renormalized values (see Eqs. (5.12),(5.16),(5.20) and (5.23)). Note that since $\xi \ll \lambda\bar{R}^{(0)}$ for gels obtained away from the cross-link saturation threshold, the mesoscopic range extends to wavelengths smaller that the average mesh size $\lambda\bar{R}^{(0)}$ (we showed that this quantity describes the mesh size; see Eq. (5.32)).

In this range, the renormalization of length scales (see the discussion following Eq. (5.12)) which leads to the renormalization of $\lambda$, affects also the wave vectors $q$, and leads to the replacement $q \to (\bar{R}/\bar{R}^{(0)})q$ in the mean-field expressions. The resulting replacements to be made in the RPA density correlators are:

(1) $a^2\bar{N}q^2 \to \bar{R}^2q^2 \equiv Q^2$ ,

i.e., the mean-field expression for the size of an average network chain is replaced by the corresponding scaling value in the final state, $\bar{R} = a(\rho a^3)^{-1/8}\bar{N}^{1/2}$.

(2) $a^2\bar{N}(\lambda \star q)^2 \to (\bar{R}^{(0)})^2(\lambda \star q)^2 = [(\bar{R}^{(0)})^2/\bar{R}^2](\lambda \star \check{q})^2Q^2$

in which the size of an average network chain is replaced by the corresponding scaling value in the initial state $\bar{R}^{(0)} = a(\rho^{(0)}a^3)^{-1/8}\bar{N}^{1/2}$ (this factor expresses the affine deformation of a chain in the initial state).

(3) $(\lambda \star q)^2/q^2 \to [(\bar{R}^{(0)})^2/\bar{R}^2](\lambda \star q)^2/q^2$ .

(4) Renormalization of the virial coefficients:

$w^{(0)} \to a^3(\rho^{(0)}a^3)^{1/4}$ , $w \to a^3(\rho a^3)^{1/4}$ .

In this way, the renormalized correlators can be obtained from their RPA analogues simply by changing the definitions of the dimensionless wave vectors ($Q$), replacing the second virial coefficients by their renormalized values and making the replacement $\lambda \to (\bar{R}^{(0)}/\bar{R})\lambda$ in the RPA expressions for the correlators $g_q, v_q, G_q$ and $C_q$ given in Section 4.

The qualitative features of the density correlators of uniaxially stretched gels in good solvents (butterfly patterns, etc.) are similar to those of gels in polymeric solvents and we will not repeat the analysis here and only present several typical results. A three-dimensional plot of the full structure factor for uniaxially stretched gels prepared close to the cross-link saturation threshold, is shown in Fig. 5.2. The enhancement of scattering parallel to the stretching direction and the suppression of scattering normal to it is clearly visible. Similar behavior is observed for gels prepared away from the cross-link saturation threshold and studied at equilibrium swelling (Fig. 5.3), when static inhomogeneities dominate. Furthermore, since the angular anisotropy of thermal fluctuations is much weaker than that of static inhomogeneities, butterfly patterns oriented along the stretching

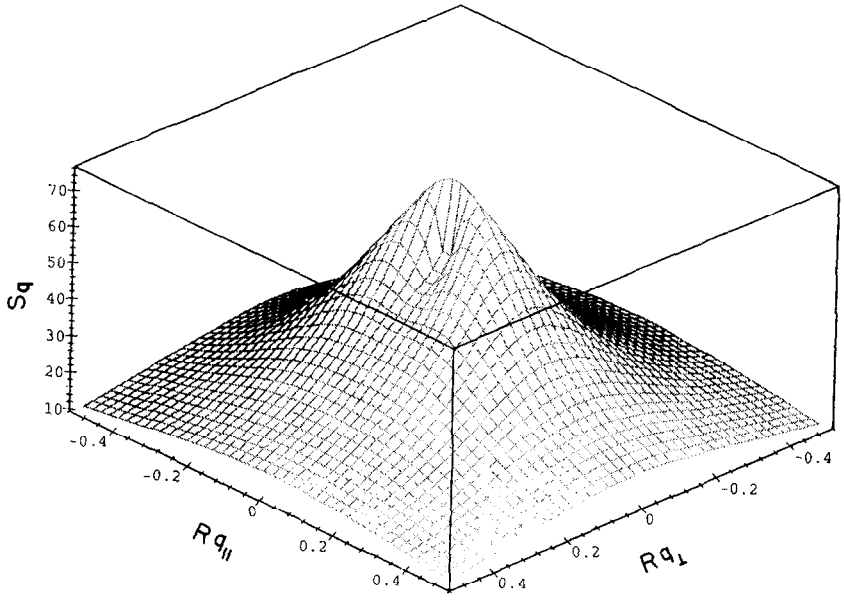


Fig. 5.2. 3-dimensional plot of the total intensity $S_q$ in the $(q_\parallel, q_\perp)$ plane, for a gel prepared close to the cross-link saturation threshold, $a^3\rho^{(0)} = a^3\rho = 0.026$, $\bar{N} = 100$ and $\alpha = 1.2$.

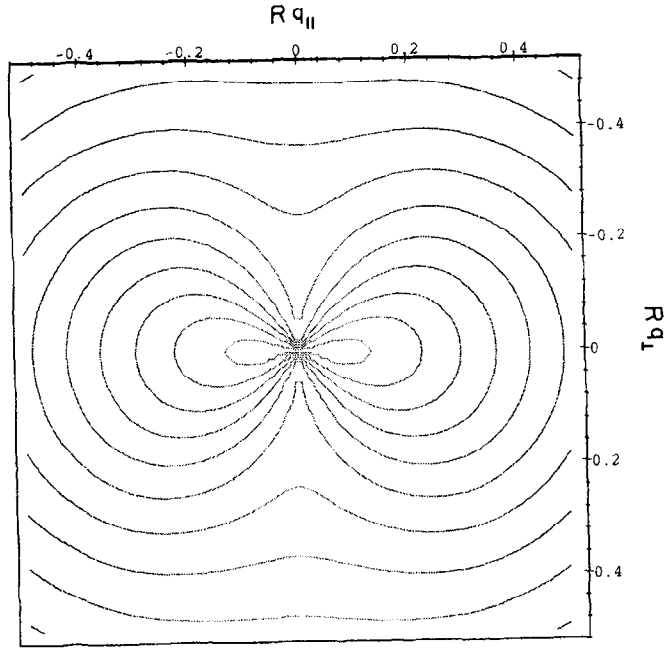


Fig. 5.3. Isointensity plot in the $(q_\parallel, q_\perp)$ plane, for a gel prepared away from the cross-link saturation threshold and swollen to equilibrium. The parameters are $\bar{N} = 100$, $a^3\rho^{(0)} = 0.3$, $a^3\rho = 0.05$ and $\alpha = 1.1$.

direction are predicted even for gels prepared away from the cross-link saturation threshold and studied at the concentration of preparation, when thermal fluctuations dominate (Fig. 5.4).

One of the striking predictions of our theory is the existence of a *maximum in the thermal structure factor of neutral polymer gels in good solvents, at a finite wave vector* $q_*$ (this follows from the discussion in Section 4.5.4, where we replace the RPA parameters by their renormalized good solvent counterparts). Although the maximum is located at a wave vector which lies outside the range of our mesoscopic (or short wavelength) analytical expressions, scaling considerations suggest that for gels in the state of preparation or for uniaxially swollen ones, the predicted peak in the thermal structure factor appears at a wavelength of the order of the average mesh size of the network. The maximum is shifted to $q_* = 0$ when the gel is isotropically compressed to 93% of its volume in the state of preparation (this Lifshitz point is defined by the condition $\alpha(\check{q}) = 0$, with $\alpha$ obtained by substituting the renormalized good solvent parameters into the RPA expression, Eq. 4.40).

Since static scattering experiments measure the sum of the contributions of thermal fluctuations and static density inhomogeneities (the latter contribution is expected to be a monotonically decreasing function of $q$), the above maximum will be observed only under conditions when thermal fluctuations make a significant contribution to the scattering. As will be shown in the next subsection (5.4.2), scattering from static inhomogeneities always dominates at high degrees of cross-linking (near the cross-link saturation threshold), and even away from this threshold, for gels swollen to equilibrium in excess solvent. We therefore expect to observe a pronounced maximum

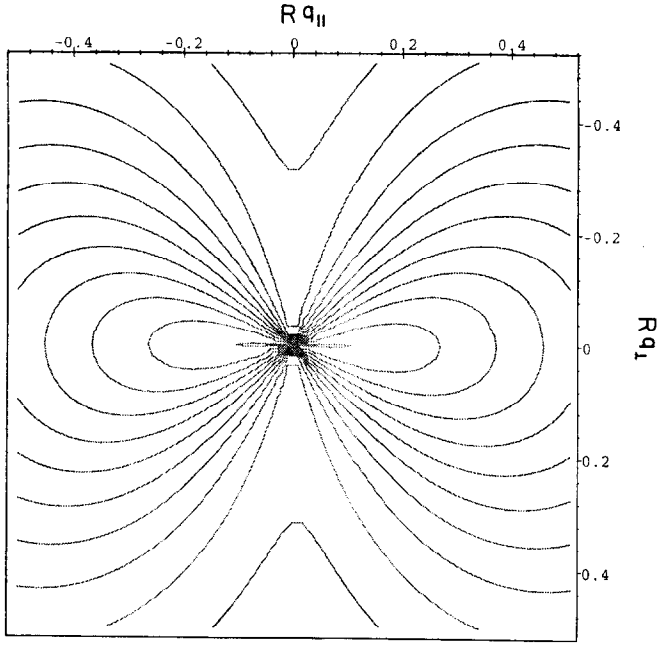


Fig. 5.4. Isointensity plot in the $(q_\parallel, q_\perp)$ plane of the scattering vector (parallel and normal to the stretching direction), for a gel prepared away from the cross-link saturation threshold and studied at the concentration of prepration, $a^3\rho^{(0)} = a^3\rho = 0.3$. The parameters are $\bar{N} = 100$ and $\alpha = 1.1$.

at $q = 0$ (due to scattering from static inhomogeneities), followed by a smaller maximum or a "shoulder" at intermediate $q$ values (due to thermal scattering) in plots of the total scattered intensity, for lightly cross-linked gels and for gels studied at the state of preparation. The "shoulder" should disappear with progressive swelling of the network and at higher degrees of cross-linking. Both effects were observed in experiments [66–69]. The complex shape of the scattering curves has been fitted by the sum of a Lorentzian form for the thermal contribution and a Gaussian form for the contribution of scattering from static inhomogeneities [70] (to the best of our knowledge, the possibility of a finite $q$ maximum in the thermal structure factor of neutral gels, has not been mentioned by any of the previous investigators).

Note that the effect of the maximum on the static scattering spectrum should become more pronounced with the approach to the $\Theta$-point (poor solvent conditions), where thermal fluctuations are expected to diverge. Although this effect has been observed for charged gels [55], it was attributed to the interplay between electrostatic and poor solvent phenomena [71, 72], and similar experiments on neutral gels are needed to test our prediction.

*5.4.2. Long wavelength limit*

Exact analytical expressions for the density correlation functions of a gel in a good solvent can be obtained in the long wavelength limit ($q \to 0$). When a network prepared at density $\rho^{(0)}$ undergoes an isotropic density change to a concentration $\rho$, the correlators of thermal fluctuations and of static inhomogeneities become

$$G_0 = \frac{2\rho\bar{N}(\rho/\rho^{(0)})^{5/12}}{1 + 2(\rho/\rho^*)^{5/4}(\rho/\rho^{(0)})^{5/12}} \tag{5.37}$$

and

$$C_0 = \frac{3\rho\bar{N}[2(\rho^{(0)}/\rho^*)^{5/4} + 1]}{[(\rho^{(0)}/\rho^*)^{5/4} - 1][1 + 2(\rho/\rho^*)^{5/4}(\rho/\rho^{(0)})^{5/12}]^2} \,. \tag{5.38}$$

Note that the contribution of static inhomogeneities $C_0$ diverges near the cross-link saturation threshold, $\rho^{(0)} = \rho^*$ (Eq. (5.21)) and we predict that, for networks prepared close to $\rho^*$ conditions, practically all the observed scattered intensity comes from these inhomogeneities. We can define the network *heterogeneity parameter*

$$X \equiv 1/[(\rho^{(0)}/\rho^*)^{5/4} - 1] \,, \tag{5.39}$$

which diverges at the cross-link saturation threshold. For $X \to \infty$, the density in the initial state coincides with that in the equilibrium swelling state (swelling is suppressed with the approach to the cross-link saturation threshold, i.e., $\rho_{eq} \approx \rho^{(0)} \approx \rho^*$; see Eq. (5.24)) and the correlators are given by

$$G_0 \approx \frac{2\bar{N}^{1/5}}{3a^3} \,, \qquad C_0 \approx \frac{\bar{N}^{1/5}}{a^3[(\rho^{(0)}/\rho^*)^{5/4} - 1]} \,. \tag{5.40}$$

If the gel is prepared close to the cross-link saturation threshold ($\rho^{(0)} \to \rho^*$) and then strongly compressed ($\rho \gg \rho^*$), we get

$$G_0|_{comp} \approx 1/a^3(a^3\rho)^{1/4} \,, \tag{5.41}$$

and

$$C_0|_{\text{comp}} \approx \frac{9}{4a^3\bar{N}^{5/3}(a^3\rho)^{7/3}[(\rho^{(0)}/\rho^*)^{5/4}-1]} .$$

Thermal fluctuations are independent of the degree of cross-linking and their intensity decreases slowly with increasing compression. Near the cross-link saturation threshold static inhomogeneities increase with increasing degree of cross-linking (as $\bar{N}^{-5/3}$) and are rapidly suppressed by compression (as $\rho^{-7/3}$).

For networks prepared away from the cross-link saturation threshold ($\rho^{(0)} \gg \rho^*$), we can distinguish between experiments in which the scattering is performed (1) on the gel in the state of preparation, (2) on the gel swollen to equilibrium in excess solvent and (3) on a gel compressed (isotropically) with respect to the state of preparation ($\rho \gg \rho^{(0)}$).

(1) State of preparation, $\rho = \rho^{(0)}$. In this case,

$$G_0|_{\rho=\rho^{(0)}} \approx \frac{1}{a^3(a^3\rho^{(0)})^{1/4}} , \qquad C_0|_{\rho=\rho^{(0)}} \approx \frac{3}{2a^3\bar{N}(a^3\rho^{(0)})^{3/2}} , \tag{5.42}$$

i.e., the thermal component of the scattering does not depend on the density of cross-links (for fixed monomer density in the initial state). The scattering from static inhomogeneities increases with the density of cross-links and rapidly decreases with the concentration $\rho^{(0)}$. The ratio $Y \equiv C_0/G_0$ of the contributions of the static inhomogeneities and the thermal fluctuations is given by

$$Y_{\rho=\rho^{(0)}} \approx \tfrac{3}{2}(\rho^*/\rho^{(0)})^{5/4} \ll 1 , \tag{5.43}$$

i.e., the thermal scattering dominates in the state of preparation. Note that, in this case, the scattering from the gel is expected to be very close to that from an equivalent solution, in agreement with experimental observations [47, 57].

(2) Swelling equilibrium, $\rho = \rho^*(\rho^{(0)}/\rho^*)^{1/4}$ (from Eq. (5.24)):

$$Y_{\text{eq}} \approx (\rho^{(0)}/\rho^*)^{5/16} \gg 1 , \tag{5.44}$$

i.e., the scattering comes mostly from static heterogeneities. Note that for gels swollen with respect to the state of preparation, the scattering is expected to increase with swelling, $G_0 \sim \rho^{-1/4}$ and $C_0 \sim \rho^{-7/3}$ (the effect is especially strong for scattering from static heterogeneities). This effect was also observed in experiments [47, 57].

(3) Isotropic compression, $\rho \gg \rho^{(0)} \gg \rho^*$:

$$G_0|_{\text{comp}} \approx \frac{1}{a^3(a^3\rho)^{1/4}} , \qquad C_0|_{\text{comp}} \approx \frac{3(\rho^{(0)})^{5/6}}{2a^{15/2}\bar{N}\rho^{7/3}} . \tag{5.45}$$

The corresponding ratio is

$$Y_{\text{comp}} \approx \tfrac{3}{2}(\rho^{(0)}/\rho)^{5/6}(\rho^*/\rho)^{5/4} \ll 1 , \tag{5.46}$$

i.e., thermal fluctuations dominate.

We now consider uniaxially stretched gels (with deformation ratio $\alpha$). The intensity of thermal fluctuations at small wave vectors parallel to the direction of elongation, is

$$G_0^{\parallel} = \frac{(2/\alpha^2)\rho\bar{N}(\rho/\rho^{(0)})^{5/12}}{1 + (2/\alpha^2)(\rho/\rho^*)^{5/4}(\rho/\rho^{(0)})^{5/12}} \tag{5.47}$$

and the corresponding contribution of static heterogeneities is given by

$$C_0^{\parallel} = \frac{3\rho\bar{N}[2(\rho^{(0)}/\rho^*)^{5/4} + 1]}{[(\rho^{(0)}/\rho^*)^{5/4} - 1][1 + (2/\alpha^2)(\rho/\rho^*)^{5/4}(\rho/\rho^{(0)})^{5/12}]^2} \,. \tag{5.48}$$

Near the cross-link saturation threshold ($\rho^{(0)} \to \rho^*$) the scattering is always dominated by static inhomogeneities.

Away from the cross-link saturation threshold, we distinguish between cases (1) and (2) (as above). In the state of preparation (1), the ratio increases from

$$Y^{\parallel}_{\rho=\rho^{(0)}} \approx \tfrac{3}{2}\alpha^4(\rho^*/\rho^{(0)})^{5/4} < 1 \tag{5.49}$$

for moderate values of the deformation ratio $\alpha$ ($\alpha^2 \ll 2(\rho^{(0)}/\rho^*)^{5/4}$), to

$$Y^{\parallel}_{\rho=\rho^{(0)}} \approx 3\alpha^2 \gg 1 \tag{5.50}$$

for $\alpha^2 \gg 2(\rho^{(0)}/\rho^*)^{5/4}$, i.e., the contribution of static inhomogeneities to the scattering in the direction of elongation dominates in the strong stretching limit. Therefore, the parallel component of small angle scattering from gels in the state of preparation, changes from thermally dominated to static inhomogeneity dominated regime with increasing stretching.

Under equilibrium swelling conditions (2), the ratio of the corresponding structure factors is given by

$$Y^{\parallel}_{\mathrm{eq}} \approx [3\alpha^4/(2 + \alpha^2)](\rho^{(0)}/\rho^*)^{5/16} \gg 1 \tag{5.51}$$

and therefore, scattering from static heterogeneities is always dominant.

We now proceed to study the long wavelength scattering in the direction normal to the stretching axis. The thermal component of the scattering perpendicular to the direction of elongation is

$$G_0^{\perp} = \frac{2\alpha\rho\bar{N}(\rho/\rho^{(0)})^{5/12}}{1 + 2\alpha(\rho/\rho^*)^{5/4}(\rho/\rho^{(0)})^{5/12}} \tag{5.52}$$

and the perpendicular scattering from the static heterogeneities is

$$C_0^{\perp} = \frac{3\rho\bar{N}[2(\rho^{(0)}/\rho^*)^{5/4} - 1]}{[(\rho^{(0)}/\rho^*)^{5/4} - 1][1 + 2\alpha(\rho/\rho^*)^{5/4}(\rho/\rho^{(0)})^{5/12}]^2} \,. \tag{5.53}$$

As before, near the cross-link saturation threshold most of the scattering comes from static inhomogeneities. Away from the cross-link saturation threshold we get

1. In the state of preparation

$$Y^{\perp}_{\rho=\rho^{(0)}} \approx (3/2\alpha^2)(\rho^*/\rho^{(0)})^{5/4} \ll 1 \,, \tag{5.54}$$

i.e., thermal scattering always dominates the scattered intensity in the direction normal to the stretching axis.

2. At equilibrium swelling

$$Y_{eq}^{\perp} \approx \frac{3}{\alpha(2+\alpha)} (\rho^{(0)}/\rho^*)^{5/16}, \tag{5.55}$$

i.e., scattering from static inhomogeneities is stronger than that from thermal ones at small deformations but the situation is reversed in the large deformation limit.

*5.4.3. State of preparation*

An exact expression for the total structure factor can be obtained for gels in the state of preparation by replacing the RPA parameters by their renormalized values in Eq. (4.31) (this expression is valid for all wave vectors in the range $|\boldsymbol{q}| \ll 1/\xi^{(0)}$):

$$S_q^{(0)} = \frac{\rho^{(0)}\bar{N}}{(\rho^{(0)}/\rho^*)^{5/4} - 1 + (R^{(0)})^2 \boldsymbol{q}^2/2} \tag{5.56}$$

The correlation length, $R^{(0)}[(\rho^{(0)}/\rho^*)^{5/4} - 1]^{-1/2}$, diverges at the cross-link saturation threshold at which the length scale associated with the static heterogeneities becomes infinite and our RPA approximation for the frozen fluctuations of network structure breaks down.

Away from the cross-link saturation threshold ($\rho^{(0)}/\rho^* \gg 1$) this expression reduces to

$$S_q^{(0)} \cong \frac{(\rho^{(0)})^{-1/4} a^{-15/4}}{1 + (\xi^{(0)})^2 \boldsymbol{q}^2/2}, \tag{5.57}$$

i.e., the correlation length coincides with the size of a blob in the state of preparation (Eq. (5.14)).

We found that frozen heterogeneities of network structure give the dominant contribution to the scattering from gels prepared near the cross-link saturation threshold of the initial state (close to $c^*$ conditions). Away from the cross-link saturation threshold, thermal fluctuations dominate the scattering from an unstretched gel in the state of preparation, but static inhomogeneities dominate and the intensity of small angle scattering increases [70] when the gel is swollen to equilibrium.

When the gel is uniaxially stretched, we predict that the angular dependence of the scattering intensity (at small wave vectors) will be always dominated by the static inhomogeneities and that butterfly patterns (in isointensity plots) oriented along the stretching direction will be observed. This holds even for gels prepared away from the cross-link saturation threshold and studied at the concentration of preparation (i.e., when thermal fluctuations dominate), since the angular anisotropy of static inhomogeneities is stronger than that of thermal fluctuations.

## 6. Connection with continuum theory of elasticity

In the previous sections we derived exact expressions for the density correlators which describe the static density inhomogeneities and the thermal density fluctuations in a deformed network. We found that the total structure factor is dominated, under most conditions, by the static density inhomogeneities and that under uniaxial extension, the predicted long wavelength angular anisotropy and the dependence on the deformation ratios are in excellent agreement with experimental

observations and reproduce the butterfly effect observed in small angle neutron scattering and light scattering experiments.

Although we have presented what we believe to be a complete description of the butterfly effect, and found that it is related to the anisotropy of the elastic restoring forces in the stretched network and to the existence of an inhomogeneous equilibrium state of a deformed gel, a simple intuitive explanation proved to be quite elusive. Our problem can be traced back to the usual difficulty in representing polymer elasticity in the language of collective coordinates (i.e., density field) [23]. In this language, mechanical force balance conditions have to be reformulated in terms of equilibrium conditions on chemical potentials (the gradients of these chemical potentials are the thermodynamic forces which govern the response to monomer density changes) and, while we have good intuition about how osmotic forces can be described in these terms, we are much less familiar with the way in which elastic forces are represented in this formulation (note, however, that this problem has been considered in the literature in other contexts – see e.g. [73]).

Can we describe the physics of the inhomogeneous equilibrium state of deformed gels in terms of mechanical equilibrium between ordinary forces? From the knowledge that forces are conjugate to displacements, we have to reformulate the problem in terms of displacement fields. Following this line of argument, we will try to recast the physics of gels into the language of the ordinary theory of elasticity of solids, generalized to the case of inhomogeneous deformed continua. Note that although such a continuum description cannot capture the small-sale behavior of gels, it should be able to reproduce long wavelength phenomena such as the butterfly effect.

### 6.1. *Anisotropic moduli of homogeneous deformed networks*

We begin with the mean-field free energy of a *homogeneous* gel, with a constant density of cross-links $\nu$ (Eq. (3.30)), and note that the change in the elastic free energy associated with the deformation along the principal axes can be written as (for simplicity we assume that the temperature is the same in the initial and the final states):

$$\frac{\mathscr{F}_{\mathrm{el}}\{\lambda_\alpha\}}{T} = \frac{\nu}{2} V \sum_\alpha (\lambda_\alpha^2 - 1) . \tag{6.1}$$

We would like to extend this expression to a general class of deformations characterized by an arbitrary displacement field $\boldsymbol{u}^{(0)}(\boldsymbol{x}^{(0)}) \equiv \boldsymbol{x} - \boldsymbol{x}^{(0)}$ which describes the displacement of a point $\boldsymbol{x}^{(0)} \to \boldsymbol{x}$ in a solid under a given deformation. We can follow the path of the usual continuum theory of elasticity of homogeneous and isotropic solids [21] by expanding the free energy in the gradients of this displacement field. However, since we are interested in large deformations (strains of order of or larger than unity), we must retain the nonlinear terms in the definition of the strain tensor (the importance of introducing second-order strains in the present context was emphasized by Alexander [22])

$$u_{\alpha\beta}(\boldsymbol{x}^{(0)}) \equiv \frac{1}{2}\left[\frac{\partial u_\alpha^{(0)}}{\partial x_\beta^{(0)}} + \frac{\partial u_\beta^{(0)}}{\partial x_\alpha^{(0)}} + \sum_\gamma \frac{\partial u_\gamma^{(0)}}{\partial x_\alpha^{(0)}} \frac{\partial u_\gamma^{(0)}}{\partial x_\beta^{(0)}}\right] . \tag{6.2}$$

Furthermore, in principle, we must keep all higher (than second) orders in the strain tensor in the expansion of the free energy. The expansion coefficients will be determined by the requirement that,

for deformations given by $\boldsymbol{u}^{(0)}(\boldsymbol{x}^{(0)}) = \lambda \star \boldsymbol{x}^{(0)} - \boldsymbol{x}^{(0)}$, our free energy is given by Eq. (6.1). Thus,

$$\frac{\mathscr{F}_{\mathrm{el}}[\boldsymbol{u}^{(0)}]}{T} = \int \mathrm{d}\boldsymbol{x}^{(0)} \Bigg[ \nu^{(0)} \sum_{\alpha} u_{\alpha\alpha}(\boldsymbol{x}^{(0)}) + \theta \sum_{\alpha,\beta} u_{\alpha\beta}^2(\boldsymbol{x}^{(0)}) + \kappa \sum_{\alpha} u_{\alpha\alpha}^2(\boldsymbol{x}^{(0)}) + \cdots \Bigg], \tag{6.3}$$

where the scalar form of the expansion coefficients is dictated by the isotropy of the undeformed solid (the assumption of local isotropy has to be modified in the presence of static heterogeneities which will be considered later).

Substituting the displacement $\boldsymbol{u}^{(0)}(\boldsymbol{x}^{(0)}) = \lambda \star \boldsymbol{x}^{(0)} - \boldsymbol{x}^{(0)}$ into the definition of the strain tensor, Eq. (6.2), gives

$$u_{\alpha\beta} = \tfrac{1}{2}(\lambda_\alpha^2 - 1)\delta_{\alpha\beta} . \tag{6.4}$$

Inserting this expression into Eq. (6.3) and comparing with Eq. (6.1), we conclude that the term linear in $u_{\alpha\alpha}$ reproduces our mean-field elastic free energy and therefore, that the coefficients of all higher-order terms must vanish identically. Furthermore, since the integration in Eq. (6.3) is over the volume of the undeformed gel, $V^{(0)} = V/(\lambda_x\lambda_y\lambda_z)$, the coefficient $\nu^{(0)}$ is given by $\nu^{(0)} = \nu\lambda_x\lambda_y\lambda_z$ and can be interpreted as the density of cross-links in the initial state. We conclude that the generalization of our elastic free energy for arbitrary deformations (because of the contribution of second-order strains this diagonal form describes shear deformations as well as volume changes) is given by

$$\frac{\mathscr{F}_{\mathrm{el}}[\boldsymbol{u}^{(0)}]}{T} = \int \mathrm{d}\boldsymbol{x}^{(0)} \nu^{(0)} \sum_{\alpha} u_{\alpha\alpha}(\boldsymbol{x}^{(0)}) . \tag{6.5}$$

Note that terms linear in the strain tensor (such as above) are usually neglected in ordinary continuum theories of elasticity of solids [21]. The reason for omitting them is that the theory of elasticity is an expansion about the equilibrium state of the solid and it is usually assumed that there are no internal stresses in this state. A different situation exists in a polymer gel which is solid permeated by a liquid. The equilibrium state of a gel is achieved by balancing the entropic tension in the chains against the osmotic pressure (which appears in the full free energy of the gel, equation (3.30)) and, therefore, non-vanishing elastic stresses exist in the network even in the absence of externally applied deformation [22].

We proceed to calculate the elastic modulus which governs the response to small fluctuations in the final deformed state of the homogeneous gel and, to this end, we consider a *small displacement with respect to the deformed state*. Referred to the initial undeformed state, the displacement can be written as

$$\boldsymbol{u}^{(0)}(\boldsymbol{x}^{(0)}) = \lambda \star \boldsymbol{x}^{(0)} - \boldsymbol{x}^{(0)} + \boldsymbol{u}(\lambda \star \boldsymbol{x}^{(0)}) , \tag{6.6}$$

where $\boldsymbol{u}(\lambda \star \boldsymbol{x}^{(0)}) = \boldsymbol{u}(\boldsymbol{x})$ is a small displacement of the point $\boldsymbol{x} = \lambda \star \boldsymbol{x}^{(0)}$ in the affinely stretched state of the network (Fig. 6.1).

We now express the free energy, Eq. (6.5), in terms of the displacement field, referred to the final deformed (and, depending on the deformation, possibly anisotropic) state. For this we need to

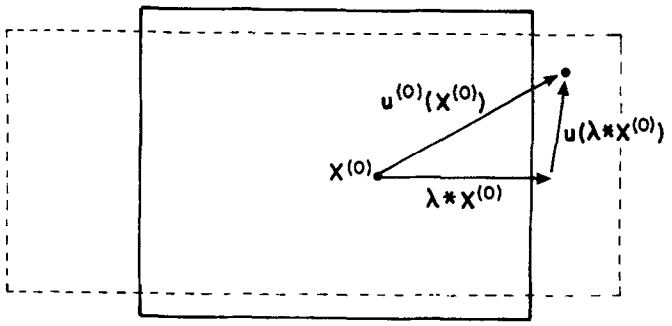


Fig. 6.1. The displacements $u^{(0)}(x^{(0)})$ and $u(\lambda \star x)$ of the point $x^{(0)}$ referred to the coordinates of the undeformed and the deformd gel, respectively. The undeformed and the deformed network is shown by solid and broken lines, respectively.

substitute Eq. (6.6) into Eq. (6.2), insert the expression for $u_{\alpha\alpha}$ into (6.5) and introduce the change of variables $x^{(0)} \to x$. Under this transformation, the gradient operators in the two states are related by

$$\partial/\partial x_\alpha^{(0)} = \lambda_\alpha \partial/\partial x_\alpha \tag{6.7}$$

and the volume element transforms as

$$dx^{(0)} = dx/\lambda_x\lambda_y\lambda_z \,. \tag{6.8}$$

Substituting these replacements into Eq. (6.5) and noticing that, upon integration, the terms linear in $\partial u_\alpha(x)/\partial x_\alpha$ contribute a surface term which balances the externally applied force (this term is omitted in the following), we obtain the elastic free energy functional

$$\mathscr{F}_{el}[u] = \mathscr{F}_{el}\{\lambda_\alpha\} + T\int dx \frac{\nu}{2}\sum_{\alpha\beta}\left(\lambda_\alpha \frac{\partial u_\beta(x)}{\partial x_\alpha}\right)^2 , \tag{6.9}$$

where $\mathscr{F}_{el}\{\lambda_\alpha\}$ is given by our mean-field expression, Eq. (6.1), and defines the *reference free energy of the deformed homogeneous state.*

In the Fourier representation, the free energy associated with small deformations and fluctuations about the affinely deformed state can be written as

$$\Delta\mathscr{F}_{el}[u] \equiv \mathscr{F}_{el}[u] - \mathscr{F}_{el}\{\lambda_\alpha\} = T\int \frac{dq}{(2\pi)^3}\frac{\nu}{2}(\lambda \star q)^2(u_q \cdot u_{-q}) \,. \tag{6.10}$$

Comparing this expression to the general form of the elastic free energy valid for small deformations with respect to the anisotropically stretched state

$$\Delta\mathscr{F}_{el}[u] = \frac{1}{2}\int \frac{dq}{(2\pi)^3}\sum_{ijkl} \Lambda_{ij;kl} q_i q_k (u_q)_j (u_{-q})_l \,, \tag{6.11}$$

we find that the effective elastic modulus for small fluctuations about the deformed state is given by

$$\Lambda_{ij;kl} = T\nu\lambda_i^2 \delta_{ik}\delta_{jl} \,. \tag{6.12}$$

We conclude that *the modulus of an anisotropically deformed network (for which some of the* $\{\lambda_i\}$ *differ from each other) depends on the externally imposed deformation and is, in general, anisotropic.*

### 6.2. Equilibrium state of deformed inhomogeneous gels and the butterfly effect

Up to this point we have constructed the expansion of the elastic free energy in terms of displacement field $\boldsymbol{u}(\boldsymbol{x})$, with respect to a deformed homogeneous state. Such a homogeneous state can no longer be considered as the equilibrium state of randomly cross-linked networks whose state of preparation is characterized by a spatially non-uniform distribution of cross-links and, therefore, a linear term in $\boldsymbol{u}(\boldsymbol{x})$ should appear in the above expansion. The coefficient of the linear term can be interpreted as a restoring force ($\boldsymbol{f}(\boldsymbol{x})$) produced by the internal elastic stresses, which drives the network towards its new inhomogeneous equilibrium state. This restoring force depends, in general, on the concrete realization of network structure $\boldsymbol{S}$ and on its deformation $\{\lambda_i\}$. In order to obtain the full free energy, we need to include also the osmotic term ($w\rho^2(\boldsymbol{x})/2$) which accounts for the excluded volume forces that tend to swell the network. The full free energy associated with deviations from an affinely deformed homogeneous reference state is

$$\Delta\mathscr{F}[\boldsymbol{u}] = T\int\frac{\mathrm{d}\boldsymbol{q}}{(2\pi)^3}\left[\frac{v}{2}(\lambda\star\boldsymbol{q})^2(\boldsymbol{u}_{\boldsymbol{q}}\cdot\boldsymbol{u}_{-\boldsymbol{q}}) + \boldsymbol{f}_{\boldsymbol{q}}\cdot\boldsymbol{u}_{-\boldsymbol{q}} + \frac{w\rho^2}{2}(\boldsymbol{q}\cdot\boldsymbol{u}_{\boldsymbol{q}})(\boldsymbol{q}\cdot\boldsymbol{u}_{-\boldsymbol{q}})\right], \tag{6.13}$$

where we have used the relation

$$\rho_{\boldsymbol{q}} = -\mathrm{i}\rho\boldsymbol{q}\cdot\boldsymbol{u}_{\boldsymbol{q}} \equiv -\mathrm{i}\rho|\boldsymbol{q}|u_{\boldsymbol{q}}^{\parallel} \tag{6.14}$$

to express the osmotic contributions in terms of the longitudinal components of the displacement field ($u_{\boldsymbol{q}}^{\parallel}$). The above equation can be obtained by Fourier transforming the geometric relation $\nabla\cdot\boldsymbol{u}(\boldsymbol{x}) = -\delta\rho(\boldsymbol{x})/\rho$ (which follows from the network mass conservation law) between the displacement $\boldsymbol{u}(\boldsymbol{x})$ and the monomer density change $\delta\rho(\boldsymbol{x})$ [21].

The displacement field $\langle\boldsymbol{u}(\boldsymbol{x})\rangle$ which describes the inhomogeneous equilibrium state of the deformed gel (referred to the affinely deformed homogeneous state) is obtained by minimizing this free energy with respect to $\boldsymbol{u}_{\boldsymbol{q}}$

$$v(\lambda\star\boldsymbol{q})^2\langle\boldsymbol{u}_{\boldsymbol{q}}\rangle + \boldsymbol{f}_{\boldsymbol{q}} + w\rho^2\boldsymbol{q}(\boldsymbol{q}\cdot\langle\boldsymbol{u}_{\boldsymbol{q}}\rangle) = 0\,. \tag{6.15}$$

The above relation can be interpreted as a *force balance condition which defines the mechanical equilibrium in the network.* The first term describes the elastic forces which arise due to the elastic response of stretched chains and tend to compress the network and, as was shown above, such a term is present even in a homogeneous network. The second term is a network-structure-dependent force which drives the deformed gel towards the inhomogeneous equilibrium state. The third (purely longitudinal) term gives the osmotic force which tends to swell the network. The vectorial equation can be decomposed into three scalar ones, one for the longitudinal component $\langle u_{\boldsymbol{q}}^{\parallel}\rangle$ (equivalent to the density – see Eq. (6.14)) and two for the transverse components $\langle\boldsymbol{u}_{\boldsymbol{q}}^{\perp}\rangle$ (shear displacements). Since earlier in this work we only considered density modes, we will focus on the force balance equation for the longitudinal component which can be written as

$$\langle u_{\boldsymbol{q}}^{\parallel}\rangle = -\frac{\boldsymbol{q}\cdot\boldsymbol{f}_{\boldsymbol{q}}}{v(\lambda\star\boldsymbol{q})^2 + w\rho^2\boldsymbol{q}^2}\,. \tag{6.16}$$

Using Eq. (6.14), the above equation can be recast into the form

$$\rho_{\boldsymbol{q}}^{\mathrm{eq}} = n_{\boldsymbol{q}}^{\mathrm{LW}}/(1 + wg_{\boldsymbol{q}}^{\mathrm{LW}})\,, \tag{6.17}$$

where we defined

$$g_q^{LW} \equiv \rho^2 q^2 / v(\lambda \star q)^2 \tag{6.18}$$

and

$$n_q^{LW} \equiv i\rho(q \cdot f_q)/v(\lambda \star q)^2 \,. \tag{6.19}$$

Note that since the density of cross-links is given by $v = \rho/2\bar{N}$, the above definition of $g_q^{LW}$ coincides with the long wavelength limit of the previously derived expression for the thermal correlator of the elastic reference state, $g_q$ (Eq. (4.33)). Furthermore, if we identify the expression for $n_q^{LW}$ with the long wavelength limit of the density in the elastic reference state, $n_q$, the expression for the Fourier components of the density profile, Eq. (6.17), is identical to the expression for the density profile of the inhomogeneous equilibrium state of the deformed gel, Eq. (4.20) (the finite value of $n_{q\to 0}$ in Eq. (4.34) is consistent with the requirement that, since $f(x)$ describes the internal restoring forces in the network, its integral over the volume of the gel must vanish and therefore $f_{q\to 0} = 0$). The equality $n_q^{LW} = n_{q\to 0} = \text{const.}$ (see Eq. (4.34) for the structure averaged correlator of $n_{q\to 0}$) allows us to write the longitudinal component of the restoring force $f_q^{\parallel}$ as

$$f_q^{\parallel} = -i[v(\lambda \star q)^2/\rho|q|]\, n_{q\to 0} \,. \tag{6.20}$$

When the gel is subjected to uniaxial deformation, the amplitudes of the elastic restoring force which would be present even in a homogeneous network (the first term in Eq. (6.15)), and of the force $f_q^{\parallel}$, increase in the stretching direction and decrease normal to it. We conclude that both forces originate in the elastic response of stretched chains to further deformation. This response is stronger in the direction of the applied deformation and the condition of mechanical equilibrium implies that the amplitude of the osmotic force must also increase along this direction, with the result that *the amplitude of the density modulation which characterizes the inhomogeneous equilibrium state of the deformed gel, must increase along the stretching direction and decrease normal to it.* This density profile produces the butterfly-shaped isointensity lines observed in scattering experiments.

In order to complete the connection between the present formulation and our RPA density functional results, let us now consider the thermal fluctuations about the inhomogeneous equilibrium state of the deformed gel. Since we are interested in the density fluctuations we will consider only the contribution of the longitudinal fluctuations of the displacement field ($\delta u^{\parallel}(x) = u^{\parallel}(x) - \langle u^{\parallel}(x)\rangle$) to the fluctuation free energy. Expanding the free energy, Eq. (6.13), in the fluctuations of the longitudinal component of the displacement field yields

$$\Delta\mathscr{F}^{\parallel}_{\text{fluct}}[u] = \frac{T}{2}\int \frac{dq}{(2\pi)^3}\,[v(\lambda \star q)^2 + w\rho^2 q^2]\,\delta u_q^{\parallel}\delta u^{\parallel}_{-q} \,. \tag{6.21}$$

Using the relation between the thermal density fluctuations and the longitudinal fluctuations of the displacement field (see Eq. (6.14)), $\rho_q^{th} = -i\rho|q|\delta u_q^{\parallel}$, in the equipartition theorem $\langle \delta u_q^{\parallel}\delta u^{\parallel}_{-q}\rangle = [v(\lambda \star q)^2 + w\rho^2 q^2]^{-1}$, we obtain the correlator of thermal density fluctuations about the inhomogeneous equilibrium state of the deformed gel

$$\langle \rho_q^{th}\rho^{th}_{-q}\rangle = g_q^{LW}/(1 + w g_q^{LW}) \,. \tag{6.22}$$

where we used the definition of $g_q^{LW}$, Eq. (6.18). The above result is identical to the previously derived expression for the long wavelength limit of the thermal correlator $G_q$ (Eq. (4.27)). We

therefore conclude that the continuum theory of elasticity of inhomogeneous deformed networks is equivalent to the long wavelength limit of our RPA density functional formulation.

The above discussion gives an explanation of the butterfly effect in the familiar language of balance of forces. We now understand that the *butterfly effect reveals the anisotropic and inhomogeneous character of the equilibrium state of the deformed network. The angular anisotropy factor* $(\lambda \star \boldsymbol{q})^2$ *expresses the fact that the elastic moduli of a deformed network (whether a homogeneous or an inhomogeneous one) depend on the magnitude and the direction of the deformation. The amplitude of the effect and the direction of the butterfly pattern (parallel to the stretching direction) are determined by the presence of static heterogeneities (non-vanishing* $n_{q\to 0}$*) and the effect would disappear in the absence of such inhomogeneities* (note that the thermal fluctuation contribution to the structure factor is much smaller than that of static inhomogeneities and the direction of angular anisotropy is perpendicular to the observed one – see Eq. (6.22)).

## 7. Discussion

In this work we studied the statistical mechanics of randomly cross-linked, arbitrarily deformed polymer networks. Starting from a "microscopic" Hamiltonian, we have used replica field theory in order to account for the heterogeneous structure of polymer networks and obtained extensive statistical information about the macroscopic, mesoscopic and microscopic behavior of polymer gels. Our solution of the statistical mechanics of this problem is on the same level of mathematical rigor as that of the well-established (static) theory of polymer solutions.

We have shown that once it is formed, a polymer network has a unique state of microscopic equilibrium which depends on temperature, quality of solvent, average monomer density and externally imposed deformation. This state of equilibrium is characterized by a unique set of average monomer positions (which change affinely with the macroscopic deformation of the network) or, equivalently, by a unique inhomogeneous monomer density profile. We have given a complete statistical characterization of this equilibrium profile in terms of the moments of the static equilibrium density profile.

We found that the intrinsic inhomogeneity of structure of the gel is determined by the density of cross-links in the state of preparation and by a dimensionless inhomogeneity parameter which measures the distance from the cross-link saturation threshold. Gels prepared by instantaneous cross-linking away from the cross-link saturation threshold (but still at much higher cross-link density compared to the gel point) have microscopic density heterogeneities, on length scales comparable to the mesh size (the wavelength associated with these heterogeneities increases with the degree of cross-linking and diverges at the cross-link saturation threshold). We have shown that gels prepared by cross-linking from semi-dilute solution away from the threshold are characterized by strong interpenetration of network chains, i.e., there are many cross-links in the volume spanned by a single chain (the shortest contour distance between two cross-links).

We showed that the elastic restoring forces in gels subjected to anisotropic deformation, depend both on the magnitude and the direction of the deformation and that the condition of mechanical equilibrium between the opposing elastic and osmotic forces, leads to the anisotropic density

profile which characterizes the inhomogeneous equilibrium state of stretched networks. This static anisotropic profile gives rise to the butterfly patterns in isointensity contours observed in static light and small angle neutron scattering experiments. Thermal fluctuations (which can be observed by dynamic light scattering) about the anisotropic equilibrium state are also anisotropic, but with anisotropy axes rotated by 90° with respect to those of the equilibrium profile.

Although the physical picture which emerges from our work is very different from that of the classical theories of polymer gels, many of our thermodynamic results (on the RPA level) agree qualitatively with the classical theories of elasticity of polymer networks [6, 8] and give rise to similar stress–strain relations. Such theories give a good description of the elasticity of swollen gels [74] but fail to predict the elastic response of dense networks for which Mooney–Rivlin corrections [75] have to be introduced. These corrections are usually attributed to entanglement effects which are important for concentrated, sparsely cross-linked ($\bar{N} \geq N_e$, where $N_e$ is the entanglement length) networks and which are not considered in this work.

New thermodynamic predictions made in our work concern phase separation in polymer networks swollen by low molecular weight solvents. We found that swollen gels will undergo microphase separation on a length scale of the order of the mesh size, at some temperature below the $\Theta$-point. Macrophase separation (by spinodal decomposition) will result under compression, or under uniaxial extension in the state of preparation (due to the divergence of thermal fluctuations in the directions normal to the stretching axis). Similar effects (stretching-induced segregation of free chains dispersed in the network) are predicted for gels swollen by polymeric solvents. Although we are unaware of any experimental studies on strain-induced spinodal decomposition in gels, shear effects on phase separation were recently observed in polymer solutions [76, 77], and blends [19]. In these systems, other mechanisms (notably the concentration dependence of the viscosity [78]) not considered in our work, are believed to play an important role.

New thermodynamic results were also obtained in the case of semi-dilute gels in good solvents. We found that fluctuations renormalize not only the osmotic but also the elastic part of the free energy which depends in a non-trivial way on the swelling of the gel. This leads to the breakdown of the classical additivity assumption and to the prediction of increased chain interpenetration upon compression (and desinterpenetration upon reswelling). Other interesting effects are the prediction of the concentration dependence of the shear modulus which differs from the classical one, and the emergence of a negative effective Poisson ratio at finite elongations [64].

A wealth of phenomena were predicted for the mesoscopic range of wavelengths probed by scattering experiments. We showed that the butterfly effect is the characteristic signature of the continuum theory of elasticity of polymer networks which gives rise to a deformation-dependent anisotropic elastic modulus, and that the observed enhancement of the scattering in the direction of stretching is dominated by the static inhomogeneities. Note that since the predicted angular dependence of the elastic modulus survives in the continuum limit, it can be observed, in principle, even by ultrasonic measurements on stretched networks.

Our detailed expressions for the structure factors of deformed networks allow us to use the results of scattering experiments to obtain (average) structural information about the network in its state of preparation, such as the average chain length between cross-links $\bar{N}$ and the value of the

heterogeneity parameter $X$ (which tells us how close to the cross-link saturation threshold the gel was prepared). Information about the distribution of chain lengths in the network can also be obtained by comparison with the scattering from reference polymer solutions (characterized by different molecular weight distributions). Although the present theory is restricted to the case of randomly (instantaneously) cross-linked networks, many of its qualitative predictions are applicable to networks made by end-linking of monodisperse polymer solutions. We hope that future experiments will be able to reproduce this aspect of our model (by preparing networks cross-linked by irradiation from solution) and attempt a quantitative comparison with our theory.

We would like to comment on the limitations and the possible extensions of our theory. While it does not include some of the features of real polymer gels (such as entanglement contributions to elasticity [79] and the non-Gaussian character of real chains [80]), it does capture what we consider to be the most important characteristics of polymer gels: the frozen randomness of their structure introduced by the statistical character of their preparation, and the interplay between short-range ("liquid") osmotic and long-range ("solid") elastic forces. Moreover, entanglement effects can be included by a proper generalization of the present model, which accounts for the effective "tube" introduced by the topological constraints [81]. This will allow one to study the transition from Mooney–Rivlin to Flory-type elasticity, with progressive swelling from the dense state of preparation to the semi-dilute, equilibrium swelling regime. Although our model strictly applies only to semi-dilute gels in which the second virial approximation holds (with the exception of the case of free chains dissolved in the network, where strong screening gives rise to a broader range of applicability of mean-field arguments), the generalization to the concentrated regime by replacing the second virial approximation by a concentration-dependent osmotic free energy, is straightforward.

The theory can be extended (work in progress) to the important case of weakly charged polyelectrolyte gels [82]. Another possible extension involves heterogeneous networks formed by random cross-linking of two different polymers. The most non-trivial extension involves the dynamics of gels and temporary networks [12]. This requires the introduction of viscous friction and consideration of temporary entanglements and offers a new perspective for the study of the viscoelastic behavior of polymers.

We would like to conclude this work with some general comments on the nature of randomly cross-linked polymer gels. Polymer gels are fundamentally different from both crystalline solids and amorphous solids (such as glasses). Unlike glasses, once they are formed by cross-linking, they have a unique state of equilibrium in which the average positions of all "atoms" (i.e., monomers) are completely defined by the thermodynamic conditions. Although, in the above sense, gels resemble ordinary crystalline solids, there are several important differences:

1. There is no long-range order in gels, whether periodic (as in crystals) or non-periodic (as in quasi-crystals). This is a consequence of the fact that the structure of a gel resembles a snapshot of the polymer solution from which it was formed.

2. In ordinary solids, fluctuations take place only on length scales smaller than the distance between the neighboring atoms (otherwise they melt, according to the Lindemann criterion). In gels, thermal fluctuations take place on length scales of the order of the distance between topologically neighboring cross-links (i.e., cross-links which are nearest neighbors along the chain contour), which is much larger than the distance between spatially neighboring cross-links (since

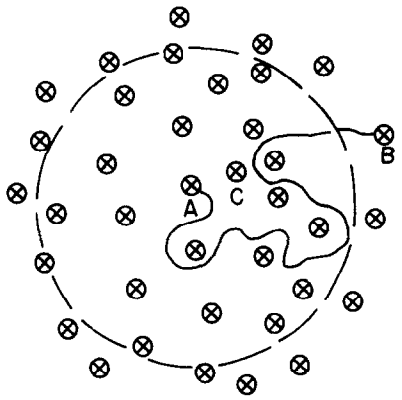


Fig. 7.1. Schematic drawing of spatially (A and C) and topologically (A and B) neighboring cross-links. The localization volume of cross-link A (the length scale of its thermal fluctuations) is indicated by the dashed circle.

there are many cross-links in the volume of a single mesh) – see Fig. 7.1. Nevertheless, since permanent cross-links are formed by strong covalent bonds, these large-scale thermal fluctuations do not result in melting and gels maintain their solid character as long as network chains remain unbroken.

3. In ordinary solids the attractive interactions are usually of the nearest-neighbor type. In polymer networks, the attractive interaction between cross-links is only due to the connecting chains and since the average distance between cross-links which are neighbors along the chain contour is much larger than the distance between cross-links which are neighbors in space (Fig. 7.1), the attractive interaction has a long-range character. This also means that the length of the average minimal cycle (the minimal contour length of a closed path emanating from a cross-link) is much larger than the mesh size. Since this contour length determines the length scale on which the shear rigidity of a solid is established [22] (there would be no resistance to shear at all, in the absence of such cycles, in a non-entangled polymer network), gels are soft solids.

The above discussion suggests that polymer gels are the only known example of a new class of materials which can be called *soft disordered equilibrium solids.*

## Acknowledgements

We are extremely grateful to S. Alexander for many stimulating conversations and numerous insightful comments on our manuscript. Valuable discussions with S. Edwards and written correspondence with P. Goldbart are also acknowledged. Finally, we would like to thank P. Pekarski and A. Feigel for helping with the figures and for useful comments. One of us (SP) would like to acknowledge the hospitality of the Department of Physics of Bar-Ilan University, where this work was done. This research was supported by grants from the Israeli Academy of Sciences and Humanities, the Israeli Ministry of Science and Technology and the Bar-Ilan University.

## Appendix A. Field theoretical preliminaries

### A.1. Functional integrals

We start with the following fundamental identity for a *Gaussian* field $\psi(x)$:

$$\left\langle \exp\left\{\int dx h(x)\psi(x)\right\}\right\rangle_{\psi}$$
$$\equiv \int D\psi(x) P[\psi(x)] \exp\left\{\int dx h(x)\psi(x)\right\}$$
$$= \exp\left\{\frac{1}{2}\int dx \int dx' h(x) g(x,x') h(x')\right\}, \tag{A.1}$$

where the averaging is performed with the weight

$$P[\psi] = \frac{\exp\left\{-\frac{1}{2}\int dx \int dx' \psi(x) g^{-1}(x,x')\psi(x')\right\}}{\int D\psi(x) \exp\left\{-\frac{1}{2}\int dx \int dx' \psi(x) g^{-1}(x,x')\psi(x')\right\}}. \tag{A.2}$$

In Eq. (A.1) $h(x)$ is an auxiliary vector field and $g$ is an arbitrary positive-definite operator. Its inverse, $g^{-1}$, is defined by

$$\int dx'' g^{-1}(x,x'') g(x'',x') = \delta(x - x'). \tag{A.3}$$

Identity (A.1) can be proved by introducing a shift

$$\psi(x) \to \psi(x) + \int dx' g(x,x') h(x')$$

into the second term in Eq. (A.1). Differentiating the third term in this equation with respect to the field $h$ and taking the limit $h = 0$, yields

$$g(x,x') = \frac{\delta^2}{\delta h(x)\delta h(x')} \left\langle \exp\left\{\int dx h(x)\psi(x)\right\}\right\rangle_{\psi}\Bigg|_{h=0}$$
$$= \int D\psi \psi(x)\psi(x') P[\psi(x)] \equiv \langle \psi(x)\psi(x')\rangle_{\psi}. \tag{A.4}$$

Here we have used the usual definition of a functional derivative

$$\delta I[h] \equiv I[h + \delta h] - I[h] = \int dx \, \delta h(x) \frac{\delta I[h]}{\delta h(x)}, \tag{A.5}$$

which holds to first order in the arbitrarily small variation $\delta h$.

In the case when the function $g$ depends only on the difference of its arguments, $g(\boldsymbol{x},\boldsymbol{x}') = g(\boldsymbol{x}-\boldsymbol{x}')$, it is convenient to write down Eqs. (A.1)–(A.4), in terms of the Fourier coefficients.

$$\left\langle \exp\left\{ \int \frac{d\boldsymbol{q}}{(2\pi)^3} h_{\boldsymbol{q}} \psi_{-\boldsymbol{q}} \right\} \right\rangle_{\psi} \equiv \exp\left\{ \frac{1}{2} \int \frac{d\boldsymbol{q}}{(2\pi)^3} \frac{h_{\boldsymbol{q}} h_{-\boldsymbol{q}}}{g_{\boldsymbol{q}}} \right\} . \tag{A.6}$$

The averaging is performed with the weight

$$P[\psi] = \exp\left\{ \frac{1}{2} \int \frac{d\boldsymbol{q}}{(2\pi)^3} \left[ \ln(2\pi g_{\boldsymbol{q}}) - \frac{\psi_{\boldsymbol{q}} \psi_{-\boldsymbol{q}}}{g_{\boldsymbol{q}}} \right] \right\} , \tag{A.7}$$

where the $\ln(2\pi g_{\boldsymbol{q}})$ contribution comes from integrating the denominator in Eq. (A.2). In deriving the above equation we used the fact that Eq. (A.3) becomes a trivial identity in the Fourier representation, $g_{\boldsymbol{q}}^{-1} = 1/g_{\boldsymbol{q}}$. Eq. (A.4) transforms into

$$g_{\boldsymbol{q}} = \langle \psi_{\boldsymbol{q}} \psi_{-\boldsymbol{q}} \rangle_{\psi} . \tag{A.8}$$

*A.2. Field representation for Gaussian chains*

Eq. (A.4) can be used to construct the field theoretical representation of the partition function of a Gaussian chain of $N$ monomers with ends fixed at points $\boldsymbol{x}$ and $\boldsymbol{x}'$, in an external field $h(\boldsymbol{x})$. This function is given by the functional integral

$$G_N\{\boldsymbol{x},\boldsymbol{x}';[h]\} = \int_{\boldsymbol{x}}^{\boldsymbol{x}'} D\boldsymbol{x}(s) \exp\left\{ - \int_0^N ds \left[ \frac{1}{2a^2} \left( \frac{d\boldsymbol{x}}{ds} \right)^2 + h(\boldsymbol{x}(s)) \right] \right\} , \tag{A.9}$$

which is the solution of the diffusion-like equation

$$\left[ \frac{\partial}{\partial N} - a^2 \nabla^2 + h(\boldsymbol{x}) \right] G_N\{\boldsymbol{x},\boldsymbol{x}';[h]\} = 0 , \tag{A.10}$$

with the "initial" condition

$$G_N\{\boldsymbol{x},\boldsymbol{x}';[h(\boldsymbol{x})]\}|_{N=0} = \delta(\boldsymbol{x}-\boldsymbol{x}') . \tag{A.11}$$

It is convenient to introduce the grand canonical analog of this partition function by the Laplace transform:

$$G\{\boldsymbol{x},\boldsymbol{x}';[h]\} = \int_0^{\infty} dN e^{-\mu N} G_N\{\boldsymbol{x},\boldsymbol{x}';[h]\} , \tag{A.12}$$

where $\mu$ is the chemical potential of monomers. Using the Laplace transform of Eq. (A.10) with the initial condition (A.11), it can be shown that this function obeys the equation

$$[\mu - a^2 \nabla^2 + h(\boldsymbol{x})] G\{\boldsymbol{x},\boldsymbol{x}';[h]\} = \delta(\boldsymbol{x}-\boldsymbol{x}') . \tag{A.13}$$

Comparison of Eqs. (A.3) and (A.13) shows that the inverse operator $G^{-1}\{\boldsymbol{x},\boldsymbol{x}';[h]\}$ is defined by

$$G^{-1}\{\boldsymbol{x},\boldsymbol{x}';[h]\} = \delta(\boldsymbol{x}-\boldsymbol{x}')[\mu - a^2 \nabla^2 + h(\boldsymbol{x})] . \tag{A.14}$$

We proceed to derive an explicit field theoretical expression for the grand canonical partition function of a Gaussian chain. Substituting the operator $G^{-1}$ into (A.2), performing the integration over $x'$ with the aid of the $\delta$-function, and transforming the Laplacian into a square gradient by integration in parts, we finally obtain

$$G\{x,x';[h]\} = \frac{\int D\varphi \varphi(x)\varphi(x') \exp\{-H_0[h,\varphi]\}}{\int D\varphi \exp\{-H_0[h,\varphi]\}}, \tag{A.15}$$

where the effective (dimensionless) Hamiltonian $H_0$ is defined as

$$H_0[h,\varphi] = \int dx \left[ \tfrac{1}{2}(\mu + h(x))\varphi^2(x) + \frac{a^2}{2}(\nabla\varphi(x))^2 \right] \tag{A.16}$$

In order to avoid dealing with the denominator in Eq. (A.15) we introduce de Gennes' $n = 0$ model. The trick consists of introducing an $n$-component vector field $\boldsymbol{\varphi}(x)$ with components $\varphi_i(x)$; $i = 1, \ldots, n$ and noticing that Eq. (A.15) can be formally written as

$$G\{x,x';[h]\} = \lim_{n\to 0}\left[ \int D\varphi \exp\{-H_0[h,\varphi]\} \right]^{n-1} \times \int D\varphi_1 \varphi_1(x)\varphi_1(x') \exp\{-H_0[h,\varphi_1]\}. \tag{A.17}$$

Since, for integer $n$ one can write

$$\left[ \int D\varphi \exp\{-H_0[h,\varphi]\} \right]^{n-1} = \prod_{i=2}^{n} \int D\varphi_i \exp\{-H_0[h,\varphi_i]\}, \tag{A.18}$$

Eq. (A.17) can be recast into the simple expression:

$$G\{x,x'\ [h]\} = \int D\boldsymbol{\varphi} \varphi_1(x)\varphi_1(x') \exp\{-H_0[h,\boldsymbol{\varphi}]\}, \tag{A.19}$$

where an analytic continuation over the number of components of the field $\boldsymbol{\varphi}$, from integer values of $n$ to the limit $n = 0$ is implied. Here, $H_0[h,\boldsymbol{\varphi}]$ is defined by replacing $\varphi$ by $\boldsymbol{\varphi}$ in $H_0[h,\varphi]$ and using

$$\boldsymbol{\varphi}^2(x) \equiv \sum_{i=1}^{n} \varphi_i^2(x), \quad (\nabla\boldsymbol{\varphi}(x))^2 = \sum_{i=1}^{n} (\nabla\varphi_i(x))^2. \tag{A.20}$$

## Appendix B. Mean-field Hamiltonian

### *B.1. Replica space integration*

We start with expression (3.29) for the mean-field Hamiltonian (reproduced here again, for convenience):

$$H_{mf} = \int d\hat{x}\, \tilde{H}(\varsigma) + \frac{w^{(0)}}{2} V^{(0)}(\rho^{(0)})^2 + m\frac{w}{2} V\rho^2. \tag{B.1}$$

We first calculate the replica integrals $\int d\hat{x}\tilde{H}(\varsigma) = \int dx_L \int dx_T \tilde{H}(\varsigma)$. Since the integrand depends only on the variable $\varsigma \equiv \frac{1}{2}(\hat{x}_T)^2$, the $x_T$ integration can be splitted into the product of a trivial angular factor $\int d\Omega$ which gives the surface area of a $3m$-dimensional unit sphere, $S_{3m} = 2\pi^{3m/2}/\Gamma(3m/2)$ ($\Gamma$ is the gamma-function), and an integral of the form $\int d|x_T|\,|x_T|^{3m-1}$. The last integral can be written as $\int_0^\infty d\varsigma(2\varsigma)^{3m/2-1}$ and combining both contributions and integrating by parts, we obtain

$$\int dx_T \tilde{H}(\varsigma) = S_{3m}\int_0^\infty d\varsigma(2\varsigma)^{3m/2-1}\tilde{H}(\varsigma)$$

$$= -\int_0^\infty d\zeta \frac{(2\pi\varsigma)^{3m/2}}{(3m/2)\cdot\Gamma(3m/2)}\frac{d\tilde{H}(\varsigma)}{d(\varsigma)}. \tag{B.2}$$

In obtaining the last equality we have used the relation $\tilde{H}(\infty) = 0$, which follows from the observation that the integrand (the Hamiltonian density, $\tilde{H}(\zeta)$) is a polynomial in $\varphi_{mf}(\varsigma)$, and thus it decreases exponentially fast with $\zeta$, for $\varsigma \to \infty$ (see Eqs. (3.24) and (3.26)). Expanding to first order in $m$ and using the relations $(3m/2)\cdot\Gamma(3m/2) = \Gamma(1 + 3m/2) \to 1 - 3m\gamma/2$ ($\gamma$ is Euler's constant) and $(2\pi\varsigma)^{3m/2} \to 1 + (3m/2)\ln(2\pi\varsigma)$, yields

$$\int dx_T \tilde{H}(\varsigma) \xrightarrow{m\to 0} \tilde{H}(0) - \frac{3m}{2}\int_0^\infty d\varsigma \ln(2\pi\zeta e^\gamma)\frac{d\tilde{H}(\varsigma)}{d\varsigma}. \tag{B.3}$$

In order to calculate the above integral it is convenient to introduce the dimensionless variable $t$ defined in Eq. (3.24). Writing $\ln\varsigma = \ln(a^2\bar{N}) + \ln t$ and neglecting the $\ln t$ term, yields $\tilde{H}(0)[1 + m\ln(a\sqrt{\bar{N}})^3]$.

The exponentially fast decrease (with $\varsigma$) of the integrand in Eq. (B.2), means that dominant contribution to the integral comes from values of $\varsigma$ in the interval between zero and $a^2\bar{N}$. We can use this fact to perform the remaining $dx_L$ integration, which goes over an infinite region (the integrand does not depend on the coordinates $x_L$). Note that the condition $\varsigma = 0$ is equivalent to $y_\alpha^{(k)} = 0$ or, equivalently to $x_\alpha^{(k)} = \lambda_\alpha x_\alpha^{(0)}$ (see Eq. (3.10)). Substituting the latter relation into the definition of $x_L$ (Eq. (3.19)),

$$x_{L\alpha} \equiv \sum_{k=0}^{m} e_\alpha^{(k)} x_\alpha^{(k)} = \frac{x_\alpha^{(0)} + \sum_{k=1}^{m}\lambda_\alpha x_\alpha^{(k)}}{(1 + m\lambda_\alpha^2)^{1/2}} = (1 + m\lambda_\alpha^2)^{1/2} x_\alpha^{(0)} \tag{B.4}$$

and integrating over $x^{(0)}$ we find that the integration over $x_{L\alpha}$ contributes the factor

$$V_L \equiv V^{(0)}\prod_\alpha (1 + m\lambda_\alpha^2)^{1/2}, \tag{B.5}$$

where $V^{(0)}$ is the initial volume of the gel. Finally, multiplying the results of the transverse and longitudinal integrations and expanding to first order in $m$ yields

$$\int dx \tilde{H}(\zeta) = \tilde{H}(0)V^{(0)}\left[1 + m\left(\ln(a\sqrt{\bar{N}})^3 + \frac{1}{2}\sum_\alpha \lambda_\alpha^2\right)\right], \tag{B.6}$$

where $\tilde{H}(0)$ is obtained from Eq. (3.19), $\tilde{H}(0) = \mu\rho_{mf}^{(0)} - z_c(\rho_{mf}^{(0)})^2$.

We proceed to calculate the contribution of the second term on the right-hand side of Eq. (B.1). The density in the zeroth replica is evaluated using the equality

$$N_{\rm tot} = \int \mathrm{d}\boldsymbol{x}^{(0)} \rho^{(0)} = \int \mathrm{d}\hat{\boldsymbol{x}} \rho_{\rm mf}(\varsigma) \,, \tag{B.7}$$

where the second equality is obtained from the definition (2.33). Notice that since no assumptions about the precise functional form of $\tilde{H}(\varsigma)$ were used in the derivation of Eq. (B.6), we can write (using $\rho_{\rm mf}(0) = \rho_{\rm mf}^{(0)}$)

$$N_{\rm tot} = \rho_{\rm mf}^{(0)} V^{(0)} \left[ 1 + m \left( \ln(a\sqrt{\bar{N}})^3 + \frac{1}{2} \sum_{\alpha} \lambda_{\alpha}^2 \right) \right] . \tag{B.8}$$

This defines the density in the replica of the initial state, $\rho^{(0)} = N_{\rm tot}/V^{(0)}$.

Collecting all the terms in (B.1) and using Eqs. (3.4) and (3.5), after some algebra we arrive at the expression

$$H_{\rm mf} = \tfrac{1}{2} \mu (\rho_{\rm mf}^{(0)})^2 V^{(0)} + m \left[ N_{\rm c} \left( \frac{1}{2} \sum_{\alpha} \lambda_{\alpha}^2 + \ln(a\sqrt{\bar{N}})^3 \right) + \frac{w}{2} V \rho^2 \right] . \tag{B.9}$$

### *B.2. The longitudinal subspace*

We now show that the condition $\varsigma = 0$ is equivalent to demanding that the deformation is affine in each of the replicas of the deformed state, i.e., $\boldsymbol{x}^{(k)} = \lambda \star \boldsymbol{x}^{(0)}$. Using Eq. (3.20), the former condition can be written as

$$\begin{aligned} &\sum_{k=0}^{m} (\boldsymbol{x}^{(k)})^2 - \sum_{\alpha} \frac{1}{1 + m\lambda_{\alpha}^2} \left[ \boldsymbol{e}_{\alpha} \cdot \boldsymbol{x}^{(0)} + \sum_{k=1}^{m} \lambda_{\alpha} \boldsymbol{e}_{\alpha} \cdot \boldsymbol{x}^{(k)} \right]^2 \\ &\quad = \sum_{\alpha} \left[ \sum_{k=1}^{m} (y_{\alpha}^{(k)})^2 - \frac{\lambda_{\alpha}^2}{1 + m\lambda_{\alpha}^2} \left( \sum_{k=1}^{m} y_{\alpha}^{(k)} \right)^2 \right] \\ &\quad = \sum_{\alpha} \sum_{k,l=1}^{m} \left( \delta_{kl} - \frac{\lambda_{\alpha}^2}{1 + m\lambda_{\alpha}^2} \right) y_{\alpha}^{(k)} \, y_{\alpha}^{(l)} = 0 \,, \end{aligned} \tag{B.10}$$

where the first equality is obtained, upon some algebra, from the definition (3.10), $\boldsymbol{y}^{(k)} = \boldsymbol{x}^{(k)} - \lambda \star \boldsymbol{x}^{(0)}$. All the eigenvalues of the matrix in brackets can be shown to be positive and, therefore, the last equality can be satisfied only if $y_{\alpha}^{(k)} = 0$ (for all $\alpha$ and $k$), which completes our proof. We conclude that the condition $\varsigma = 0$ defines a 3-dimensional surface in the replica space, on which the affine relation between the coordinates of the initial and the final replicas is satisfied. This surface will be called the *longitudinal* subspace in the following. Its volume $V_{\rm L}$ was calculated in Eq. (B.5). Since the mean-field solution decays on a length scale of the order of the average distance between cross-links, $a\bar{N}^{1/2}$ (see Eq. (3.26)), we conclude that the *average* positions of all the monomers in the replicas of the deformed state are uniquely defined by their positions in the initial undeformed state (they can be obtained from the latter by the affine transformation $\boldsymbol{x}^{(0)} \to \lambda \star \boldsymbol{x}^{(0)}$), and that deviations from affinity can only take place due to thermal fluctuations about these average positions, on distances of the order of the mesh size.

## Appendix C. Spectrum of fluctuations

An arbitrary fluctuation $\delta\varphi$ can be represented as a linear combination of the eigenmodes $\psi$. Since $\psi$ is the solution of a linear equation, it is only defined up to a multiplicative constant. In the following, we will choose this constant to be unity so that for each fluctuation mode we have

$$\delta\varphi(\hat{x}) = \psi(\hat{x}) . \tag{C.1}$$

### *C.1. Homogeneous solution*

The first step is to calculate the spectrum of eigenvalues of the operator $K^{\parallel}$ (Eq. (3.35)) evaluated on the constant solution $\varphi_{\mathrm{mf}}(\hat{x}) = \text{const}$. We will show that some of the eigenvalues of this operator are negative and therefore will not study further the spectrum of the operator $K^{\perp}$ for the homogeneous mean-field solution. The secular equation is obtained by substituting Eq. (3.35) into Eq. (3.36) and removing $\delta(\hat{x} - \hat{x}')$ by integrating over $\hat{x}'$:

$$(-z_c\varphi_{\mathrm{mf}}^2 - a^2\hat{\nabla}^2)\psi^{\parallel}(\hat{x}) + \varphi_{\mathrm{mf}}^2 \sum_{k=0}^{m} w^{(k)} \prod_{l\neq k} \int \mathrm{d}x^{(l)}\psi^{\parallel}(\hat{x}) = \Lambda^{\parallel}\psi^{\parallel}(\hat{x}). \tag{C.2}$$

As can be verified by direct substitution into the resulting equation, the solutions are plane waves, $\psi^{\parallel}(\hat{x}) \sim \exp(\mathrm{i}\hat{q}\cdot\hat{x})$. Using the identities: $\int \mathrm{d}x \exp(\mathrm{i}q\cdot x) = 0$ for $q \neq 0$ and $\int \mathrm{d}x \exp(\mathrm{i}q\cdot x) = V$ for $q = 0$ ($V$ is the volume of the final system), we have the following scenarios, depending on the direction of the wave vector $\hat{q}$:

1. For wave vectors which lie in the $i$th ($\hat{q}^{(i)} \equiv (0, \ldots q^{(i)}, \ldots 0)$) sector of replica space, the only contribution comes from the $i$th term in the sum (since otherwise, one of the integrations over the $l \neq k$ replicas will be over the coordinate $x^{(i)}$ and the corresponding integral will vanish). In this case the factor $\exp(\mathrm{i}\hat{q}\cdot\hat{x})$ can be taken outside the integrals and the integrations will result in the product of the volumes of all replicas except the $i$th one. We have to distinguish between two cases:

(a) For wave vectors lying completely in the 0th (i.e., $\hat{q}^{(0)} \equiv (q^{(0)}, 0, \ldots, 0)$) replica, the integration produces a factor of $V^m$ and taking the limit $m \to 0$ and collecting the terms in Eq. (C.2), we find the eigenvalues

$$\Lambda^{\parallel}(\hat{q}^{(0)}) = (w^{(0)} - z_c)\varphi_{\mathrm{mf}}^2 + a^2(q^{(0)})^2 \tag{C.3}$$

(b) For wave vectors which lie completely in the $k$th (i.e., $\hat{q}^{(k)} \equiv (0, \ldots q^{(k)}, 0)$) sector of replica space ($k \neq 0$), the integration produces a factor of $V^{(0)}V^{m-1}$ and in the limit $m \to 0$ we find the eigenvalues

$$\Lambda^{\parallel}(q^{(k)}) = (wV^{(0)}/V - z_c)\varphi_{\mathrm{mf}}^2 + a^2(q^{(k)})^2 . \tag{C.4}$$

2. For all other wave vectors, which are not restricted to these sectors (i.e., $\hat{q} \equiv (q^{(0)}, \ldots, q^{(k)}, \ldots, q^{(m)})$), the sum in Eq. (C.2) does not contribute to the eigenvalue equation and we obtain

$$\Lambda^{\parallel}(\hat{q}) = -z_c\varphi_{\mathrm{mf}}^2 + a^2\hat{q}^2 . \tag{C.5}$$

The presence of the negative eigenvalues in Eq. (C.5) (for small enough values of $q$) shows that the constant solution corresponds to a saddle point, rather than to a minimum of the Hamiltonian. We conclude that the solution which has the full translational invariance of $H$ does not represent its ground state, and proceed to examine the stability of solutions with spontaneously broken translational symmetry.

### C.2. *Inhomogeneous solution*

We turn to the calculation of the solutions of the secular equations, (3.36), which correspond to the inhomogeneous mean-field solution $\varphi_{\mathrm{mf}}(\hat{x}) = \varphi_{\mathrm{mf}}(\varsigma)$ (Eq. (3.24)). Note that the mean-field solution does not depend on the 3-dimensional vector $\boldsymbol{x}_{\mathrm{L}}$, defined by the projection $x_{\mathrm{L}\alpha}$ of the replica space vector $\hat{x}$ on the *longitudinal* subspace spanned by the three vectors $\hat{e}_\alpha$, $\alpha = x, y, z$ (Eqs. (3.18) and (3.19)). This fact can be used to simplify the calculations by performing a partial Fourier transform with respect to the coordinates $x_{\mathrm{L}\alpha}$

$$f(\hat{x}) = \int \frac{\mathrm{d}\boldsymbol{q}_{\mathrm{L}}}{(2\pi)^3} f_{q_{\mathrm{L}}}(\boldsymbol{x}_{\mathrm{T}}) \exp(\mathrm{i}\boldsymbol{q}_{\mathrm{L}} \cdot \boldsymbol{x}_{\mathrm{L}}) , \tag{C.6}$$

where $\boldsymbol{x}_{\mathrm{T}}$ is a $3m$-dimensional vector in the *transverse* subspace defined as the orthogonal complement to the longitudinal subspace (here $f(\hat{x})$ is an arbitrary function of replica space coordinates). The advantage of this representation becomes evident by noticing that when the Laplacian $\hat{\nabla}^2$ is applied to the function $f(\hat{x})$, we obtain

$$\hat{\nabla}^2 f(\hat{x}) = \int \frac{\mathrm{d}\boldsymbol{q}_{\mathrm{L}}}{(2\pi)^3} (\nabla_{\mathrm{T}}^2 - \boldsymbol{q}_{\mathrm{L}}^2) f_{q_{\mathrm{L}}}(\boldsymbol{x}_{\mathrm{T}}) \exp(\mathrm{i}\boldsymbol{q}_{\mathrm{L}} \cdot \boldsymbol{x}_{\mathrm{L}}) , \tag{C.7}$$

where the Laplacian $\nabla_{\mathrm{T}}^2$ is taken only with respect to the $\boldsymbol{x}_{\mathrm{T}}$ coordinates.

In the following, we will express all eigenfunctions $\psi(\hat{x})$, in terms of their longitudinal Fourier components

$$\psi(\hat{x}) = \psi_{q_{\mathrm{L}}}(\boldsymbol{x}_{\mathrm{T}}) \exp(\mathrm{i}\boldsymbol{q}_{\mathrm{L}} \cdot \boldsymbol{x}_{\mathrm{L}}) , \tag{C.8}$$

and label the corresponding eigenvalues as $\Lambda(\boldsymbol{q}_{\mathrm{L}})$.

#### C.2.1. *Rotational modes*

The eigenvalues and eigenfunctions of the operator $K^{\perp}$ can be obtained by substituting the mean-field solution $\varphi_{\mathrm{mf}}(\varsigma)$ into Eq. (3.36). Using the above-defined Fourier representation for the eigenfunctions $\psi^{\perp}(\hat{x})$, the corresponding secular equation becomes

$$[1/\bar{N} - a^2 \nabla_{\mathrm{T}}^2 + a^2 \boldsymbol{q}_{\mathrm{L}}^2 - \Lambda^{\perp}(\boldsymbol{q}_{\mathrm{L}}) - (z_{\mathrm{c}}/2)\varphi_{\mathrm{mf}}(\varsigma)]\psi_{q_{\mathrm{L}}}^{\perp}(\boldsymbol{x}_{\mathrm{T}}) = 0 . \tag{C.9}$$

The general solution of this equation, which satisfies the orthogonality condition $\boldsymbol{\psi}_{q_{\mathrm{L}}}^{\perp}(\boldsymbol{x}_{\mathrm{T}}) \cdot \boldsymbol{n} = 0$, is of the form $\boldsymbol{\psi}_{q_{\mathrm{L}}}^{\perp}(\boldsymbol{x}_{\mathrm{T}}) = \psi_{q_{\mathrm{L}}}^{\perp}(\boldsymbol{x}_{\mathrm{T}})\delta\boldsymbol{n}_{q_{\mathrm{L}}}$, where $\delta\boldsymbol{n}_{q_{\mathrm{L}}}$ is an arbitrary vector which satisfies the condition $\delta\boldsymbol{n}_{q_{\mathrm{L}}} \cdot \boldsymbol{n} = 0$. The function $\psi_{q_{\mathrm{L}}}^{\perp}(\boldsymbol{x}_{\mathrm{T}})$ is obtained from the scalar variant of Eq. (C.9). Since the vector $\delta\boldsymbol{n}_{q_{\mathrm{L}}}$ has $n-1$ independent components, each of the eigenvalues $\Lambda^{\perp}(\boldsymbol{q}_{\mathrm{L}})$ is $n-1$-fold degenerate.

Notice that the above equation has the form of a Shröedinger equation with a spherically symmetric potential. As is well-known from quantum mechanics, the ground state solution which

corresponds to the minimal value of $\Lambda^{\perp}$ is spherically symmetric [83]. Although there are also non-spherically symmetric solutions, they have higher energy and do not have to be considered in the present context (study of the stability of the inhomogeneous solution, $\varphi_{\mathrm{mf}}(\varsigma)$).

The spherically symmetric solution can be found from the observation that Eq. (C.9) is identical in form to the mean-field Eq. (3.1) and, therefore, the solution is simply

$$\psi^{\perp}_{q_{\mathrm{L}}}(x_{\mathrm{T}}) = \varphi_{\mathrm{mf}}(\varsigma)\,\delta n_{q_{\mathrm{L}}}\,, \tag{C.10}$$

where $\varsigma = x_{\mathrm{T}}^2/2$. The corresponding eigenvalues are obtained by substituting this solution back into Eq. (C.9) and using Eq. (3.1):

$$\Lambda^{\perp}(q_{\mathrm{L}}) = a^2 q_{\mathrm{L}}^2\,. \tag{C.11}$$

These eigenfunctions and eigenvalues are associated with the rotations of the vector $\boldsymbol{n}$ in the abstract $n$-dimensional space. This can be demonstrated by showing how the field $\boldsymbol{\varphi}$ transforms under the infinitesimal rotation $\boldsymbol{n} \to \boldsymbol{n} + \delta\boldsymbol{n}$, with $\delta\boldsymbol{n}(\hat{x}) \equiv \delta\boldsymbol{n}_{q_{\mathrm{L}}} \exp(i\boldsymbol{q}_{\mathrm{L}} \cdot \boldsymbol{x}_{\mathrm{L}})$. Under this rotation

$$\delta^{\perp}\boldsymbol{\varphi}(\hat{x}) = \boldsymbol{\varphi}_{\mathrm{mf}}(\varsigma)|_{\boldsymbol{n} \to \boldsymbol{n} + \delta\boldsymbol{n}} - \boldsymbol{\varphi}_{\mathrm{mf}}(\varsigma) = \varphi_{\mathrm{mf}}(\varsigma)\delta\boldsymbol{n}(\hat{x})\,. \tag{C.12}$$

Since $\delta\boldsymbol{n}(\hat{x})$ is orthogonal to $\boldsymbol{n}$, the deviation (C.12) corresponds to the transverse mode of the fluctuations. These solutions are gapless Goldstone modes, i.e., their eigenvalues are positive definite and vanish in the long wavelength limit. The situation is equivalent to that of a ferromagnet (with $n \to 0$ spin components) where the Goldstone modes describe "soft" ($q \to 0$) rotations of the magnetization vector [36], although in our case these modes do not have a simple physical interpretation.

We proceed to calculate the spectrum of the operator $K^{\shortparallel}$. The secular equation (3.36) is obtained by substituting the mean-field solution, expression (3.24), into Eq. (3.35), where for simplicity of notation, we drop the superscript $^{\shortparallel}$ everywhere in the following:

$$[1/\bar{N} - a^2\hat{\nabla}^2 - 3(z_{\mathrm{c}}/2)\varphi^2_{\mathrm{mf}}(\varsigma)]\psi(\hat{x}) + \varphi_{\mathrm{mf}}(\varsigma)\sum_{k=0}^{m} w^{(k)}\,\delta\rho^{(k)}(x^{(k)}) = \Lambda\psi(\hat{x})\,, \tag{C.13}$$

with $w^{(k)} = w$ for $k = 1, \ldots, m$. Here,

$$\delta\rho^{(k)}(x^{(k)}) = \int \mathrm{d}\hat{x}'\,\delta(x^{(k)} - x'^{(k)})\varphi_{\mathrm{mf}}(\varsigma')\psi(\hat{x}') \tag{C.14}$$

is the density fluctuation in the $k$th replica (this identification follows from Eqs. (2.32), (2.46) and (C.1)).

Eqs. (C.13) and (C.14) admit two types of solutions which can be classified according to whether the density fluctuations $\delta\rho^{(k)}$ do or do not vanish identically in all the replicas (i.e., for all $k$).

### C.2.2. *Shear modes*

Consider the case

$$\delta\rho^{(k)}(x^{(k)}) = 0 \quad \text{for all } k\,. \tag{C.15}$$

Such fluctuations correspond to *pure shear* modes, i.e., to displacements in replica space which do not affect the density in each of the replicas. Substituting the partial Fourier transform, Eq. (3.37), into Eq. (C.13) we can recast the latter into the form:

$$[1/\bar{N} - a^2\nabla_{\mathrm{T}}^2 + a^2\boldsymbol{q}_{\mathrm{L}}^2 - \Lambda(\boldsymbol{q}_{\mathrm{L}}) - 3(z_{\mathrm{c}}/2)\varphi_{\mathrm{mf}}^2(\varsigma)]\psi_{\boldsymbol{q}_{\mathrm{L}}}(\boldsymbol{x}_{\mathrm{T}}) = 0\,. \tag{C.16}$$

It is convenient to represent this equation in a dimensionless form by introducing the $3m$-dimensional vector $\boldsymbol{r} \equiv \boldsymbol{x}_{\mathrm{T}}/(a\bar{N}^{1/2})$. Defining $\psi_{\boldsymbol{q}_{\mathrm{L}}}(\boldsymbol{x}_{\mathrm{T}}) \equiv \xi(\boldsymbol{r})$ and $t \equiv \boldsymbol{r}^2/2$, yields the dimensionless eigenvalue equation

$$(1 - \nabla_r^2 - 3\chi^2(t))\,\xi(\boldsymbol{r}) = \varpi\xi(\boldsymbol{r})\,, \tag{C.17}$$

where $\chi$ is defined in Eq. (3.24) and where the eigenvalues $\Lambda$ and $\varpi$ are related by

$$\Lambda(\boldsymbol{q}_{\mathrm{L}}) = a^2\boldsymbol{q}_{\mathrm{L}}^2 + \varpi/\bar{N}\,. \tag{C.18}$$

Eq. (C.17) has the standard form of a Shröedinger equation in a spherically symmetric potential. Its solution can be represented as a product of a radial (function of $t$ only) and an angular (function of the direction of $\boldsymbol{r}$ only) part [83]. The latter is an eigenfunction of the angular momentum operator (in the $3m$-dimensional space) and is labelled by the angular momentum quantum number $l = 0, 1, 2, \ldots$ (the eigenvalue $\varpi_l$ is $(3m-1)l + 1$ degenerate).

The lowest "energy" solution is spherically symmetric ($l = 0$) and is therefore a function of $t$ only. Substitution into Eq. (C.14) shows that such a solution cannot satisfy the condition (C.15) and thus must be rejected. The $l = 1$ case corresponds to the dipole-type solution $\xi_1(\boldsymbol{r}) = \nabla_r\chi(t)$, with the eigenvalue $\varpi_1 = 0$. This solution will be studied in detail below. Solutions which correspond to higher harmonics (with $l > 1$) have positive definite $\varpi_l$ which increase monotonically with $l$. The corresponding fluctuations have positive-definite eigenvalues (Eq. (C.18)) and therefore do not affect the stability of our mean-field solutions. They describe complicated distortions in replica space and will not be considered further in this appendix (their contribution will be included when we derive the fluctuation corrections to the partition function, in Appendices D and F).

We now return to the case $l = 1$ and note that an equation of the same form as (C.16), can be obtained by applying the $\nabla_{\mathrm{T}}$ operator to Eq. (3.1) and, therefore, $\nabla_{\mathrm{T}}\varphi_{\mathrm{mf}}(\varsigma)$ is a solution of Eq. (C.16). The general solution of (C.13) is obtained by multiplying the transverse gradient by a constant vector $\bar{\boldsymbol{u}}_{\mathrm{T}}$:

$$\psi_{\boldsymbol{q}_{\mathrm{L}}}(\boldsymbol{x}_{\mathrm{T}}) = (\bar{\boldsymbol{u}}_{\mathrm{T}} \cdot \nabla_{\mathrm{T}})\,\varphi_{\mathrm{mf}}(\varsigma)\,. \tag{C.19}$$

This solution has to satisfy the $1 + m$ conditions $\delta\rho^{(k)}(\boldsymbol{x}^{(k)}) = 0$, or in terms of their Fourier transforms,

$$\rho^{(k)}_{\boldsymbol{q}^{(k)}} \equiv \int \mathrm{d}\hat{\boldsymbol{x}}\,\exp(-\mathrm{i}\hat{\boldsymbol{q}}^{(k)}\cdot\hat{\boldsymbol{x}})\,\varphi_{\mathrm{mf}}(\varsigma)\psi(\hat{\boldsymbol{x}}) = 0\,, \tag{C.20}$$

where, as before, we define $\hat{\boldsymbol{q}}^{(k)} \equiv (0, \ldots \boldsymbol{q}^{(k)}, \ldots 0)$. The integral can be calculated by separating the integration into longitudinal and transverse components, $\mathrm{d}\hat{\boldsymbol{x}} \to \mathrm{d}\boldsymbol{x}_{\mathrm{L}}\,\mathrm{d}\boldsymbol{x}_{\mathrm{T}}$. In order to perform the integration over the longitudinal component, it is convenient to define the projections of these replica space wave vectors on the parallel and the perpendicular directions to the subspace spanned by the three unit vectors $\hat{\boldsymbol{e}}_\alpha$ (Eq. (3.18)). The corresponding projections are given by $\hat{\boldsymbol{q}}_{\mathrm{L}}^{(k)} = \sum_\alpha q_{\mathrm{L}\alpha}^{(k)}\hat{\boldsymbol{e}}_\alpha$

and $\hat{\boldsymbol{q}}_{\mathrm{T}}^{(k)} \equiv \hat{\boldsymbol{q}}^{(k)} - \hat{\boldsymbol{q}}_{\mathrm{L}}^{(k)}$, where $q_{\mathrm{L}\alpha}^{(k)} = \hat{\boldsymbol{q}}^{(k)} \cdot \hat{\boldsymbol{e}}_\alpha$ can be treated as the components of a three-dimensional vector $\boldsymbol{q}_{\mathrm{L}}^{(k)}$. Similarly, the $3m$-dimensional vector $\boldsymbol{q}_{\mathrm{T}}^{(k)}$ is defined by the projection of the replica vector $\hat{\boldsymbol{q}}^{(k)}$ on the transverse subspace. Substituting Eq. (3.18) for $\hat{\boldsymbol{e}}_\alpha$ yields (in the limit $m \to 0$)

$$\boldsymbol{q}_{\mathrm{L}}^{(0)} = \boldsymbol{q}^{(0)}, \quad (\boldsymbol{q}_{\mathrm{T}}^{(0)})^2 = 0 , \quad \boldsymbol{q}_{\mathrm{L}}^{(k)} = \lambda \star \boldsymbol{q}^{(k)} \quad \text{for } k \neq 0 , \tag{C.21}$$

where the second equality is obtained from the first one by noticing that $(\hat{\boldsymbol{q}}_{\mathrm{T}}^{(0)})^2 \equiv (\hat{\boldsymbol{q}}^{(0)})^2 - (\hat{\boldsymbol{q}}_{\mathrm{L}}^{(0)})^2 = 0$. The rather strange peculiarity of vectors in replica space is that, in the limit $m \to 0$, we may have $(\hat{\boldsymbol{q}}_{\mathrm{T}}^{(0)})^2 = 0$ but $\hat{\boldsymbol{q}}_{\mathrm{T}}^{(0)} \cdot \boldsymbol{q}_{\mathrm{T}}^{(k)} \neq 0$ (an example is given by an $3m$-component vector $\boldsymbol{a}_{\mathrm{T}} = (1, 1, \ldots, 1)$ whose elements are all different from zero but whose norm vanishes in the limit $m \to 0$).

With the above definitions, the replica space product in the exponent of Eq. (C.20) can be written as the sum of longitudinal and transverse contributions:

$$\hat{\boldsymbol{q}}^{(k)} \cdot \hat{\boldsymbol{x}} = \boldsymbol{q}_{\mathrm{L}}^{(k)} \cdot \boldsymbol{x}_{\mathrm{L}} + \boldsymbol{q}_{\mathrm{T}}^{(k)} \cdot \boldsymbol{x}_{\mathrm{T}} . \tag{C.22}$$

Making the above replacement in Eq. (C.20) and using Eq. (3.37), the integration over $\mathrm{d}\boldsymbol{x}_{\mathrm{L}}$ gives a $\delta$-function, $\delta(\boldsymbol{q}_{\mathrm{L}}^{(k)} - \boldsymbol{q}_{\mathrm{L}})$. Substituting Eq. (C.7) into the remaining integral over $\mathrm{d}\boldsymbol{x}_{\mathrm{T}}$ and moving the constant $\bar{\boldsymbol{u}}_{\mathrm{T}}$ outside the integral, condition (C.20) becomes

$$\bar{\boldsymbol{u}}_{\mathrm{T}} \cdot \int \mathrm{d}\boldsymbol{x}_{\mathrm{T}} \exp(-\mathrm{i}\boldsymbol{q}_{\mathrm{T}}^{(k)} \cdot \boldsymbol{x}_{\mathrm{T}}) \varphi_{\mathrm{mf}}(\varsigma) \nabla_{\mathrm{T}} \varphi_{\mathrm{mf}}(\varsigma) = 0 . \tag{C.23}$$

Using $\varphi_{\mathrm{mf}}(\varsigma) \nabla_{\mathrm{T}} \varphi_{\mathrm{mf}}(\varsigma) = \nabla_{\mathrm{T}} \varphi_{\mathrm{mf}}^2(\varsigma)/2$ and integrating by parts, we finally obtain (the surface term vanishes since $\varphi_{\mathrm{mf}}(\varsigma \to \infty) \to 0$)

$$(\bar{\boldsymbol{u}}_{\mathrm{T}} \cdot \boldsymbol{q}_{\mathrm{T}}^{(k)}) \int \mathrm{d}\boldsymbol{x}_{\mathrm{T}} \exp(-\mathrm{i}\boldsymbol{q}_{\mathrm{T}}^{(k)} \cdot \boldsymbol{x}_{\mathrm{T}}) \varphi_{\mathrm{mf}}^2(\varsigma) = 0 . \tag{C.24}$$

Since the above integral is, in general, non-vanishing, the vector $\bar{\boldsymbol{u}}_{\mathrm{T}}$ must obey the condition $\bar{\boldsymbol{u}}_{\mathrm{T}} \cdot \boldsymbol{q}_{\mathrm{T}}^{(k)} = 0$.

The eigenvalues are calculated by comparing Eq. (C.16) with the equation for $\nabla_{\mathrm{T}} \varphi_{\mathrm{mf}}(\varsigma)$ (obtained by applying the gradient to Eq. (3.1)). This gives

$$\Lambda_{\mathrm{S}}(\boldsymbol{q}_{\mathrm{L}}) = a^2 \boldsymbol{q}_{\mathrm{L}}^2 , \tag{C.25}$$

i.e., shear modes are gapless Goldstone modes. We show below that the eigenfunctions (C.19) describe the infinitesimal displacement $\boldsymbol{x}_{\mathrm{T}} \to \boldsymbol{x}_{\mathrm{T}} + \boldsymbol{u}_{\mathrm{T}}(\boldsymbol{x}_{\mathrm{L}})$ of the coordinate $\boldsymbol{x}_{\mathrm{T}}$ (in the abstract transverse $3m$-dimensional subspace). Under the displacement $\boldsymbol{u}_{\mathrm{T}}(\boldsymbol{x}_{\mathrm{L}}) = \boldsymbol{u}_{\mathrm{T}q} \exp(\mathrm{i}\boldsymbol{q} \cdot \boldsymbol{x}_{\mathrm{L}})$, the variation of the field $\varphi(\hat{\boldsymbol{x}})$ has the form

$$\delta_{\mathrm{S}} \varphi(\hat{\boldsymbol{x}}) = \varphi_{\mathrm{mf}}(\varsigma)|_{\boldsymbol{x}_{\mathrm{T}} \to \boldsymbol{x}_{\mathrm{T}} + \boldsymbol{u}_{\mathrm{T}}} - \varphi_{\mathrm{mf}}(\varsigma) = \boldsymbol{u}_{\mathrm{T}}(\boldsymbol{x}_{\mathrm{L}}) \cdot \nabla_{\mathrm{T}} \varphi_{\mathrm{mf}}(\varsigma) = \psi_{\boldsymbol{q}_{\mathrm{L}}}(\boldsymbol{x}_{\mathrm{T}}) . \tag{C.26}$$

Under this displacement, the argument of the function $\varphi_{\mathrm{mf}}(\varsigma)$ changes as $\varsigma \to \varsigma + \boldsymbol{x}_{\mathrm{T}} \cdot \boldsymbol{u}_{\mathrm{T}}$ and, expanding to first order in $\boldsymbol{u}_{\mathrm{T}}$, we obtain the second equality in Eq. (C.26). The third equality follows from comparison with (C.19), upon identifying the arbitrary vector $\bar{\boldsymbol{u}}_{\mathrm{T}}$ with the displacement $\boldsymbol{u}_{\mathrm{T}}$. The additional condition $\boldsymbol{u}_{\mathrm{T}} \cdot \boldsymbol{q}_{\mathrm{T}}^{(k)} = 0$ (see Eq. (C.24)) means that the displacement $\boldsymbol{u}_{\mathrm{T}}$ has to be orthogonal to the $m + 1$ vectors $\boldsymbol{q}_{\mathrm{T}}^{(k)}$. This condition imposes $m + 1$ constraints on the $3m$ components of the vector $\boldsymbol{u}_{\mathrm{T}}$ and we conclude that the shear modes are $2m - 1$-degenerate.

We now return to Eq. (C.14) and consider the general case in which at least one of the density fluctuations $\delta\rho^{(k)}(x^{(k)})$ is not identically zero. It is convenient to work with functions over the usual three-dimensional space (i.e., $x^{(k)}$) in each of the replicas, instead of the $3(1+m)$-dimensional replica space. This is achieved by recasting Eq. (C.13) into an equation for $\delta\rho^{(k)}(x^{(k)})$. This equation can be used to express $\psi$ through $\delta\rho^{(k)}$,

$$\psi(\hat{x}) = -\int d\hat{x}' D(\Lambda;\hat{x},\hat{x}')\varphi_{mf}(\varsigma')\sum_{k=0}^{m} w^{(k)}\delta\rho^{(k)}(x'^{(k)}) , \tag{C.27}$$

where $D$ is defined by the equation

$$[1/\bar{N} - \Lambda - a^2\hat{\nabla}^2 - 3(z_c/2)\varphi_{mf}^2(\hat{x})]\, D(\Lambda;\hat{x},\hat{x}') = \delta(\hat{x}-\hat{x}') . \tag{C.28}$$

Substituting (C.27) into (C.14), we obtain a closed system of linear integral equations for $\delta\rho^{(k)}$:

$$\delta\rho^{(k)}(x) + \sum_{l=0}^{m} w^{(l)} \int dx'\, g_{\Lambda}^{kl}(x,x')\delta\rho^{(l)}(x') = 0 , \tag{C.29}$$

where we define the replica space density correlation functions:

$$g_{\Lambda}^{kl}(x,x') \equiv \int d\hat{x}\,\varphi_{mf}(\varsigma)\delta(x - x^{(k)}) \int d\hat{x}'\,\varphi_{mf}(\varsigma')\delta(x' - x'^{(l)})\, D(\Lambda;\hat{x},\hat{x}') . \tag{C.30}$$

The problem can be further simplified by Fourier transforming Eq. (C.29). For this we have to calculate the Fourier transform of the functions $g_{\Lambda}^{kl}(x,x')$,

$$g_{\Lambda}^{kl}(q^{(k)},q^{(l)}) \equiv \int d\hat{x}\,\varphi_{mf}(\varsigma)\int d\hat{x}'\,\varphi_{mf}(\varsigma')D(\Lambda;\hat{x},\hat{x}')\exp(i\hat{q}^{(k)}\cdot\hat{x} - i\hat{q}^{(l)}\cdot\hat{x}') . \tag{C.31}$$

Changing the integration $d\hat{x} \to dx_L\, dx_T$ (and $d\hat{x}' \to dx'_L\, dx'_T$) and performing the integrations over the longitudinal coordinates using Eq. (C.22), yields

$$g_{\Lambda}^{kl}(q^{(k)},q^{(l)}) = \delta(q_L^{(k)} - q_L^{(l)})\, g_{\Lambda}^{kl}(q_L^{(k)}) , \tag{C.32}$$

$$g_{\Lambda}^{kl}(q_L^{(k)}) = \int dx_T\,\varphi_{mf}(\varsigma)\int dx'_T\,\varphi_{mf}(\varsigma')$$
$$\times D(\Lambda - a^2(q_L^{(k)})^2; x_T, x'_T)\exp(iq_T^{(k)}\cdot x_T - iq_T^{(l)}\cdot x'_T) . \tag{C.33}$$

In deriving Eq. (C.33), we used the replacement $\hat{\nabla}^2 \to \nabla_T^2 - (q_L^{(k)})^2$, which introduced the shift $\Lambda \to \Lambda - a^2(q_L^{(k)})^2$ (Eq. (C.7)) into the longitudinal Fourier transform of Eq. (C.28). In calculating the above integrals we only consider the usual *continuous* description of a solid in which one only considers wavelengths that are much larger than the characteristic microscale (in our case, this microscale corresponds to the average spatial distance between cross-links, $a\bar{N}^{1/2}$). Since this distance is the characteristic length scale for the decay of the classical solution ($\varphi_{mf}(\varsigma \gg a^2\bar{N}) \to 0$), in evaluating the integrals we can expand the exponentials and keep only terms to second order in $q_T^{(k)}\cdot x_T$. Furthermore, since $|q_T^{(k)}|$ and $|q_L^{(k)}|$ can differ only by a factor of order unity (i.e., by a multiplicative factor of $\lambda$), the functions $g_{\Lambda}^{kl}(q_L^{(k)})$ have to be calculated also only to order $(q_L^{(k)})^2$. This calculation is carried out in Appendix E.

Fourier transforming Eq. (C.29) and eliminating the integrations using the $\delta$-functions in (C.32), yields a set of algebraic relations between the Fourier coefficients of the solutions $\delta\rho^{(0)}(\boldsymbol{x}) = \rho^{(0)}_{\boldsymbol{q}^{(0)}} \exp(\mathrm{i}\boldsymbol{q}^{(0)}\cdot\boldsymbol{x})$ and $\delta\rho^{(k)}(\boldsymbol{x}) = \rho^{(k)}_{\boldsymbol{q}} \exp(\mathrm{i}\boldsymbol{q}\cdot\boldsymbol{x})$, with $\boldsymbol{q}^{(0)} = \lambda \star \boldsymbol{q} = \boldsymbol{q}_{\mathrm{L}}$

$$
\begin{aligned}
&[1 + w^{(0)} g_{\Lambda}^{00}(\boldsymbol{q}_{\mathrm{L}})]\rho^{(0)}_{\boldsymbol{q}^{(0)}} + w g_{\Lambda}^{01}(\boldsymbol{q}_{\mathrm{L}}) \sum_{k=1}^{m} \rho^{(k)}_{\boldsymbol{q}} = 0 \,, \\
&[1 + w(g_{\Lambda}^{11}(\boldsymbol{q}_{\mathrm{L}}) - g_{\Lambda}^{12}(\boldsymbol{q}_{\mathrm{L}}))]\rho^{(k)}_{\boldsymbol{q}} + w^{(0)} g_{\Lambda}^{10}(\boldsymbol{q}_{\mathrm{L}})\rho^{(0)}_{\boldsymbol{q}^{(0)}} + w g_{\Lambda}^{12}(\boldsymbol{q}_{\mathrm{L}}) \sum_{k=1}^{m} \rho^{(k)}_{\boldsymbol{q}} = 0 \,,
\end{aligned}
\tag{C.34}
$$

where we used the identity of the $k \neq 0$ replicas to replace the general replica indices $(k, l)$ in the functions (C.33), by those of the first and the second replicas. This symmetry can be used in Eq. (C.29), in order to recast it into a system of equations for the fields $\rho^{(0)}_{\boldsymbol{q}^{(0)}}$ and $\eta_{\boldsymbol{q}} \equiv \sum_{k=1}^{m} \rho^{(k)}_{\boldsymbol{q}}$:

$$
\begin{aligned}
&[1 + w^{(0)} g_{\Lambda}^{00}(\boldsymbol{q}_{\mathrm{L}})]\rho^{(0)}_{\boldsymbol{q}^{(0)}} + w g_{\Lambda}^{01}(\boldsymbol{q}_{\mathrm{L}})\eta_{\boldsymbol{q}} = 0 \,, \\
&[1 + w(g_{\Lambda}^{11}(\boldsymbol{q}_{\mathrm{L}}) - g_{\Lambda}^{12}(\boldsymbol{q}_{\mathrm{L}}) + m g_{\Lambda}^{12}(\boldsymbol{q}_{\mathrm{L}}))]\eta_{\boldsymbol{q}} + m w^{(0)} g_{\Lambda}^{10}(\boldsymbol{q}_{\mathrm{L}})\rho^{(0)}_{\boldsymbol{q}^{(0)}} = 0 \,.
\end{aligned}
\tag{C.35}
$$

The eigenvalues $\Lambda(\boldsymbol{q}_{\mathrm{L}})$ are obtained from the condition of solvability of this linear system of equations,

$$
\begin{aligned}
&[1 + w^{(0)} g_{\Lambda}^{00}(\boldsymbol{q}_{\mathrm{L}})]\,[1 + w(g_{\Lambda}^{11}(\boldsymbol{q}_{\mathrm{L}}) - g_{\Lambda}^{12}(\boldsymbol{q}_{\mathrm{L}}) + m g_{\Lambda}^{12}(\boldsymbol{q}_{\mathrm{L}}))] \\
&\quad = m w^{(0)} w [g_{\Lambda}^{01}(\boldsymbol{q}_{\mathrm{L}})]^2 \,.
\end{aligned}
\tag{C.36}
$$

Strictly speaking, we can set $m \to 0$ in the above equation and find the two eigenvalues from the condition that one of the two terms in the square brackets vanishes. Extra care must be taken in calculating the corresponding eigenfunctions since Eq. (C.36) admits three different types of eigenmodes, two of which become degenerate in the limit $m \to 0$.

*C.2.3. Density modes in initial state*

The first type of eigenmodes corresponds to eigenvalues $\Lambda_{\mathrm{D}}^{(0)}(\boldsymbol{q}_{\mathrm{L}})$ which, in the limit $m \to 0$, are determined by setting to zero the term in the first square bracket on the left-hand side of Eq. (C.36),

$$
1 + w^{(0)} g_{\Lambda}^{00}(\boldsymbol{q}_{\mathrm{L}}) = 0 \tag{C.37}
$$

Substituting the expressions (Appendix E) for $g_{\Lambda}^{00}$ (in the limit $m \to 0$) into (C.37) we find

$$
\Lambda_{\mathrm{gap}}(\boldsymbol{q}_{\mathrm{L}}) = (w^{(0)} - z_{\mathrm{c}})\,\varphi_{\mathrm{mf}}^2 + a^2(\boldsymbol{q}_{\mathrm{L}})^2 \,. \tag{C.38}
$$

Since this eigenvalue does not vanish, in general, in the limit $q \to 0$, following the usual terminology we say that the corresponding solution is *massive* (i.e., has an energy gap). The gap vanishes at

$$
z_{\mathrm{c}} = 1/\rho^{(0)} \bar{N}^{\min} = w^{(0)} \,, \tag{C.39}
$$

which can be interpreted as the cross-link saturation threshold that defines the highest density of cross-links that can be achieved by instantaneous cross-linking of a polymer solution.

Further inspection of eqs. (C.34) and (C.35) leads to the conclusion that the above solution corresponds to the case of identical densities $\rho^{(k)}_{\boldsymbol{q}}$ in all the replicas of the final state ($k = 1, \ldots, m$).

Furthermore, in the limit $m \to 0$ (taken in the above defined sense), these modes obey the affine relation between the densities $\rho_q^{(k)} = \rho_{\Lambda \star q}^{(0)}$ in the final and the initial states.

In order to construct the eigenfunctions of the density modes which correspond to the eigenvalues (C.38), we have to Fourier transform (see Eq. (C.6)) Eq. (C.27) for the functions $\psi(\hat{x})$:

$$\psi_{q_L}(x_T) = \int dx'_T \, \varphi_{mf}(\varsigma') \, D\,(\Lambda - a^2 q_L^2; x_T, x'_T) \sum_{k=0}^{m} w^{(k)} \rho_q^{(k)} \exp(i q_T^{(k)} \cdot x'_T) \,. \tag{C.40}$$

Using the rapid decrease of $\varphi_{mf}(\varsigma')$ with $\varsigma' = (x'_T)^2/2$, one can expand the exponentials in the above expression to second order in $q_T^{(k)} \cdot x'_T$ and, taking into account the definitions of the functions $\Phi$ and $\Psi$ (Eqs. (E.4) and (E.11), Appendix E), one arrives at the general result

$$\psi_{q_L}(x_T) = \sum_{k=0}^{m} \rho_q^{(k)} [\Phi(\Lambda - a^2 q_L^2; \varsigma) + i q_T^{(k)} \cdot x_T \, \Psi(\Lambda - a^2 q_L^2; \varsigma)] \,. \tag{C.41}$$

Explicit expressions for the eigenfunctions can be obtained from (C.41) by substituting the corresponding eigenvalues $\Lambda$ and using the appropriate relations between the $\rho_q^{(k)}$ coefficients in each of the modes, Eq. (C.34) and (C.35). Since we are interested in the continuum limit, we can set $q_L = 0$ in $\Phi$ in the above expression. The next step is to realize that for the massive mode ($\Lambda_{gap} \to$ *constant* as $q \to 0$), the function $\Psi$ remains finite in the limit $q \to 0$. In this case, the second term on the right-hand side of Eq. (C.41) is of order $q_T^{(k)} \cdot x_T$ and can be neglected with respect to the first term. This gives

$$\psi_{gap}(\hat{x}) = \Phi((w^{(0)} - z_c) \varphi_{mf}^2; \varsigma) \exp(i q_L \cdot x_L) \,, \tag{C.42}$$

where the function $\Phi$ is defined as the solution of Eq. (E.6), Appendix E, and where we dropped the (constant) $\rho_q^{(k)}$ terms which appear in (C.41), since the latter only affect the (arbitrary) normalization of the eigenfunctions. An analytic expression for $\Phi$ can be obtained only at the cross-link saturation threshold, $\Phi(0; \varsigma) = \bar{N}^2 \partial \varphi_{mf} / \partial \bar{N}$ (Eq. (E.9), Appendix E).

*C.2.4. Density modes in final state*

In the limit $m \to 0$, the eigenvalue equation for the density modes in the final state is obtained by setting to zero the term in the second square bracket on the left-hand side of Eq. (C.36)

$$1 + w(g_\Lambda^{11}(q_L) - g_\Lambda^{12}(q_L)) = 0 \,. \tag{C.43}$$

The functions $g_\Lambda^{11}$ and $g_\Lambda^{12}$ are calculated in the continuous limit ($q^2 a^2 \bar{N} \ll 1$) in Appendix E. The gapless density modes $\Lambda_D(q_L) \sim q_L^2$ are obtained by noticing that for this modes, $\Psi(\Lambda - a^2 q_L^2; \varsigma) \sim q_L^{-2}$ (Eq. (E.18), Appendix E) and therefore, the second term on the right-hand side of Eq. (C.41) dominates in the long wavelength limit. Substituting the relation $x_T \partial \varphi_{mf}(\varsigma)/\partial \varsigma = \nabla_T \varphi_{mf}(\varsigma)$ into Eq. (E.18) we obtain the eigenfunctions given in Eq. (3.42):

$$\Lambda_D(q_L) = a^2 q_L^2 + 2 w \rho^{(0)} a^2 \bar{N} (\lambda^{-1} \star q_L)^2 \,. \tag{C.44}$$

Since $\Lambda_D(q_L \to 0) \to 0$, the corresponding fluctuations are Goldstone modes. Note that the condition $\Lambda_D(q_L) > 0$ is always satisfied when the final state of the gel corresponds to good solvent conditions ($w > 0$). In fact, for large deformations the positivity condition can be satisfied even for

moderately poor solvent ($w < 0$), since the network can be stabilized against collapse by the external forces applied to its surface.

The next step is to calculate the eigenfunctions corresponding to the above eigenvalue. We find that there are $m$ degenerate eigenfunctions (in the limit $m \to 0$!) and therefore, before taking this limit we have to consider the case of arbitrary integer $m$.

Consider modes for which $\rho^{(0)}_{q^{(0)}} = \eta_q = 0$ but $\rho^{(k)}_q \neq 0$ (for $k = 1, \ldots, m$). In this case we cannot use the secular equation (C.36) and have to return to Eq. (C.34). This gives the eigenvalue equation

$$J_m(\Lambda_D(\boldsymbol{q}_L)) = 0 , \tag{C.45}$$

where we define

$$J_m(\Lambda) \equiv 1 + w(g^{11}_\Lambda(\boldsymbol{q}_L) - g^{12}_\Lambda(\boldsymbol{q}_L)) .$$

The $(m-1)$-degenerate eigenfunctions corresponding to this eigenvalue are obtained by calculating the integrals in Eq. (C.27),

$$\psi_j(\hat{\boldsymbol{x}}) = \sum_{k=1}^{m} S^{(k)}_j \left( \frac{\mathrm{i}\boldsymbol{q}^{(k)}_T}{\rho^{(0)} q^2} \cdot \nabla_T \varphi_{mf}(\zeta) \right) \exp(\mathrm{i}\boldsymbol{q}_L \cdot \boldsymbol{x}_L) , \quad j = 1, \ldots, m-1 . \tag{C.46}$$

Here, $\rho^{(0)}$ is the mean density in the initial state. The arbitrary coefficients $S^{(k)}_j$ obey the relation

$$\sum_{k=1}^{m} S^{(k)}_j = 0 , \tag{C.47}$$

which follows from the condition $\eta_q = 0$ (this can be checked by substituting $\psi_j$ into Eq. (C.20) and summing over $k$). The condition of orthogonality of the eigenfunctions, $\int \mathrm{d}\hat{\boldsymbol{x}} \psi_i(\hat{\boldsymbol{x}}) \psi^*_j(\hat{\boldsymbol{x}}) = 0$ for $i \neq j$ (where * denotes a complex conjugate and where the volume of the system is kept finite during the integration over $\boldsymbol{x}_T$), imposes another relation between the $S^{(k)}_j$ coefficients:

$$\sum_{k,l=1}^{m} S^{(k)}_i S^{(l)}_j \, (\delta_{kl} - \boldsymbol{q}^2_L/\boldsymbol{q}^2) = 0 \quad \text{for } i \neq j . \tag{C.48}$$

In order to gain some insight into the physical meaning of the above eigenfunctions we note that the gradient term (C.46) describes the infinitesimal displacement $\boldsymbol{x}_T \to \boldsymbol{x}_T + \boldsymbol{u}_T(\boldsymbol{x}_L)$ of the coordinate $\boldsymbol{x}_T$ (see Eq. (C.26)), where

$$\boldsymbol{u}_T(\boldsymbol{x}_L) = \frac{\mathrm{i}\boldsymbol{q}^{(k)}_T}{q^2 \rho^{(0)}} \exp(\mathrm{i}\boldsymbol{q}_L \cdot \boldsymbol{x}_L) , \tag{C.49}$$

The displacements $\boldsymbol{u}_T$ given by Eq. (C.49) are orthogonal to the displacements which lead to pure shear modes (in replica space) derived in a previous subsection. Unlike the former, they correspond to fluctuations in the densities of the replicas.

We now consider $\eta_q \neq 0$ (and, consequently, $\rho^{(0)}_{q^{(0)}} \neq 0$), in which case all the $\rho^{(k)}_q$ are equal and the eigenvalue spectrum is obtained from the secular equation (C.36), which can be rewritten

in the form

$$J_m(\Lambda) = mw\left[\frac{w^{(0)}(g_\Lambda^{01}(\boldsymbol{q}_\perp))^2}{1 + w^{(0)}g_\Lambda^{00}(\boldsymbol{q}_\perp)} - g_\Lambda^{12}(\boldsymbol{q}_\perp)\right]. \tag{C.50}$$

Using this expression we obtain, to first order in $m$,

$$\Lambda(\boldsymbol{q}_\perp) = \Lambda_D(\boldsymbol{q}_\perp) + m\Lambda'_D(\boldsymbol{q}_\perp)\,, \tag{C.51}$$

where

$$\Lambda'_D(\boldsymbol{q}_\perp) \equiv \frac{w}{\partial J_0/\partial\Lambda}\left[\frac{w^{(0)}(g_\Lambda^{01}(\boldsymbol{q}_\perp))^2}{1 + w^{(0)}g_\Lambda^{00}(\boldsymbol{q}_\perp)} - g_\Lambda^{12}(\boldsymbol{q}_\perp)\right] \tag{C.52}$$

should be evaluated in the limit $m \to 0$. The corresponding fluctuations do not affect the density in the initial state since in this limit $\rho_{q^{(0)}}^{(0)} \sim \eta_q = m\rho_q^{(1)} \to 0$.

The eigenfunction corresponding to the eigenvalue (C.51) is obtained by calculating the integrals in Eq. (C.27)

$$\psi_0(\hat{\boldsymbol{x}}) = \sum_{k=1}^{m}\left(\frac{i\boldsymbol{q}_T^{(k)}}{\rho^{(0)}q^2}\cdot\nabla_T\varphi_{mf}(\varsigma) - w\frac{\partial\varphi_{mf}(\varsigma)}{\partial\mu}\right)\exp(i\boldsymbol{q}_\perp\cdot\boldsymbol{x}_\perp)\,. \tag{C.53}$$

Comparing this equation with the expression for the degenerate eigenmodes, Eq. (C.46) and using Eq. (C.47), we can write down a general expression for all $m$ density eigenmodes ($j = 0, \ldots, m-1$)

$$\psi_j(\hat{\boldsymbol{x}}) = \sum_{k=1}^{m} S_j^{(k)}\left(\frac{i\boldsymbol{q}_T^{(k)}}{\rho^{(0)}q^2}\cdot\nabla_T\varphi_{mf}(\varsigma) - w\frac{\partial\varphi_{mf}(\varsigma)}{\partial\mu}\right)\exp(i\boldsymbol{q}_\perp\cdot\boldsymbol{x}_\perp)\,, \tag{C.54}$$

where all $S_0^{(k)}$ are equal to each other. From Eq. (C.48) and the automatic orthogonality of eigenfunctions corresponding to different eigenvalues, we can write the general ortho-normality condition

$$\sum_{k,l=1}^{m} S_i^{(k)}S_j^{(l)}\,(\delta_{kl} - \boldsymbol{q}_\perp^2/\boldsymbol{q}^2) = \delta_{ij}\,, \tag{C.55}$$

where a convenient choice of normalization was made.

We end this appendix with a brief summary. We proved that the homogeneous solution is unstable against fluctuations which mix the replicas and does not correspond to a minimum of the Hamiltonian. We then proceeded to study the fluctuations about the inhomogeneous mean-field solution $\varphi_{mf}(\varsigma)$. We showed that, for this solution, all the eigenvalues $\Lambda$ of the second derivative operator $\boldsymbol{K}$ are positive for networks prepared in sufficiently good solvents. We found that all the fluctuations increase the energy of the system and, therefore, the above solution corresponds to a true minimum of the Hamiltonian. There are six different types of fluctuation modes, the first two of which do not have a direct physical interpretation:

1. Rotational modes of the $n$-vector model, which are related to excluded volume effects.
2. Massive (i.e., with an energy gap) shear modes which do not affect the densities in the replicas (they correspond to spherical harmonics with $l > 1$; see the discussion following Eq. (C.18)).

The other four modes describe shear and density fluctuations in the space of the replicas and are summarized as

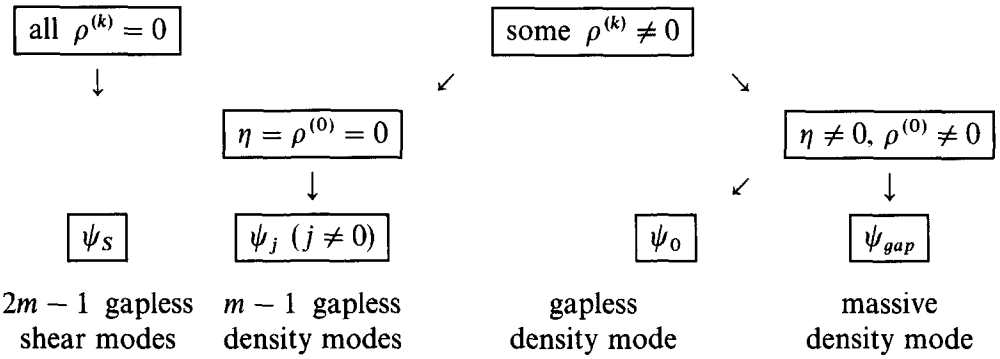


The appearance of Goldstone modes is the consequence of the fact that the ground state of the stretched network corresponds to a solution with spontaneously broken symmetry with respect to translations in replica space, which describes a disordered solid.

The above classification contains information about the quenched (frozen) versus annealed (thermal) character of the fluctuations described by the $3m$ physical modes. Shear modes mix both types of fluctuations. The degenerate $\psi_j (j \neq 0)$ density modes correspond to independent density fluctuations in the replicas of the final state ($\rho^{(k)}$ are only constrained by the relation $\eta = 0$) and therefore describe purely annealed thermal fluctuations of the final density. The non-degenerate modes $\psi_0$ and $\psi_{gap}$ describe density fluctuations which are identical in the replicas of the final state ($\rho^{(1)} = \rho^{(2)} = \cdots = \rho^{(m)}$) and thus correspond to pure quenched fluctuations.

## Appendix D. Ultra-short wavelength corrections to free energy

We proceed to calculate the fluctuation corrections to the mean-field free energy, Eq. (3.30). To this end one has to account for fluctuations at arbitrary wave vectors $\boldsymbol{q}$ (we will show that the dominant contributions come from ultra-short wavelength fluctuations).

We have shown in Appendix C that any small fluctuation around the mean-field solution can be expressed as a sum of orthogonal rotational, shear and density modes

$$\delta\varphi(\hat{\mathbf{x}}) = \delta_R\varphi(\hat{\mathbf{x}}) + \delta_S\varphi(\hat{\mathbf{x}}) + \delta_D\varphi(\hat{\mathbf{x}}) \,. \tag{D.1}$$

It is convenient to separate the fluctuation contributions to the grand canonical partition function which come from the integration over the rotational modes ($\Xi_m^R$), and rewrite Eq. (2.47) in the form

$$\Xi_m(\mu, z_c) = \exp(-H_{mf})\,(\Xi_m^R)^{n-1}\,\Xi_m^{SD} \,, \tag{D.2}$$

where we have taken into account the $n - 1$-fold degeneracy of the rotational modes (in the space of the $n$-vector model) and defined the rotational partition function by integrating over

the scalar field $\delta\varphi$:

$$\Xi_m^{\mathrm{R}} = \int \mathrm{D}[\delta\varphi] \exp(-\Delta H^{\perp}[\delta\varphi]) , \tag{D.3}$$

$\Xi_m^{\mathrm{SD}}$ contains the contributions of shear and density fluctuations and is given by

$$\Xi_m^{\mathrm{SD}} = \int \mathrm{D}[\delta\varphi] \exp(-\Delta H^{\parallel}[\delta\varphi]) . \tag{D.4}$$

In the limit $n \to 0$, Eq. (D.2) becomes

$$\Xi_m(\mu, z_c) = \exp(-H_{\mathrm{mf}}) \Xi_m^{\mathrm{SD}} / \Xi_m^{\mathrm{R}} . \tag{D.5}$$

*D.1. Rotational partition function*

The rotational Hamiltonian in Eq. (D.3) is given by

$$\Delta H^{\perp}[\delta\varphi] \equiv \frac{1}{2} \int \mathrm{d}\hat{\boldsymbol{x}}\, \mathrm{d}\hat{\boldsymbol{x}}'\, \delta\varphi(\hat{\boldsymbol{x}}) K^{\perp}(\hat{\boldsymbol{x}}, \hat{\boldsymbol{x}}') \delta\varphi(\hat{\boldsymbol{x}}') , \tag{D.6}$$

where $K^{\perp}$ was defined in Eq. (3.34). The Gaussian integral in Eq. (D.3) can be calculated by expanding a general fluctuation in a linear combination of the normalized eigenfunctions of the operator $K^{\perp}$,

$$\delta\varphi(\hat{\boldsymbol{x}}) = \sum_{i,\boldsymbol{q}_{\mathrm{L}}} C_i(\boldsymbol{q}_{\mathrm{L}}) \psi^{\perp}_{i,\boldsymbol{q}_{\mathrm{L}}}(\boldsymbol{x}_{\mathrm{T}}) \exp(\mathrm{i}\boldsymbol{q}_{\mathrm{L}} \cdot \boldsymbol{x}_{\mathrm{L}}) \tag{D.7}$$

and replacing the $\delta\varphi$ integration by the integration over the expansion coefficients $C_i$:

$$\Xi_m^{\mathrm{R}} = \prod_{i,\boldsymbol{q}_{\mathrm{L}}} \int \frac{\mathrm{d}C_i(\boldsymbol{q}_{\mathrm{L}})}{2\pi} \exp[-\tfrac{1}{2} \Lambda_i^{\perp}(\boldsymbol{q}_{\mathrm{L}}) C_i^2(\boldsymbol{q}_{\mathrm{L}})] . \tag{D.8}$$

Performing the Gaussian integration we obtain

$$\begin{aligned} \Xi_m^{\mathrm{R}} &= \left[ \prod_{i,\boldsymbol{q}_{\mathrm{L}}} \Lambda_i^{\perp}(\boldsymbol{q}_{\mathrm{L}}) \right]^{-1/2} = \exp\left\{ -\frac{1}{2} \sum_{i,\boldsymbol{q}_{\mathrm{L}}} \ln \Lambda_i^{\perp}(\boldsymbol{q}_{\mathrm{L}}) \right\} \\ &\to \exp\left\{ -\frac{1}{2} \textstyle\sum_i V_{\mathrm{L}} \int \dfrac{\mathrm{d}\boldsymbol{q}_{\mathrm{L}}}{(2\pi)^3} \ln \Lambda_i^{\perp}(\boldsymbol{q}_{\mathrm{L}}) \right\} , \end{aligned} \tag{D.9}$$

where the eigenvalues $\Lambda_{\perp}$ of the rotational eigenmodes are defined by Eq. (C.9) and $V_{\mathrm{L}}$ is the volume of the longitudinal subspace, defined in Eq. (B.5) (Appendix B).

The logarithmic singularity coming from Goldstone modes with eigenvalues $\Lambda^{\perp}(\boldsymbol{q}_{\mathrm{L}}) = a^2 \boldsymbol{q}_{\mathrm{L}}^2$ that vanish in the limit $\boldsymbol{q}_{\mathrm{L}} \to 0$, disappears upon integration. The expression in the exponent of Eq. (D.9) is dominated by the $\boldsymbol{q}_{\mathrm{L}} \to \infty$ and $i \to \infty$ contributions (the eigenvalues increase monotonically with $i$). In this limit the spectrum becomes continuous and we can replace the discrete index $i$ by the

continuous wave vector $q_T$ and write

$$\sum_i V_L \int \frac{dq_L}{(2\pi)^3} \ln \Lambda_i^{\perp}(q_L) \to V^{(0)} V^m \int \frac{d\hat{q}}{(2\pi)^{3(1+m)}} \ln \Lambda^{\perp}(\hat{q}) , \tag{D.10}$$

where $\hat{q} = \hat{q}_L + \hat{q}_T$. In order to calculate the contribution of $\Lambda^{\perp}(\hat{q})$ we note that in the limit $|\hat{q}| \gg (a\bar{N}^{1/2})^{-1}$, the operator in the eigenvalue equation, (C.9), is dominated by the transverse Laplacian and therefore, the normalized eigenfunctions are plane waves $\psi(\hat{x}) = (V^{(0)} V^m)^{-1/2} \times \exp(i\boldsymbol{q}\cdot\hat{x})$. Recalling the Shröedinger-like form of this equation and following the usual quantum mechanical procedure [83], the contribution of the other terms in this equation can be calculated in first-order perturbation expansion (using the above zeroth-order eigenfunctions):

$$\Lambda^{\perp}(\hat{q}) = \frac{1}{\bar{N}} + a^2\hat{q}^2 - \frac{z_c}{2V^{(0)}V^m} \int d\hat{x} \varphi_{mf}^2(\varsigma) . \tag{D.11}$$

Substituting Eq. (D.11) into Eq. (D.10), we observe that the resulting integral over $\hat{q}$ diverges. In the following we show that an identical divergence occurs in the calculation of $\Xi_m^{SD}$ and that the leading divergences cancel each other in the ratio $\Xi_m^{SD}/\Xi_m^{R}$, which appears in the derivation of the total partition function, Eq. (D.5).

*D.2. Partition function of shear and density modes*

We now return to Eq. (D.4) and write

$$\Delta H^{\parallel}[\delta\varphi] \equiv \frac{1}{2} \int d\hat{x}\, d\hat{x}'\, \delta\varphi(\hat{x}) K^{\parallel}(\hat{x}, \hat{x}')\, \delta\varphi(\hat{x}') , \tag{D.12}$$

where the operator $K^{\parallel}$ is defined in Eq. (3.35). The calculation of the Gaussian integrals follows the same steps as in the preceding subsection, with the result

$$\Xi_m^{SD} = \left[ \prod_{i,q_L} \Lambda_i^n(q_L) \right]^{-1/2} \to \exp\left[ -\frac{V^{(0)}V^m}{2} \int \frac{d\hat{q}}{(2\pi)^{3(1+m)}} \ln \Lambda^{\parallel}(\hat{q}) \right] , \tag{D.13}$$

where the main contribution to the integral comes, again, from large wave vectors. The eigenvalues of $K^{\parallel}$ can be calculated from Eq. (C.13), by expanding about the (high $\hat{q}$) plane wave solutions, $\psi(\hat{x}) = (V^{(0)}V^m)^{-1/2} \exp(i\hat{q}\cdot\hat{x})$. This gives

$$\Lambda^{\parallel}(\hat{q}) = 1/\bar{N} + a^2\hat{q}^2 - \frac{3z_c}{2V^{(0)}V^m} \int d\hat{x} \varphi_{mf}^2(\varsigma) + \delta\Lambda(\hat{q}) , \tag{D.14}$$

where

$$\delta\Lambda(\hat{q}) \equiv \sum_{k=0}^{m} \frac{w^{(k)}}{V^{(0)}V^m} \int d\hat{x} \varphi_{mf}(\varsigma) \int d\hat{x}' \varphi_{mf}(\varsigma') \delta(\hat{x}^{(k)} - \hat{x}'^{(k)}) \exp[-i\hat{q}\cdot(\hat{x} - \hat{x}')] . \tag{D.15}$$

### D.3. Elimination of divergences

Using Eq. (D.9) and (D.13), the short wavelength contribution to the total partition function can be represented as

$$\left.\frac{\Xi_m^{SD}}{\Xi_m^R}\right|_{sw} = \exp\left\{ -\frac{V^{(0)}V^m}{2}\int \frac{d\hat{q}}{(2\pi)^{3(1+m)}} \ln\left[\frac{\Lambda^{\parallel}(\hat{q})}{\Lambda^{\perp}(\hat{q})}\right]\right\}. \tag{D.16}$$

We now substitute expressions (D.11) and (D.14) for the eigenvalues and expand the logarithm of their ratio in the limit $a^2(q^{(k)})^2 \gg \max\{\bar{N}^{-1}, w^{(k)}\rho^{(k)}\}$ (in the following we will assume that $\bar{N}^{-1} \ll w^{(k)}\rho^{(k)}$). This leads to exact cancellation of the leading divergences and yields

$$\ln\left[\frac{\Lambda^{\parallel}(\hat{q})}{\Lambda^{\perp}(\hat{q})}\right] \to \frac{1}{a^2\hat{q}^2}\left[ -\frac{z_c}{V^{(0)}V^m}\int d\hat{x}\varphi_{mf}^2(\zeta) + \delta\Lambda(\hat{q})\right]. \tag{D.17}$$

Substituting Eq. (D.17) into expression (D.16) we realize that although we have removed the most divergent terms, the remaining integrals (in Eq. (D.22)) still diverge due to *ultra-short* wavelength contributions from wave vectors $|q| \sim 1/a$. The origin of the problem can be traced back to the inadequacy of our Gaussian chain model for the description of the polymers on spatial scales $\leq a$. This follows from the observation that all the divergent integrals are of the form

$$Q_m^{gauss}(\hat{x}) \equiv 2\int \frac{d\hat{q}}{(2\pi)^{3(1+m)}} \frac{\exp(-i\hat{q}\cdot\hat{x})}{a^2\hat{q}^2} \tag{D.18}$$

and can be written as

$$Q_m^{gauss}(\hat{x}) = \int_0^{\infty} dN \prod_{k=0}^{m} P_N^{gauss}(x^{(k)}), \tag{D.19}$$

where $P_N^{gauss}(x)$ is the normalized end-to-end distribution function (i.e., probability density) of a Gaussian chain of $N$ monomers,

$$P_N^{gauss}(x) = (2\pi a^2 N)^{-3/2}\exp[-x^2/(2a^2N)]. \tag{D.20}$$

The divergence of $Q_N^{gauss}(0)$ in Eq. (D.18) reflects an unphysical aspect of the Gaussian chain model which allows the formation of loops on arbitrarily small scales.

In order to eliminate the divergence in Eq. (D.18), we have to revise the continuous model of the polymer and take into consideration the stiffness of polymer chains on small spatial scales (loops cannot form on length scales smaller than the size of a single chemical monomer!). This revision has no influence on the large-scale behavior and leads only to the replacement of $P_N^{gauss}$ by the end-to-end probability distribution of *real* chains, $P_N$:

$$Q_m^{gauss}(\hat{x}) \to Q_m(\hat{x}) \equiv \sum_{N=1}^{\infty}\prod_{k=0}^{m} P_N(x^{(k)}), \tag{D.21}$$

which is finite for all $\hat{x}$.

Inserting eq. (D.17) into (D.16) and using the substitution (D.21), we arrive at the following expression for the logarithm of the grand canonical partition function (Eq. (D.5)):

$$-\ln \Xi_m(\mu, z_c)|_{sw} = H_{mf} - \frac{z_c}{2} Q_m(0) \int d\hat{x} \varphi_{mf}^2(\varsigma) + \int d\hat{x} \varphi_{mf}(\varsigma) \int d\hat{x}' \varphi_{mf}(\varsigma') Q_m(\hat{x} - \hat{x}') \sum_{k=0}^{m} \frac{w^{(k)}}{2} \delta(x^{(k)} - x'^{(k)}) . \tag{D.22}$$

Since $Q_m(0)$ is a finite quantity (related to the probability of formation of small loops in a real polymer), and the integral over $\hat{x}$ converges, we conclude that the second term on the right-hand side of Eq. (D.22) is now well-defined. The last term on the right-hand side of the above equation can be simplified by noticing that

$$\delta(x^{(k)} - x'^{(k)}) Q_m(\hat{x} - \hat{x}') = \delta(x^{(k)} - x'^{(k)}) \sum_{N=1}^{\infty} P_N(0) \prod_{l \neq k} P_N(x^{(l)} - x'^{(l)}) . \tag{D.23}$$

The functions $P_N(x^{(l)} - x'^{(l)})$ in the above product, decay over length scales of the order of $aN^{1/2}$. We note that in the derivation of Eq. (D.22) we have used the short wavelength approximation, $a^2(q^{(k)}) \gg w^{(k)}\rho^{(k)}$ (which allowed us to consider only terms linear in $w^{(k)}$ in the expansion of the logarithm, Eq. (D.17)). This means only length scales $|x^{(l)} - x'^{(l)}| \ll \xi^{(k)} \equiv a(w^{(k)}\rho^{(k)})^{-1/2}$ (screening length) contribute in Eq. (D.22). For $\xi^{(k)} \ll a\bar{N}^{1/2}$ (the characteristic length scale for the decay of $\varphi_{mf}(\varsigma)$), the functions $\varphi_{mf}(\varsigma')$ in the integrals can be replaced by

$$\varphi_{mf}(\varsigma') = \varphi_{mf}(\varsigma) + \sum_{k=0}^{m} \sum_{\alpha} (x_\alpha^{(k)} - x'^{(k)}_\alpha) \nabla_\alpha^{(k)} \varphi_{mf}(\varsigma) + \frac{1}{2} \sum_{k=0}^{m} \sum_{\alpha} (x_\alpha^{(k)} - x'^{(k)}_\alpha)(x_\beta^{(l)} - x'^{(l)}_\beta) \nabla_\alpha^{(k)} \nabla_\beta^{(l)} \varphi_{mf}(\varsigma) . \tag{D.24}$$

With this substitution and changing the integration variables $\hat{x}' \to \hat{x}' - \hat{x}$, Eq. (D.22) is recast into the form

$$-\ln \Xi_m(\mu, z_c)|_{sw} = H[\varphi_{mf}] - \left[\frac{z_c}{2} Q_m(0) - \frac{w^{(0)} + mw}{2} Q_0(0)\right] \int d\hat{x} \varphi_{mf}^2(\varsigma) - \frac{1}{2} \int d\hat{x} \varphi_{mf}(\varsigma) \sum_{k=0}^{m} \Delta (a^{(k)})^2 (\nabla^{(k)})^2 \varphi_{mf}(\varsigma) , \tag{D.25}$$

where

$$\Delta(a^{(0)})^2 \equiv -mw^{(0)} \sum_{N=1}^{\infty} P_N(0) \int dx x^2 P_N(x) \tag{D.26}$$

and

$$\Delta(a^{(k)})^2 \equiv -[w^{(0)} + (m-1)w] \sum_{N=1}^{\infty} P_N(0) \int dx x^2 P_N(x) \tag{D.27}$$

for $k > 0$. The above integrals can be estimated by introducing a cutoff on a length scale $\xi^{(k)}$ and, in the limit $m \to 0$, we obtain

$$\Delta(a^{(0)})^2 = 0\,, \quad \Delta(a^{(k)})^2 = a^2[(w/a^6\rho)^{1/2} - (w^{(0)}/a^6\rho^{(0)})^{1/2}] \tag{D.28}$$

The last term in Eq. (D.25) can be recast, through integration by parts, in the form

$$\frac{1}{2}\int d\hat{x} \sum_{k=0}^{m} \Delta(a^{(k)})^2 (\nabla^{(k)}\varphi_{mf}(\varsigma))^2\,. \tag{D.29}$$

Comparing the coefficients of the $(\nabla^{(k)}\varphi)^2$ terms in this expression and in the expression for the Hamiltonian, Eq. (2.48), we conclude that this term describes the renormalization of the size of a statistical segment ("monomer") due to thermal fluctuations. Upon adding the contributions of the $(\nabla^{(k)}\varphi)^2$ terms, the coefficient in front of the squared gradient must be interpreted as $(a^{(k)})^2/2$, where $a^{(k)}$ is the observed size of the effective monomer, which is related to the end-to-end distance $\langle R^{(k)2}\rangle$ of a chain of contour length $L \equiv Na_{bare}$ by $\langle R^{(k)2}\rangle = 3(a^{(k)})^2 N$ ($N$ is the dimensionless chain length expressed in units of the size of monomers in the absence of excluded volume interactions, $a_{bare}$).

The renormalization corrections to $a$ are small if [23] $(w^{(k)}/a^6\rho^{(k)})^{1/2} \ll 1$, for all $k$. If these conditions are not satisfied, our short wavelength approximation breaks down and we have to include contributions to Eq. (D.27) which come from increasingly larger length scales. This problem is identical to the usual difficulties with the application of mean field theory to semi-dilute polymer solutions, and has to be treated by non-perturbative methods (e.g., renormalization group [27, 84, 85] and scaling [3]). Such a treatment will be presented in Section 5.

We return to Eq. (D.25) and dropping the last term on the right-hand side of this equation (this term is absorbed in the renormalization of the monomer size $a$), rewrite it in the form

$$\begin{aligned} -\ln \Xi_m(\mu, z_c)|_{sw} &= H_{eff}[\varphi_{mf}] \\ &\equiv H[\varphi_{mf}] - \left[\frac{z_c}{2} Q_m(0) - [(w^{(0)} + mw)/2]\, Q_0(0)\right]\int d\hat{x}\varphi_{mf}^2(\varsigma)\,. \end{aligned} \tag{D.30}$$

The unphysical divergences which appeared in the original expression for the partition function, eq. (D.16), are replaced by sums over the probability densities $P_N(0)$ of finding closed loops of $N$ monomers. Note that, for $N \gg 1$, $P_N(0) \to P_N^{gauss}(0)$ and since the latter decreases as $N^{-3/2}$ with $N$, only the smallest loops (with size of the order of the persistence length) contribute to the sum for $Q_m(0)$ in Eq. (D.21). For such small $N$, the function $P_N(0)$ is non-universal and must be calculated from models (e.g., persistent, freely rotating, rotational isomer, etc. [32]) which account for the local stiffness of real polymer chains.

The small loop corrections to the mean-field partition function have a simple physical interpretation. The term with the coefficient $z_c Q_m(0)$ describes the *reduction* of the elastic modulus of the network (simultaneously in all the replicas) due to permanent *wasted loops* which do not transmit stresses in the network but contribute to monomer and cross-link density [1]. The second term, with the coefficient $(w^{(0)} + mw)Q_0(0)$, reflects the *increase* in the excluded volume interactions between neighboring monomers (in each of the replicas, separately) due to temporary small loops which form in the network due to thermal fluctuations.

*D.4. Wasted loops corrections to free energy*

Although the small loop contributions enter only additively into the replica free energy $\mathscr{F}_m$ (see Eqs. (D.25) and (2.28)), this additivity is the consequence the Gaussian approximation which assumes that the fluctuation corrections to the mean-field Hamiltonian are small and can be treated in first-order perturbation theory. While (as was shown in the previous subsection) corrections due to ultra-short wavelength ($a|\boldsymbol{q}| \sim 1$) fluctuations are not infinite for networks made of real polymers, they are not necessarily small compared to the mean-field Hamiltonian. This suggests that the one loop approximation may not suffice and that one must resort to non-perturbative resummation methods.

The contribution from all small loops can be summed up exactly by the *effective action* method [31, 27]. This method allows us to use the results of the first-order perturbation expansion, in order to construct all the higher-order contributions of terms of such type and to obtain a new ground state which includes *exactly* the effect of the dominant ultra-short wavelength fluctuations. We begin by writing

$$-\ln \Xi_m(\mu, z_c)|_{sw} = \min_{\varphi} H_{eff}[\varphi] , \tag{D.31}$$

where $\varphi_{min}(\hat{\boldsymbol{x}}) \equiv \varphi_{sw}(\hat{\boldsymbol{x}})$ is found by minimizing the *effective* Hamiltonian $H_{eff}[\varphi]$ (instead of minimizing the *bare* Hamiltonian $H[\varphi]$ in Eq. (2.48)), defined by replacing $\varphi_{mf} \to \varphi$ in the argument of $H_{eff}$, in Eq. (D.30). Upon this replacement, the calculation of the solution which minimizes the effective Hamiltonian proceeds in exactly the same way as that of $\varphi_{mf}(\varsigma)$.

For $m = 0$, the extremum condition gives the following expression for $\varphi_{sw}$

$$\varphi_{sw}^2 = [2\mu/(z_c - w^{(0)})] - Q_0(0) , \tag{D.32}$$

which, in the case $Q_0(0) = 0$ (vanishing probability of loop formation) is identical to Eq. (3.4).

Using Eqs. (2.29), the parameters $\mu$ and $z_c$ are expressed through the physically observable $\rho^{(0)}$ and $\bar{N}$:

$$\mu = (\rho^{(0)} + Q_0(0)/2)\,[1/(\rho^{(0)} + Q_0(0)) - w^{(0)}] , \tag{D.33}$$

and

$$z_c = 1/\bar{N}(\rho^{(0)} + Q_0(0)) . \tag{D.34}$$

The above equations reduce to expressions (3.5), for $Q_0(0) = 0$. The cross-link saturation threshold condition becomes (Eq. (3.41)):

$$w^{(0)} = z_c = [\bar{N}(\rho^{(0)} + Q_0(0))]^{-1} . \tag{D.35}$$

In order to calculate the short-wavelength corrections to the free energy, we have to find the solution $\varphi_{sw}(\hat{\boldsymbol{x}})$ which minimizes the effective Hamiltonian for finite $m$. This can be done simply by noticing that $H_{eff}[\varphi]$ can be obtained from the bare Hamiltonian by the substitution

$$\mu \to \mu - (z_c/2)Q_m(0) + [(w^{(0)} + mw)/2]\,Q_0(0) \tag{D.36}$$

and the renormalization of the monomer size in the final state with respect to that in the initial state. The latter effect is assumed to be small in concentrated gels and will be neglected in this section (this approximation will be relaxed when we consider semi-dilute gels in good solvents). We conclude that the only effect of including the contribution of ultra-short wavelength fluctuations is to introduce the replacement

$$\bar{N} \to \bar{N}(1 + Q_0(0)/\rho^{(0)}) \tag{D.37}$$

in the expressions for the inhomogeneous mean-field solution (Eq. (3.24)), the cross-link saturation threshold (Eq. (3.41)) and the mean-field free energy (Eq. (3.30)).

Neglecting logarithmic corrections and constants, the renormalized free energy which includes ultra-short wavelength (coming from length scales $\sim a$) fluctuation corrections, is given by

$$\frac{\mathscr{F}_{sw}\{\lambda_\alpha\}}{VT} = \frac{\nu}{2}\Gamma_{wl}\sum_\alpha \lambda_\alpha^2 + \frac{1}{2}w\rho^2 . \tag{D.38}$$

The correction due to permanent wasted loops formed in the process of cross-linking

$$\Gamma_{wl} \equiv [1 + Q_0(0)/\rho^{(0)}]^{-1} \tag{D.39}$$

depends only on the local stiffness of the chain and on the concentration of the network in the state of preparation. Recall that $Q_0(0)$ is expressed in terms of the probability densities of loop formation,

$$Q_0(0) \equiv \sum_{N=1}^{\infty} P_N(0) . \tag{D.40}$$

Note that neglecting the corrections to the monomer size, the renormalization of the free energy by ultra-small-scale fluctuations does not affect the fundamental additivity property of the mean-field free energy, which can be expressed as the sum of purely elastic and purely osmotic terms. Violation of additivity will play an important role in semi-dilute networks in good solvents, for which one must include the effect of fluctuations on intermediate scales (between the monomer and the mesh sizes). Such effects will be treated by a combination of renormalization group and scaling methods in Section 5.

## Appendix E. Correlation functions of the replica system

We proceed to calculate the replica space correlation functions

$$g_\Lambda^{kl}(\boldsymbol{q}_L) \equiv \int d\boldsymbol{x}_T \varphi_{mf}(\varsigma) \int d\boldsymbol{x}'_T \varphi_{mf}(\varsigma') \times D(\Lambda - a^2(\boldsymbol{q}_L^{(k)})^2; \boldsymbol{x}_T, \boldsymbol{x}'_T) \exp(i\boldsymbol{q}_T^{(k)} \cdot \boldsymbol{x}_T - i\boldsymbol{q}_T^{(l)} \cdot \boldsymbol{x}'_T) , \tag{E.1}$$

where the function $D$ is the solution of the differential equation

$$[1/\bar{N} - (\Lambda - a^2\boldsymbol{q}_L^2) - a^2\nabla_T^2 - (3z_c/2)\varphi_{mf}^2(\varsigma)]D(\Lambda - a^2\boldsymbol{q}_L^2; \boldsymbol{x}_T, \boldsymbol{x}'_T) = \delta(\boldsymbol{x}_T - \boldsymbol{x}'_T) . \tag{E.2}$$

*E.1. Calculation of $g_{\Lambda}^{00}$*

The function $g_{\Lambda}^{00}$ can be represented in the form (recall that $(\boldsymbol{q}_{\mathrm{T}}^{(0)})^2 = 0$; see Eq. (C.21))

$$g_{\Lambda}^{00}(\boldsymbol{q}_{\mathrm{L}}) = \int \mathrm{d}\boldsymbol{x}_{\mathrm{T}} \varphi_{\mathrm{mf}}(\varsigma)\, \Phi(\Lambda - a^2\boldsymbol{q}_{\mathrm{L}}^2; \varsigma)\,, \tag{E.3}$$

where $\Phi$ is defined by

$$\Phi(\Lambda - a^2\boldsymbol{q}_{\mathrm{L}}^2; \varsigma) \equiv \int \mathrm{d}\boldsymbol{x}'_{\mathrm{T}} \varphi_{\mathrm{mf}}(\varsigma')\, D(\Lambda - a^2\boldsymbol{q}_{\mathrm{L}}^2; \boldsymbol{x}_{\mathrm{T}}, \boldsymbol{x}'_{\mathrm{T}})\,. \tag{E.4}$$

Due to the spherical symmetry of the differential operator in Eq. (E.2), $\Phi$ depends only on the scalar combination $\varsigma = \boldsymbol{x}_{\mathrm{T}}^2/2$. The integral (E.3) is calculated in the same way as in eqs. (B.2) and (B.3) (Appendix B) in which we replace $\tilde{H}(\varsigma)$ by $\varphi_{\mathrm{mf}}(\varsigma)\Phi(\Lambda - a^2\boldsymbol{q}_{\mathrm{L}}^2; \varsigma)$ and take the limit $m \to 0$ (note that in calculating $\int \mathrm{d}\boldsymbol{x}_{\mathrm{T}} \tilde{H}(\varsigma)$ we only used the property that $\varphi_{\mathrm{mf}}(\varsigma)$ is an exponentially decreasing function of $\varsigma$). This yields

$$g_{\Lambda}^{00}(\boldsymbol{q}_{\mathrm{L}}) = \varphi_{\mathrm{mf}}(0)\, \Phi(\Lambda - a^2\boldsymbol{q}_{\mathrm{L}}^2; 0)\,. \tag{E.5}$$

In order to calculate the function $\Phi$, we apply the differential operator in Eq. (E.2) to the left-hand side of eq. (E.4) and remove the resulting $\delta$-function by integrating over $\boldsymbol{x}'_{\mathrm{T}}$ on the right-hand side of the resulting equation. This gives the following equation for $\Phi$:

$$[1/\bar{N} - (\Lambda - a^2\boldsymbol{q}_{\mathrm{L}}^2) - 2a^2\varsigma(\partial^2/\partial\varsigma^2) - (3z_{\mathrm{c}}/2)\,\varphi_{\mathrm{mf}}^2(\varsigma)]\, \Phi(\Lambda - a^2\boldsymbol{q}_{\mathrm{L}}^2; \varsigma) = \varphi_{\mathrm{mf}}(\varsigma)\,. \tag{E.6}$$

For $\varsigma = 0$ the equation reduces to an algebraic relation

$$\Phi(\Lambda - a^2\boldsymbol{q}_{\mathrm{L}}^2; 0) = \frac{\varphi_{\mathrm{mf}}(0)}{-2/\bar{N} - \Lambda + a^2\boldsymbol{q}_{\mathrm{L}}^2} \tag{E.7}$$

and, upon inserting this expression into Eq. (E.5), we finally get

$$g_{\Lambda}^{00}(\boldsymbol{q}_{\mathrm{L}}) = \frac{2\rho^{(0)}}{-2/\bar{N} - \Lambda + a^2\boldsymbol{q}_{\mathrm{L}}^2}\,. \tag{E.8}$$

Substituting $g_{\Lambda}^{00}$ into the eigenvalue equation, (C.37), Appendix C, we obtain the eigenvalue $\Lambda_{\mathrm{gap}}$ of the "massive" density mode. We will show in the following that the corresponding eigenfunction is simply $\Phi(\Lambda_{\mathrm{gap}}(\boldsymbol{q}_{\mathrm{L}}) - a^2\boldsymbol{q}_{\mathrm{L}}^2; \varsigma)$. Its functional form cannot be given, in general, since for arbitrary $\varsigma$, Eq. (E.6) can only be solved numerically. There is, however, one important case in which we can find a simple analytical solution:

$$\Phi(0; \varsigma) = -\frac{\partial\varphi_{\mathrm{mf}}(\varsigma)}{\partial\mu} = \bar{N}^2\frac{\partial\varphi_{\mathrm{mf}}(\varsigma)}{\partial\bar{N}}\,. \tag{E.9}$$

This result can be checked by differentiating Eq. (3.1) for $\varphi_{\mathrm{mf}}(\varsigma)$ with respect to $\mu$ and comparing the resulting expression with Eq. (E.6).

*E.2. Calculation of $g_\Lambda^{kl}$*

We now proceed to calculate the replica space correlation function $g_\Lambda^{kl}$ for general $k$, $l$. In order to obtain the $q^2$ corrections to $g^{kl}$, we have to expand the exponential in Eq. (E.1) to fourth order in $q_T$ (linear terms vanish due to angular integrations):

$$g_\Lambda^{kl}(q_L) = g_\Lambda^{00}(q_L) + \int dx_T \varphi_{mf}(\varsigma) \int dx'_T \varphi_{mf}(\varsigma')\, D(\Lambda - a^2 (q_L^{(k)})^2; x_T, x'_T)$$
$$\times [ -\tfrac{1}{2}(q_T^{(k)} \cdot x_T - q_T^{(l)} \cdot x'_T)^2 + \tfrac{1}{24}(q_T^{(k)} \cdot x_T - q_T^{(l)} \cdot x'_T)^4 ] . \tag{E.10}$$

In order to calculate the above integrals, it is convenient to introduce the function

$$x_T \Psi(\Lambda - a^2 q_L^2; \varsigma) \equiv \int dx'_T \varphi_{mf}(\varsigma')\, D(\Lambda - a^2 q_L^2; x_T, x'_T) x'_T . \tag{E.11}$$

Returning to the definition of $\Phi$, Eq. (E.4) and using the symmetry of the integrand in Eq. (E.10) under the replacement $x_T \leftrightarrow x'_T$, we can rewrite the latter in the form

$$g_\Lambda^{kl}(q_L) = g_\Lambda^{00}(q_L) + \int dx_T \varphi_{mf}(\varsigma) \{ -\tfrac{1}{2}\Phi(\Lambda - a^2 q_L^2; \varsigma)$$
$$\times [(q_T^{(k)} \cdot x_T)^2 + (q_T^{(l)} \cdot x_T)^2] + \Psi(\Lambda - a^2 q_L^2; \varsigma) [(q_T^{(k)} \cdot x_T)(q_T^{(l)} \cdot x_T)$$
$$- \tfrac{1}{6}(q_T^{(k)} \cdot x_T)^3 (q_T^{(l)} \cdot x_T) - \tfrac{1}{6}(q_T^{(k)} \cdot x_T)(q_T^{(l)} \cdot x_T)^3] \} . \tag{E.12}$$

The angular integrations over the direction of the vector $x_T$ in Eq. (E.12) are performed with the aid of the formulae

$$\int d\Omega x_{Ti} x_{Tj} = S_{3m} \frac{x_T^2}{3m} \delta_{ij} ,$$
$$\int d\Omega x_{Ti} x_{Tj} x_{Tl} x_{Tk} = S_{3m} \frac{(x_T^2)^2}{3m(3m+2)} (\delta_{ij}\delta_{kl} + \delta_{ik}\delta_{jl} + \delta_{il}\delta_{jk}) , \tag{E.13}$$

where $S_{3m} = 2\pi^{3m/2}/\Gamma(3m/2)$ is the surface area of a unit $3m$-dimensional sphere ($\Gamma$ is the gamma function). In the limit $m \to 0$ this yields

$$g^{kl}(q_L) = g^{00}(q_L) - \frac{1}{2}\int_0^\infty d\varsigma \varphi_{mf}(\varsigma) [(q_T^{(k)})^2 + (q_T^{(l)})^2]$$
$$\times \Phi(\Lambda - a^2 q_L^2; \varsigma) + \int_0^\infty d\varsigma \varphi_{mf}(\varsigma) (q_T^{(k)} \cdot q_T^{(l)}) \Psi(\Lambda - a^2 q_L^2; \varsigma)$$
$$- \frac{1}{2}\int_0^\infty d\varsigma\varsigma \varphi_{mf}(\varsigma) [(q_T^{(k)})^2 + (q_T^{(l)})^2] (q_T^{(k)} \cdot q_T^{(l)}) \Psi(\Lambda - a^2 q_L^2; \varsigma) . \tag{E.14}$$

*E.2.1. Long wavelength limit, $q \to 0$*

We first calculate the functions $g^{kl}$, defined by Eq. (E.14), in the limit $q \to 0$. From the definition of $\boldsymbol{q}_{\mathrm{T}}^{(k)}$, Eq. (C.21),

$$\begin{aligned}\boldsymbol{q}_{\mathrm{T}}^{(k)} \cdot \boldsymbol{q}_{\mathrm{T}}^{(l)} &= \hat{\boldsymbol{q}}^{(k)} \cdot \hat{\boldsymbol{q}}^{(l)} - \boldsymbol{q}_{\mathrm{L}}^{(k)} \cdot \boldsymbol{q}_{\mathrm{L}}^{(l)} \\ &= (\lambda^{-1} \star \boldsymbol{q}_{\mathrm{L}})^2 \delta_{kl} - \boldsymbol{q}_{\mathrm{L}}^2 , \quad k \neq 0 , \quad l \neq 0 \end{aligned} \tag{E.15}$$

and, consequently, $(\boldsymbol{q}_{\mathrm{T}}^{(k)})^2 = (\boldsymbol{q}_{\mathrm{T}}^{(l)})^2$ for $k, l \neq 0$. Using these relations, we express the combination $g_{\Lambda}^{11}(\boldsymbol{q}_{\mathrm{L}}) - g_{\Lambda}^{12}(\boldsymbol{q}_{\mathrm{L}})$ in Eq. (C.43), in terms of the function $\Psi$

$$g_{\Lambda}^{11}(\boldsymbol{q}_{\mathrm{L}}) - g_{\Lambda}^{12}(\boldsymbol{q}_{\mathrm{L}}) = (\lambda^{-1} \star \boldsymbol{q}_{\mathrm{L}})^2 \int_0^{\infty} \mathrm{d}\varsigma \varphi_{\mathrm{mf}}(\varsigma) \Psi(\Lambda - a^2 \boldsymbol{q}_{\mathrm{L}}^2; \varsigma) . \tag{E.16}$$

The function $\Psi$ can be calculated from the following equation (which can be obtained by applying the differential operator in Eq. (E.2) to both sides of Eq. (E.11)):

$$\begin{aligned}&\left[\frac{1}{\bar{N}} - (\Lambda - a^2 \boldsymbol{q}_{\mathrm{L}}^2) - 2a^2 \varsigma \frac{\partial^2}{\partial \varsigma} - 2a^2 \frac{\partial}{\partial \varsigma} - 3 \frac{z_{\mathrm{c}}}{2} \varphi_{\mathrm{mf}}^2(\varsigma)\right] \\ &\quad \times \Psi(\Lambda - a^2 \boldsymbol{q}_{\mathrm{L}}^2; \varsigma) = \varphi_{\mathrm{mf}}(\varsigma) . \end{aligned} \tag{E.17}$$

In general, the function $\Psi(\Lambda - a^2 \boldsymbol{q}_{\mathrm{L}}^2; \varsigma)$ has to be calculated numerically. Note, however, that the differential operator in Eq. (E.17) has an eigenvalue $a^2 \boldsymbol{q}_{\mathrm{L}}^2 - \Lambda$, with an eigenfunction of the form $\partial \varphi_{\mathrm{mf}}(\varsigma)/\partial \varsigma$ (this can be checked by differentiating the mean-field equation (3.23), with respect to $\varsigma$ and comparing to Eq. (E.17)). Thus, when looking for the solution of the equation (E.17) in the form of an expansion over eigenfunctions of this operator, in the limit $\Lambda - a^2 \boldsymbol{q}_{\mathrm{L}}^2 \to 0$ we can retain only the contribution of this eigenfunction (ground state dominance):

$$\Psi(\Lambda - a^2 \boldsymbol{q}_{\mathrm{L}}^2; \varsigma) \to \frac{C_0}{a^2 \boldsymbol{q}_{\mathrm{L}}^2 - \Lambda} \frac{\partial \varphi_{\mathrm{mf}}(\varsigma)}{\partial \varsigma} , \tag{E.18}$$

where $C_0$ is obtained from the normalization condition which yields

$$C_0 = \int_0^{\infty} \mathrm{d}\varsigma \varphi_{\mathrm{mf}}(\varsigma) \frac{\partial \varphi_{\mathrm{mf}}(\varsigma)}{\partial \varsigma} \Big/ \int_0^{\infty} \mathrm{d}\varsigma \left(\frac{\partial \varphi_{\mathrm{mf}}(\varsigma)}{\partial \varsigma}\right)^2 . \tag{E.19}$$

Substituting this expression into Eq. (E.16) we obtain

$$g_{\Lambda}^{11}(\boldsymbol{q}_{\mathrm{L}}) - g_{\Lambda}^{12}(\boldsymbol{q}_{\mathrm{L}}) = C \frac{(\lambda^{-1} \star \boldsymbol{q}_{\mathrm{L}})^2}{a^2 \boldsymbol{q}_{\mathrm{L}}^2 - \Lambda} , \tag{E.20}$$

where the constant $C$ is given by

$$C = \left(\int_0^{\infty} \mathrm{d}\varsigma \varphi_{\mathrm{mf}}(\varsigma) \frac{\partial \varphi_{\mathrm{mf}}(\varsigma)}{\partial \varsigma}\right)^2 \Big/ \int_0^{\infty} \mathrm{d}\varsigma \left(\frac{\partial \varphi_{\mathrm{mf}}(\varsigma)}{\partial \varsigma}\right)^2 . \tag{E.21}$$

The numerator and the denominator in this expression are readily calculated by integrating by parts

$$\int_0^\infty d\varsigma \varphi_{mf}(\varsigma) \frac{\partial \varphi_{mf}(\varsigma)}{\partial \varsigma} = \frac{\varphi_{mf}^2(\varsigma)}{2}\Big|_0^\infty = -\frac{\varphi_{mf}^2}{2} \tag{E.22}$$

and

$$\begin{aligned}\int_0^\infty d\varsigma \left(\frac{\partial \varphi_{mf}(\varsigma)}{\partial \varsigma}\right)^2 &= -2\int_0^\infty d\varsigma \frac{\partial \varphi_{mf}(\varsigma)}{\partial \varsigma} \varsigma \frac{\partial^2 \varphi_{mf}(\varsigma)}{\partial \varsigma^2} \\ &= -\int_0^\infty d\varsigma \frac{\partial \varphi_{mf}(\varsigma)}{\partial \varsigma} \frac{[1/\bar{N} - (z_c/2)\varphi_{mf}^2(\varsigma)]\varphi_{mf}(\varsigma)}{a^2} \\ &= (\varphi_{mf}^2/(2\bar{N}) - z_c\varphi_{mf}^4/8)/a^2 = \varphi_{mf}^2/(4a^2\bar{N}) ,\end{aligned} \tag{E.23}$$

where, in obtaining the second equality, we have used Eq. (3.23) for $\varphi_{mf}(\varsigma)$. Substituting the above into Eq. (E.21) gives

$$C = 2\rho^{(0)} a^2 \bar{N} . \tag{E.24}$$

The eigenvalues corresponding to the gapless density modes are found by substituting the expression for $g_\Lambda^{11}(\boldsymbol{q}_L) - g_\Lambda^{12}(\boldsymbol{q}_L)$ (Eqs. (E.20) and (E.23)) into the eigenvalue equation, (C.43). This gives the eigenvalues, Eqs. (3.42).

*E.2.2. Long wavelength limit, $q^2$ corrections*

We proceed to calculate the $q^2$ corrections to the functions $g^{kl}$, defined by Eq. (E.14). Since all what we need are the functions $D$, $\Phi$ and $\Psi$ defined for $\Lambda = 0$, we can simplify the notation by *omitting* the argument $\Lambda$. Begin with the calculation of the function $\Psi$, defined by Eq. (E.11) (with $\Lambda = 0$),

$$[1/\bar{N} + a^2\boldsymbol{q}_L^2 - 2a^2\varsigma(\partial^2/\partial\varsigma^2) - 2a^2(\partial/\partial\varsigma) - (3z_c/2)\varphi_{mf}^2(\varsigma)]\,\Psi(\varsigma) = \varphi_{mf}(\varsigma) . \tag{E.25}$$

To solve this equation, let us rewrite its right-hand side as the sum of two terms,

$$\varphi_{mf}(\varsigma) = C_0 \frac{\partial \varphi_{mf}(\varsigma)}{\partial \varsigma} + \tilde{\varphi}_{mf}(\varsigma) , \quad \int_0^\infty d\varsigma \tilde{\varphi}_{mf}(\varsigma) \frac{\partial \varphi_{mf}(\varsigma)}{\partial \varsigma} = 0 , \tag{E.26}$$

the first of which is "parallel" to the eigenfunction $\partial\varphi_{mf}(\varsigma)/\partial\varsigma$ of the differential operator in Eq. (E.25) and the second one is orthogonal to it. The constant $C_0$ was calculated earlier (Eq. (E.19)). The solution of the equation can be represented in the same form as in Eq. (E.26)

$$\Psi(\varsigma) = \frac{C_0}{a^2\boldsymbol{q}_L^2} \frac{\partial \varphi_{mf}(\varsigma)}{\partial \varsigma} + \tilde{\Psi}(\varsigma) , \quad \int_0^\infty d\varsigma \tilde{\Psi}(\varsigma) \frac{\partial \varphi_{mf}(\varsigma)}{\partial \varsigma} = 0 , \tag{E.27}$$

where the function $\tilde{\Psi}(\varsigma)$ is the solution of Eq. (E.25), where on the right-hand side we replace the function $\varphi_{mf}(\varsigma)$ by $\tilde{\varphi}_{mf}(\varsigma)$. Since we are interested only in terms of order $\boldsymbol{q}^2$, we can omit the $a^2\boldsymbol{q}_L^2$ term in this equation.

To solve this equation let us introduce the dimensionless function

$$\tilde{\Psi}(\varsigma) = -\sqrt{\frac{2\bar{N}}{z_c}}\,\vartheta(t)\,, \quad t = \frac{\varsigma}{2a^2\bar{N}}\,, \tag{E.28}$$

which obeys the equation

$$(1 - 3\chi^2(t))\,\vartheta(t) - t\vartheta''(t) - \vartheta'(t) = \chi(t) + \chi'(t)\,, \tag{E.29}$$

with $\chi(t)$ defined in Eq. (3.24). Although we do not know the explicit analytical expression for the function $\chi(t)$, the general solution of the differential equation can be found, since we know one of the solutions ($\chi'(t)$) of the corresponding homogeneous equation. This general solution can be written as

$$\vartheta(t) = \tfrac{1}{2}[\chi(t) + t\chi'(t)] + \chi'(t)\left[C_1 + C_2\int^t \frac{\mathrm{d}t'}{t'(\chi'(t))^2}\right], \tag{E.30}$$

where $C_1$ and $C_2$ are integration constants. Since the integral diverges we have to take $C_2 = 0$. Also, we must have $C_1 = 0$ because of the orthogonality condition, Eq. (E.27).

We now turn to the calculation of the functions $g^{kl}$, Eq. (E.14). Substituting the expression $\Phi(\varsigma) = \bar{N}^2\partial\varphi_{\mathrm{mf}}(\varsigma)/\partial\bar{N}$, Eq. (E.4), in the first integral, we find

$$\int_0^\infty \mathrm{d}\varsigma\,\varphi_{\mathrm{mf}}(\varsigma)\Phi(\varsigma) = \bar{N}^2\frac{\partial}{\partial\bar{N}}\int_0^\infty \mathrm{d}\varsigma\frac{\varphi_{\mathrm{mf}}^2(\varsigma)}{2} = \frac{2a^2\bar{N}^2}{z_c}\frac{\partial}{\partial\bar{N}}\int_0^\infty \mathrm{d}t\chi^2(t) = 0\,. \tag{E.31}$$

Substituting the expressions (E.27) and (E.28) into Eq. (E.14) we find

$$g^{kl}(\boldsymbol{q}_{\mathrm{L}}) = g^{00}(\boldsymbol{q}_{\mathrm{L}}) + \int_0^\infty \mathrm{d}\varsigma\,\tilde{\Psi}(\varsigma)\tilde{\varphi}_{\mathrm{mf}}(\varsigma)\,(\boldsymbol{q}_{\mathrm{T}}^{(k)}\cdot\boldsymbol{q}_{\mathrm{T}}^{(l)})$$
$$+ \frac{(\boldsymbol{q}_{\mathrm{T}}^{(k)}\cdot\boldsymbol{q}_{\mathrm{T}}^{(l)})}{a^2\boldsymbol{q}_{\mathrm{L}}^2}\left\{C + \frac{C_0 I_1}{4}[(\boldsymbol{q}_{\mathrm{T}}^{(k)})^2 + (\boldsymbol{q}_{\mathrm{T}}^{(l)})^2]\right\}, \tag{E.32}$$

where

$$I_1 \equiv \int_0^\infty \mathrm{d}t\chi^2(t) = 0.524\,. \tag{E.33}$$

Using the definition (E.28), we can rewrite the corresponding integral in Eq. (E.32) in the form

$$\int_0^\infty \mathrm{d}\varsigma\,\tilde{\Psi}(\varsigma)\tilde{\varphi}_{\mathrm{mf}}(\varsigma) = 2\rho^{(0)}\bar{N}I_2 \tag{E.34}$$

$$I_2 \equiv \int_0^\infty \mathrm{d}t(\chi(t) + t\chi'(t))\,(\chi(t) + \chi'(t))\,. \tag{E.35}$$

Let us estimate the integrals which appear in Equation (E.35). Multiplying Equation (3.25) for the function $\chi(t)$ by $t\chi'(t)$ and $\chi(t)$ and integrating by parts, we obtain

$$\int_0^\infty dt t(\chi'(t))^2 = \frac{1}{2}\int_0^\infty dt\,\chi^2(t) - \frac{1}{4}\int_0^\infty dt\,\chi^4(t)\,, \tag{E.36}$$

$$\frac{1}{2} - \int_0^\infty dt t(\chi'(t))^2 = \int_0^\infty dt\,\chi^2(t) - \int_0^\infty dt\,\chi^4(t)\,, \tag{E.37}$$

respectively. Combining these two equations, we find

$$\int_0^\infty dt t(\chi'(t))^2 = \frac{1}{5}\int_0^\infty dt\,\chi^2(t) - \frac{1}{10}\,. \tag{E.38}$$

Multiplying Eq. (3.25) by factors $\chi'(t)$ and integrating by parts, yields

$$\int_0^\infty dt(\chi'(t))^2 = \frac{1}{2}\,. \tag{E.39}$$

Using these relations we finally obtain

$$I_2 = \frac{2}{5} - \frac{7}{10}\int_0^\infty dt\,\chi^2(t) = 0.033\,. \tag{E.40}$$

*E.2.3. Short wavelength limit*

We now calculate the functions $g^{kl}(\boldsymbol{q}_L)$, defined in Eq. (E.1), with $\Lambda = 0$, in the short wavelength limit $a^2\bar{N}(\lambda \star \boldsymbol{q})^2 \gg 1$. In this limit the Laplacian gives the leading contribution to the differential operator in Eq. (E.2). Its eigenfunctions are plane waves, $\exp(i\boldsymbol{q}_T\boldsymbol{x}_T)$, and corresponding eigenvalues are

$$\varepsilon(\boldsymbol{q}_T^2) = \frac{1}{\bar{N}} + a^2(\boldsymbol{q}_L^2 + \boldsymbol{q}_T^2) - \frac{3z_c}{2V^m}\int d\boldsymbol{x}_T\varphi_{mf}^2(\varsigma)\,. \tag{E.41}$$

In the limit $m \to 0$ this takes the form

$$\varepsilon(\boldsymbol{q}_T^2) = a^2(\boldsymbol{q}_L^2 + \boldsymbol{q}_T^2) - 2/\bar{N}\,. \tag{E.42}$$

The short wavelength limit of the function $D$ is

$$D(\boldsymbol{x}_T, \boldsymbol{x}_T') = \int \frac{d\boldsymbol{q}_T}{(2\pi)^{3m}}\frac{e^{i\boldsymbol{q}_T\cdot(\boldsymbol{x}_T - \boldsymbol{x}_T')}}{\varepsilon(\boldsymbol{q}_T^2)}\,, \tag{E.43}$$

where, for the sake of simplicity, we omit the argument $\Lambda$.

Substituting this function into Eq. (E.1) we find

$$g^{kl}(\boldsymbol{q}_L) = \int \frac{d\boldsymbol{q}_T}{(2\pi)^{3m}}\frac{\varphi(\boldsymbol{q}_T - \boldsymbol{q}_T^{(k)})\varphi(-\boldsymbol{q}_T + \boldsymbol{q}_T^{(l)})}{\varepsilon(\boldsymbol{q}_T^2)}\,, \tag{E.44}$$

where the function $\varphi(\boldsymbol{q}_T)$ is the Fourier transform (in the transverse subspace) of the function $\varphi_{mf}(\varsigma)$

$$\varphi(\boldsymbol{q}_T) \equiv \int d\boldsymbol{x}_T \varphi_{mf}(\varsigma) e^{-i\boldsymbol{q}_T \cdot \boldsymbol{x}_T} . \tag{E.45}$$

Since this function has a very sharp peak at the origin and falls down exponentially at infinity, we can estimate the integral (E.45) in the limit of large $q_*^2 \equiv (\boldsymbol{q}_T^{(k)})^2 = (\boldsymbol{q}_T^{(l)})^2$ as

$$g^{kl}(\boldsymbol{q}_L) \approx \frac{1}{\varepsilon(q_*^2)} \int \frac{d\boldsymbol{q}_T}{(2\pi)^{3m}} \varphi(\boldsymbol{q}_T - \boldsymbol{q}_T^{(k)}) \varphi(-\boldsymbol{q}_T + \boldsymbol{q}_T^{(l)})$$

$$= \frac{1}{\varepsilon(q_*^2)} \int d\boldsymbol{x}_T \varphi_{mf}^2(\varsigma) \exp[i(\boldsymbol{q}_T^{(k)} - \boldsymbol{q}_T^{(l)})\boldsymbol{x}_T] . \tag{E.46}$$

We now split the $\boldsymbol{x}_T$ integration into an angular integration and an integration over $|\boldsymbol{x}_T|$. In calculating the former we use the equality

$$\int d\Omega e^{i\boldsymbol{q}_T \cdot \boldsymbol{x}_T} = S_{3m} \Gamma\left(1 + \frac{3m}{2}\right) \left(\frac{2^{1/2}}{|\boldsymbol{q}_T| \varsigma^{1/2}}\right)^{3m/2} J_{3m/2}(|\boldsymbol{q}_T| \sqrt{2\varsigma}) . \tag{E.47}$$

Substituting it into expression (E.46) we find (in the limit $m \to 0$):

$$g^{kl}(\boldsymbol{q}_L) \approx -\frac{1}{\varepsilon(q_*^2)} \int_0^\infty d\varsigma \frac{d\varphi_{mf}^2(\varsigma)}{d\varsigma} J_0(|\boldsymbol{q}_T^{(k)} - \boldsymbol{q}_T^{(l)}| \sqrt{2\varsigma}) . \tag{E.48}$$

In the short wavelength limit this equation reduces to

$$g^{kl}(\boldsymbol{q}_L) = \frac{2\rho^{(0)}}{a^2(\lambda^{-1} \star \boldsymbol{q}_L)^2 - 2/\bar{N}} \quad \text{for } k = l . \tag{E.49}$$

In the case $k \neq l$ we use the equality

$$(\boldsymbol{q}_T^{(k)} - \boldsymbol{q}_T^{(l)})^2 = (\hat{\boldsymbol{q}}^{(k)} - \hat{\boldsymbol{q}}^{(l)})^2 = 2(\lambda^{-1} \star \boldsymbol{q}_L)^2 \tag{E.50}$$

and find from Eq. (E.48):

$$g^{kl}(\boldsymbol{q}_L) \approx -\frac{1}{\varepsilon(q_*^2)} \left.\frac{d\varphi_{mf}^2(\varsigma)}{d\varsigma}\right|_{\varsigma=0} \int_0^\infty d\varsigma \theta(\varsigma) J_0(2\sqrt{(\lambda^{-1} \star \boldsymbol{q}_L)^2 \varsigma}) , \tag{E.51}$$

where $\theta(0) = 1$ and, according to eqs. (E.30) and (3.26), the function $\theta(\varsigma)$ decreases when $\varsigma \to \infty$ as $\exp\{-4[\varsigma/(2a^2\bar{N})]^{1/2}\}$. Since the asymptotics under consideration does not depend on the form of this function, we can use this exponent for $\theta(\varsigma)$ in the entire region of variation of $\varsigma$. This gives

$$g^{kl}(\boldsymbol{q}_L) = \frac{\rho^{(0)}|\chi'(0)|}{a^2(\lambda^{-1} \star \boldsymbol{q}_L)^2 [a^2\bar{N}(\lambda^{-1} \star \boldsymbol{q}_L)^2 - 2]} \quad \text{for } k \neq l , \tag{E.52}$$

where numerical calculations give $\chi'(0) = -1.21$.

Notice that in the derivation of expressions (E.50) and (E.52) we neglected terms of order of $q_L^{-6}$.

## F. Derivation of the entropy density functional

### *F.1. Elimination of shear fluctuations and of density fluctuations in the initial state*

An explicit expression for the entropy in the final state ($k = 1, \ldots, m$), $\Delta S_m[\{\delta\rho^{(k)}\}]$, Eq. (4.7), is found by introducing the Fourier representation of the $\delta$-function through the auxiliary fields $\{h^{(k)}(x)\}$ (the field $h^{(k)}$ is conjugate to $\delta\rho^{(k)}$):

$$\delta\left[\delta\rho^{(k)}(x) - \int d\hat{x}\varphi_{mf}(\varsigma)\delta\varphi(\hat{x})\delta(x - x^{(k)})\right] = \int D[h^{(k)}]$$
$$\times \exp\left(i\int dx\delta\rho^{(k)}(x)h^{(k)}(x) - i\int d\hat{x}\varphi_{mf}(\varsigma)\delta\varphi(\hat{x})h^{(k)}(x^{(k)})\right), \tag{F.1}$$

where we used $\delta(x - x^{(k)})$ to integrate over $x$, in the second term on the right-hand side of this expression. Substituting into Eq. (4.7) and moving the integration over $\{h^{(k)}(x)\}$ to the leftmost side of the resulting expression, gives

$$\exp(\Delta S_m[\{\delta\rho^{(k)}\}])$$
$$= \int D\{h^{(k)}\}\exp\left(i\sum_{k=1}^{m}\int dx\delta\rho^{(k)}(x)h^{(k)}(x)\right)I[\{h^{(k)}\}], \tag{F.2}$$

where

$$I[\{h^{(k)}\}] \equiv \int D[\delta\varphi]\exp\left\{-i\int d\hat{x}\varphi_{mf}(\varsigma)\delta\varphi(\hat{x})\sum_{k=1}^{m}h^{(k)}(x^{(k)})\right.$$
$$\left. - \frac{1}{2}\int d\hat{x}\int d\hat{x}'\,\delta\varphi(\hat{x})K_0^{\|}(\hat{x},\hat{x}')\delta\varphi(\hat{x}')\right\}. \tag{F.3}$$

The operator $K_0^{\|}$ is defined by expression (3.35) for $K^{\|}$, in which we take $w = 0$.

In order to perform the integration over $\delta\varphi$ in the functional $I$, it is convenient to remove the term linear in $\delta\varphi$ by shifting the integration variables, $\delta\varphi(\hat{x}) \to \delta\varphi(\hat{x}) + \phi_h(\hat{x})$ and demanding that the field $\phi_h$ obeys the relation:

$$\int d\hat{x}'\,K_0^{\|}(\hat{x},\hat{x}')\phi_h(\hat{x}') \equiv i\varphi_{mf}(\varsigma)\sum_{k=1}^{m}h^{(k)}(x^{(k)}). \tag{F.4}$$

The remaining Gaussian integration can be easily carried out with the result

$$I[\{h^{(k)}\}] = [\det K_0^{\|}]^{-1/2}\exp\left[-\frac{i}{2}\int d\hat{x}'\varphi_{mf}(\varsigma')\phi_h(\hat{x}')\sum_{k=1}^{m}h^{(k)}(x^{(k)})\right]. \tag{F.5}$$

The determinant $\det K_0^{\|}$ is given by the product of the eigenvalues $\Lambda_0(q_L)$ of the operator $K_0^{\|}$ which are obtained by substituting $w = 0$ in the eigenvalues of the operator $K^{\|}$. We have shown that all the eigenvalues are positive and therefore $\det K_0^{\|}$ is a well-defined quantity which introduces fluctuation corrections to the mean-field free energy. Since these corrections were calculated in the previous section, we will omit them in the following.

Eq. (F.4) for the response field $\phi_h(\hat{x})$ can be rewritten as

$$[1/\bar{N} - a^2\hat{\nabla}^2 - 3(z_c/2)\varphi_{mf}^2(\varsigma)]\,\phi_h(\hat{x}) + \varphi_{mf}(\varsigma)w^{(0)}\rho_h^{(0)}(x^{(0)}) = i\varphi_{mf}(\varsigma)\sum_{k=1}^{m} h^{(k)}(x^{(k)})\,, \tag{F.6}$$

where

$$\rho_h^{(0)}(x^{(0)}) = \int d\hat{x}'\,\delta(x^{(0)} - x'^{(0)})\varphi_{mf}(\varsigma')\,\phi_h(\hat{x}') \tag{F.7}$$

can be interpreted as the density variation in the 0th replica of initial state, induced by the fields $\{h^{(k)}\}$ in the replicas of final state. Since the $\{h^{(k)}\}$ fields were introduced as conjugate fields to the densities $\{\delta\rho^{(k)}\}$ in the replicas of the final state, the fact that the density in the initial state is also affected by $\{h^{(k)}\}$ appears strange at first sight. Further reflection reveals that the above relation expresses the simple physical fact that the densities in the initial and the final state are strongly correlated, since the structure of the network is identical in all the replicas.

Returning to Eq. (F.6), we notice that this equation is the inhomogeneous variant of the homogeneous equation, (C.13), Appendix C and solve Eq. (F.6) by recasting it into an equation for the field $\rho_h^{(0)}(x^{(0)})$. We first express $\phi_h$ through $\rho_h^{(0)}$,

$$\phi_h(\hat{x}) = -\int d\hat{x}'\,D(0;\hat{x},\hat{x}')\,\varphi_{mf}(\varsigma')\left[w^{(0)}\rho_h^{(0)}(x'^{(0)}) - i\sum_{k=1}^{m} h^{(k)}(x')\right], \tag{F.8}$$

where $D$ is defined by Eq. (C.28), with the substitution $\Lambda = 0$. Substituting this expression into Eq. (F.5) yields

$$I[\{h^{(k)}\}] = \exp\left\{-\frac{1}{2}\int dx \int dx'\left[\sum_{k,l=1}^{m} g^{kl}(x,x')h^{(k)}(x)h^{(l)}(x') + iw^{(0)}\rho_h^{(0)}(x)g^{01}(x,x')\sum_{k=1}^{m} h^{(k)}(x')\right]\right\}, \tag{F.9}$$

where we define the Green's function $g^{kl}$ by

$$g^{kl}(x,x') \equiv g_\Lambda^{kl}(x,x')|_{\Lambda=0}\,, \tag{F.10}$$

with $g_\Lambda^{kl}(x,x')$ defined in Eq. (C.30) (the long wavelength and short wavelength limits of the Fourier transforms of these functions are calculated in Appendix E).

We now proceed to eliminate $\rho_h^{(0)}$ in the expression for $I[\{h^{(k)}\}]$. Inserting Eq. (F.8) into Eq. (F.6), we obtain a linear integral equation for the function $\delta\rho_h^{(0)}(x)$:

$$\delta\rho_h^{(0)}(x) + w^{(0)}\int dx'\,g^{00}(x,x')\,\delta\rho_h^{(0)}(x') = i\int dx'\,g^{01}(x,x')\sum_{k=1}^{m} h^{(k)}(x')\,. \tag{F.11}$$

Fourier transforming equation (F.11) we find (analogously to Eq. (C.34)),

$$[1 + w^{(0)}g^{00}(q^{(0)})]\,\rho_{q^{(0)}}^{(0)} = i\,g^{01}(q^{(0)})\sum_{k=1}^{m} h_q^{(k)}\,, \tag{F.12}$$

where the wave vectors $\boldsymbol{q}^{(0)}$ and $\boldsymbol{q}$ in the initial and the final states, respectively, are related by the affine transformation

$$\boldsymbol{q}^{(0)} = \lambda \star \boldsymbol{q} \,. \tag{F.13}$$

Substituting this solution into Eq. (F.5) yields an explicit expression for $I[\{h^{(k)}\}]$ in terms of the Fourier components $\{h_q^{(k)}\}$:

$$I[\{h^{(k)}\}] = \exp\left\{ - \int \frac{\mathrm{d}\boldsymbol{q}}{(2\pi)^3} \left[ \frac{g_q}{2} \sum_{k=1}^{m} h_q^{(k)} h_{-q}^{(k)} + \frac{v_q}{2} \sum_{k=1}^{m} h_q^{(k)} \sum_{l=1}^{m} h_{-q}^{(l)} \right] \right\}, \tag{F.14}$$

with the coefficients

$$g_q \equiv \frac{g^{11}(\lambda \star \boldsymbol{q}) - g^{12}(\lambda \star \boldsymbol{q})}{\lambda_x \lambda_y \lambda_z} \tag{F.15}$$

and

$$v_q \equiv \frac{1}{\lambda_x \lambda_y \lambda_z} \left[ g^{12}(\lambda \star \boldsymbol{q}) - \frac{w^{(0)} [g^{01}(\lambda \star \boldsymbol{q})]^2}{1 + w^{(0)} g^{00}(\lambda \star \boldsymbol{q})} \right], \tag{F.16}$$

where the functions $g^{kl}$ are the replica space correlation functions calculated in Appendix E. The fact that the wave vectors transform as $\boldsymbol{q}^{(0)} = \lambda \star \boldsymbol{q}$, automatically implies that the coordinates transform as $\boldsymbol{x} = \lambda \star \boldsymbol{x}^{(0)}$, where $\boldsymbol{x}$ and $\boldsymbol{x}^{(0)}$ are the coordinates of a point in the deformed and the undeformed network, respectively. The factor $\lambda_x \lambda_y \lambda_z = V/V^{(0)}$ in Eqs. (F.15) and (F.16) reflects the change of volume in going from the initial to the final (deformed) state of the network.

### *F.2. Diagonalization in the replicas*

Note that expression (F.14) contains non-diagonal terms in the replicas. The "interaction" between the replicas reflects the fact that all replicas have identical network structure. This observation is made more transparent if we diagonalize these terms using the identity (Eq. (A.6) in Appendix A, with the replacement $\psi \to n$)

$$\exp\left\{ - \int \frac{\mathrm{d}\boldsymbol{q}}{(2\pi)^3} \frac{v_q}{2} \sum_{k=1}^{m} h_q^{(k)} \sum_{l=1}^{m} h_{-q}^{(l)} \right\} \equiv \left\langle \exp\left\{ - \mathrm{i} \int \frac{\mathrm{d}\boldsymbol{q}}{(2\pi)^3} n_q \sum_{l=1}^{m} h_{-q}^{(l)} \right\} \right\rangle_n , \tag{F.17}$$

where $n_q$ is a Fourier component of a random Gaussian field whose correlator (see Eq. (A.8), in Appendix A) is

$$\langle n_q n_{-q} \rangle_n = v_q \,. \tag{F.18}$$

The probability distribution of this random field can be obtained from Eq. (A.7)

$$P[n] = \exp\left\{ \frac{1}{2} \int \frac{\mathrm{d}\boldsymbol{q}}{(2\pi)^3} \left[ \ln(2\pi v_q) - \frac{n_q n_{-q}}{v_q} \right] \right\}. \tag{F.19}$$

We can now use identity (F.17) to represent Eq. (F.14) in the diagonal in the replicas form

$$I[\{h^{(k)}\}] = \left\langle \prod_{k=1}^{m} \exp\left\{ -\int \frac{d\boldsymbol{q}}{(2\pi)^3}\left[\frac{g_q}{2} h_q^{(k)} h_{-q}^{(k)} - i h_q^{(k)} n_{-q}\right]\right\}\right\rangle_n . \tag{F.20}$$

Upon inserting this relation into Eq. (F.2) and performing the Gaussian integrals over $\{h^{(k)}\}$ we get

$$\exp \Delta S_m[\{\rho^{(k)}\}] = \left\langle \prod_{k=1}^{m} \exp \Delta S[n, \delta\rho^{(k)}]\right\rangle_n , \tag{F.21}$$

where the entropy functional is given by the simple expression:

$$\Delta S[n, \delta\rho^{(k)}] = -\int \frac{d\boldsymbol{q}}{(2\pi)^3} \frac{(\rho_q^{(k)} - n_q)\,(\rho_{-q}^{(k)} - n_{-q})}{2g_q} . \tag{F.22}$$

## Appendix G. Asymptotic expressions for correlators $g_q$ and $v_q$

We begin with the summary of the main results of Appendix E for the correlation functions $g_q^{kl}$ of the replica system (with $\Lambda = 0$), and then derive exact asymptotic expressions for the long and the short wavelength limits of the correlators $g_q$ and $v_q$.

An exact (to all orders in $\boldsymbol{q}^2$) expression for $g^{00}$ is given in Eq. (E.8). Substituting $\Lambda = 0$ in the above expression we find

$$g^{00}(\lambda \star \boldsymbol{q}) = \frac{2\rho^{(0)}\bar{N}}{-2 + Q^2} , \tag{G.1}$$

where we introduced the dimensionless wave vector $Q$, defined as $Q^2 \equiv a^2 \bar{N} \boldsymbol{q}^2$. Due to the symmetry of the replica Hamiltonian with respect to permutations of all the replicas in the case of an undeformed network ($\{\lambda_\alpha = 1\}$), we find (see Appendix E) that all $g^{kl}$ are equal for $k \neq l$ and that $g^{kk} = g^{00}$ for $k = 1, \ldots, m$. Substituting eqs. (F.15) and (F.16) into eqs. (4.27)–(4.30) and using these symmetry relations, we find upon some algebra that all dependence of the total structure factor on the non-diagonal elements of $g^{kl}$ drops out, and we obtain

$$S_q^{(0)} = g^{00}(\boldsymbol{q})/[1 + w^{(0)} g^{00}(\boldsymbol{q})] . \tag{G.2}$$

In the general case, $\{\lambda_\alpha \neq 1\}$, the replica space correlation functions have been calculated in Appendix E only in the long wavelength ($Q \ll 1$) and the short wavelength ($Q \gg 1$) limits. Combining the expressions for the functions $g^{kl}$ obtained in the above appendix, we write

$$g^{11}(\lambda \star \boldsymbol{q}) - g^{12}(\lambda \star \boldsymbol{q}) = \begin{cases} \dfrac{2\rho^{(0)}\bar{N}}{(\lambda \star \check{\boldsymbol{q}})^2}[1 + \alpha(\check{\boldsymbol{q}})Q^2] & \text{for } Q \ll 1, \\ \dfrac{2\rho^{(0)}\bar{N}}{Q^2}(1 + I_3/Q^2) & \text{for } Q \gg 1 , \end{cases} \tag{G.3}$$

where we introduce the unit vector $\check{\boldsymbol{q}} = \boldsymbol{q}/|\boldsymbol{q}|$ in the direction of the wave vector $\boldsymbol{q}$, and

$$\alpha(\check{\boldsymbol{q}}) = 2I_1[(\lambda \star \check{\boldsymbol{q}})^2 - 1] + I_2(\lambda \star \check{\boldsymbol{q}})^2 , \tag{G.4}$$

with the constants $I_1 \simeq 0.524$, $I_2 \simeq 0.033$ and $I_3 \simeq 1.395$.

In the same approximation, we find the long and short wavelength limits of the function $g^{00} - g^{12}$

$$g^{00}(\lambda \star \boldsymbol{q}) - g^{12}(\lambda \star \boldsymbol{q}) = \begin{cases} 2\rho^{(0)}\bar{N}[1 + \alpha(\check{\boldsymbol{q}})Q^2] & \text{for } Q \ll 1 , \\ \dfrac{2\rho^{(0)}\bar{N}}{Q^2}(1 + I_3/Q^2) & \text{for } Q \gg 1 . \end{cases} \tag{G.5}$$

We complete our consideration of replica correlation functions with the function $g^{00} - g^{10}$,

$$g^{00}(\lambda \star \boldsymbol{q}) - g^{10}(\lambda \star \boldsymbol{q}) = \begin{cases} 2\rho^{(0)}\bar{N}[1 + \alpha_0(\check{\boldsymbol{q}})Q^2] & \text{for } Q \ll 1 , \\ \dfrac{2\rho^{(0)}\bar{N}}{Q^2}(1 + I_3/Q^2) & \text{for } Q \gg 1 , \end{cases} \tag{G.6}$$

where $\alpha_0(\check{\boldsymbol{q}})$ is defined by the expression

$$\alpha_0(\check{\boldsymbol{q}}) = I_1[(\lambda \star \check{\boldsymbol{q}})^2 - 1] + I_2(\lambda \star \check{\boldsymbol{q}})^2 . \tag{G.7}$$

The knowledge of these functions is sufficient to calculate the correlators in the elastic reference state $g_{\boldsymbol{q}}$ and $v_{\boldsymbol{q}}$ defined by Eqs. (F.15) and (F.16). The function $g_{\boldsymbol{q}}$ is directly expressed through the following combination of replica correlation functions:

$$g_{\boldsymbol{q}} \equiv \frac{g^{11}(\lambda \star \boldsymbol{q}) - g^{12}(\lambda \star \boldsymbol{q})}{\lambda_x\lambda_y\lambda_z} . \tag{G.8}$$

The correlator of static inhomogeneities $v_{\boldsymbol{q}}$ can be rewritten in the form

$$\begin{aligned} v_{\boldsymbol{q}} &\equiv \frac{1}{\lambda_x\lambda_y\lambda_z}\left[g^{12}(\lambda \star \boldsymbol{q}) - \frac{w^{(0)}[g^{01}(\lambda \star \boldsymbol{q})]^2}{1 + w^{(0)}g^{00}(\lambda \star \boldsymbol{q})}\right] \\ &= 2\rho\bar{N}A_{\boldsymbol{q}} + B_{\boldsymbol{q}}\frac{S^{(0)}_{\lambda \star \boldsymbol{q}}}{\lambda_x\lambda_y\lambda_z} , \end{aligned} \tag{G.9}$$

where all the dependence on preparation condition enters through the function $S^{(0)}_{\lambda \star \boldsymbol{q}}$ (see Eq. (4.31), with the substitution $\boldsymbol{q} \to \lambda \star \boldsymbol{q}$),

$$\frac{S^{(0)}_{\lambda \star \boldsymbol{q}}}{\lambda_x\lambda_y\lambda_z} = \frac{2\rho}{-2/\bar{N} + 2\rho^{(0)}w^{(0)} + a^2(\lambda \star \boldsymbol{q})^2} , \tag{G.10}$$

and where we defined the functions

$$A_{\boldsymbol{q}} \equiv \frac{1}{2\rho^{(0)}\bar{N}}\left\{g^{12}(\lambda \star \boldsymbol{q}) - \frac{[g^{01}(\lambda \star \boldsymbol{q})]^2}{g^{00}(\lambda \star \boldsymbol{q})}\right\} \tag{G.11}$$

and

$$B_{\boldsymbol{q}} \equiv g^{01}(\lambda \star \boldsymbol{q})/g^{00}(\lambda \star \boldsymbol{q}) . \tag{G.12}$$

Using the asymptotic expressions for the functions $g^{kl}$ which were derived in this appendix, we obtain the following asymptotics for the functions $A_q$ and $B_q$:

$$A_q = \begin{cases} 3 - (1 + \alpha(\check{q}) - 6\alpha_0(\check{q}))Q^2 & \text{for } Q \ll 1\,, \\ (2 - I_3)^2 Q^{-4} & \text{for } Q \gg 1\,, \end{cases} \tag{G.13}$$

$$B_q = \begin{cases} 9 - 6(1 - 2\alpha_0(\check{q}))Q^2 & \text{for } Q \ll 1\,, \\ (2 - I_3)^4 Q^{-4} & \text{for } Q \gg 1\,, \end{cases} \tag{G.14}$$

## References


[1] R.T. Deam and S.F. Edwards, Philos. Trans. R. Soc. London Ser. A, 280 (1976) 317.
[2] M. Warner and S.F. Edwards, J. Phys. A 11 (1978) 1649.
[3] P.-G., de Gennes, Scaling Concepts in Polymer Physics (Cornell University Press, Ithaca, New York, 1979).
[4] P.W. Anderson, Basic Notions of Condensed Matter Physics (Benjamin, Reading, MA, 1984).
[5] S.V. Panyukov, JETP Lett. 55 (1992) 608.
[6] P.J. Flory and J. Rehner, J. Chem. Phys. 11 (1943) 521.
[7] P.J. Flory, Principles of Polymer Chemistry (Cornell University Press, Ithaca, New York, 1971).
[8] H.M. James and E. Guth, J. Chem. Phys. 11 (1943) 455.
[9] S.F. Edwards and P.W. Anderson, J. Phys. (Paris) F 5 (1975) 1965.
[10] S.V. Panyukov, JETP Lett. 58 (1993) 119.
[11] S. Panyukov, Y. Rabin and A. Feigel, Europhys. Lett. 28 (1994) 149.
[12] A. Ramzi et al., J. de Phys. 4; Colloque C8 Supp. J. de Phys. 1, Vol. 3 (1993).
[13] C. Rouf et al., Phys. Rev. Lett. 73 (1994) 830.
[14] T. Takebe et al., J. Chem. Phys. 91 (1989) 4360.
[15] S.V. Panyukov, Sov. Phys. JETP 76 (1993) 631.
[16] R. Oeser, C. Picot and J. Hertz, Springer Proc. Phys. 29 (1988) 104.
[17] J. Bastide, M. Buzier and F. Boué, Springer Proc. Phys. 29 (1988) 112.
[18] F. Boué, J. Bastide and M. Buzier, Springer Proc. Phys. 42 (1989) 48.
[19] T. Takebe and T. Hashimoto, Polym. Commun. 29 (1988) 261.
[20] R.C. Ball and S.F. Edwards, Macromolecules 13 (1980) 748.
[21] L.D. Landau and E.M. Lifshitz, Theory of Elasticity (Pergamon Press, Oxford, 1970).
[22] S. Alexander, J. Phys. (Paris) 45 (1984) 1939; in: Physics of Finely Divided Matter, eds. N. Boccara and M. Daoud (Springer, Berlin, 1985).
[23] M. Doi and S.F. Edwards, The Theory of Polymer Dynamics (Clarendon, Oxford, 1986).
[24] G.S. Grest, K. Kremer and E.R. Duering, Physica A. 194 (1993) 330.
[25] S.F. Edwards and T.A. Vilgis, Rep. Prog. Phys. 51 (1988) 243.
[26] P.M. Goldbart and N. Goldenfeld, Phys. Rev. A 39 (1989) 1412.
[27] J. des Cloizeaux and G. Jannink, Polymers in Solution. Their Modelling and Structure (Clarendon Press, Oxford, 1990).
[28] H.E. Castillo, P.M. Goldbart and A. Zippelius, Europhys. Lett. 28 (1994) 519.
[29] S.V. Panyukov, Sov. Phys. JETP 76 (1993) 808.
[30] A. Zippelius, P.M. Goldbart and N. Goldenfeld, Europhys. Lett. 23 (1993) 451.
[31] J. Zinn-Justin, Quantum Field Theory and Critical Phenomena (Clarendon Press, Oxford, 1989).
[32] P.J. Flory, Statistical Mechanics of Chain Molecules (Wiley, New York, 1969).
[33] M. Mezard, G. Parisi and M. Virasoro, Spin Glass Theory and Beyond (World Scientific, Singapore, 1987).
[34] P.M. Goldbart and N. Goldenfeld, Phys. Rev. Lett. 58 (1987) 2676.
[35] P.M. Goldbart and A. Zippelius, J. Phys. A: Math. Gen. 27 (1994) 6375.

[36] D. Forster, Hydrodynamic Fluctuations, Broken Symmetry and Correlation Functions (Addison-Wesley, New York, 1983).
[37] D. Sherrington and S. Kirkpatrick, Phys. Rev. Lett. 32 (1975) 1792.
[38] H.M. James, J. Chem. Phys. 15 (1947) 651.
[39] J. Bastide, C. Picot and S. Candau, J. Macromol. Sci. Phys. 19 (1981) 13.
[40] M. Daoud, E. Bouchaud and G. Jannink, Macromolecules 19 (1986) 1955.
[41] Y. Rabin and R. Bruinsma, Europhys. Lett. 20 (1992) 79; R. Bruinsma and Y. Rabin, Phys. Rev. E. 49 (1994) 554.
[42] P.M. Goldbart and A. Zippelius, Phys. Rev. Lett. 71 (1993) 2256.
[43] J.G. Joosten, J.L. McCarthy and P.N. Pusey, Macromolecules 24 (1991) 6690.
[44] M.J. Orkisz, Ph.D. Thesis, MIT, 1994.
[45] N. Micali et al., Phys. Rev. E. 48 (1993) 4501.
[46] J. Bastide, R. Dupplesix, C. Picot and S. Candau, Macromolecules 17 (1984) 83.
[47] J. Bastide et al., Macromol. Chem., Macromol. Symp. 40 (1990) 81.
[48] F. Zielinski, Ph.D. Thesis, Paris 6, 1991.
[49] M. Mendes, Ph.D. Thesis, Louis Pasteur, Strasbourg, 1991.
[50] J. Bastide and L. Leibler, Macromolecules 21 (1988) 2647.
[51] J. Bastide, L. Leibler and J. Prost, Macromolecules 23 (1990) 1821.
[52] A. Onuki, J. de Phys. II. 2 (1992) 45.
[53] A. Ramzi, Ph.D. Thesis, Paris 6, 1994.
[54] F.S. Bates and G.H. Fredrickson, Ann. Rev. Phys. Chem. 41 (1990) 525.
[55] M. Shibayama, T. Tanaka and C.C. Han, J. Chem. Phys. 97 (1992) 6829.
[56] R. Hornreich, M. Luban and S. Shtrikman, Phys. Rev. Lett. 35 (1982) 1678.
[57] M. Mendes et al., Phys. Rev. Lett. 66 (1991) 1595.
[58] B.J. Bauer, R.M. Briber and C.C. Han, Macromolecules 22 (1988) 940.
[59] S.-K. Ma, Modern Theory of Critical Phenomena (Benjamin, Reading, MA, 1976).
[60] S.V. Panyukov, Sov. Phys. JETP 67 (1988) 930.
[61] A.Y. Grosberg and A.R. Khokhlov, Statistical Physics of Macromolecules (AIP Press, New York, 1994).
[62] S.V. Panyukov, JETP Lett. 51 (1990) 253; S.V. Panyukov, Sov. Phys. JETP 71 (1990) 372.
[63] S.P. Obukhov, M. Rubinstein and R.H. Colby, Macromolecules 27 (1994) 3191.
[64] P. Pekarski, A. Tkachenko and Y. Rabin, Macromolecules 27 (1994) 7192.
[65] A.J. Staverman, Adv. Polym. Sci. 44 (1982) 73.
[66] S. Mallam et al., Macromolecules 22 (1989) 3356.
[67] F. Horkay et al., Macromolecules 24 (1991) 2896.
[68] A.N. Falcao, J. Skov Pedersen and K. Mortensen, Macromolecules 26 (1993) 5350.
[69] J. Bastide and S.J. Candau, preprint.
[70] E. Geissler, F. Horkay and A.-M. Hecht, Phys. Rev. Lett. 71 (1993) 645.
[71] V. Borue and I. Erukhimovich, Macromolecules 21 (1988) 3240.
[72] J.F. Joanny and L. Leibler, J. Phys. (Paris) 51 (1990) 545.
[73] F. Brochard and P.G. de Gennes, Phys. Chem. Hydrodyn. 4 (1983) 313.
[74] A.-M. Hecht et al., Macromolecules 24 (1991) 4183.
[75] M. Mooney, J. Appl. Phys. 19 (1948) 434; R.S. Rivlin, Philos. Trans. R. Soc. London Ser. A 241 (1948) 379.
[76] X.L. Wu, D.J. Pine and P.K. Dixon, Phys. Rev. Lett. 66 (1991) 2408.
[77] J.W. van Egmond, D.E. Werner and G.G. Fuller, J. Chem. Phys. 96 (1992) 7742.
[78] E. Helfand and G.H. Fredrickson, Phys. Rev. Lett. 62 (1989) 2468.
[79] P.J. Flory and B. Erman, Macromolecules 15 (1982) 801.
[80] J.E. Mark and J.G. Curro, J. Chem. Phys. 79 (1983) 5705.
[81] S.V. Panyukov, Sov. Phys. JETP 67 (1988) 2274; S.V. Panyukov, Sov. Phys. JETP 69 (1989) 342.
[82] R. Skouri et al., Europhys. Lett. 23 (1993) 635.
[83] L.D. Landau and E.M. Lifshitz, Quantum Mechanics (Pergamon, Oxford, 1984).
[84] Y. Oono, in: Advances in Chem. Phys. Vol. 61, eds., I. Prigogine and S.A. Rice (Wiley, New York, 1985).
[85] K.F. Freed, Renormalization Group Theory of Macromolecules (Wiley, New York, 1987).